

UNIVERSITY OF ALBERTA

THE EFFECT OF FABRIC ON THE MECHANICAL BEHAVIOUR
OF A TAILINGS SAND

by

DONALD JAMES LAW

A THESIS

SUBMITTED TO THE FACULTY OF GRADUATE STUDIES AND RESEARCH
IN PARTIAL FULFILLMENT OF THE REQUIREMENTS FOR THE DEGREE
OF MASTER OF SCIENCE

DEPARTMENT OF CIVIL ENGINEERING


EDMONTON, ALBERTA

SPRING, 1991


UNIVERSITY OF ALBERTA

FACULTY OF GRADUATE STUDIES AND RESEARCH


THE UNDERSIGNED CERTIFY THAT THEY HAVE READ, AND
RECOMMEND TO THE FACULTY OF GRADUATE STUDIES AND
RESEARCH FOR ACCEPTANCE, A THESIS ENTITLED
**THE EFFECT OF FABRIC ON THE MECHANICAL
BEHAVIOUR OF A TAILINGS SAND,**
SUBMITTED BY DONALD JAMES LAW
IN PARTIAL FULFILLMENT OF THE REQUIREMENTS FOR
THE DEGREE OF MASTER OF SCIENCE.



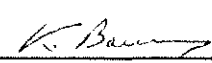
D. C. Sego, Supervisor



N. R. Morgenstern



P. K. Robertson



K. Barron

March 8, 1991

ABSTRACT

This thesis investigates the relationship between fabric and the mechanical behaviour of a tailings sand. Fabric differences among depositional methods used to place the tailings sand are investigated using the Scanning Electron Microscope. The mechanical behaviour of the sand is investigated to determine if fabric differences affect the strength, deformation and pore pressure generation properties of the tailings sand as determined in the consolidated-undrained triaxial test. An assessment of the appropriateness of the laboratory representation of the field fabric is made. The effect of small gradational changes on mechanical behaviour is also investigated.

The analysis of fabric and mechanical behaviour of this material failed to show a significant fabric effect among the three depositional methods studied; pluviation, flume and field hydraulic deposition. A technique was developed to allow the viewing of undisturbed tailings sand in the Scanning Electron microscope, and a practical method of obtaining and analyzing orientation data from the SEM micrographs is outlined.

The pre-shear and steady state conditions were determined for this material in terms of dry density and relative density. Less scatter was observed with the use of the relative density representation of the state conditions. A parameter based on relative density and the state parameter concept was developed which somewhat normalizes the observed mechanical behaviour in terms of state and small gradational differences among the specimens tested. Dilative test results were used to characterize the steady state condition above the 1000 kPa effective stress level, and the results linked well with those determined from contractive test data.

ACKNOWLEDGEMENTS

The author would like to thank his supervisor, Dr. D. Segó, and Professor N. Morgenstern for the suggestion of this topic and for their guidance and advice throughout this research. Also gratefully acknowledged is Angela Kupper, whose council and patience were instrumental in the completion of this thesis.

Funding for the research was provided through grants from the Natural Sciences and Engineering Research Council (NSERC), and from Esso Resources Canada Ltd. Test data from Syncrude Canada Ltd. were generously provided by Mr. G. Handford, and support services were provided by Thurber Engineering Ltd. of Edmonton. Many thanks are extended to these sources for their support.

The author is grateful for the technical assistance (anything from cold room work to electronics) provided by Steve Gamble, Christine Hereygers, Jay Khajuria and Gerry Cyre, and for the Scanning Electron Microscopy expertise provided by George Braybrook. Much appreciation is also expressed to my fellow graduate students and the staff of the Department of Civil Engineering for their support and comradery during this research. The personal friendships that have grown over these years of study will last a lifetime.

Finally, the author wishes to express his deep appreciation for the patience and support provided by his wife Jo, and apologize for the countless hours spent away from the family to this end. This work is dedicated to Johanna Rose and Graeme Benjamin Wegner Law.

TABLE OF CONTENTS

CHAPTER	PAGE
1. INTRODUCTION.....	1
1.1. Background.....	1
1.2. Objective of Thesis.....	1
1.3. Scope of Study	2
1.4. Organization of Thesis.....	3
2. PREVIOUS WORK RELATING FABRIC TO MECHANICAL BEHAVIOUR.....	5
2.1. Fabric.....	5
2.2. Anisotropy Effects	6
2.2.1. Moderate Strain Effects.....	6
2.2.2. Large Strain Effects.....	11
2.3. Specimen Preparation Effects.....	11
2.4. Summary.....	15
3. FABRIC ANALYSIS.....	18
3.1. Introduction.....	18
3.2. Specimen Preparation and Viewing.....	19
3.2.1. Mounting Method A - No Lateral Support	20
3.2.2. Mounting Method B - Lateral Support.....	22
3.2.3. SEM Viewing.....	22
3.3. Micrograph Analyses	23
3.3.1. Qualitative Analysis.....	23
3.3.2. Quantitative Analysis.....	27
3.3.2.1. Data Collection.....	28
3.3.2.2. Data Analysis.....	29
3.4. Results.....	35
3.4.1. Qualitative Analysis Results.....	35
3.4.1.1. Attached Clay.....	35
3.4.1.2. Silt Sizes	36
3.4.1.3. Long Grains.....	37
3.4.1.4. Planarity.....	38
3.4.1.5. Contact Areas.....	39

3.4.1.6.	Degree of Interlock	40
3.4.1.7.	Packing.....	40
3.4.1.8.	Void Size and Homogeneity.....	41
3.4.1.9.	Orientation	42
3.4.1.10.	Conclusions	44
3.4.2.	Quantitative Analysis Results	45
3.4.2.1.	Vector Magnitude and Direction.....	45
3.4.2.2.	Mean Aspect Ratio.....	47
3.5.	Summary of Fabric Analysis Results.....	49
4.	MECHANICAL BEHAVIOUR DURING SHEAR	66
4.1.	Introduction	66
4.2.	Behaviour of Cohesionless Materials During Shear.....	67
4.2.1.	Steady State of Deformation	68
4.2.2.	Drained Behaviour	69
4.2.3.	Undrained Behaviour	71
4.3.	Laboratory Testing.....	72
4.3.1.	Overview	72
4.3.2.	Present Study	74
4.3.2.1.	Material Tested	74
4.3.2.2.	Specimen Preparation	75
4.3.2.2.1.	Pluviation.....	75
4.3.2.2.2.	Flume	81
4.3.2.2.3.	Field.....	82
4.3.2.3.	Triaxial Test Procedure.....	83
4.3.2.3.1.	Preparation	85
4.3.2.3.2.	Assembly	86
4.3.2.3.3.	Thaw	88
4.3.2.3.4.	Saturation.....	88
4.3.2.3.5.	B-Test.....	89
4.3.2.3.6.	Consolidation	90
4.3.2.3.7.	Shear	91
4.3.2.3.8.	Dismantle	91

4.3.2.4.	General Comments	92
4.3.3.	Other Testing Programs	93
4.3.3.1.	Source 1.....	93
4.3.3.2.	Source 2.....	95
4.3.3.3.	Source 3.....	97
4.3.3.4.	Source 4.....	98
4.3.3.5.	Source 5.....	100
4.3.4.	Summary of Testing Programs.....	102
4.3.4.1.	Potential Sources of Error	104
4.4.	Results.....	105
4.4.1.	Direct Comparison	106
4.4.2.	Normalized Comparison.....	109
4.4.2.1.	Pre-Shear Conditions.....	110
4.4.2.2.	Steady State Characterization.....	111
4.4.2.3.	Relative Density Parameter	117
4.5.	Summary of Results	120
5.	CONCLUSIONS.....	166
5.1.	General	166
5.2.	Limitations Of The Study.....	167
5.3.	Recommendations For Further Study.....	169
	REFERENCES.....	170
	APPENDIX	
A	Selected SEM Micrographs and Rose Diagrams.....	176
B	Triaxial Apparatus Calibrations.....	195
C	Present Study Triaxial Test Results	197
D	Grain Size Analysis Summary and Results	250
E	Relationship Between the Relative Density Parameter and Various Moderate Strain Parameters	266

LIST OF TABLES

TABLE	PAGE
3.1 Summary of Qualitative Analysis.....	51
3.2 Comparison of Qualitative Analyses	55
3.3 Summary of Quantitative Analyses.....	59
3.4 Comparison of Orientation Results.....	60
4.1 Dry Density Variation due to Method and Spatial Location	123
4.2 Specimen State Summary	124
4.3 Triaxial Testing Conditions Summary	127
4.4 Stress-Strain/Pore Pressure Response Parameters at Elbow: Comparison Among Methods of Deposition	128
4.5 Stress-Strain/Pore Pressure Response Parameters at Elbow: Control Group.....	129
4.6 Stress-Strain/Pore Pressure Response Parameters at Elbow: Comparison of Ranges of Observed Values Between Control and Comparison Groups	130
4.7 Average Gradational and Max/Min Properties	131
B-1 Calibration Data	196
C-1 PL 2 Triaxial Test Result Summary.....	199
C-2 PL 3 Triaxial Test Result Summary.....	201
C-3 PL 6 Triaxial Test Result Summary.....	203
C-4 PL 7 Triaxial Test Result Summary.....	205
C-5 PL 8 Triaxial Test Result Summary.....	207
C-6 PL 9 Triaxial Test Result Summary.....	209
C-7 PL 10 Triaxial Test Result Summary	211
C-8 PL 12 Triaxial Test Result Summary	213

C-9	PL 13 Triaxial Test Result Summary	215
C-10	PL 14 Triaxial Test Result Summary	217
C-11	PL 15 Triaxial Test Result Summary	219
C-12	PL 16 Triaxial Test Result Summary	221
C-13	PL 17 Triaxial Test Result Summary	223
C-14	PL 19 Triaxial Test Result Summary	225
C-15	FL 2 Triaxial Test Result Summary.....	227
C-16	FL 3 Triaxial Test Result Summary.....	229
C-17	FL 4 Triaxial Test Result Summary.....	231
C-18	FL 5 Triaxial Test Result Summary.....	233
C-19	FL 6 Triaxial Test Result Summary.....	235
C-20	FL 7 Triaxial Test Result Summary.....	237
C-21	FL 8 Triaxial Test Result Summary.....	239
C-22	FL 9 Triaxial Test Result Summary.....	241
C-23	FL 10 Triaxial Test Result Summary	243
C-24	UF 1 Triaxial Test Result Summary	245
C-25	FD 1 Triaxial Test Result Summary	247
C-26	FD 2 Triaxial Test Result Summary	249
D-1	Grain Size Summary.....	251

LIST OF FIGURES

FIGURE	PAGE
3.1 Confidence Level Using the Rayleigh Test of Significance	61
3.2 Vector Magnitude vs Aspect Ratio	62
3.3 Intergranular Fabric Classification	63
4.1 Idealized Triaxial Shear Results (Consolidated-Drained).....	134
4.2 Idealized Triaxial Shear Results (Consolidated-Undrained).....	135
4.3 Range of Grain Size Distributions for Tailings Sand Investigated	136
4.4 Multiple Sieve Pluviation Device	137
4.5 Pluviation Mould.....	138
4.6 Pluviation Test Specimen Layout (Ottawa Sand).....	139
4.7 Average Density Variation due to Change in Height of Drop.....	140
4.8 Variation in Density With Opening Diameter.....	141
4.9 Schematic of Tailings Disposal.....	142
4.10 Shape of Test Specimens After Shear.....	143
4.11 Triaxial Apparatus.....	144
4.12 Platen Design and Initial Specimen Dimensions.....	145
4.13 Non-Uniformity of Strains Developed During Shear Using Conventional End Platens.....	146
4.14 Pre-Shear Void Ratio Change vs Initial Void Ratio	147
4.15 Typical Stress Path, Stress-Strain and Pore Pressure Response Results.....	148
4.16 Behaviour Comparison at Elbow: Deviatoric Stress and Change in Pore Pressure	149
4.17 Behaviour Comparison at Elbow: p' and Pore Pressure Parameter 'A'	150

4.18	Behaviour Comparison at Elbow: Strain and Stress Ratio	151
4.19	Behaviour Comparison at Elbow: Initial Tangent Modulus and Foreslope Modulus	152
4.20	Typical Stress-Strain, Pore Pressure Response and Stress Path Response	153
4.21	Pre-Shear Specimen State Grouped by Stress-Strain Type (Dry Density)	154
4.22	Pre-Shear and Steady State Relationship	155
4.23	Pre-Shear Specimen State Grouped by Stress-Strain Type (Relative Density).....	156
4.24	Steady State Conditions (Dry Density)	157
4.25	Steady State Conditions (Relative Density)	157
4.26	Relative Density Representation of Steady State Condition	158
4.27	Effect of D_{50} and C_u on Maximum and Minimum Density	159
4.28	Effect of Fines Content on C_u for Similar Gradations.....	160
4.29	Maximum Dry Density Corresponding to Measured D_{50} and C_u	161
4.30	Minimum Dry Density Corresponding to Measured D_{50} and C_u	162
4.31	State Parameter Definition.....	163
4.32	Steady State Diagram Showing Correction of S_{US}	164
4.33	Steady State Shear Strength vs RD Parameter	165
C-1	PL 2 Triaxial Test Results.....	198
C-2	PL 3 Triaxial Test Results.....	200
C-3	PL 6 Triaxial Test Results.....	202
C-4	PL 7 Triaxial Test Results.....	204
C-5	PL 8 Triaxial Test Results.....	206
C-6	PL 9 Triaxial Test Results.....	208
C-7	PL 10 Triaxial Test Results.....	210

C-8	PL 12 Triaxial Test Results	212
C-9	PL 13 Triaxial Test Results	214
C-10	PL 14 Triaxial Test Results	216
C-11	PL 15 Triaxial Test Results	218
C-12	PL 16 Triaxial Test Results	220
C-13	PL 17 Triaxial Test Results	222
C-14	PL 19 Triaxial Test Results	224
C-15	FL 2 Triaxial Test Results.....	226
C-16	FL 3 Triaxial Test Results.....	228
C-17	FL 4 Triaxial Test Results.....	230
C-18	FL 5 Triaxial Test Results.....	232
C-19	FL 6 Triaxial Test Results.....	234
C-20	FL 7 Triaxial Test Results.....	236
C-21	FL 8 Triaxial Test Results.....	238
C-22	FL 9 Triaxial Test Results.....	240
C-23	FL 10 Triaxial Test Results	242
C-24	UF 1 Triaxial Test Results	244
C-25	FD 1 Triaxial Test Results	246
C-26	FD 2 Triaxial Test Results	248
D-1	Grain Size Distribution for PL 3 and PL 5.....	254
D-2	Grain Size Distribution for PL 6 and PL 7.....	255
D-3	Grain Size Distribution for PL 8 and PL 9.....	256
D-4	Grain Size Distribution for PL 10 and PL 12.....	257
D-5	Grain Size Distribution for PL 15 and PL16.....	258
D-6	Grain Size Distribution for PL 17 and PL 18.....	259

D-7	Grain Size Distribution for PL 19 and FL 3	260
D-8	Grain Size Distribution for FL 4 and FL 5.....	261
D-9	Grain Size Distribution for FL 6 and FL 7.....	262
D-10	Grain Size Distribution for FL 8 and FL 9.....	263
D-11	Grain Size Distribution for FL 10 and UF 1.....	264
D-12	Grain Size Distribution for FD 4.....	265
E-1	Initial Tangent Modulus vs RD Parameter	271
E-2	Foreslope Modulus vs RD Parameter.....	271
E-3	Stress Ratio vs RD Parameter	272
E-4	'A' Parameter vs RD Parameter	272

LIST OF PLATES

PLATE		PAGE
3.1	Micrograph Showing Attached Clay, Solution Pitting and Etching (Field).....	64
3.2	Micrograph Showing Clay Bridge Between Sand Grains (Field).....	64
3.3	Micrographs Showing Minor Segregation (Flume).....	65
A-1	Micrograph 32 011 (Pluviated), Rose and Histogram Diagrams.....	177
A-2	Micrograph 33 014 (Pluviated), Rose and Histogram Diagrams.....	178
A-3	Micrograph 33 016 (Pluviated), Rose and Histogram Diagrams.....	179
A-4	Micrograph 13 038 (Flume), Rose and Histogram Diagrams	180
A-5	Micrograph 13 050 (Flume), Rose and Histogram Diagrams	181
A-6	Micrograph 13 054 (Flume), Rose and Histogram Diagrams	182
A-7	Micrograph 46 037 (Flume), Rose and Histogram Diagrams	183
A-8	Micrograph 44 030 (Flume), Rose and Histogram Diagrams	184
A-9	Micrograph 45 033 (Flume), Rose and Histogram Diagrams	185
A-10	Micrograph 60 078 (Flume), Rose and Histogram Diagrams	186
A-11	Micrograph 56 061 (Flume), Rose and Histogram Diagrams	187
A-12	Micrograph 61 083 (Flume), Rose and Histogram Diagrams	188
A-13	Micrograph 63 092 (Field), Rose and Histogram Diagrams.....	189
A-14	Micrograph 62 086 (Field), Rose and Histogram Diagrams.....	190
A-15	Micrograph 05 008 (Field), Rose and Histogram Diagrams.....	191
A-16	Micrograph 64 095 (Field), Rose and Histogram Diagrams.....	192
A-17	Micrograph 65 101 (Field), Rose and Histogram Diagrams.....	193
A-18	Micrograph 06 002 (Field), Rose and Histogram Diagrams.....	194

LIST OF SYMBOLS

SYMBOL	MEANING
A, B	Parameters relating pore pressure response with undrained total stress change
BP	Back pressure
C_u	Uniformity coefficient ($C_u = D_{10}/D_{60}$)
CU	Consolidated-undrained triaxial test
D_n	Mean particle diameter greater than n percent by weight of the soil particles in a sample
D_r	Relative density
e	Void ratio
e_{ss}	Steady state void ratio
Δe	Change in void ratio
FD	Field
FL	Flume
G_s	Specific gravity
l/d	Length to diameter ratio
L	Long axis resultant vector magnitude, %
LVDT	Linear voltage displacement transducer
MSP	Multiple sieve pluviation
n	Observation vector magnitude

N	Number of observations
% fines	Percent of material finer than 0.075 mm, by weight
p	Probability of randomness
PL	Pluviated
p_o'	Initial effective confining pressure
p'	Effective normal stress component, $(\sigma_1' + \sigma_3')/2$
q	Shear stress component, $(\sigma_1 - \sigma_3)/2$
r	Long axis resultant vector magnitude
RD	Relative density parameter
RTD	Resistive thermal device
SEM	Scanning Electron Microscopy
Δu	Change in pore pressure
ϕ'	Effective angle of internal shearing resistance
σ_1'	Major principal effective stress
$\Delta \sigma_1$	Change in major total stress
σ_3'	Minor principal effective stress
$\Delta \sigma_3$	Change in minor total stress
$(\sigma_1 - \sigma_3)$	Deviatoric stress or principal stress difference
σ_1'/σ_3'	Effective stress ratio
θ	Long axis azimuth
$\bar{\theta}$	Long axis resultant vector azimuth

1. INTRODUCTION

1.1. Background

The effect of the inherent fabric on the mechanical behaviour of granular materials has been the subject of much recent study in the geotechnical community. The knowledge of the behaviour of these soils can be critical to the understanding and prediction of the performance of granular structures. Significant safety and economic benefits may be possible through refined analytical techniques and design methods derived from a better understanding of material behaviour.

The tailings dyke at Syncrude Canada Ltd.'s oil sand mining facility north of Fort McMurray, Alberta, is among the largest granular structures in the world. The granular material used in this study is the sand portion of the waste by-product of the oil extraction process performed at Syncrude. Upon completion over 470 million cubic metres of the tailings sand material will have been hydraulically placed in the 18 kilometer dyke structure to contain roughly 400 million cubic metres of sludge and 50 million cubic metres of free water (Yano and Handford, 1988).

An appreciation for the effects of fabric on the mechanical behaviour of the tailings sand mass is expected to allow a more complete understanding of the nature of the strength and pore pressure generation characteristics of the tailings dyke.

1.2. Objective of Thesis

The objective of the study is to determine if definitive fabric differences exist dependent upon the depositional method used to place the tailings sand. The mechanical

behaviour of the sand is then investigated to determine if fabric differences affect the strength, deformation and pore pressure generation properties of the tailings sand. An assessment of the appropriateness of the laboratory representation of the field fabric is made. The effect of small gradational changes on mechanical behaviour is also investigated.

1.3. Scope of Study

The study is divided into three areas.

First, a study of the fabric produced by three placement techniques is presented. These techniques include field deposition (beaching), laboratory deposition (flume modelling of the field deposition process), and pluviation through air. This study includes a qualitative analysis of Scanning Electron Microscope (SEM) images to obtain a visual assessment of the differences in fabric developed, followed by a quantitative analysis of selected images using a digitizing technique and statistical analysis to confirm the qualitative assessment.

Second, a laboratory testing program is presented that attempts to uncover differences in mechanical behaviour (stress-strain and pore pressure response) due to a difference in fabric produced by the varying placement techniques. The strain controlled consolidated-undrained triaxial testing method was used to test specimens of the Syncrude tailings sand, with testing procedures modified to minimize the disturbance of the inherent fabric produced by the placement techniques. To complement the results obtained in this study, Syncrude has provided the results of steady state tests performed on the tailings sand over the past twelve years which allowed the comparison of another method of placement (compaction) with the present study results as well as the comparison of

contractive test results with the dilative results obtained in this study. A new parameter is developed that ties together the state parameter concept with relative density, in an attempt to allow a more direct comparison of the results from tests on materials with somewhat different grain size characteristics.

Finally, an interpretation of the results obtained in the fabric analysis investigation and mechanical behaviour determination is presented. Conclusions, limitations of the investigation and recommendations for further study are also presented.

This investigation was performed in conjunction with a study of the depositional process of the Syncrude tailings sand by Kupper (1991). Complete details of the flume and field deposition methods used to create the inherent fabrics studied are found therein. The Scanning Electron Microscope study and qualitative and quantitative fabric analyses of the undisturbed tailings sand specimens were performed together.

1.4. Organization of Thesis

Much work has been performed in the past 60 years on the behaviour of sand. A complete review of this literature is beyond the scope of this thesis. A selection of this literature is reviewed in Chapter 2, highlighting some of the relevant work carried out in the areas of anisotropic fabric and mechanical behaviour, and effects of specimen preparation on mechanical behaviour. Generalized behaviour of sands during shear is discussed at the beginning of Chapter 4.

Chapter 3 outlines the procedures and results of the fabric analysis portion of the study. Selected micrographs and rose diagrams displaying the preferred grain orientation are presented in Appendix A.

The mechanical behaviour of the tailings sand is investigated in Chapter 4. Electronic measurement equipment calibration details are included in Appendix B, and the detailed results from the triaxial tests are presented in Appendix C. Grain size analysis results are compiled in Appendix D, and the investigation of the relationship between the Relative Density parameter and a number of small strain parameters is presented in Appendix E.

Conclusions from the results of the previous chapters are summarized in Chapter 5, and limitations of the study are outlined. Also, recommendations for further study are made in this chapter.

2. PREVIOUS WORK RELATING FABRIC TO MECHANICAL BEHAVIOUR

Numerous studies relating the mechanical behaviour of cohesionless materials to the fabric of the material have been performed in the past twenty years. Following is a selected overview highlighting some of the relevant past studies relevant to this area of study. The term 'fabric' is discussed and a definition of the term as used in this study is given. Work involving the effects of fabric anisotropy on mechanical behaviour is then discussed, followed by specimen preparation effects.

2.1. Fabric

Various definitions of fabric exist in the literature. Brewer (1964) defines soil fabric as "the physical constitution of a soil material as expressed by the spatial arrangement of the solid particles and associated voids." Geologists and soil scientists separate 'fabric' (meaning particle arrangement and orientation) from the term structure (meaning 'fabric' and the size and shape of the individual grains and voids). The engineering community tends to use the terms interchangeably (Mahmood and Mitchell, 1974). In this study, fabric is defined in the broader sense as the spatial arrangement of particle sand voids as well as the characteristics of individual grains and voids such as relative size and shape.

Oda (1976) breaks the definition of fabric into two areas; homogeneous and heterogeneous fabric. Granular assemblies having a heterogeneous fabric are composed of groups of homogeneous parts or sub-masses having different kinds and degrees of particle configuration. The three-dimensional distribution and orientation of these homogeneous sub-masses and their mutual relation are, according to Oda, the most important structural

feature prevailing in the heterogeneous assembly. Oda states that the orientation of individual particles (orientation fabric) and the mutual relationship of individual particles to one another (packing) are separate concepts that are included in the definition of a homogeneous fabric. The overall fabric of a sand is therefore ideally described in terms of three elements; orientation fabric and packing within homogeneous sub-masses, and the interrelationship among the sub-masses within the sand matrix.

2.2. Anisotropy Effects

Arthur and Menzies (1972) provide an overview of studies performed prior to 1972 in which the existence of both inherent and induced anisotropy have been confirmed. Casagrande and Carillo (1944) have defined inherent anisotropy as "a physical characteristic inherent in the material and entirely independent of the applied strains". Induced anisotropy is defined as a physical characteristic "due exclusively to the strain associated with an applied stress." These definitions apply to observed strength anisotropy as well as stress-strain and fabric anisotropy.

The effect of anisotropy on mechanical behaviour can be separated for discussion of behavioural differences noted prior to peak strength (moderate strain effects), and those noted after peak strength has been achieved (large strain effects). Small strain effects, such as fabric effects observed as differences in shear (S) or compression (P) wave velocity and/or attenuation measured through the soil medium, are not considered herein.

2.2.1. Moderate Strain Effects

Arthur and Menzies (1972) had found that an inherent geometrical anisotropy was produced in specimens constructed of a rounded sand deposited through air and water. It

was found that the long axis of the sand particles tended to align to the horizontal (i.e. perpendicular to the direction of deposition). A series of drained cubic triaxial compression tests were performed on specimens of similar initial porosity (and at the same initial confining pressure), prepared such that the direction of the principal stress axes varied with the direction of deposition. Differences in axial strains observed to a given stress ratio of well over 200% were observed, depending on the angle between the direction of applied principal stress and the direction of deposition. A strength increase of 10% in the stress ratio at failure (corresponding to a ϕ' increase of 2°) was observed as the angle between the pouring direction and the direction of the major principal stress changed from 90° to 0° .

Dunstan (1972) expanded on this study by performing direct shear tests with differing principal stress directions relative to the direction of deposition, using four sand gradations and three stress levels. It was found that the variation in gradation "had little effect on the difference in strength caused by the anisotropic packing." It was also concluded that the anisotropic difference in shear strength tends to decrease as the normal stress increases.

Wong and Arthur (1985) have shown with tests in a directional shear cell that drained shear strength is largely independent of induced anisotropy and varies with inherent anisotropy even after moderate strains. They state that this persistence of inherent anisotropy can frequently control the magnitude of drained peak shear resistance. Conversely the induced anisotropy, developed after as little as 0.5% shear strain has taken place, can cause very large variations in the measured stiffness of sand and the associated capability for porewater pressure generation in undrained tests.

In drained triaxial compression, plane strain and cubical triaxial tests on a sand with a high aspect (length to width) ratio and an anisotropic fabric, Ochiai and Lade (1983)

found that the major principal strain was smallest and the rate of dilation was highest when the major principal stress acted perpendicular to the long axes of the sand grains. The effects of the inherent fabric were mainly observed in the prefailure stress-strain behaviour, whereas sufficient changes in the fabric had occurred (induced fabric) at relatively large strains (ie. at failure) to produce failure conditions which resembled those observed for isotropic sands.

A number of papers published by Oda since 1972 have attempted to determine a rationale for the observed differences in behaviour due to initial fabric anisotropy, as well as developing methods by which to quantify the changes in fabric observed during and after a specimen is stressed. In his 1972 work, Oda developed a direct method for measuring sand fabric. This technique involved using resin to 'lock' the fabric in place, allowing thin sections to be taken. Using a petrographic microscope, actual measurements of pertinent fabric features were made from these thin sections.

In drained triaxial compression tests, Oda (1972a) found that continuous reconstruction of the initial fabric with increase of axial strain occurred mainly by preferred directional sliding along the unstable contacts among neighbouring grain particles, and partially by rolling of each grain to make preferred re-orientation of long axes of grains perpendicular to the maximum principal stress direction.

Oda (1972b) reports on a series of drained triaxial tests (similar to those of Arthur and Menzies, 1972) from which the effect of the variance of the angle of deposition with respect to the major principal stress axis is demonstrated. Two sands were tested, with one material (Sand D) having more rounded particles on average than the other material (Sand B).

It was found that the mobilized maximum stress ratio at similar initial void ratios is higher in Sand B specimens tested such that the maximum principal stress direction is perpendicular to the average long axis direction of the sand particles, especially at low initial void ratios. The same trend was not apparent in tests on Sand D specimens.

The secant deformation modulus (determined at 50% of peak strength) was found to vary significantly with the direction of applied maximum principal stress at the same initial void ratio, with consistently higher moduli measured for the specimens prepared such that the maximum principal stress direction is perpendicular to the average long axis direction of the sand particles. This trend was observed in the tests performed on both sands. A scatter of up to 20% was noted in the tests where the highest moduli were measured, reflecting the accuracy with which this parameter can be measured.

These results are explained by the rationalization that the re-arrangement and re-orientation of sand grains may occur more easily (i.e. at a lower strain) in Sand D, consisting of relatively spherical particles, than in Sand B, having relatively flat or elongated grains. It appears that the effect of the inherent anisotropy on the mechanical behaviour is dependent on the shape of the grains of the sand investigated, and that this effect is noticeable over a larger range of strain in materials with flat or elongated particles.

The importance of the distribution of the directions normal to tangents at contact points between particles within a mass of granular material to determining its mechanical behaviour is developed in Oda (1972b, c) and, more completely, in Oda (1976). In these papers Oda develops the concept of fabric index which is defined by the three-dimensional distribution of the contact tangent normal directions, and shows that the fabric index is intimately related to the mobilized stress ratio and the dilatancy rate. Oda also determined that the fabric change induced by a stress change occurs following the same basic

mechanism through pre-peak loading to the peak stress condition, and is characterized generally by preferred sliding between particles along unstable contacts and partially by rolling of particles to preferentially orient their long axes perpendicular to the maximum principal stress axis. According to Oda, this concentration of contact tangent normal directions toward the maximum principal stress direction is believed to play the most essential role in the hardening process of granular material, because it is in this orientation that granular particles are most effective in supporting the axial stress.

Oda et. al. (1980) expanded further on the above work, introducing the term fabric ellipsoid. This term (fabric ellipsoid) is regarded as the mathematical approximation of the distribution of contact tangent normal directions, which allows the combination of the effects of particle long axis orientation, particle shape, and packing within the granular mass to explain the observed differences in mechanical behaviour in terms of fabric differences. In this work the authors found that the principal axes of the fabric ellipsoid generally coincide with those of the stress ellipsoid (the mathematical approximation of the stress state within the specimen) and this appears to hold whether the principal stress axes rotate gradually or discontinuously during deformation. In a strain hardening matrix, the fabric ellipsoid (or distribution of contact tangent normal directions) appears to continuously change with strain such that the ability of the material to withstand increased applied stress is enhanced. Depending on the initial packing of the assembly of particles and their proximity to one another, the strength response to continued straining will be either hardening (an increase in strength to a constant value) or softening (a decrease in strength after peak to a constant value). According to Oda, it is the change of fabric during deformation that results in the hardening (or softening) behaviour of granular materials during deformation.

In a summary of some of Oda's work, Feda (1982) concluded that "the fabric of granular materials has a distinct geometrical anisotropy provided that it is a consequence of a directional load (sedimentation, consolidation and flow pressures, pouring, compression, pressing, etc.). This condition manifests itself by the majority of the contact planes becoming perpendicular to the direction of the maximum pressure. The structure thus assumes its most stable arrangement for which the dissipation of strain energy is maximal, and for which the contact forces are largely normal to the contact planes. A consequence of this geometrical anisotropy is mechanical anisotropy."

2.2.2. Large Strain Effects

As determined by Castro (1969), the undrained steady state strength of sand is only a function of its void ratio and not of its initial stress state, type of undrained loading (monotonic or cyclic), nor its initial fabric. This premise is further supported by testing as outlined in Castro (1975) and Castro et. al. (1982). He states that "the shape of the stress strain curve prior to reaching steady state is a function of the initial structure of the soil; however, its steady state is not, since at steady state the soil is thoroughly remoulded and has lost all 'memory' of its initial structure."

However, Phillips and May (1967) report seeing an appreciable strength difference between specimens sheared with and across the dominant particle long axis direction even when the material is shearing at a constant void ratio.

2.3. Specimen Preparation Effects

A number of authors describe their work on the influence of specimen preparation on fabric and observed mechanical behaviour during shear. A change in preparation

method is an artificial means of imposing a different inherent anisotropy on a specific specimen, and therefore can give insight into the expected effects of natural variances in granular fabric due to varying depositional environments or stress histories.

Mahmood and Mitchell (1974) investigated the relationship between fabric and mechanical behaviour of an artificially prepared (crushed) silty sand sized basalt composed of elongate, angular grains. Fabric characteristics were determined from grain orientations measured from thin vertical sections taken through resin impregnated specimens, and from the pore size distribution determined using a mercury intrusion porosimetry technique. Three placement techniques were used to prepare specimens. These were dry pluviation (gentle pouring through air), static compaction (slow piston loading), and dynamic compaction (tapping).

The placement method was found to substantially affect the measured orientation of the apparent long axes of the grains, with the loose dry pluviated specimen (Relative Density (D_r) = 62%) exhibiting a strong horizontal orientation while both compacted specimens (D_r = 90%) showing a random or weakly oriented particle orientation. As expected, the pore sizes determined for the loose specimen were substantially higher than those of the compacted (dense) specimens, with the dynamic method being more effective in reducing the average pore diameter. Arthur and Menzies (1972) and Miura and Toki (1982) also found a strong orientation associated with pluviated specimens.

In a subsequent study, Mahmood et. al. (1976) found that pluviated specimens prepared using a sand where the grains are only slightly elongate and rounded showed no strong preferred orientation. This fabric condition was evident in specimens prepared to both a loose and a dense state. To explain the observed fabric differences the authors propose that on a horizontal surface, pluviated sands with elongated grains are more likely

to come to rest with their long axes normal to the direction of fall whereas sands with nearly round grains come to rest in random positions.

Specimen preparation has also been found to have a major influence on the liquefaction behaviour of a sand. In cyclic undrained triaxial tests, Ladd (1974) found that two commonly used preparation methods (dry-vibration and wet-tamping) required a significantly different number of cycles to achieve the same strain when tested at the same pre-shear void ratio. The specimens prepared by the dry-vibration method were significantly weaker during cyclic loading than the specimens prepared using the wet-tamping method. Ladd concluded that different inherent fabrics created by the two specimen preparation techniques was likely an important reason for the observed differences in liquefaction behaviour.

Mitchell et. al. (1976) concluded that specimens prepared using dry pluviation (raining) showed a much lower drained triaxial strength under cyclic loading than specimens prepared using moist tamping and moist vibration techniques, especially at lower relative densities. Thus, for the three methods of compaction used to prepare specimens of this sand, "it appears that for a given relative density the greater the intensity of preferred long axis orientation in a direction normal to the direction of the applied cyclic deviator stress, the less the resistance to liquefaction under triaxial loading conditions." As well, "the greater the proportion of interparticle contacts oriented normal to the direction of the major principal stress in triaxial compression the greater the resistance to deformation and liquefaction...." This trend was strongly observed in specimens prepared at $D_r = 50\%$, but not as strongly at $D_r = 80\%$.

Mulilis et. al. (1977) conducted an investigation to determine the effects of eleven methods of specimen preparation on the liquefaction characteristics of saturated sands

under undrained, stress-controlled cyclic triaxial test conditions. Differences in cyclic stress ratio causing liquefaction were found to be in the order of 100% for one sand tested, depending on the method of specimen preparation used. Tests on other sands indicate that the magnitude of the effect of the method of preparation used is a function of the type of sand. A fabric study of thin sections taken from resin-impregnated specimens indicated that the observed differences in the orientation of the contacts between sand grains and in packing were likely the primary reasons for the observed differences in the dynamic strength of the sand.

Nemat-Nasser and Tobita (1982) also studied the effect of the inherent anisotropy produced during specimen preparation on the observed mechanical behaviour of specimens during cyclic triaxial and cyclic simple shear tests. They have shown that although the moist tamping preparation method has produced specimens more resistant to liquefaction than dry pluviated specimens in cyclic triaxial tests (Mulilis et. al., 1977), the opposite trend was observed in their cyclic simple shear testing program using the same sand. Further extensive testing was recommended to attempt to understand why this differing behaviour was observed.

Campbell (1985) recognized the problem of the labour intensive methods in use to quantify fabric measurement, such as thin sectioning after resin impregnation followed by manual determination of fabric characteristics from these thin sections. In his work, Campbell used an ultrasonic (indirect) technique on post-shear sugar-cemented specimens to infer fabric, with confirmation of this inference made utilizing the more standard thin section (direct) method. The amount of data analyzed using the thin section technique was greatly increased by using a digitizing method, cutting the analysis time by over 90%. However, correlation of the thin section data to stress-strain behaviour in cubic triaxial tests

was not possible because the changes in fabric observed over the moderate strains induced were not considered large enough to be meaningful.

2.4. Summary

A summary of the conclusions drawn from the above work is presented below:

1. Large differences in the deformation modulus observed prior to failure and modest peak strength differences are apparent when specimens are stressed in different directions relative to a prevalent anisotropic grain orientation.
2. The influence of the inherent fabric is observed early in the shear strength test, with some previous work suggesting that this influence continues past the point of failure. The strain to which the inherent fabric influence is observed appears to be dependent on the shape of the grains, and is noticeable over a larger strain in materials with elongated or flat grains.
3. Pluviated specimens can develop a significant anisotropic fabric, but the intensity of the preferred orientation appears dependent on the grain shape. Sands with less elongate grains will likely show less orientation upon pluviation. Other methods of sample preparation (rodding, tapping, and vibration) tend to provide a more random fabric.
4. Cyclic strength varies with specimen preparation method, but specific trends associated with each method are not well defined and appear to depend on grain shape and method of loading.

It is evident that the effect of fabric on mechanical behaviour of granular materials is a complicated area of study that requires much future work to fully understand. Some of the difficulties encountered in past studies stem from the problems associated with obtaining and testing cohesionless specimens and problems inherent with the accurate determination of the fabric linked with specific methods of specimen preparation or field deposition.

In the present study, the distribution of the orientations of apparent long axes of the sand grains is used as a quantitative measure of the fabric of the specimens prepared using differing placement techniques. It is recognized that other aspects of fabric may also have an important influence on the observed mechanical behaviour of the sand during shear. These fabric elements include the distribution of the normals to interparticle contact planes, pore sizes and pore distributions, particle clustering, void variability within specimens, and particle size segregation (Mitchell et. al., 1976).

A full assessment of fabric was beyond the scope of this study. The qualitative assessment of fabric was undertaken to augment the collection of long axis orientation data. This was done to minimize the enormous task of data gathering and still allow an assessment of the effect of other fabric elements on the behaviour of this material during shear.

It can be argued that the distribution of long axis orientations is a two dimensional approximation of the fabric ellipsoid for soils that contain grains that have a substantial aspect (width to length) ratio. If a preferred orientation exists, the long grains will tend to contact each other along the long sides of the grains which would produce a contact tangent normal direction approximately 90° to that of the long axis of the grain. By finding the

apparent long axis orientation on three adjacent faces of a cube taken from the specimen, the orientation of the fabric ellipsoid may be inferred.

This method has limitations because it does not account for other factors important to the total fabric description of an assemblage of particles. Of these missing parameters, the individual particle shape and group packing characteristics (i.e. coordination number) of the sand mass appear to be the most important, and are intrinsically accounted for in the fabric ellipsoid representation. It is considered that for this sand, however, the long axis orientation representation will still be a meaningful indicator of initial fabric.

As pointed out by Oda (1976) and Fedá (1982), representative measures of fabric are ideally made from samples large enough to exhibit the heterogeneous fabric (made up of homogeneous structural units) that natural soils are generally composed of. The observations made in the present study are limited to small specimens (nominally 15 mm square) which may not contain the macrofabric considered critical to the mechanical behaviour of soils by these authors.

3. FABRIC ANALYSIS

3.1. Introduction

The purpose of this analysis was to determine the extent of fabric differences (if any) that exist among three placement methods. The placement methods investigated included field deposition (typically spigotted or overboarded at 60% solids content), flume deposition (laboratory simulation of the field deposition method), and dry pluviation ('raining' of sand through air). The field and flume depositional methods are briefly described in Chapter 4 and are described in detail by Kupper (1991). The flume and field methods were chosen for analysis to determine if a difference in fabric exists between the flume representation of the field conditions, and the field conditions themselves. The depositional method of pluviation through air was considered a significant departure from the other depositional methods, and therefore the results from the pluviated specimens were used to determine if this sample preparation method produces a significant change in fabric from that encountered in the field. The pluviation technique used in the present study is described in detail in Chapter 4.

Two methods of fabric determination were considered for this study; thin sectioning and scanning electron microscopy (SEM). Thin sectioning was attempted by Kupper (1991) but differentiation between the sand grains and the resin used to fix the grains in position was not possible under polarized light. Because of the nature of polarized light, only some of the grains were visible at one time making the digitizing process difficult and excessively time consuming. A coloured resin was experimented with in an attempt to allow the definition of all grains under natural light, but the addition of the colouring agent detrimentally affected the characteristics of the resin upon hardening. This problem had not been solved prior to the fabric analysis portion of the testing program hence the thin

sectioning method was abandoned. The SEM method was adopted as a means for the fabric determination.

Difficulties inherent to working with cohesionless sands were encountered during SEM specimen preparation but with a preparation method modification, undisturbed specimens were obtained for SEM viewing. The method used to obtain specimens for the SEM analysis is described next, followed by details of both the qualitative and quantitative analyses performed on the micrographs obtained from the SEM observations. The results of the analyses are then discussed, followed by the conclusions drawn from these results.

3.2. Specimen Preparation and Viewing

Frozen samples obtained from the laboratory (flume and pluviated) and from the field were trimmed in a -25°C cold room and then chilled on a bed of CO_2 pellets to -78°C . Specimens were created with fresh (undisturbed) faces by striking the sample with a hammer and small chisel to obtain an approximately cubical shape with a side dimension of 5 mm. The reduced temperature of the trimmed specimens prior to chiselling increased the ease with which clean, fresh faces were created, and allowed more time to work with the samples at room temperature. A bed of CO_2 pellets was kept nearby to re-chill the specimens during the creation of fresh faces, when necessary. Care was taken to attempt to maintain a record of the orientations of the faces with respect to the horizontal and the flow direction (if any) throughout the specimen preparation and the SEM observations, but some of the orientations may be suspect.

Two series of specimen preparation were undertaken, and each series used a different technique to mount the specimens for SEM viewing. The first technique used (Method A, Section 3.2.1) is a standard method used to mount objects that have inherent cohesion, and allows full view of the object from any angle. Although the material used in

this study is considered cohesionless, some strength upon drying has been observed in field samples.

An attempt was made in the first series to mount the frozen specimens using Method A, and determine if sufficient cohesion exists to allow the specimens to survive undisturbed during the SEM preparation and viewing. Method B (Section 3.2.2) was developed to allow SEM study of specimens that required lateral support to withstand the necessary preparation and viewing procedures.

3.2.1. Mounting Method A - No Lateral Support

This method follows the standard technique used to mount any object with significant internal cohesion. It involves the coating of the top surface of a circular aluminum mounting stub with a silver-based conductive contact cement. A frozen specimen was then placed on the stub, and a thread of the contact cement was placed up from the stub to the top face of the specimen along one of the corners of the specimen. This allowed for a better conductive path between the stub and the gold coating on the top face, thus creating better quality images from the SEM equipment.

Specimens can be dried after mounting using one of the techniques discussed below. In this study, all surviving specimens were allowed to thaw and air-dry for a minimum of 24 hours in a desiccated environment. Drying is necessary if the specimen contains more than a minimal amount of moisture to prevent sample disturbance during the evacuation of both the gold coating and SEM vacuum chambers. If the shrinkage behaviour of the material is such that upon oven or air-drying the structure is disturbed, then freeze-drying (vacuum sublimation after rapid freezing) or another technique such as substitution drying or critical point drying (Sides, 1971, Tovey and Wong, 1973) is

required. Shrinkage is expected to occur only when drying clays or sands with significant plastic fines content. Since the focus of this study is on the orientation of the larger particles in the specimens and the clay content is estimated to be very small (not measurable with hydrometer analysis), the shrinkage that occurs upon air-drying is not expected to influence the orientation of the grains of interest.

Gold coating is necessary to create a continuously conductive viewing surface which reduces the 'charging' that is sometimes observed during SEM viewing. Charging occurs when a single grain fails to make good electrical contact with its neighbouring grains, resulting in a dark halo around the particle. This halo significantly obscures the view of the particles surrounding the charging grain. The gold coating process places a 50 to 75 angstrom thick coating on the specimen surface while in a vacuum chamber. Two layers of the gold coating were required to eliminate most of the charging. The gold layer does not interfere with the image resolution at the magnification used in this study (up to 1000X). Unfortunately, both the freeze-drying and gold coating equipment imparted small vibrations on the specimens, which disturbed specimens without sufficient cohesion.

A number of problems surfaced while working with the first series of specimens. The inherent cohesion that normally keeps objects intact during the freeze-drying (if necessary) and gold coating stages of sample preparation, as well as during stage rotation and tipping while viewing the object with the SEM equipment, was not found in some of the specimens. None of the placement techniques (flume, pluviated, nor field) produced specimens that, when prepared using mounting Method A, survived the freeze-drying process. This method of drying was subsequently abandoned in favour of the air-drying method. Some of the sand specimens mounted using this method were able to withstand the smaller vibrations generated during the gold coating stage of preparation. The surviving specimens included most of the field specimens and a few of the flume

specimens. None of the pluviated specimens survived this preparation stage. As well, a few of the specimens that survived the gold coating process did not maintain their integrity during stage tilting while being viewed in the SEM vacuum chamber.

A second series of specimen preparation (using Method B to mount specimens) was undertaken to replace the specimens mounted using Method A that were damaged during the gold coating or SEM viewing stages.

3.2.2. Mounting Method B - Lateral Support

To circumvent the problems discussed above, a mounting technique was developed by which lateral support was given to the specimen during thaw, gold coating and subsequent SEM viewing. This method allowed only one face to be observed for each specimen. A wall of cellophane tape was placed around the head of the mounting stub, creating a cylindrical form which was partially filled with the viscous contact cement used in Method A. The frozen specimen was then placed into the form, with care taken not to disturb the upper (viewing) face. The cement was displaced until the specimen was surrounded, leaving only the top face of the specimen exposed. The assembly was then allowed to thaw and air-dry for a minimum of 24 hours in a desiccated environment. Some minor shrinkage was observed in the specimens and in the contact cement, but the specimens did not appear to be disturbed to the point of changing the orientations of the individual grains. The specimens prepared in this manner were then able to withstand the vibrations of the gold coating process.

3.2.3. SEM Viewing

A Cambridge Stereoscan scanning electron microscope (Model S-240) was used for this study. Specimens were placed on the stage in the vacuum chamber (10^{-5} torr) of the

SEM, the secondary electron emissions at an excitation level of 20 kV were viewed directly on a CRT screen, and over 160 micrographs were taken of random areas on the tailings sand specimens. The stage allows for tipping and rotation of the specimens to enable the face of interest to be oriented normal to the scanning electron beam. Approximately 100 of the micrographs were taken such that approximately 150 'large' grains (grains with a visible length greater than about 0.075 mm) were observed within the viewing area. This corresponded to a magnification of 50X for the sand being investigated. These micrographs were then analyzed qualitatively, and 18 selected micrographs were analyzed quantitatively, as described in the next section.

3.3. Micrograph Analyses

Two methods were chosen to analyze the fabric characteristics of the specimens. The first was an observational method developed to qualitatively investigate nine factors considered important to the determination of fabric for this material. The second was a quantitative method using image analysis techniques aimed at determining the orientation characteristics of the specimen faces by studying the orientation of individual particles with a statistical basis.

3.3.1. Qualitative Analysis

The visual (qualitative) determination of nine fabric characteristics that were considered important and somewhat variable was performed after a cursory examination of the micrographs taken of the undisturbed specimens. These nine characteristics were established by the author in conjunction with Kupper, 1991. Table 3.1, found at the end of this chapter, summarizes the specimen faces observed and the values assigned to each face for all the characteristics studied. These characteristics included:

Attached Clay: This is the amount of clay observed that adheres to the surface of the grains and creates bridges or connectors between particles. The possible descriptive terms used in Table 3.1 are none, very little, and some.

Silt Sizes: This variable reflects the number of observed particle sizes below 0.075 mm but above 0.002 mm with respect to the overall number of grains visible. Possible descriptive terms used include very few, few, and some.

Long Grains: This is the amount of particles observed to have a long to short axis ratio of approximately 1.5 to 1 or greater. Possible descriptive terms include few, some, and many.

Planarity of the Face: This is the relative flatness of the observed face. This variable may indicate that the face observed coincides with a plane preferred orientation. Descriptive terms used include none and some.

Size of Contact Area: This variable describes the observed apparent size of the area of contact between grains. Possible descriptive terms include small, small/few medium, small/some medium, small/medium, and medium.

Degree of Interlock: Interlocking can occur when proximal grains are of the required shape and orientation to interlock. The degree of interlock observed is described with the terms low, medium, and high.

Packing: The degree of packing observed reflects the closeness of the particles on a particular face. Possible descriptive terms are loose, medium, and dense.

Void Size and Homogeneity: This variable describes both the size of the observed voids with respect to other faces and also the homogeneity of the voids within the face. Descriptive terms for this variable include small and large, indicating that the voids are generally all one size. Other terms are small/some large, and small/large, indicative of a heterogeneous matrix that may include arching.

Orientation of Grains and Voids: This description is determined by a visual estimation of the preferred direction of the apparent long axes of the grains and void spaces (termed the orientation direction), and the magnitude of this observation (i.e. strong, weak, none). This orientation is described related to the bedding (horizontal) direction and/or the flow direction (if any) during placement.

Specimens were generally examined on three planes; horizontal, vertical parallel to flow (if any), and vertical perpendicular to flow. These planes are described as Face 1, Face 2 and Face 3, respectively. The micrographs from each face examined (ranging in number from 2 to 12) constitute a group (labelled P-pluviated, L-flume and F-field). The micrographs from each group were examined together to determine the average characteristics for that particular face and specimen. To be as unbiased as possible, judgements of the above fabric characteristics were made from the micrographs without knowledge of the flow direction, viewing face or method of placement by which the specimen was created. The results were then tabulated (Table 3.1), comparisons were made among the different faces within each deposition method, and like faces were compared among the deposition methods (Table 3.2). As well, the observed (qualitative) and measured (quantitative) orientation results were compared with the known flow and bedding directions (Table 3.4). These results are discussed in Section 3.4.

To fully describe the orientation direction, both the face observed (horizontal, vertical parallel and vertical perpendicular to flow) and the orientation of that face in relation to the flow and bedding directions must be known as viewed in the micrograph¹. The bedding direction is seen on the two vertical faces of each specimen, and the flow direction is visible on the horizontal and vertical (parallel to flow) faces. Although some difficulty was encountered in maintaining the specimen orientation relative to flow and bedding directions during specimen preparation, it is believed that the knowledge of the face being observed was maintained (as listed in Table 3.1). However, for eight of the flume specimens and one of the field specimens, the orientation of the face with respect to the flow/bedding direction as viewed in the micrograph was not maintained. Because of the ability of the SEM stage to rotate, tilt and translate, specimen faces can be viewed either upright (as mounted) or on one side, causing a 90° shift in the micrograph view orientation. The importance of this distinction was not fully appreciated at the time of the SEM study.

In Table 3.1, comments regarding the orientation direction are made relative to the micrograph view. A reference note (1, 2, or ?) is given in the comments for all but one of the micrograph groups relating the direction of the bedding and/or flow to the micrograph orientation². A (1) indicates that the bedding/flow direction is oriented horizontally on the micrograph, while a (2) is indicative of a vertical orientation. A (?) indicates that the orientation of the face is unknown in relation to the bedding/flow direction. In Table 3.2 the particle orientation direction is compared keeping the bedding/flow direction in mind.

¹ Bedding direction is considered to be perpendicular to the direction of the force of gravity (horizontal) for the purposes of this discussion.

² For the case of the horizontal face of the specimen created by pluviation, neither flow nor bedding can be viewed from this face orientation.

3.3.2. Quantitative Analysis

Another method was desired to determine the fabric orientation of the sand grains for comparison to the results obtained in the qualitative analysis, and this led to the use of a quantitative approach to determine this characteristic. Image analysis techniques were used to obtain orientation data that is directly comparable to the visual orientation observations, and also allows a statistical analysis to be performed. This information was used to supplement the qualitative results described previously, allowing the confidence in the visual orientation observations to be estimated.

To fully evaluate the orientation of an assemblage of particles, the required parameters include the preferred orientation direction, the degree of preferred orientation observed, and confidence that the result is not merely random. Orientation measurements, because of their angular nature, are difficult to analyze statistically in the conventional linear manner. Curray (1956) describes a procedure whereby these three results are achieved, using a circular approach. A resultant vector is determined for the circular distribution, with its direction and magnitude defining the preferred orientation direction and its degree, respectively. The generated data is also compared to a circular distribution that simulates the distribution of a random assemblage of particles. The probability that the results are not purely random is estimated, based on the number of observations made and the magnitude of the resultant vector determined for the face studied.

Other methods of orientation data analysis are available, as described in Pincus (1953), Smart (1973) and Tovey (1973). The method of analysis proposed by Curray (1956) was used successfully by Mitchell et. al. (1976) for the statistical analysis of

particle long axis orientation measurements collected for fabric determination, hence this approach was adopted for this study.

3.3.2.1. Data Collection

Eighteen selected micrographs representing the full range of deposition methods and orientations with respect to flow (if any) were analyzed using an image analysis technique. These micrographs are included in Appendix A, along with the rose diagrams (histograms) of preferred orientation associated with each micrograph as derived from the long axis orientation results. The process involved the manual tracing of individual grains using a digitizing device and its associated software (Mop Videoplan Image Analysis System, developed by Kontron Ltd.). Two variables were determined for each grain traced, including:

1. Aspect Ratio (Ratio of apparent* short to long axis length), and
2. Angle of apparent long axis with respect to the horizontal.

*Note: The term 'apparent' indicates that the variables describe only the projections of the variable visible on the face observed, and not the actual variable (i.e. longest axis) describing the grain.

The aspect ratio is estimated by the software using a moment of inertia technique. The axes lengths generated are not true apparent lengths, but represent the lengths of the axes of the generated elliptical representation of the grain. The long axis angle is the angle between the apparent long axis of the grain and horizontal as observed in the micrograph.

The selection of the 18 micrographs was made based on three factors. First, photographic quality was considered to ensure accurate grain tracing could be undertaken. Second, micrographs were chosen such that the full range of methods and orientations relative to the horizontal and flow (if any) directions was included in the group. Finally, the results of the qualitative study were used to select micrographs that may help to clarify some the ambiguities encountered in this portion of the study.

3.3.2.2. Data Analysis

Curry (1956) presents a vector method and significance test developed specifically to determine the direction, magnitude, and relevance of two-dimensional orientation data. The long axis orientation of each grain is considered to be a vector in the observed direction, with either a unit magnitude or a magnitude weighted by another factor such as the particle size or shape. In the present study, both unweighted and weighted analyses were performed with the weighting based on the aspect ratio. The weighting puts more emphasis on those particles that are 'long' (small aspect ratio) and therefore are considered more meaningfully oriented. It is noted that the orientation of a long particle is intuitively more meaningful than that of a particle that is close to being round in shape, in that its elongated shape contributes more to an anisotropic fabric (and therefore anisotropic mechanical behaviour) than an equi-dimensional particle would.

The resultant vector magnitude (L) and azimuth (θ) were determined for both the unweighted and weighted cases, giving the overall long axis orientation direction and a measure of its magnitude (or alternatively the amount of dispersion from a singular direction) for each face of the specimen examined.

No distinction is made of one end of the particle from the other; hence the observed range of azimuths is from 0° to 180° . To ensure a true measure of the orientation magnitude

and direction without dependence on the reference axis chosen, the angles measured were doubled prior to calculating the resultant vector. If the data were simply used twice by adding 180° to each of the observations, a resultant vector magnitude of zero would always be obtained because of symmetry. Performing the vector resolution on the 180° distribution would not reflect the true central tendency, and this is explained by Curray (1956) with the following example. If the 180° range lies in the eastern semicircle, the distribution has no westerly components. The northerly components would tend to cancel out the south components in such a way that the resultant vector would always have a strong easterly direction even if the true central tendency was north-south. Conversely, grains oriented at right angles to each other would produce a resultant vector direction between the two individual long axis directions, rather than cancelling out. By doubling the individual azimuth observations before computing the components and then halving the resultant azimuth, a non-symmetrical periodic distribution is obtained resulting in a true measure of the central tendency $\bar{\theta}$ and its magnitude L .

This magnitude can be likened to a measure of the dispersion of the data in conventional linear statistical analysis, but rather than being a measure of how closely the data approximates a straight line, it is a measure of how much unlike a circular (or random) distribution the data approximate. The calculations are outlined as follows:

$$\text{Horizontal component}^* = \sum n \cos 2q \quad (3.1)$$

$$\text{Vertical component}^* = \sum n \sin 2q \quad (3.2)$$

* as viewed in the micrograph

$$\tan 2\bar{\theta} = \frac{\sum n \sin 2\theta}{\sum n \cos 2\theta} \quad (3.3)$$

$$r = \sqrt{(\sum n \sin 2\theta)^2 + (\sum n \cos 2\theta)^2} \quad (3.4)$$

$$L = \frac{r}{\Sigma n} 100 \quad (3.5)$$

$$\bar{\theta} = \frac{1}{2} \tan^{-1} \frac{\Sigma n \sin 2\theta}{\Sigma n \cos 2\theta} \quad (3.6)$$

where:

θ = azimuth from 0° to 360° of each observation or group of observations,

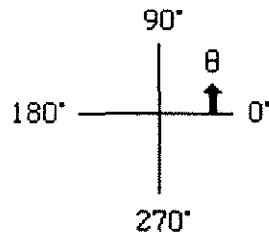
$\bar{\theta}$ = azimuth of resultant vector,

n = observation vector magnitude
($n=1$ if data is unweighted, $n=[1-\text{Aspect Ratio}]$ for the weighted case),

r = magnitude of the resultant vector, and

L = magnitude of the resultant vector in terms of percent.

The angle θ is measured as follows:



The significance of the calculated vector direction and magnitude was evaluated by determining the probability that the results are likely random or, conversely, the confidence that the results are not random. Rayleigh (1894) devised a significance test for the differentiation between random and non-random amplitude changes in the study of the combination of sound waves. Curry (1956) adapted this test for the analysis of geological orientation data and this adaptation was used directly in the present study. The following form of Rayleigh's equation was used:

$$p = e^{(-N[L/100])^2} \quad (3.7)$$

where:

p = probability of obtaining a greater magnitude from a random assemblage of particles,

N = number of observations, and

L = vector magnitude in terms of percent.

The confidence level attained is then determined using the relation:

$$\text{Confidence Level (\%)} = 100(1 - p) \quad (3.8)$$

Table 3.3 provides a summary of the quantitative analysis results. This table describes the method of deposition, the face and number of grains observed in each micrograph studied, as well as the vector direction, magnitude, and confidence level measured for both the unweighted and weighted cases. The mean aspect ratio of all 2736 grains traced is 0.65, with a standard deviation of 0.15. Rose diagrams for each micrograph constructed using the unweighted data are presented in Appendix A, giving a graphical representation of the long axis orientation for the observed face relative to that expected for a purely random assemblage of particles.

A rating system was derived giving a verbal description to the measured orientation magnitude. Based on a review of the rose diagrams generated for each micrograph (Appendix A), faces observed with vector magnitude (L) values above 30% were considered to display a very strong degree of orientation. Values of L between 18% and 30% were considered strongly oriented, while weakly oriented faces displayed L values

between 12% and 18%. A degree of orientation of 'none' was defined for those faces exhibiting L values less than 12%. These designations of preferred degree of orientation are included in Table 3.3, and are compared directly with the qualitative long axis orientation results in Table 3.4.

Rayleigh's equation (equation 3.7, expressed in terms of confidence level) is shown graphically in Figure 3.1, showing the confidence level attained by the calculated vector magnitude for the number of observations made. This graph can be used as a guideline for the rational determination of the number of observations required to achieve a specific level of confidence that the results are not random.

The graph of Figure 3.1 shows that the number of observations required depends directly on the magnitude of the resultant vector, as well as the level of confidence desired. It is evident that a group of observations with a large vector magnitude (i.e. a strong degree of orientation) requires a smaller number of observations to achieve the same level of confidence than a group of observations with a small vector magnitude. A large range of vector magnitudes were observed in this study, especially using the unweighted data where L ranged from 3.8 to 61.8%. From Figure 3.1, over 2000 observations would be required to be 95% confident that $L=3.8\%$ and its corresponding azimuth were not random occurrences, whereas less than 10 observations would be required to have the same level of confidence for $L=61.8\%$ and its corresponding azimuth. Therefore, it takes many more observations to conclude with confidence that a group of observations with a low resultant vector magnitude is representative than for a group of observations with a high resultant vector magnitude.

From the results presented in Table 3.3, micrographs that exhibit at least some degree of orientation have L values greater than 12.6% in the unweighted case

(Micrograph 61 083) and 14.9% in the weighted case (Micrograph 06 002). From Equation 3.7 (or Figure 3.1) the required N values are 189 and 135 for the unweighted and weighted cases, respectively, for the 95% confidence level. Therefore to achieve this level of differentiation among the orientations of the different faces (i.e. to ensure that these lower vector magnitudes are significant), the above N values are considered to be minimum for the respective unweighted and weighted analyses.

In five of the analyses performed for the unweighted case and in three of the analyses performed for the weighted case, the number of grains traced was not sufficient to achieve a confidence level of 95% or higher. The orientation results described as 'weak' and 'none' may therefore be suspect, and a larger number of observations would be desirable for these micrographs to determine if the results are a true representation of the orientation displayed or that of a random assemblage of particles. An iterative process is recommended for future work whereby the confidence level achieved is calculated prior to finishing the traces for each individual micrograph. If necessary, more grains could then be traced until the appropriate confidence level was attained. A minimum of 200 observations is required to achieve a confidence level of 95% when a weak orientation is to be defined ($12\% \leq L \leq 18\%$). As seen in Table 3.2, smaller N values still allow for high confidence levels to be achieved for cases where a high degree of orientation is expected.

When the vector magnitude is plotted against the aspect ratio (Figure 3.2), it is evident that for micrographs studied where a lower average width to length ratio is observed, the magnitude of the observed orientation tends to be higher.

3.4. Results

3.4.1. Qualitative Analysis Results

The results of the qualitative analysis are tabulated in Table 3.1, and comparisons were made both among the different faces within each deposition method and among similarly oriented faces across the three depositional methods (Table 3.2). Each of the nine characteristics is discussed separately with regard to an overall assessment of the characteristic for the three placement methods investigated. As well, specific comparisons of the characteristic with regard to the faces and depositional methods are discussed (as summarized in Table 3.2).

3.4.1.1. Attached Clay

Very little clay was observed in the micrographs in general, with more clay observed in field specimens than in the laboratory prepared specimens. Most of the clay observed was either attached to the sand size particles (Plate 3.1a) or acted as bridges or connectors between sand particles (Plate 3.1b). Plate 3.1a also shows solution pitting and etching that was evident on many of the sand grains. The field specimens displayed a range of observed quantities of attached clay (from virtually none to some) which in the latter case tended to obscure the contacts between a significant number of sand grains.

The comparisons made in Table 3.2 for the attached clay characteristic indicate a similar result among the faces within each deposition method, but a wide range of descriptions was evident for the same face across depositional methods. The amount of attached clay observed varies, with the most seen in field specimens and the least observed in pluviated specimens. A likely reason for the observed difference is that the source materials may be slightly different for each deposition method. This trend may be expected

because of the treatment of the sand prior to the fabric study. The flume tests were conducted with tailings sand collected from the field tests. This material was prepared prior to flume placement using a commercial drying process in which some of the fines were lost. The material to be used for the pluviated samples was then collected from the flume after test completion, oven dried and pluviated in the dry state. Some fines may have been lost in this process as well.

The amount of clay observed in the micrographs was small. One hydrometer test was run on a field sample that had significant internal cohesion upon air drying, and therefore likely had more clay bridging the sand particles together than some of the other field samples tested and therefore likely more clay than either the flume or pluviated samples tested. The sample was soaked overnight in a deflocculant solution, and vigorously shaken prior to performing the test. The results of this test indicated that no measurable amount of clay (designated as material finer than 0.002 mm in diameter) was found in the sample tested.

3.4.1.2. Silt Sizes

Particles with a minor axis length visually estimated to be between clay size (0.002 mm) and fine sand size (0.075 mm) were used in this characterization. The number of silt sized particles observed was generally small, with an increasing amount observed depending on the placement method. Silt sizes were least apparent in the pluviated specimens and most apparent in the field specimens. As for the attached clay characteristic, the successive drying and reuse of the field material for the flume and pluviation methods is the likely cause of increasingly fewer fines observed in the order field, flume and pluviation.

The number of silt sized particles observed appeared similar among the three faces observed for the pluviated and flume specimens, but a relatively large range was observed among faces of the field specimens. This is possibly due to the higher variability of the fines content of this material exhibited in the field samples, as shown in the range of grain size distributions determined for the field case (Figure 4.3, Chapter 4). A wide range of descriptions was evident among depositional methods for Faces 1 and 2 (horizontal and vertical parallel to flow, respectively), but few silt particles were observed in Face 3 (vertical perpendicular to flow), even for the field specimens. This may be because voids that are filled with silt particles in the other faces are kept open by the flow of water normal to this face.

The average fines content was determined to be generally in the range of 5 to 12% by grain size analysis, with the exception of a few of the field samples tested (up to 19%). Fines content in this thesis corresponds to the percentage of material passing the #200 sieve (0.075 mm), by weight. Some minor segregation of large and small particles was observed, for example in a flume specimen on a vertical face oriented perpendicular to the flow direction (Micrographs 42 019 and 42 020, shown in Plate 3.2).

3.4.1.3. Long Grains

In general, the difference in the observed number of 'long' grains among the specimens was small. A grain was considered long if its major axis is visually determined to be about 1.5 times as long as its minor axis. The number of long grains observed in relation to the number of grains in the micrograph was estimated and related to the other micrographs through the descriptors few, some, and many.

The pluviated specimens tended to show a more consistent ratio of long grains across the faces than the flume or field specimens. A wide range of descriptions were

determined for all specimens among the different faces. A higher ratio of long grains was found to be consistent for all placement methods for Face 2 (vertical parallel to flow).

3.4.1.4. Planarity

It was observed that in all of the pluviated specimens created, all faces displayed at least some planarity. Some of the micrographs appeared strikingly flat in comparison to most of the other micrographs taken of the flume and field specimens. As well, during specimen preparation, the pluviated samples appeared to break more easily than their flume and field counterparts and they generally broke along a curved plane whereas the flume and field samples tended to break along a flat plane.

The pluviated specimens revealed a similar amount of planarity on all faces, whereas the flume and field specimens indicated a range of planarity among the faces. A range of planarity was also observed among methods of placement for all three faces.

An expected trend was to see more planarity in the horizontal face (Face 1) than in the other two faces because of the nature of both pluviation and hydraulic deposition. It is possible that as the particle loses energy as a result of transferring it to the particles below (impact during pluviation and drag during hydraulic deposition), the particles would tend to align horizontally to mimic the particles immediately below. In the case of pluviation, this likely depends on the flow rate of the particles into the mould because a faster flow rate would tend to maintain 'long' particles in an upright position (long axis normal to the horizontal) if they were in this position during impact. This is plausible because the proximal particles are closer during pluviation with a high flow rate than with a low rate, thereby not allowing much room to align horizontally (as gravity would force it to do if the space were available).

In the hydraulic deposition case, the particles are generally deposited under a flow condition which imparts a component of horizontal force to the sand grains. Under these conditions it is likely that a particle will be oriented such that it provides the least resistance to the flow occurring directly above. This orientation is probably such that the flattest side is up with the long axis direction aligned either essentially with the flow direction or perpendicular to the flow direction, depending if the flow regime was such that the sand grains were rolling prior to final deposition.

Another factor appears to be the variability in the flow regime. The meandering nature of hydraulic deposition means some areas of the beach are aggrading while others are degrading, and the locations of these two conditions is constantly changing. Large channels of concentrated flow many metres across can also be formed in the field case, causing major changes to the depositional pattern in local areas.

Both of these scenarios (micro and macro) may occur concurrently, leaving a more or less heterogeneous orientation on the macro scale with localized areas of homogeneous orientation.

3.4.1.5. Contact Areas

The areas of contact between grains were looked at to evaluate whether long side contact was prevalent or whether point contact between grains was more common. Types of contacts fit broadly into four categories as shown in Figure 3.3, modified from Dusseault (1977). In general, a wide range of contact areas was observed, from mostly point or tangential contacts (small area) to many long side or straight contacts (medium area), with some micrographs revealing a significant number of interpenetrative contacts.

The pluviated specimens again seemed to be the most consistent, with an approximately equal number of small and medium contact areas for all faces investigated. The full range of descriptors were determined for both the flume and field specimens across all faces. A large range of observed descriptions is also found when comparing similarly oriented faces among the depositional methods.

3.4.1.6. Degree of Interlock

The degree of interlock observed in all specimens was low, but lowest overall in the field specimens. Some localized areas of some of the micrographs showed a high degree of interlock. A remark of 'high' in Table 3.1 or 3.2 is taken to mean relative to the other micrographs observed, and is certainly low when compared to the degree of interlocking observed in the in-situ oilsands as reported by Dusseault (1977).

3.4.1.7. Packing

The degree of packing observed (as used in this study) is differentiated from the void ratio or density of the sand mass because it is a two-dimensional observation. This allows differences among the faces to be assessed, allowing an anisotropic effect (if it exists) to be visually determined using this technique. In making this observation, only the sand size grains (larger than 0.075 mm) were considered, therefore voids filled with finer material were not considered to add to the packed nature of the mass. In general, the pluviated specimens appeared to be more tightly packed than their flume and field counterparts. This characteristic, however, is very dependent on the level of disturbance that occurs during specimen preparation and viewing. Some disturbance inevitably would have occurred during this process therefore less emphasis should be placed on this characteristic.

Comparisons of the faces within each depositional method (Table 3.2) reveal that the packing was similar among the faces within each method of placement. All faces of the flume specimens exhibited a wide range of packing (loose in some areas, dense in others), whereas field specimens were generally loosely packed and pluviated specimens were normally more tightly packed.

In the comparison among depositional methods, each face displayed a wide range of descriptors except Face 3 (vertical perpendicular to flow), where generally looser packing was observed for the flume and field specimens. This result may be expected because the face perpendicular to flow would likely reveal a lower degree of packing, perhaps reflecting water flow in this direction during and after deposition is complete.

3.4.1.8. Void Size and Homogeneity

This characteristic is similar to the packing category previously outlined, except that it describes the void sizes observed and their distribution, rather than describing the particles themselves. This characteristic is also related to the void ratio but attempts to display a fabric anisotropy not revealed by the void ratio measurement. The specimens created using pluviation appeared different from the flume and field specimens by exhibiting generally small voids throughout, as would be expected with a generally tighter packing arrangement.

The comparisons among faces revealed a wide range of void size and homogeneity displayed within each of the flume and field specimen groups. These ranged from all small voids, through a mixture of small and large voids, to all larger voids. This was in contrast to the pluviated case, which yielded small voids for each face investigated. The comparisons revealed a wide range of descriptors for each face across the depositional

methods, but the field specimens were more consistently made up of a heterogeneous matrix of both small and large voids for Face 3 (vertical perpendicular to flow).

The above result for the field case may be expected for the same reasons outlined above in the packing category. Only one specimen revealed a consistently small void size for Face 3 from the flume deposition group, hence this single variance from the expected behaviour could be due to the observed meandering within the flume during all of the tests. As this aberration may be explained by a sample taken in a location of severe meandering (i.e. greater than 45° from the average flume direction), it is considered that the general trend of both looser packing and variable void sizes in the plane perpendicular to flow is confirmed for both the flume and field specimens.

3.4.1.9. Orientation

The observed orientation of the particles was divided into two categories; direction and magnitude. The results for each group of micrographs viewed (as displayed in Table 3.1) indicate a wide variety of observed orientation magnitudes from none to strong, but generally an orientation coincident with the flow and/or bedding direction was noted.

The pluviated specimens displayed no preferred grain orientation direction except in one vertical face observation, where it was found to strongly coincide with the bedding direction. The field specimens generally displayed a particle orientation direction coincident with the flow and/or bedding direction, if any was observed at all. As explained previously, the majority of the flume specimen face orientations with respect to the flow and/or bedding directions are unknown. However, a consistently strong degree of orientation was observed in the flume specimens where the faces were oriented perpendicular to the flow of water.

It was expected that the faces oriented horizontal and vertical (parallel to flow) on the flume and field specimens would reveal an orientation direction that would reflect the depositional flow regime. It is not clear, however, whether the orientation of the long axes should be similar to that of the direction of flow or perpendicular to it. Feda (1982) suggests that two basic factors affect the orientation of particles: the direction of pressure or force (in this case gravity and water flow), and the direction of motion (shear forces imparted by the water flow). As Feda explains, the first factor causes the plane of maximum stability (defined as the plane perpendicular to the smallest dimension of the particle) to orient itself perpendicular to the resultant of the pressures. The second makes the particle rotate such that its long axis is parallel to the direction of motion. Which process governs the actual particle orientation after placement is likely dependent at least upon the flow regime (including flow rate and sedimentation load), particle size and shape, and particle roughness. Because of the complicated flow regimes in which the flume and field specimens were prepared, both factors may act concurrently to create a complex orientation fabric. The pluviated specimens are expected to exhibit a preferred horizontal orientation on vertical faces due to the first factor described by Feda (1982) above (gravitational forces). An essentially random distribution of long axis orientation may be expected on the horizontal faces of specimens created by pluviation.

In general, a trend of long axis orientation coincident with the flow and/or bedding direction is supported by the qualitative orientation results. However, this trend is not consistently visible on all faces and with all methods of deposition. The flume specimens showed the most consistently strong particle orientation.

Variability in the orientation direction results may be expected. In the case of field sampling, orientation of flow was determined from a visual examination of surface channel and meander patterns prior to sampling. Below the surface the sand grains may have been

deposited with a flow direction substantially different from that observed at the surface due to the meandering nature of the flow. This rationale also applies to the flume case, although direction of flow due to meandering did not vary as much as for the field case because of the confined flow conditions.

3.4.1.10. Conclusions

The results of the comparisons indicate that, for all of the characteristics investigated except the degree of interlock, similar descriptions were evident for the pluviated specimens regardless of the face investigated. Flume specimens gave similar descriptions among faces for the attached clay visible, the quantity of silt sizes evident, and the degree of packing observed, whereas all other characteristics displayed a wide range of descriptions among faces. The field specimens were slightly more varied than the flume specimens across faces, yielding similar descriptions for only the attached clay, the degree of interlock, and the orientation direction observed. It is likely that the less variable conditions inherent to the pluviation deposition method is the major reason that the results are less varied for these specimens when compared to the flume and field specimens. As well, the grain size distribution of the flume and field material is considerably more variable than that of the pluviated material, as referred to previously in Figure 4.3, Chapter 4.

Comparing like faces among the depositional methods, all characteristics except the particle orientation direction were relatively different from one another. Also, no fabric orientation was visible for the horizontal face of the pluviated specimen studied while a trend to orientation with the flow direction was observed in the field specimens for this face. Conversely, the vertical faces exhibited similar orientations (generally either no orientation or coincident with the flow/bedding direction) for the pluviated and field cases.

From this limited study it is concluded that, in general, the overall fabric of the pluviated specimens is similar regardless of the direction of pluviation except for the orientation fabric, where it may be preferentially horizontally oriented when pluviation is vertical (due to gravity). For flume and field deposition, the overall fabric generally appears to vary substantially depending on the flow and/or bedding direction operative during placement except for the orientation direction characteristic, which tends to be coincident with these directions. It is therefore concluded that any differences in mechanical behaviour observed during the testing program (discussed in Chapter 4) would likely be due to any or all of the first eight characteristics outlined above. The orientation fabric differences observed are likely not pervasive enough to impact the mechanical behaviour of this material.

3.4.2. Quantitative Analysis Results

3.4.2.1. Vector Magnitude and Direction

The results of this analysis are tabulated in Table 3.3 for the pluviated, flume and field specimen micrographs selected for examination. For the purposes of this study, an orientation measurement was determined to be very strong when the vector magnitude was greater than about 30%, strong if between 18% and 30%, weak if between 12% and 18%, and non-existent if less than about 12%. These descriptive terms were used to allow the comparison of orientation results between the qualitative and quantitative approaches. The 'weak' and 'none' orientation results are considered to be suspect because of the low confidence levels associated with these vector magnitudes, as discussed earlier. The results of the quantitative analysis of the weakly oriented specimens were therefore used only to complement the results of the orientation characteristic analysis described previously.

Rose diagrams for each micrograph analyzed are presented in Appendix A below its respective micrograph and were used to help categorize the degree of orientation apparent in the selected micrographs. The rose diagrams are essentially histograms, but display the data in a circular form with the dashed circle representing a distribution with the same number of observations in each class interval (i.e. isotropic in the observed plane). Used in conjunction with the calculated vector magnitude and confidence level, this method of data presentation was found to enhance the understanding of the variability of the orientation results.

The vector directions, magnitudes and confidence levels were determined using unweighted and weighted analyses (based on the aspect ratio), as explained previously in Section 3.3.2.2. The weighted data reveal a slightly higher vector magnitude for all but one micrograph studied, indicating that the 'long' particles were more likely to be preferentially aligned than the shorter particles. This result did not affect the overall conclusions, however, because of the generally small difference in the vector directions and magnitudes calculated using the two methods. The unweighted data was used for comparative purposes in Table 3.4, and for preparation of the rose diagrams.

Similar particle orientation direction was determined in twelve of the eighteen micrographs analyzed using both the methods of analysis while eleven of the eighteen revealed similar orientation magnitudes between the methods. This match is shown in Table 3.4 and assumes a match when the directions are within approximately $\pm 10^\circ$ and the magnitudes are similar (i.e. none \approx weak and strong \approx very strong). In five of the six cases where no orientation direction match was found between analyses, an insignificant (weak to none) orientation magnitude was determined in the visual examination but a strong to very strong magnitude was revealed using the image analysis technique. It is possible that

the image analysis techniques can identify preferential grain orientation direction that is not evident upon visual examination.

The vector directions as measured using the image analysis techniques did not match the flow and/or bedding directions in the field case as consistently as for the qualitative analysis. As well, the vector magnitudes determined using the quantitative method revealed that the field specimens gave generally lower values than the flume specimens, indicating a weaker field particle orientation preference. These two factors may be due to the higher fine content observed in the micrographs of the field specimens which allowed for poorer resolution of the actual outline of the sand grains.

The pluviated specimens gave vector magnitudes within the range of the magnitudes found for the flume and field specimens. This indicates that the magnitude of orientation created by the pluviation method is not significantly different from that of the hydraulically placed specimens.

3.4.2.2. Mean Aspect Ratio

The mean aspect ratio for each micrograph analyzed was determined, along with its standard deviation (Table 3.3). Relatively consistent results were determined for all faces and methods of placement, with a range of mean values from 0.60 to 0.69. The calculated coefficient of variation ranged from 20% to 27%, and an essentially normal distribution of aspect ratio values was determined. A weak correlation exists between the aspect ratio and the vector magnitude, as shown in Figure 3.2. The higher the mean aspect ratio (i.e. the greater percentage of particles with higher short to long axis ratios on a particular face), the lower the vector magnitude recorded for that face.

Two reasons for the observed trend in Figure 3.2 are possible. First, an assemblage of particles exhibiting a low mean aspect ratio (more elongate particles) has the ability to produce a higher magnitude of orientation than an assemblage with a high aspect ratio (more round shaped particles) because more particles are of a shape where, due to external forces acting during placement, the grains may be oriented in a preferred direction rather than randomly. A higher magnitude of orientation may not necessarily occur with a low mean aspect ratio, however, as the vector magnitude is dependent on the effectiveness of the placement method to produce a preferred orientation. As observed previously, the range of mean aspect ratio values calculated is relatively small. This is to be expected within this specific material type because the grain size is uniform.

Secondly, the method of placement may create faces in which more particles are oriented in such a manner as to display the 'long' sides of the particles, whereas other faces may display the particles from an end perspective. This would give the result of some faces with low average aspect ratios and others with high average aspect ratios. No correlation of the aspect ratio with face or method of placement was observed, however, indicating that the relatively small range of differences in aspect ratio observed may be due to material differences between specimens alone, and not due to the placement method or the relation of the face with respect to the direction of flow of water through the specimen prior to sampling.

The pluviated results again gave the most consistent mean aspect ratio values, both within the same sample across the faces examined, and between samples from which the specimens were obtained. A range of mean aspect ratio values between 0.66 and 0.67 were obtained, with a range of variation coefficients of 20% to 24%. This again is most likely attributable to the greater degree of control on the material and the placement conditions used to create specimens than those of the flume and field cases.

It is considered that 200 observations is a sufficient number to assure a meaningful orientation result (95% Confidence Level or greater) using quantitative methods, if the vector magnitude of the orientation observed is greater than about 12%. Fewer numbers of observations may still be statistically meaningful in cases where the measured vector magnitude is high, but large numbers of grains are needed for analysis when the vector magnitude is low. When weighted data based on the aspect ratio are utilized, higher vector magnitudes are expected.

3.5. Summary of Fabric Analysis Results

No definitive fabric characteristic was found to be generated by one or more of the placement techniques used in this study. In general, the characteristics tended to overlap among the placement methods and among the faces examined, leaving no clear definition of the fabric associated with a particular method of placement. The pluviated specimens tended to be more uniform than their flume and field counterparts as indicated by most of the characteristics investigated. This is thought to be a result of the controlled placement conditions inherent in the pluviation method, and a result of having the least variable grain size among the placement methods. The aspect ratio results also revealed more uniform specimens for the pluviation method of placement, but did not reveal a significant difference in the ratio of short to long axis length due to method of placement or in relation to the direction of water flow during placement, if any.

The qualitative orientation results were generally confirmed by the quantitative analysis performed using image analysis techniques. It is noted that the quantitative orientation results would have been enhanced if more grains had been analyzed in some cases. An iterative process would be useful when obtaining orientation data to ensure the

number of grains analyzed is adequate to confidently describe the orientation and magnitude of the preferred grain direction prior to completing the analysis.

In summary, conclusive evidence was not found to unequivocally distinguish differences in the fabric characteristics studied herein among the methods of placement, nor among the studied face orientations in relation to the direction of pluviation or water flow during hydraulic deposition. Specifically, pluviated specimens were not found to have particles oriented in a significantly different manner either visually or statistically from their flume and field counterparts. As well, the magnitude of the measured particle orientation for the pluviated case was not significantly different from the flume and field cases. In the following chapter an attempt is made to determine if a difference exists due to the variations in the fabric characteristics caused by these and other placement methods, based on the mechanical behaviour observed in undrained triaxial tests.

PLUVIATED		Attached Clay	Silt Sizes	Long Grains	Planarity	Contact Areas	Degree of Interlock	Packing	Void Size and Homogeneity	Orientation*
FACE										
Group/Micrograph # Sample										
HORIZONTAL										
P5 32 (B8 to B12) FM 12 C2	none	very few	some	small/ medium	low	medium to dense	small	none		
VERTICAL										
P4 31 (B1 to B7) FM 13	very little	few	many	small/ some med.	medium	medium to dense	small	none (1)		
P6 33 (B13 to B16) FM 12 C2	none	very few	some	small/ some med.	high	medium	small	horizontal (1) (strong)		

* As viewed on micrograph. Number denotes direction of bedding and/or flow (as viewed on micrograph) as follows:
 (1) 0° or 180°
 (2) 90°
 (?) Unknown

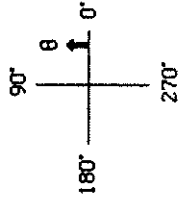


TABLE 3.1: SUMMARY OF QUALITATIVE ANALYSIS (1 of 4)

FLUME FACE	Attached Clay	Silt Sizes	Long Grains	Planarity	Contact Areas	Degree of Interlock	Packing	Void Size and Homogeneity	Orientation*
Group/Micrograph # Sample									
HORIZONTAL									
L3 13 (A37 to A39) TS 36 2-3	very little	some	many	none	medium	high	dense	small	diagonal down to right (?) (strong)
L3 13 (A40 to A44) TS 36 2-3	very little	few	many	none	medium	high	dense	small	none (?)
L11 46 (B35 to B37) TS 34	very little	few	few	some	small	medium	loose	small/ some large	diagonal down to right (2) (weak)
VERTICAL (0° to Flow)									
L5 41 (B17 to B18) TS 33 6-7	very little	few	some	none	small/ some med.	medium	medium to dense	small	horizontal (?) (strong)
L9 44 (B29 to B30) TS 34	very little	few	some	none	small/ some med.	low	loose	large	none (?)
VERTICAL (90° to Flow)									
L6 42 (B19 to B24) TS 33 6-7	very little	few	some	none	small/ some med.	low	loose to medium	small/large	diagonal down to left (?) (strong)
L8 43 (B25 to B28) TS 34	very little	few	some	none	medium	medium	medium	small/large	horizontal (?) arching (strong)
L10 45 (B31 to B34) TS 34	very little	few	many	some	medium	medium	loose	small	diagonal up to right (1) (strong)
VERTICAL (? to Flow)									
L3 13 (A48 to A52) TS 36 2-3	very little	very few	some	none	medium	medium	dense	small	out of plane (?)
VERTICAL (?+90° to Flow)									
L3 13 (A53 to A56) TS 36 2-3	very little	very few	some	none	medium	high	dense	small	horizontal (?) (strong)

* See first page of table for notes

TABLE 3.1: SUMMARY OF QUALITATIVE ANALYSIS

(2 of 4)

FIELD	Attached Clay	Silt Sizes	Long Grains	Planarity	Contact Areas	Degree of Interlock	Packing	Void Size and Homogeneity	Orientation*
FACE									
Group/Micrograph # Sample									
HORIZONTAL									
F2 63 (B89 to B93) T1 SG 6	very little	few	some	some	small	low	loose	small/large	not obvious (2) out of plane?
F4 (A33-36 and B102-104) T4 SG 9	some	some	some	remarkable	small/ medium	low	medium	small/ large filled	none (2)
F6 64 (B94 to B97) T4 SG 22	very little	few	some	none	small	low	loose to medium	small/large	none (2)
F8 51 (B38 to B41) T1 SG 27	very little	very few	few	some	small/ some med.	medium	medium	small/large	not obvious (2) horizontal?
F9 52 (B42 to B45) T2 SG 3	some	some	some	none	small	low	loose	small/large	horizontal (1) (weak)
F10 60 (B75 to B79) T2 SG 3	some	some	some	some	small	low	medium	small/large	none (1)
F11 57 (B62 to B66) T1 SG 27	very little	very few	some	none	small/ some med.	low	medium	large	slightly down to right (2) (strong)
F12 58 (B67 to B71) T1 SG 27	very little	very few	few	none	small/ some med.	low	medium	small/large	horizontal (1) (strong)

* See first page of table for notes

TABLE 3.1: SUMMARY OF QUALITATIVE ANALYSIS

(3 of 4)

FIELD	Attached Clay	Silt Sizes	Long Grains	Planarity	Contact Areas	Degree of Interlock	Packing	Void Size and Homogeneity	Orientation*
FACE									
Group/Micrograph # Sample									
VERTICAL (0° to Flow)									
F2 62 (B85 to B88) T1 SG 6	very little	few	some	none	small	low	loose to medium	small/large	not obvious (2) (down to left?)
F4 (A29 to A30) T4 SG 9	some	some	many	some	small/ some med.	low	loose to medium	small/large	not obvious (2) vertical?
F6 65 (B98 to B101) T4 SG 22	some	few	some	none	small/ medium	low	loose	small/large	vertical or down right (2) (weak)
F8 55 (B53 to B56) T1 SG 27	some	few	some	none	small	low	medium	small	slightly down to right (?) (strong)
F9 54 (B50 to B52) T2 SG 3	some	few	some	none	small/ some med.	medium	dense	small/ some large	not obvious (1) horizontal?
F10 56 (B57 to B61) T2 SG 3	some	some	many	some	small/ some med.	low	loose to medium	small/large	not obvious (1) horizontal?
F12 59 (B72 to B74) T1 SG 27	very little	very few	some	some	small	low	medium	small/large	none (1)
VERTICAL (90° to Flow)									
F2 05 (A7 to A18) T1 SG 6	some	few	some	none	medium	high (localized)	medium	small/large	none (2)
F4 (A4-6 and A19-22) T4 SG 9	some	few	few	none	small	medium	medium	small/ large filled	not obvious (1) horizontal?
F6 (A1-3 and A23-28) T4 SG 22	some	few	some	none	small	low	loose	small/large	not obvious (1) (into plane, vert.)
F9 53 (B46 to B49) T2 SG 3	some	few	some	none	small/ few med.	low	loose	small/large	horizontal (1) (strong)
F10 61 (B80 to B84) T2 SG 3	very little	few	some	none	small	low	medium	small/large	none (2)

* See first page of table for notes

TABLE 3.1: SUMMARY OF QUALITATIVE ANALYSIS

CHARACTER-ISTIC	COMPARISONS AMONG FACES Same Depositional Method				COMPARISONS AMONG DEPOSITIONAL METHODS Same Face				
	METHOD OF PLACEMENT	FACE	REMARKS	CONCLUSIONS	METHOD OF PLACEMENT	FACE	REMARKS	CONCLUSIONS	
	1. Attached Clay	Pluviated	1 2/3	none none to very little	similar	Pluviated Flume Field	1	none very little very little to some	wide range
2. Silt Sizes	Flume	1	very little	same	Pluviated Flume Field	2	none to very little very little	wide range	
		2	very little						
		3	very little						
	Field	1	very little to some	range	Pluviated Flume Field	3	none to very little very little some	wide range	
		2	some						
		3	some						
	3. Long Grains	Pluviated	1	very few	similar	Pluviated Flume Field	1	very few few to some	wide range
			2/3	few to very few					
			3	few					
Flume		1	few to some	similar	Pluviated Flume Field	2	few to very few few	wide range	
		2	few						
		3	few						
Field		1	very few to some	wide range	Pluviated Flume Field	3	few to very few few	similar	
		2	few to some						
		3	few						
3. Long Grains	Pluviated	1	some	similar	Pluviated Flume Field	1	some few to many	wide range	
		2/3	some to many						
		3	some						
	Flume	1	few to many	wide range	Pluviated Flume Field	2	some to many some	similar	
		2	some						
		3	some to many						
	Field	1	few to some	wide range	Pluviated Flume Field	3	some to many some to many some to many	wide range	
		2	some to many						
		3	few to some						

Faces: 1. Horizontal 2. Vertical (0° to Flow) 3. Vertical (90° to Flow)

TABLE 3.2: COMPARISON OF QUALITATIVE ANALYSES

CHARACTER-ISTIC	COMPARISONS AMONG FACES Same Depositional Method			COMPARISONS AMONG DEPOSITIONAL METHODS Same Face				
	METHOD OF PLACEMENT	FACE	REMARKS	CONCLUSIONS	FACE	METHOD OF PLACEMENT	REMARKS	CONCLUSIONS
4. Planarity	Pluviated	1	some	same	1	Pluviated	some	range
		2/3	some			Flume	none to some	
						Field	none to some	
	Flume	1	none to some	range	2	Pluviated	some	range
		2	none			Flume	none	
		3	none to some			Field	none to some	
	Field	1	none to some	range	3	Pluviated	some	range
		2	none to some			Flume	none to some	
		3	none			Field	none	
5. Contact Areas	Pluviated	1	small/medium	similar	1	Pluviated	small/medium	wide range
		2/3	small/some medium			Flume	small to medium	
						Field	small to small/med.	
	Flume	1	small to medium	wide range	2	Pluviated	small/some medium	range
		2	small/some medium			Flume	small/some medium	
		3	small/some medium to medium			Field	small to small/med.	
	Field	1	small to small/med.	wide range	3	Pluviated	small/some medium	wide range
		2	small to small/med.			Flume	small/some medium to medium	
		3	small to medium			Field	small to medium	

Faces: 1. Horizontal 2. Vertical (0° to Flow) 3. Vertical (90° to Flow)

(2 of 4)

TABLE 3.2: COMPARISON OF QUALITATIVE ANALYSES

CHARACTER-ISTIC	COMPARISONS AMONG FACES Same Depositional Method			COMPARISONS AMONG DEPOSITIONAL METHODS Same Face			
	METHOD OF PLACEMENT	FACE	REMARKS	CONCLUSIONS/FACE	METHOD OF PLACEMENT	REMARKS	CONCLUSIONS
6. Degree of Interlock	Pluviated	1	low	wide range	1	Pluviated	low
		2/3	medium to high			Flume	medium to high
						Field	low
	Flume	1	medium to high	wide range	2	Pluviated	medium to high
		2	low to medium			Flume	low to medium
		3	medium			Field	low
	Field	1	low	similar	3	Pluviated	medium to high
		2	low			Flume	medium
		3	low to medium			Field	low to medium
7. Packing	Pluviated	1	medium to dense	similar	1	Pluviated	medium to dense
		2/3	medium to dense			Flume	loose to dense
						Field	loose to medium
	Flume	1	loose to dense	similar	2	Pluviated	medium to dense
		2	loose to dense			Flume	loose to dense
		3	loose to medium			Field	loose to medium
	Field	1	loose to medium	similar	3	Pluviated	medium to dense
		2	loose to medium			Flume	loose to medium
		3	loose to medium			Field	loose to medium

Faces: 1. Horizontal 2. Vertical (0° to Flow) 3. Vertical (90° to Flow)

TABLE 3.2: COMPARISON OF QUALITATIVE ANALYSES

(3 of 4)

CHARACTER-ISTIC	COMPARISONS AMONG FACES Same Depositional Method			COMPARISONS AMONG DEPOSITIONAL METHODS Same Face					
	METHOD OF PLACEMENT	FACE	REMARKS	CONCLUSIONS	FACE	METHOD OF PLACEMENT	REMARKS	CONCLUSIONS	
8. Void Size and Homogeneity	Pluviated	1	small	same	1	Pluviated	small	wide range	
		2/3	small			Flume	small to small/some large		
						Field	small/large to large		
	Flume	1	small to small/some large	wide range	2	Pluviated	small	wide range	
		2	small to large			Flume	small to large		
		3	small to small/large			Field	small to small/large		
		1	small/large to large			Pluviated	small		wide range
		2	small to small/large			Flume	small to small/large		
		3	small/large			Field	small/large		
	9. Orientation Direction	Pluviated	1	none	with bedding direction when orientation observed	1	Pluviated	none	range
			2/3	none to with bedding direction			Flume*	none to diagonal/down right (across flow)	
							Field	none to with flow direction	
Flume*		1	none to diagonal/down right (across flow)	-	2	Pluviated	none to with bedding direction	similar	
		2	-			Flume*	-		
		3	-			Field	none to with flow/bedding direction		
Field		1	none to with flow direction	generally with flow/bedding direction when orientation observed	3	Pluviated	none to with bedding direction	similar	
		2	none to with flow/bedding direction			Flume*	-		
		3	none to with bedding direction			Field	none to with bedding direction		

* Many orientations unknown with respect to flow/bedding directions; see Table 3.1
 Faces: 1. Horizontal 2. Vertical (0° to Flow) 3. Vertical (90° to Flow)

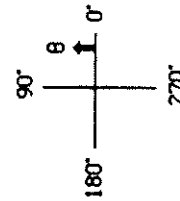
TABLE 3.2: COMPARISON OF QUALITATIVE ANALYSES

METHOD OF PLACEMENT (Sample)	MICRO-GRAPH (#)	FACE COUNT (N)	ASPECT RATIO		UNWEIGHTED			WEIGHTED*			DEGREE OF ORIENT.
			MEAN	S.D.	VECTOR DIR'N (°)	VECTOR MAGNITUDE L (%)	CONFIDENCE LEVEL (%)	VECTOR DIR'N (°)	VECTOR MAGNITUDE L (%)	CONFIDENCE LEVEL (%)	
PLUVIATED (FM12 C2)	32 011	1	0.669	0.160	170.5	13.7	90.5	178.0	16.2	96.2	WEAK
	33 014	4	0.664	0.150	177.5	20.7	99.9	174.7	25.3	100.0	STRONG
	33 016	4	0.665	0.134	8.5	34.5	100.0	7.2	41.6	100.0	V. STRONG
FLUME (TS36 2/3)	13 038	1	0.670	0.150	169.8	32.1	100.0	167.8	34.0	100.0	V. STRONG
	13 050	5	0.603	0.147	166.7	61.8	100.0	167.6	65.6	100.0	V. STRONG
	13 054	6	0.622	0.151	166.8	59.8	100.0	168.0	63.9	100.0	V. STRONG
FLUME (TS34)	46 037	1	0.669	0.151	173.5	40.5	100.0	172.6	48.3	100.0	V. STRONG
	44 030	2	0.690	0.156	24.6	3.8	25.6	20.2	7.8	70.9	NONE
	45 033	3	0.631	0.162	7.7	54.0	100.0	8.8	61.4	100.0	V. STRONG
FIELD (T2 SG3)	60 078	1	0.666	0.167	5.4	18.5	99.0	6.7	21.6	99.8	STRONG
	56 061	2	0.596	0.140	177.4	51.7	100.0	177.5	58.9	100.0	V. STRONG
	61 083	3	0.653	0.155	8.3	12.6	86.7	6.4	17.8	98.2	WEAK
FIELD (T1 SG6)	63 092	1	0.634	0.149	17.3	19.1	99.7	14.3	23.7	100.0	STRONG
	62 086	2	0.660	0.140	35.0	5.2	38.2	136.2	10.1	83.0	NONE
	05 008	3	0.613	0.167	7.1	41.8	100.0	8.7	49.8	100.0	V. STRONG
FIELD (T4 SG22)	64 095	1	0.690	0.139	14.2	22.3	99.7	15.4	27.2	100.0	STRONG
	65 101	2	0.676	0.136	147.8	15.9	93.3	137.6	15.8	93.0	WEAK
	06 002	3	0.666	0.150	158.3	14.3	95.4	161.6	14.9	96.4	WEAK

DEGREE	L (%)
NONE	less than 12
WEAK	12 to 18
STRONG	18 to 30
V. STRONG	above 30

- Faces: 1. Horizontal
 2. Vertical (0° to Flow)
 3. Vertical (90° to Flow)

4. Vertical (No Flow)
 5. Vertical (° to Flow)
 6. Vertical (7+90° to Flow)



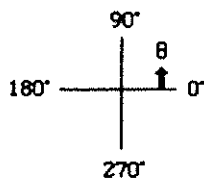
* Weighted based on the aspect ratio (ratio of short to long apparent axes lengths).

TABLE 3.3: SUMMARY OF QUANTITATIVE ANALYSES

METHOD OF PLACEMENT (Sample)	MICRO-GRAPH# [Face**]	DIRECTION OF FLOW and/or BEDDING*	LONG AXIS ORIENTATION		MATCH	
			OBSERVED* (QUALITATIVE)	MEASURED* (QUANTITATIVE)	Dir'n	Mag.
PLUVIATED (FM12 C2)	32 011 [1]	-	none	171° (WEAK)	yes	yes
	33 014 [4]	0° or 180° (bedding)	horizontal (strong)	178° (STRONG)	yes	yes
	33 016 [4]	0° or 180° (bedding)	horizontal (strong)	9° (V. STRONG)	yes	yes
FLUME (TS36 2/3)	13 038 [1]	?	diagonal down to right (strong)	170° (V. STRONG)	yes	yes
	13 050 [5]	?	out of plane	167° (V. STRONG)	no	no
	13 054 [6]	?	horizontal (strong)	167° (V. STRONG)	no	yes
FLUME (TS34)	46 037 [1]	90° (flow)	diagonal down to right (weak)	174° (V. STRONG)	yes	no
	44 030 [2]	?	none	25° (NONE)	yes	yes
	45 033 [3]	0° or 180° (bedding)	diagonal up to right (strong)	8° (V. STRONG)	yes	yes
FIELD (T2 SG3)	60 078 [1]	0° or 180° (flow)	none	5° (STRONG)	no	no
	56 061 [2]	0° or 180° (flow and bedding)	not obvious (horizontal?)	177° (V. STRONG)	yes	no
	61 083 [3]	90° (bedding)	none	8° (WEAK)	yes	yes
FIELD (T1 SG6)	63 092 [1]	90° (flow)	not obvious (out of plane?)	17° (STRONG)	no	no
	62 086 [2]	90° (flow and bedding)	not obvious (down to left?)	35° (NONE)	yes	yes
	05 008 [3]	90° (bedding)	none	7° (V. STRONG)	no	no
FIELD (T4 SG22)	64 095 [1]	90° (flow)	none	14° (STRONG)	no	no
	65 101 [2]	90° (flow and bedding)	vertical or down right (weak)	148° (WEAK)	yes	yes
	06 002 [3]	0° or 180° (bedding)	not obvious (into plane, vertical?)	158° (WEAK)	yes	yes

* as viewed on micrograph

** as defined in Table 3.3



QUANTITATIVE ORIENTATION MAGNITUDE

DEGREE	L (%)
NONE	less than 12
WEAK	12 to 18
STRONG	18 to 30
V. STRONG	above 30

TABLE 3.4: COMPARISON OF ORIENTATION RESULTS

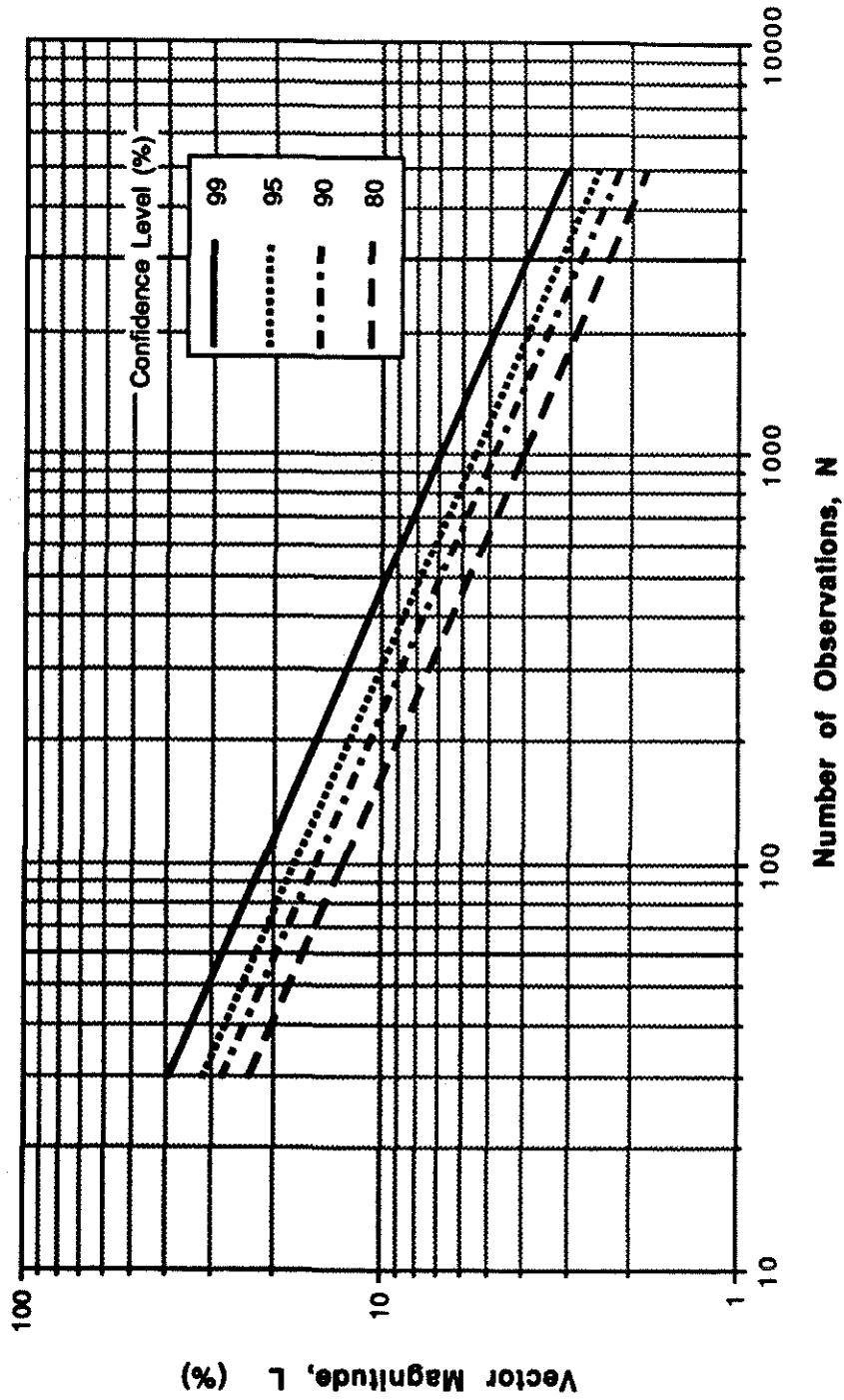


FIGURE 3.1: Confidence Level Using the Rayleigh Test of Significance
(Modified after Curray, 1956)

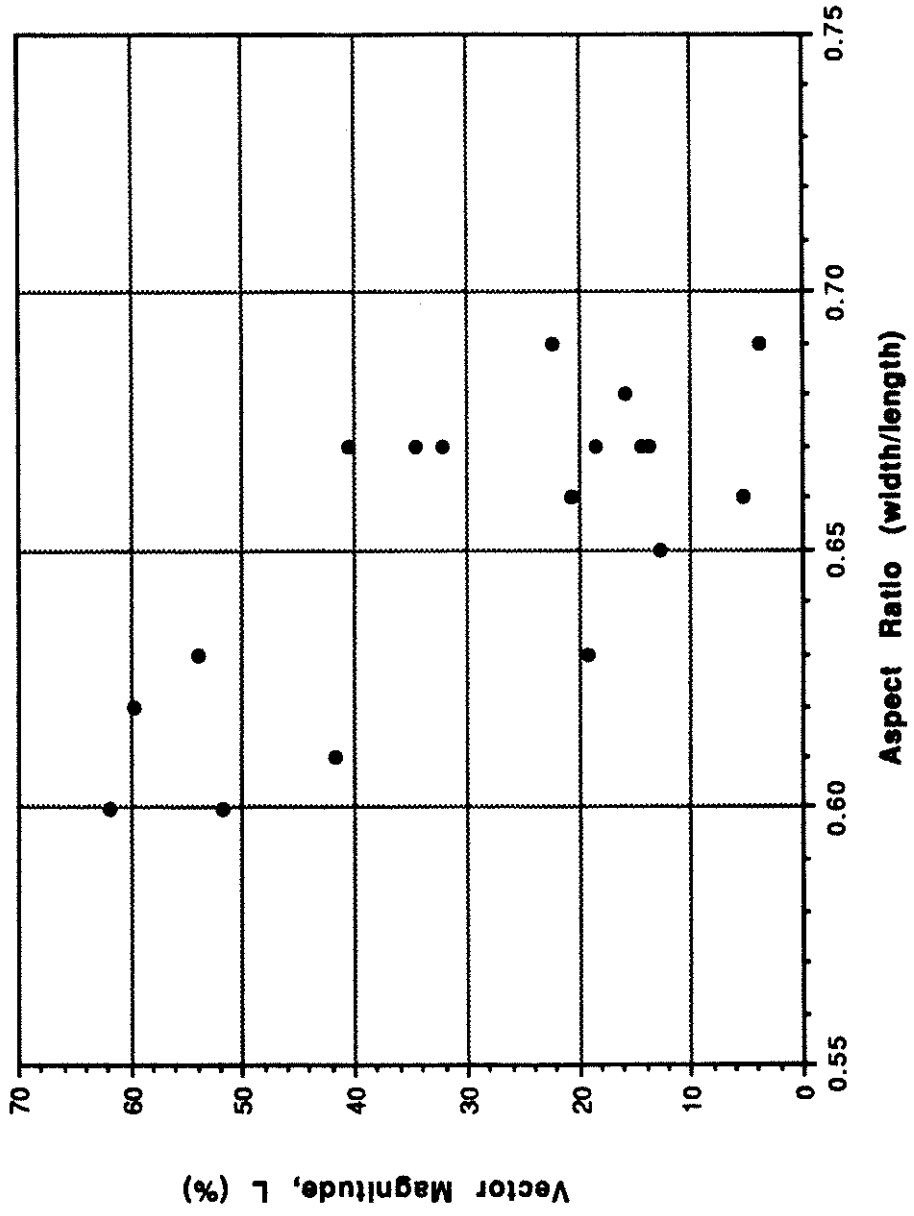


FIGURE 3.2: Vector Magnitude vs Aspect Ratio

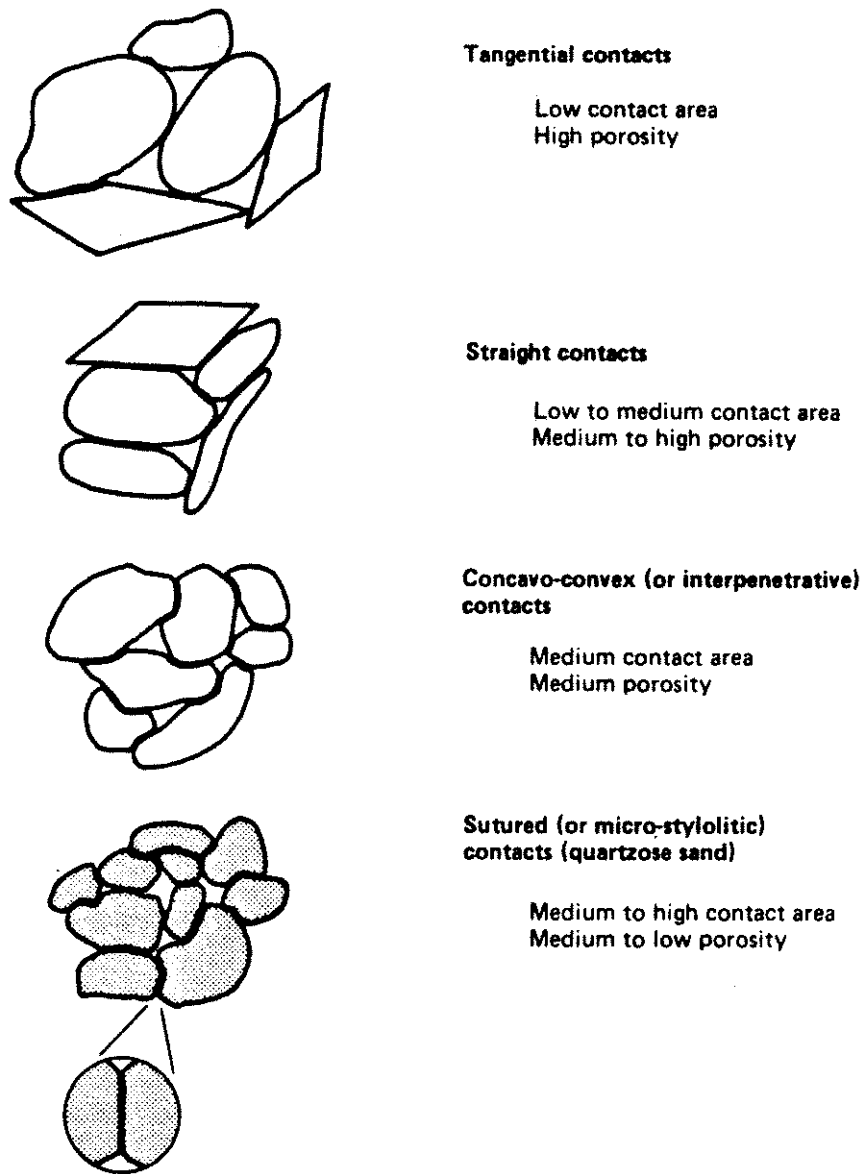


FIGURE 3.3: Intergranular Fabric Classification
 (Modified after Dusseault, 1977)

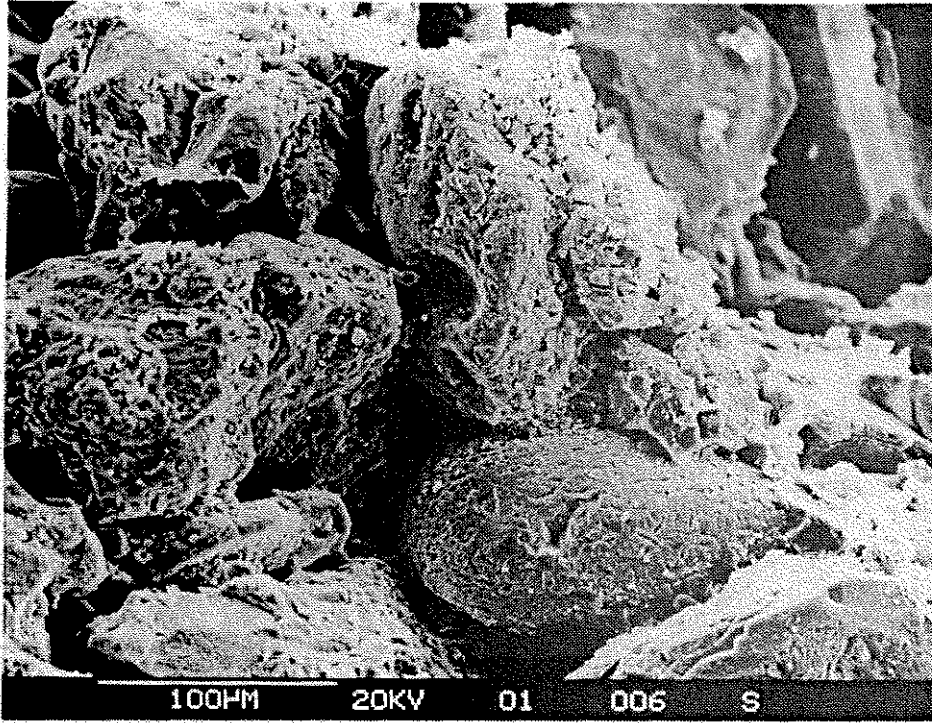


PLATE 3.1: Micrograph Showing Attached Clay,
Solution Pitting and Etching (Field)

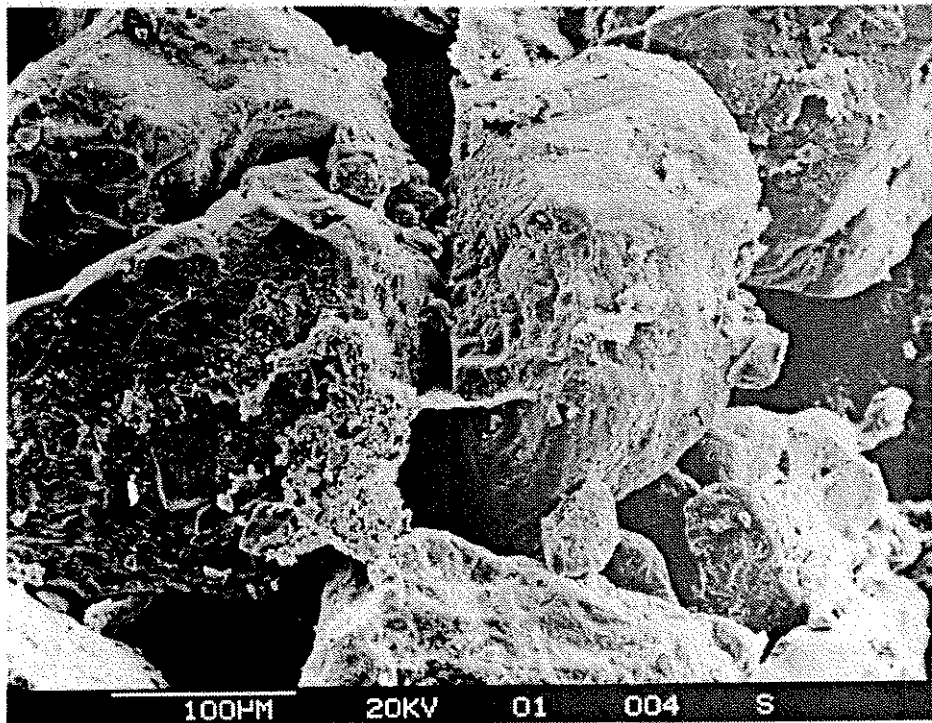


PLATE 3.2: Micrograph Showing Clay Bridge
Between Sand Grains (Field)

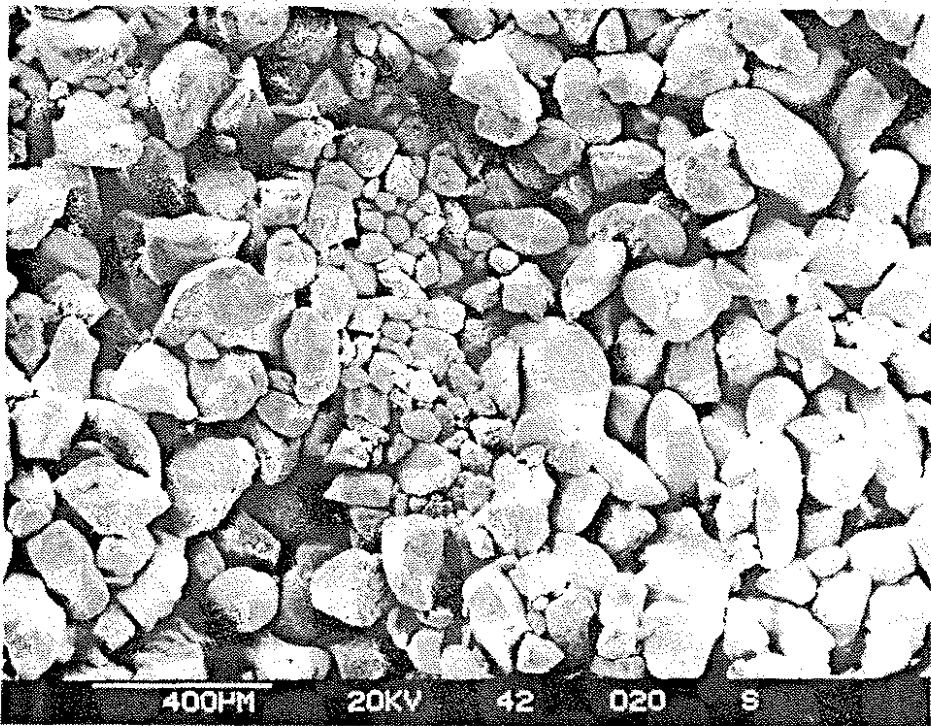
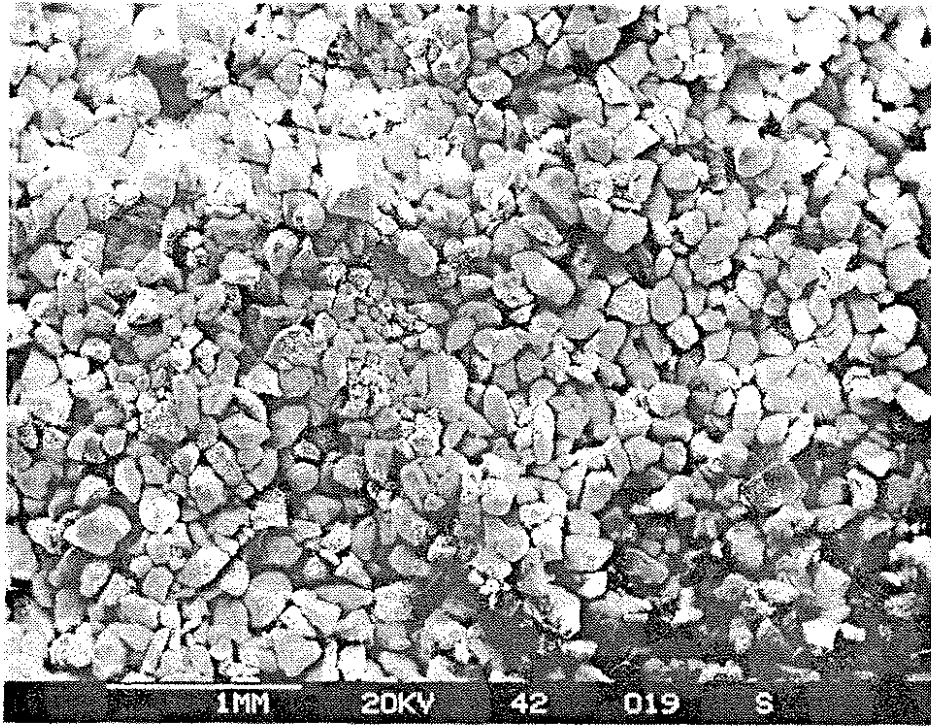


PLATE 3.3: Micrographs Showing Minor Segregation (Flume)

4. MECHANICAL BEHAVIOUR DURING SHEAR

4.1. Introduction

The understanding of the behaviour of sand undergoing shear deformation is fundamental to the correct prediction of the behaviour of embankments and natural slopes when undergoing a change in stress state. This chapter first describes the expected stress-strain behaviour of cohesionless materials during shear in terms of the steady state of deformation and generalized drained and undrained behaviour. The mechanical behaviour observed during undrained triaxial compression tests in this and other testing programs undertaken using the Syncrude tailings sand is then presented. The results of these tests are analyzed to determine if the initial placement method has a noticeable effect on the mechanical behaviour of the sand during triaxial shear.

It is appreciated that the mechanical behaviour derived from tests on laboratory samples can be substantially different from the real mechanical behaviour exhibited in the field. This is because a laboratory sample is always partially disturbed and is sometimes misrepresentative of the particulate mass being investigated. As well, the boundary conditions and the stress paths followed in laboratory tests rarely correspond with actual conditions found in the field. These points notwithstanding, a comparative study of the mechanical behaviour exhibited in the triaxial test can still be useful in determining if fabric induced behavioural differences are likely to be significant.

4.2. Behaviour of Cohesionless Materials During Shear

The behaviour of sands when stressed has been studied in great detail. The behaviour during shear is usually represented in laboratory testing by the measured relationship between stress and strain during which one of two types of drainage conditions is allowed; drained or undrained. These conditions are imposed on laboratory specimens to emulate the extreme drainage conditions possible in actual field cases, depending on the loading conditions and the drainage characteristics of the soil.

Laboratory loading can be either stress- or strain-controlled. During stress-controlled loading, the axial load applied is increased (or decreased) while the resulting strains are monitored. Strain-controlled loading induces a specific rate of axial strain on a specimen while the applied load to produce the strain is measured. In either case the applied or induced stresses are calculated from known area that the load acts upon. The change in volume (drained) or pore pressure (undrained) of the specimen due to the imposed load is often monitored to more fully describe the stress-strain behaviour in terms of effective stress.

Tests performed by Castro et al. (1982) indicate that the steady state line is unaffected by the method of axial loading chosen. Although stress-controlled loading is necessary to observe the true liquefaction phenomenon as seen in the work of Castro (1969), post-peak mechanical behaviour differences are better represented in triaxial tests where a constant rate of deformation is maintained (Saada and Townsend, 1981). Strain-controlled loading was used to provide axial load to the test specimens in this study.

Poulos (1971) has reviewed the major factors affecting the shapes of stress-strain curves and these factors are summarized below:

1. The soil type (represented chiefly by grain shape and mineralogy),
2. The initial fabric of the specimen,
3. The initial state (void ratio, effective normal and shear stresses), and
4. The method of loading (stress path followed; drained or undrained conditions).

Poulos (1971) considers all of the above factors to be very influential on the initial modulus and peak stress determined from the stress strain curve, but only the soil type has a pronounced effect on the post-peak or steady state behaviour of sands. Castro et. al. (1985) states that "the shape of the stress-strain curve prior to reaching steady state is a function of the initial structure of the soil; however, its steady state is not, since at steady state the soil is thoroughly remoulded and has lost all 'memory' of its initial structure." Some recent work suggests that the initial fabric does affect post-peak behaviour (Ladd, 1974, Mulilis et. al., 1977, Dennis, 1988), but is restricted to discussions pertaining to stress-strain behaviour during dynamic (cyclic) loading.

4.2.1. Steady State of Deformation

The steady state of deformation is defined by Poulos (1971, 1981) as "the state in which the mass is continuously deforming at constant volume, constant normal effective stress, constant shear stress, and constant velocity. The steady state of deformation is

achieved only after all particle orientation has reached a statistically steady state condition and after all particle breakage, if any, is complete so that the shear stress needed to continue deformation and the velocity of deformation remains constant." This definition is considered to apply to any mass of particles, and is achieved regardless of the initial structure or stress path followed, provided sufficient deformation occurs.

The steady state condition is similar to the critical void ratio concept first described by Casagrande (1936) from direct shear tests on sands. Castro (1969) was the first to develop this concept succinctly with undrained triaxial testing of Banding sand, and it is this work that forms the basis for most monotonically loaded steady state testing performed today. From this work came the concept of the steady state line. From a single test, the effective stress (p') at which the pore pressure remains constant with on-going strain and with no volume change is determined. The results from a number of tests performed at different pre-shear densities form the steady state line on the e -log p' plot.

4.2.2. Drained Behaviour

Drained behaviour during shear can be defined as the measured and observed responses to a change in the stress regime of a mass of soil, where the rate of change of stress and the permeability of the mass is such that the flow of pore fluid from the voids to a free surface occurs with no significant development of excess pore pressure. For the purposes of this discussion, only fully saturated sands are considered.

This behaviour is conveniently determined by triaxial or direct shear testing, the latter being better for the determination of behaviour at larger strains. The triaxial test is limited by the strains that can be imposed upon a specimen, but more flexibility can be obtained in terms of the stress path followed to failure than in the direct shear test. Other

forms of testing exist which allow better emulation of actual stress paths found in the field (such as 'true' triaxial tests or hollow cylinder tests), or allow larger strains to be investigated (ring shear tests), but these tests have other limitations and are often not practical for routine testing. Saada and Townsend (1981) provide a brief history of shear testing, review current technology in this area and evaluate the advantages and disadvantages of the various laboratory equipment available for the measurement of shear strength of soils.

Typical drained behaviour of sands undergoing shear deformation is idealized in Figure 4.1. This shows the expected stress-strain and volume change response, dependent on the state (void ratio/effective stress) in which the pre-shear specimen is found. Pre-shear is defined after consolidation of the specimen, but before any shear strain has occurred. This is in contrast to 'initial' conditions, defined as the state of the specimen prior to the imposition of any consolidation stress.

Loose specimens (specimens with pre-shear void ratios significantly larger than the steady state void ratio (e_{ss}) at the effective stress level tested) reveal a reduction of void ratio to e_{ss} with increasing strain (contraction), while the shear stress increases to a constant level. Alternatively, initially dense specimens (those with low pre-shear void ratios at the working effective stress level) show an initial reduction in void ratio but then a dilative response is observed, corresponding to an increase in void ratio to e_{ss} with increasing strain. Shear stress in the dilative case tends to peak and then reduce to a steady state value. As shown in Figure 4.1, the steady state shear stress achieved is theoretically the same for samples tested at the same stress level, regardless of the specimen's pre-shear void ratio.

4.2.3. Undrained Behaviour

Undrained behaviour during shear is defined as the response to a change in the stress regime of a mass of soil where the rate of loading and the permeability of the mass is such that no flow of pore fluid from the voids occurs, and therefore the overall volume of the mass of soil remains constant. For the purposes of this discussion, only fully saturated sands are considered. This behaviour is most easily revealed in the triaxial test when a measure of the pore pressure response during shear is desired, but again is limited by the strain that can be developed. Figure 4.2 shows the idealized stress-strain and pore pressure response for undrained loading.

Loose specimens (specimens that would contract in a drained environment) reveal an increase in pore pressure. This increase occurs to prevent contraction by reducing the effective isotropic normal stress sufficiently to negate the tendency for volume decrease caused by the shear stress. The effective shear stress increases to a peak and then falls off to the steady state shear stress. The pore pressure induced by shear is positive, and also levels off as the reduction in effective confining stress becomes sufficient to allow for steady state behaviour at the existing void ratio. Liquefaction is the special case of undrained failure where a saturated granular mass undergoes a sudden large reduction in effective stress prior to deforming at the steady state condition. This corresponds to a sudden large reduction in shear strength of the material.

Dense specimens (specimens that would dilate under drained conditions) show an initial increase in pore pressure but then a reduction is observed. This corresponds to the initially contractive, but eventually dilative, volume change observed in the drained test. The effective shear stress in the dilative case shows an early inflection point (point q,

Figure 4.2), and levels off after the increase in effective confining stress to the value corresponding to the steady state condition at that void ratio. The inflection point corresponds to the 'elbow' in the stress path plot (as described in Section 4.4.2.1.). As outlined by Mohamad and Dobry (1986), the 'elbow' is thought to be indicative of the beginning of a tendency to contract, but that tendency "is overridden by a simultaneous and stronger trend toward dilation." The steady state shear stress achieved tends to the same value for specimens tested at the same void ratio, regardless of the specimen's initial confining pressure.

It is possible that both the drained and undrained triaxial test may exhibit mechanical behavioural differences that can be attributed to fabric differences. However, the kinematic condition of constant volume during undrained shear probably greatly restricts the rebuilding of the specimen fabric during the deformation process (Fedaa, 1982). Correspondingly, the effect of initial fabric on the mechanical behaviour of undrained test specimens may be noticeable much further into the specimen deformation process than for drained test specimens. Specifically, the pore pressure response measured during undrained shear may be a key parameter in the understanding of behavioural differences due to a differing inherent fabric. The undrained method of loading was therefore chosen for this study.

4.3. Laboratory Testing

4.3.1. Overview

A laboratory program (herein called the present study) consisting of 26 isotropically consolidated undrained (CU) triaxial tests was undertaken on specimens of Syncrude tailings sand. Strain-controlled loading was performed on specimens nominally 37 mm in

diameter and 42 mm in height, with pore pressure measured at both the top and bottom of the specimens. The stress-strain and pore pressure response curves, the stress path (p' - q) plot for each of the tests performed are included in Appendix C. Also found therein is a summary of the relevant measured test parameters associated with the specific specimen.

Specimens were prepared by one of three methods; pluviation through air (designated PL tests), flume deposition (designated FL tests) or field deposition (designated FD tests). One of the flume specimens was tested from the unfrozen state (designated UF-1). All other samples were frozen uniaxially to allow undisturbed placement during set-up, and specimens were cored and trimmed from the samples. Thaw took place inside the triaxial chamber with a small confining pressure applied, and saturation was ensured prior to consolidation using a back-saturation technique at elevated cell pressures. An even distribution of stresses and pore pressures was facilitated by the use of lubricated ends for all tests except UF-1.

As well, 38 CU tests performed by other laboratories (Sources 1 through 5) on the Syncrude tailings sand over the past twelve years were also examined. Specimen dimensions are varied and somewhat larger than those of specimens tested in the present program, and testing procedures varied depending on the laboratory performing the tests. Details of the index properties of the sand tested in the present study and the procedures used to test the specimens are presented next, while the details of the other programs are found in Section 4.3.3.

4.3.2. Present Study

4.3.2.1. Material Tested

The tailings sand investigated is a uniform, fine grained quartz sand with subrounded to subangular shaped grains. It is derived from the mining of the McMurray Formation³ and forms a portion of the waste product created by the bitumen extraction process. The material used for the field and flume testing was collected from the beach area at various sites around the tailings pond, and the pluviated specimens were prepared from sand taken from the flume tests.

The D_{50} of the sand as determined from grain size analyses performed on individual specimens after testing ranged from 0.154 mm to 0.167 mm for the pluviated specimens, 0.141 mm to 0.204 mm for the flume specimens, and was approximately 0.167 mm for the two field specimens tested. The C_u ranged from 1.72 to 2.15 and 1.49 to 1.90 for the pluviated and flume specimens, respectively. The field specimens displayed a uniformity coefficient of about 2.19. Fines content ranged from 4.8% to 8.8% for pluviated specimens, 1.6% to 8.1% for flume specimens and was determined to be about 7.2% for the field specimens.

The range of grain size curves from 81 field samples and 227 flume samples reported by Kupper (1991) is presented in Figure 4.3, as well as the range of the 12 grain size curves determined for the pluviated specimens. The ranges for the field and flume deposited tailings sand were estimated from the maximum and minimum D_{10} , D_{50} , D_{90} and

³ For a geological description of the McMurray Formation and associated strata, see Dusseault (1977).

finer content measured in the grain size analyses. The grain size distribution curve determined for the Ottawa sand used to test the pluviator device is also included. The grain size analyses performed on individual test specimens are summarized in Appendix D, along with grain size distribution curves for each specimen tested.

4.3.2.2. Specimen Preparation

Isotropically consolidated undrained triaxial tests were performed on 24 laboratory prepared specimens and two specimens taken from undisturbed field samples. Fourteen of the laboratory specimens were formed by a dry pluviator technique, while the remainder were sampled from material deposited in a flume apparatus developed to model the field deposition environment.

4.3.2.2.1. Pluviation

Sample Preparation

Dry pluviator was performed in a multiple sieve pluviator (MSP) device similar to that described in Miura and Toki (1982), and shown in Figure 4.4. This consisted of a steel frame supporting six 20 cm diameter sieves, a lucite shield and a conical aluminum (funnel-like) hopper, modified at the apex such that the flow rate could be controlled. The six sieves were ASTM Designation #8 sieves, allowing all particles with a minor dimension of 3.35 mm to pass. Prior to pluviator, all material was passed through a #10 sieve (2 mm) to ensure no larger particles would clog the sieve set. Placed below the sieves was a cylindrical freezing mould into which the sand fell after being spread by the sieves. The mould was constructed of polyvinyl chloride (PVC) and is detailed, along with its brass

base plate, in Figure 4.5. The apparatus was set up and operated in a cold room maintained at a temperature of approximately +1°C.

The flow rate was controlled by changing the internal diameter of the apex of the hopper. PVC inserts were machined to allow six internal diameters, ranging from 10 mm to 35 mm, to be used to vary the flow rate of the sand. Miura and Toki have shown that a large range of densities can be obtained using this technique, and that placement density is influenced most greatly by the flow rate and only minimally by the height of drop of the material. Their tests were performed on four sands and on a graded glass bead 'sand' with uniformity coefficients varying from 1.5 to 9.0 and mean grain sizes ranging from 0.18 to 0.40 mm. Percent fines (<#200 sieve) in these materials ranged from 0 to 15%.

After pluviation, the sample was wetted by opening the valve on the base plate, thereby applying a small head across the sample. The sample surface elevation was monitored to evaluate the extent, if any, of disturbance caused by the wetting process. Sufficient time was allowed to wet the full height of the sample, which occurred in two to three hours. It was necessary to allow the Syncrude tailings sand to soak for 24 hours after wetting because of the water-repelling nature of the material. Care was taken such that the sample was not disturbed during this time period.

With wetting completed, liquid nitrogen was allowed to flow through the freezing plate. This initiated a vertically advancing freezing front through the sample, thus ensuring that a free-draining surface would always be maintained. Without this provision ice lensing could occur, severely altering the homogeneity and fabric of the sample (Baker, 1976 and Singh et. al., 1982). The sample surface elevation was monitored again to evaluate the extent of disturbance caused by the freezing process. Freezing took place in three to four

hours, after which the sample and mould were transferred to a cold room maintained at -20 to -25 °C. There the sample was allowed to equilibrate thermally for at least eight hours.

The sample was then extruded from the mould and cored in the -25 °C cold room using a 3.8 cm (inside) diameter diamond core barrel rotated at approximately 160 r.p.m. The cutting face was cleared during coring using chilled compressed dry air forced through a top-mounted swivel fitting at 250 kPa. This also served to keep the cutting face cool during coring to minimize thermal disturbance. During the initial coring attempts it was found that a relatively large curf and gap were required, as well as a slow feed, to ensure a high quality run of core. Two core runs were obtained from each sample and a number of specimens for triaxial testing were then taken from each run. Specimens were also saved from the remaining uncored sample for future density and scanning electron microscope work.

Just prior to testing, a specimen was trimmed from a core run ensuring that the ends were square. A small hole was then drilled in each end (1.5 mm diameter by 5 mm deep) to allow for the centering pins. These pins were required to prevent the specimen from becoming misaligned during set-up, which caused the initial trial specimens to slide out from between the platens during the initial stages of the shear test. The specimen was then weighed and its volume determined by measurement.

Sample Homogeneity

A study was conducted using a fine Ottawa sand, with a grain size distribution as shown in Figure 4.3, to determine the uniformity of the MSP method spatially within the freezing mould, as well as to confirm the range of dry densities that could be obtained

using this method. This was considered necessary because the MSP samples prepared in the present study were much larger than those prepared by Miura and Toki.

Eleven tests were performed using five insert diameters ranging from 15 to 35 mm to vary the flow rate. In all tests, specimens were taken from the mould after freezing and the dry density was determined using a wax/displacement method. This method involved the coating of a frozen specimen with a light paraffin/beeswax mixture and then weighing the specimen both in air and submerged in water to determine its volume. After correcting for the volume of wax, the dry density could be determined using the moisture content of the specimen.

The advantage of this method of determining the specimen volume over a measurement method is the time saved in sample trimming. With any measurement technique, specific geometric shapes (right cylindrical, square or rectangular) are necessary to determine the volume accurately, and these are difficult and time consuming to prepare in a cold room environment. With the wax/displacement method, odd shaped specimens can be used, both allowing more specimens from each test to be evaluated and reducing the specimen preparation time significantly.

In one test run of the pluviation equipment performed with Ottawa sand, 14 of the 27 specimens taken for density determination were measured to obtain their volume prior to using the wax/displacement technique. This was done to determine the accuracy of the wax/displacement method in comparison to the more standard measurement technique. After freezing, the sample was divided into 27 portions using a table saw outfitted with a diamond-studded blade, operated in a -25°C cold room. The locations of the specimens in the sample are shown in Figure 4.6. The top and bottom 12 mm were trimmed from the 20 cm high sample before two vertical cores were taken from positions A and B, using the

technique described above. The remainder of the sample was then sectioned into 44 mm thick slabs and trimmed as shown in Figure 4.6.

A comparison of the dry densities determined using both the measurement and wax/displacement techniques for volume determination is shown in Table 4.1a. The average value determined by the two methods is similar, as is the variation in the density data.

The slightly larger mean density observed in the wax/displacement series is believed to be due to a systematic error caused by trapped air between the wax shell and the frozen sample during submersion. Any trapped air would have the effect of making the sample more buoyant than it really is, thereby reducing its submerged weight. This, in turn, creates a smaller apparent volume of the sample, increasing its apparent dry density. Using care while dipping the specimen in the wax minimizes the trapped air and reduces the systematic error to a tolerable level. The observed difference in mean values of 0.007 Mg/m^3 is small (corresponding to a Δe of 0.006 based on a specific gravity (G_s) for quartz of 2.65), and well within the scatter of the data. It is concluded that the wax/displacement method is as accurate and precise as the measurement method and therefore it was used in the remainder of the program.

The same Ottawa sand sample described above was also used to determine the spatial variation of density throughout the mould. Table 4.1b indicates similar mean values and data variation between the vertical and horizontal directions. The difference between the mean density values in the horizontal and vertical directions of 0.012 Mg/m^3 is equivalent to a Δe of 0.011, again small with respect to the scatter.

The lower mean value for Level 2 is consistent with a slight variation in density with height of fall. This is shown graphically in Figure 4.7, which indicates a subtle trend towards a more dense state with increasing depth in the mould. The range in average values is 0.033 Mg/m^3 , which is only slightly higher than the standard deviations reported in Table 4.1. The results are therefore consistent with the results of Miura and Toki (1982), in that the height of fall has only a minor influence on the placement density achieved using the multiple sieve pluviation device.

The influence of the variance of flow rate (controlled by the opening diameter) on the placement density is to decrease the density with increasing flow rate, as shown in Figure 4.8. This trend is evident up to an opening diameter of 30 mm. Above this diameter the placement density appears not to be affected by an increase in opening diameter. This is explained by the observation of a buildup of sand on the top sieve at the 35 mm opening diameter, indicating that a 30 mm diameter gives the upper limit of flow rate possible for the combination of this configuration of the MSP apparatus and this material.

The results are presented in two forms: Figure 4.8a shows the overall variation in density throughout the mould, whereas Figure 4.8b indicates the density and variation found in the middle layers (layers 2 and 3, Figure 4.6). The mean densities determined for the two presentation methods are similar, but a lower variation (as indicated by the error bars) is found when comparing only the middle section densities. This is expected because of the slight variation in density with height of drop, as reported earlier. It is therefore expected that the most uniform specimens for triaxial testing can be obtained from the central layers of the sample.

It is of interest to note that the variation from the mean value decreases with increasing placement density, as shown by smaller standard deviations on the left sides of the curves of Figure 4.8. This is thought to be due to a higher susceptibility of the looser samples to disturbance during wetting and freezing. With these two points in mind, specimens were chosen from the central layers where possible, especially in the cases where the sample was prepared with a low relative density.

As the grain size distribution of the Ottawa sand is of a similar shape to that of the tailings sand investigated (Figure 4.3), and the tailings sand gradation falls in the grain size range of the materials tested by Miura and Toki (1982) described above, similar uniformity is expected with the use of the tailings sand in the MSP device.

4.3.2.2.2. Flume

Samples were obtained from a laboratory flume device developed concurrently with the present study to model the deposition of tailings sand in a mining environment (Kupper, 1991). Flume tests were performed to study the effects of the variance of placement parameters on the density achieved, the angle of deposition, and the distribution of grain size with distance from the source. Placement parameters investigated include the flow rate, the solids content (ratio of solids to total cross-sectional flow, by weight), the height of fall (from the 'spigot' to the 'beach', analogous to the field condition shown schematically in Figure 4.9), and a variation in materials deposited, including the Syncrude tailings sand.

Samples were taken from tests run using the Syncrude material using 10 cm diameter 'Shelby' type tubes with a length of 20 cm. The tubes were made of seamless, highly polished stainless steel to minimize sidewall disturbance. A tube was inserted

vertically using uniform hand pressure, and material was excavated from around the tube. Initially, samples were frozen in place by surrounding the base of the sample with frozen CO₂ pellets, increasing the height of the pellets as the approximately uniaxial freezing front migrated upwards within the sample. This method proved to be time consuming and awkward because of the confined working space within the flume, and somewhat dangerous because of the concentration of CO₂ gas that developed during sublimation of the pellets. The remaining samples were therefore carefully removed prior to freezing and placed on a horizontal bed of CO₂ pellets. Axial deformation was monitored during freezing in some of the samples to ensure that uniaxial freezing was taking place. If the measured displacement was greater than approximately 1%, the disturbance was considered too great and the sample was not used for triaxial specimen preparation.

Specimens were taken from the samples using the coring technique described in Section 4.3.2.2.1. One core run was obtained from each sample, and the triaxial specimens were prepared as described previously. Some relatively thick coarse layers (up to 8 mm) were encountered in the coring process, which usually led to poor core quality in the zone surrounding these layers. As the purpose of this study is to investigate fabric differences on a smaller scale (ie due to varying grain orientation as opposed to layering), specimens were taken from areas that appeared relatively homogeneous to the unaided eye.

4.3.2.2.3. Field

Field samples were taken during a field density/gradation program undertaken by Kupper (1991) at the Syncrude tailings pond. A number of field tests were performed where the flow rate, solids concentration, and height of fall (as shown on Figure 4.9) were varied from test to test. The pre- and post-test topography was determined by survey, and the near surface density distribution was determined by nuclear densometer and either

coring (winter) or in-situ freezing (summer) measurement methods. Numerous grab samples were taken for sieve analysis.

Two field samples were tested in this program to allow a comparison of behaviours with other methods of placement. Both samples were taken by the in-situ freezing method which is identical to the method initially used for sampling the laboratory flume, as described in Section 4.3.2.2.2. The coring method, as outlined in Section 4.3.2.2.1, was used to create triaxial specimens for undrained testing. Similar problems with core quality were encountered, as found with the preparation of the flume samples.

4.3.2.3. Triaxial Test Procedure

Specimens were prepared with a length to diameter ratio of approximately 1.1 to 1 in all tests except UF 1 (UF-unfrozen), where the ratio was 1.5 to 1. This test specimen was mounted unfrozen in the triaxial cell and the test was performed without lubricated ends and with an initial diameter of 51 mm, somewhat larger than the other specimens. All other tests were performed with lubricated ends similar to those described by Rowe and Barden (1964). A center hole was punched out of each latex disk to allow for communication between the porous stone recessed flush into the center of both the top and bottom platens and the specimen, and filter paper was placed on the porous stones. A centering post was placed in each porous stone to aid in centering the specimen during test assembly and to keep the specimen from sliding out from between the platens during shear.

Plewes (1987) performed a study of the effects of the length/diameter (l/d) ratio and the use of lubricated ends on the shape of fine Ottawa sand specimens after undrained testing. Four specimen shapes were typically observed after shear, as shown in Figure 4.10. It was found that the most uniform deformation occurred with specimens

tested with lubricated ends and with an l/d ratio of unity or less. Plewes determined that specimens tested with lubricated ends and an l/d ratio of two failed by bulging at mid-height which is most likely an indication of a non-uniform stress distribution. An l/d ratio near unity was therefore adopted for the majority of the testing performed in this study.

As summarized in Saada and Townsend (1981), Raju et. al. (1972) found the failure plane that develops in specimens of dense sand tested in compression without lubricated ends does not occur in tests with lubricated ends. Their conclusion was that the occurrence of this plane is not a property of the sand, but is due solely to the testing procedure. Lee (1978) concluded that "for medium to dense sand there was a significant increase in static undrained strength with lubricated ends as compared with tests using regular ends."

The platens (top and bottom) were designed with a larger diameter (44 mm) than the nominal sample diameter (37 mm) to allow for radial expansion of the specimen up to approximately 31% axial strain before the specimen diameter equals the platen diameter, assuming the specimen remains a right cylinder during deformation. This was done, along with the implementation of the lubricated ends, to minimize stress concentrations at the ends of the specimen during shear. Since the pore pressure was measured at the ends of the specimen, a pore pressure response more representative of the entire specimen was expected to be measured because of these refinements in the triaxial test procedure. The triaxial cell and measuring system are detailed in Figure 4.11.

The observed deformation behaviour of the Syncrude tailings specimens during shear was very uniform up to an axial strain of 20 to 25%, at which time some bulging was generally observed. Pore pressure responses during shear were measured at both the top

and bottom of the specimen independently and gave almost identical results in every test. Details of the end platen design are shown in Figure 4.12.

Dead zones are expected adjacent to the top and bottom porous stones where the lubricated ends are not acting, analogous to those postulated by Rowe and Barden (Figure 4.13). Because of their central location within the sample, the behaviour of these zones is expected to be only marginally different from that expected during general shear in an idealized element of soil. The centering posts were placed in the porous stones such that they would not protrude outside of the expected dead zones, as shown in Figure 4.12.

4.3.2.3.1. Preparation

Double de-aired water was prepared and allowed to cool to +1°C. This process involved first boiling distilled water and then agitating it within a laboratory de-airing device under vacuum. Within this device, cavitation occurs at the tips of an impeller and the air drawn out of solution is then removed by the vacuum applied at the top of the device. This process is much more efficient at elevated temperatures because the dissolution of air from water is temperature dependent.

The porous stones were de-aired by boiling them in distilled water for 20 minutes, and all ports and passages in the triaxial base were flushed with de-aired water to ensure no air was trapped. The cell pressure transducer zero value was recorded, all reservoirs were replenished if necessary and the volume change devices were checked to ensure that an appropriate stroke was available prior to set-up. The cell pressure and back pressure (lines only) were then set to 35 kPa and 20 kPa, respectively.

Calibrations of the pore pressure transducers, load cells and LVDT's used in the testing procedure were performed before and during the testing program. These calibrations and expected precision are summarized in Appendix B. The compliance of the loading system and lubricated end platens was also assessed and the correction applied to the axial strain, dependent on the loading level.

4.3.2.3.2. Assembly

The cell base, top, and top platen were all placed in the +1°C cold room and allowed to cool (minimum 1 hour). De-aired water was trickled through the back pressure (BP) connection line and top platen to remove any air bubbles. The porous stones and wetted filter paper were then placed on both the top and bottom platens. High vacuum silicone grease was applied to the latex disks acting as lubricated ends. They were then aligned around the porous stones on both the top and bottom platens.

A split ring was machined to allow the placement of the top O-rings on the top platen without removing the back pressure connection line. This O-ring stretcher was placed, with two O-rings affixed, over the top platen. The membrane stretcher was prepared with a 37 mm diameter membrane and two O-rings.

The specimen was then centered on the bottom pedestal, facilitated by aligning the 4 mm center post of the porous stone with the pre-drilled hole in the bottom of the specimen. This post prevented the specimen from becoming misaligned during mounting of the specimen, filling of the cell and during the initial portions of shearing.

The stretched membrane was then placed over the specimen and bottom pedestal and the vacuum applied to the membrane stretcher was released. The bottom O-rings were

then placed and the membrane was cut to size and rolled back over the specimen. The top platen was placed (while attached to the BP connection line) on the specimen, making sure the center post aligned with the pre-drilled hole in the top of the specimen. The membrane was then rolled up over the top platen using as small a force as necessary on the platen. The top O-rings from the split ring were then placed.

A hypodermic needle was inserted into the air extraction port through a silicone bead applied in the countersunk area. A fresh bead was then applied around the needle. Excess air from between the membrane and specimen was then removed by applying suction via the needle. The needle was removed through the fresh bead, and the suction from within then closed the hole left by the needle.

After coating the base O-ring with vacuum grease, the top of the cell was placed over the specimen, lining up the ram with the top platen ball, and the ram was locked in position. The cell top was then tightened down to the base with the wing nuts (finger tight). The RTD rod was then positioned beside the specimen and its connection was secured.

The line from the de-aired water reservoir to the cell port was then connected and a vacuum applied to the top of the cell through the bleeder cap port, removing as much air as possible. This increased the rate of filling substantially, reducing the amount of thaw that occurred prior to the application of the cell pressure. The bleeder cap was replaced and tightened, the feeder line removed from the cell port and a 15 kPa pressure locked into the cell.

4.3.2.3.3. Thaw

The cell was carefully moved from the +1°C cold room to the loading frame. The cell pressure and back pressure lines were then connected to the cell, and the two pressure transducers, the load cell and the RTD were connected to the data acquisition system.

The LVDT was set up, the initial reading taken and the cell and back pressures were applied to the cell and specimen. Axial deformations due to thaw were observed in the first hour, moving the specimen to meet the ram as necessary. Volume changes in the cell and specimen were measured every 30 minutes until the cell water temperature had stabilized for a minimum of 5 hours (usually overnight). The specimen was considered completely thawed at this time.

4.3.2.3.4. Saturation

The zero values for the back and pore pressure transducers were recorded by shutting in the perspex bleeder assembly for each port and opening the bleeder screw to atmospheric pressure. After recording the zero values, the bleeder screw was closed again and the excess pressure built up during tightening was released.

In tests PL 2 to PL 9 and FL 2 to FL 8, the cell and back pressures were then increased (lines only) to approximately 850 kPa and 835 kPa, respectively. The pressure required to saturate the sample was initially estimated using the method described by Black and Lee (1973). From an estimate of the specimen's initial saturation, both the level of back pressure required and the time to full saturation can be estimated. An elevated pore pressure also reduces the risk of cavitation for specimens tending to dilate during shear.

The lines and back pressure perspex bleeder assembly were allowed to expand for 5 minutes. The pressures to the cell and specimen were then opened (cell pressure slightly before the back pressure) and the cell volume change and pore pressure response were monitored. The specimen was allowed to back saturate for a period of approximately 5 hours.

In all other tests the cell and back pressures were increased (lines only) to a value not exceeding the proposed effective consolidation pressure for that particular specimen, and significantly lower in the cases of higher proposed confining pressure tests. The lines and back pressure perspex bleeder assembly were allowed to expand for 1 minute. The pressure to the cell was then opened and the cell volume change and pore pressure response were monitored. The back pressure was then increased until the effective confining pressure was again 15 kPa and the specimen pressure was allowed to equilibrate, this usually occurring immediately. This process was repeated until a back saturation level of about 835 kPa was reached or a B value normally greater than 0.98 was recorded. The specimen was allowed to back saturate for a period of time (often overnight) if a satisfactory B was not recorded during the previously described back saturation.

4.3.2.3.5. B-Test

The back and pore pressure ports were closed and the cell pressure was increased to the desired consolidation level above the existing back pressure (line only). This line was allowed to expand for a few minutes. The cell pressure was then opened to the cell, keeping the back pressure port closed. The pore pressure response due to the increase in cell pressure was monitored and the B value calculated as the pressures stabilized (a 10 to 15 minute period).

The B value is calculated from the pore pressure equation expressed by Skempton (1954):

$$\Delta u = B[\Delta\sigma_3 + A(\Delta\sigma_1 - \Delta\sigma_3)] \quad (4.1)$$

The value of B approaches unity when the compressibility of the soil grains is small compared to that of the pore fluid, and the compressibility of the pore fluid is very small with respect to that of the soil skeleton. This occurs when the saturation level is close to 100%, hence a measure of B is a good indication of the level of saturation of the soil specimen. During the B-test the stress level is increased isotropically, therefore the equation is reduced to the following form:

$$B = \Delta u / \Delta\sigma_3 \quad (4.2)$$

4.3.2.3.6. Consolidation

The applied cell and back pressure levels were checked to ensure the desired consolidation level would be obtained. The initial volume change zeroes were recorded and the back pressure port opened to the applied back pressure. The data was logged at five second intervals initially, doubling each successive interval appropriately with the rate of volume change observed.

The consolidation results were plotted immediately (root time versus volume change) to determine when consolidation was complete and to confirm the appropriate rate of deformation to be used during the shearing stage of the test.

4.3.2.3.7. Shear

The clutch was engaged in the loading frame prior to closing the back pressure port to avoid a buildup of pressure in the specimen. An initial set of readings were then taken and the shear was started. The sand tested is considered relatively permeable hence no pore-pressure lag is expected (Bishop and Henkel, 1964). A convenient shear rate of 0.25 mm/minute was chosen for all tests.

The test data was logged every 30 seconds until the recorded data stabilized such that two minute readings were sufficient to monitor the observed changes. This usually occurred 10 to 15 minutes into the test. The data recorded included both internal and external load (most tests), cell and pore pressures, axial deformation, cell volume change, and cell water temperature. The mode of deformation during shear was observed and the specimen shape sketched at appropriate intervals during the test. The test was terminated after recorded values ceased to change for a period of time or the strain was such that the back pressure connection line or RTD stem was interfering with the specimen strain (usually >40%).

4.3.2.3.8. Dismantle

The ram was locked and the cell pressure port closed immediately after shear was stopped. All pressure lines and electrical connections were disconnected and the cell was removed from the loading frame. The cell was drained as quickly as possible and the area around the top platen dried to prevent excess moisture from contaminating the specimen. The top O-rings were removed without disconnecting the back pressure connection line and the membrane was peeled back from the top platen.

A significant portion of the center of the specimen was removed for moisture content determination and the remainder was carefully washed into a drying pan to obtain the total dry weight of the specimen. From this information, the void ratio of the specimen during shear was determined.

4.3.2.4. General Comments

Void ratio determination prior to testing was performed by measurement of the specimen dimensions in the frozen state to determine its volume and obtaining the dry weight of the material after testing. An attempt was made to track the void ratio from the pre-assembly condition to shear using careful measurements of cell fluid volumes and assessing membrane penetration effects to determine specimen volume changes during the thaw, saturation and consolidation stages. This method proved to be very difficult because a small and variable quantity of air was generally trapped in the cell during assembly which was forced into solution during the elevation of the cell pressure, making a strict account of cell fluid volume changes impossible during the saturation stage. This method was subsequently abandoned and the post-shear moisture content was used for the determination of void ratio for all tests.

As outlined in Bishop and Eldin (1950), cavitation can occur in specimens that undergo large decreases in pore pressure during shear. Cavitation is the dissolution of gas from solution caused by a reduction of pore pressures to a threshold value (at approximately -1 atmosphere for sand). Above this value, the undrained test proceeds normally with no volume change. When the pore pressure reaches this threshold, air bubbles begin to form and the "no volume change" condition requirement is violated. Any further drop in pore pressure dictated by the dilative tendency of the specimen does not occur because the specimen volume is changing to meet the dilative need of the assembly of

particles during shear. Due to the elevated back pressures that the tests were conducted at, none of the specimens developed cavitation during shear.

In only one test (FD 1), a distinct shear plane developed and this area was taken for a moisture content separately from the central portion of the sample. The shear plane moisture content was found to be higher than that for the remainder of the specimen, indicating that more dilation had likely occurred on this plane. To maintain the no volume change conditions, a redistribution of moisture content (and therefore void ratio) must have occurred elsewhere in the specimen.

4.3.3. Other Testing Programs

The data from five testing programs performed for Syncrude Canada Ltd. were used for comparison with the results of the undrained triaxial tests performed in the present study. Below is an outline of the scope of the investigations, along with a summary of the procedures used to prepare and test the specimens for each source. Details concerning the index properties of the material used in the investigations, such as the results of grain size and maximum and minimum density determination, are also included. The complete description of each testing program and the stress-strain curves for each test are found in the individual reports referenced at the end of the text.

4.3.3.1. Source 1

The purpose of this report was to determine the degree of compaction required to preclude laboratory liquefaction of the Syncrude tailings sand. In the course of this investigation, several variables were varied, including the method of loading, oil content,

specimen diameter, and specimen preparation technique. The effect of these parameters on the resulting steady state line was observed.

Two materials were used in this investigation: Plant Site tailings and Dam Site tailings. The Plant Site material was sampled prior to placement (immediately after processing) whereas the Dam Site material was sampled after the deposition process. The beaching action associated with the Dam Site material resulted in a decrease in oil content of 0.1%, a decrease in fines content (particles passing the #200 sieve) of 11% and an upward shift in the maximum and minimum (max/min) densities of 0.03 and 0.06 Mg/m³, respectively. The grain size curves for the two materials display a higher beached uniformity coefficient (by about 1.0) and a slightly lower beached D₅₀ (0.02 mm). The following average values were determined for the Dam Site material: Fines Content = 7%, D₅₀ = 0.164 mm, C_u = 2.09 and the max/min densities are 1.616 and 1.280 Mg/m³, respectively, using the ASTM D2049 method.

The difference in the two materials was considered too great to allow the comparison of both to the present study, hence the program using the Dam Site material was chosen. The fines content in this material is within the range of that found in the material studied, whereas the Plant Site material fines content is much higher (in the order of 18%).

Five undrained, isotropically consolidated tests (R-41 to R-45) were performed on the Dam Site material. The preparation method used to perform these tests is outlined next.

After soaking for 24 hours at about 16% moisture content, the material was placed inside a rubber membrane that was stretched inside a cylindrical mould mounted on the triaxial base pedestal. The soil was placed in 20 equal layers, each compacted using a

uniform number of static load applications of a 1.3 cm diameter rod. Lubricated end platens were used to reduce end friction.

Nominal dimensions of the compacted specimen were 7.3 cm diameter by 10.8 cm high. The top cap was placed after compaction and a vacuum of 50 to 100 kPa was applied to support the specimen during assembly. After removing the mould, the specimen was accurately measured and the cell was assembled.

A confining pressure of 50 to 100 kPa was applied to the specimen and as the vacuum was dissipated, water was drawn into the specimen. Saturation was facilitated using back pressures ranging from 400 to 500 kPa, and B values of 0.95 to 1.00 were obtained for all specimens prior to consolidation. The void ratio was determined from measurements of the sample prior to saturation and the dry weight of sand used to construct the specimen, corrected for volume change measured during consolidation. Ignoring the volume change during saturation has been shown to create a systematic error, especially in samples with significant fines content (Sladen and Handford, 1987), therefore an undisclosed void ratio error may exist in this data.

The specimens were then isotropically consolidated to 588.4 kPa. Drainage valves were closed and an axial load imposed on the sample at a constant strain rate of approximately 0.5% per minute. Axial load, deformation, and pore pressure were recorded.

4.3.3.2. Source 2

Boreholes drilled in the tailings dam had revealed four locations within and beneath the dam that were considered to be relatively loose. Attempts both to determine the

susceptibility of these areas to a liquefaction failure and to develop a criterion by which to preclude such a failure were made with this report. Specimens were prepared from the sand sampled for fixed-piston density determinations to ensure that a representative material was being tested. Material index properties were somewhat variable, with D_{50} ranging from 0.126 mm to 0.176 mm, C_u ranging from 1.63 to 1.96 and fines content varying between 2.7% and 11.8%. No max/min density determinations were performed on this material.

Specimens were prepared by compacting the soil at 16% moisture content (to allow bulking to occur) in 30 equal layers within a thin rubber membrane supported by a 7.3 cm diameter split mould. Static tamping was used to compact each layer, providing 40 tamps per layer. The nominal height of specimens was 15.7 cm, providing a height to diameter ratio of 2.2. The specimens were carefully measured prior to cell assembly to later determine the initial volume and dry unit weight.

Saturation was ensured using back-saturation at levels between 390 and 880 kPa, achieving B values of 0.91 or greater. The desired consolidation level was achieved isotropically in four tests while anisotropic consolidation ($\sigma_1'/\sigma_3'=2.0$) was performed on three specimens in increments to determine compression characteristics. The anisotropically consolidated test results were not used in this comparison. The same method to determine void ratio during shear was employed as used in the Source 1 data. Again, the void ratio information may be suspect for this reason.

Specimens were sheared undrained at a rate of approximately 0.3 mm per minute (corresponding to 0.2% per minute) to between 20 and 25% axial strain, where steady state conditions were achieved. The dry unit weight of the specimen was then determined from the dry weight of the solids remaining after oven drying the sheared remains.

4.3.3.3. Source 3

The purpose of this investigation was to determine the effect of sample size on the positioning of the steady state line. Careful measurement of the density profile after shear was performed to determine if sample irregularities, possibly developed during shear, were the cause of differences attributed to scale effects in the previous testing programs performed by Sources 1 and 2. Both 7.6 and 15.2 cm diameter specimens were used in the testing program, which consisted of twelve consolidated undrained triaxial tests. Six of the tests were performed on the smaller diameter specimens with nominal heights of 11.4 cm, and the remainder of the test specimens were of the larger diameter and nominal heights of 25.9 cm.

All tests used strain-controlled loading and lubricated platens were used to reduce end effects. Pore pressure measurements were made at the top, middle, and bottom of each specimen to determine if a pore pressure gradient developed across the specimen during shear. In all tests except R-9 and R-10 (both large diameter), the specimen was prepared by pouring air-dried sand through a funnel into the membrane lined sample former. The sides of the former were tapped when a higher density was desired. Specimens R-9 and R-10 were compacted at approximately 14.5% moisture content in ten equal layers with a 1.27 cm diameter rod.

The material used is characterized by ten grain size determinations performed on samples taken from a 500 lb blended source of tailings sand provided by Syncrude Canada Ltd. The results of these tests show an average D_{50} determination of 0.17 mm, an average C_u of 1.80 and an average fines content (<#200 sieve) of 5.2%.

After preparation, a small vacuum was applied to permit removal of the former and measurement of specimen dimensions. If desired, the density was further increased by tapping the cell base. The cell was then assembled and a small cell pressure (35 to 70 kPa) was applied. The specimen was then flushed with de-aired water from bottom to top until no bubbles were observed in the back pressure connection line. Back-pressure saturation was then used to achieve B values of 0.97 or greater. Generally a 700 kPa back-pressure was required to achieve this level of saturation. Incremental isotropic consolidation was then performed, allowing drainage against the back pressure and measuring with a burette placed in the back pressure line.

Specimens were loaded at a rate of between 0.1 and 0.2 % axial strain per minute. Load, deflection, and pore pressure measurements were taken at regular intervals and tests were carried out to 20-39% strain. Samples were then frozen in the cell to allow density measurements on slices after dismantling, assuming 100% saturation.

Maximum and minimum density determinations were performed according to ASTM D2049, giving an average maximum of 1.626 Mg/m^3 and an average minimum of 1.368 Mg/m^3 . As these values of max/min density are significantly different from those reported in the other sources, it can be expected that this material may behave differently. A comparison of steady state lines reported in this report confirmed a difference in the steady state response, but it is not clear if this effect was due to material differences, specimen size differences, or both.

4.3.3.4. Source 4

The goal of this study was to provide a third independent assessment of the steady state condition for the Syncrude tailings sand in an attempt to clarify the discrepancy

observed in the results of other laboratory investigations. The range of effective stress levels investigated were increased to provide an extension to the previously reported data.

Tests were performed in a standard triaxial cell which included a rotating bushing on the loading ram to minimize piston friction. Lubricated ends were used in all samples except CU-9 and CU-10. Axial deformation, load, and both cell and pore pressure were monitored using a digital data acquisition system at a rate of 60 readings per second.

Specimens were prepared by tamping moist sand in ten equal layers within a rubber membrane supported by a split-ring mould. Nominal specimen dimensions were 70 mm in diameter by 105 mm in height for all tests except CU-9 and CU-10, where the height was increased to 150 mm. Saturation was facilitated by flushing the sample with CO₂ prior to flushing with de-aired distilled water, allowing lower back pressures to be used to obtain complete saturation. This procedure was performed prior to the placement of the top cap.

A 10 kPa suction was then applied to the sample and the mould removed. After assembly of the cell, a back pressure of 700 kPa was applied to achieve B-values equal or greater than 0.95. The saturation was performed in stages such that the effective confining pressure became no larger than 7 kPa. Isotropic consolidation was performed in four increments to the desired consolidation level.

All tests were performed strain-controlled at a rate of 0.6% to 0.8% per minute. Specimens were frozen after the cell fluid was drained to allow for a dry density determination after shear. This was shown to be significantly different from the dry density obtained by measurement of the sample prior to saturation and correction for consolidation, indicating that a significant amount of specimen densification occurs during the saturation stage. In tests CU-1 through CU-6 the specimens proved to be very unstable

after shear. To eliminate handling problems, the remainder of the specimens were consolidated to the ambient post shear cell pressure and an accurate volume change of the sample was determined by measuring the water expelled. A post-shear dry density was then calculated with this volume change taken into account.

Sieve and hydrometer analyses were performed on 25 samples; one initial sample, twelve from specimens used for maximum and minimum density testing and the remainder from the undrained triaxial tests performed on this material. The triaxial tests were performed on specimens whose material index properties were very similar (ie a small coefficient of variation was found for C_u , D_{50} , and % fines). The maximum and minimum density tests were performed on material with a 2.1% lower average fines content (7.8% versus 5.7%), a C_u with a value 0.02 lower (2.42 versus 2.40), and a 0.006 mm higher average D_{50} . These differences are not considered significant when the effects of changes in C_u , D_{50} , and % fines on relative density are examined (see Kupper, 1991).

Six maximum and six minimum density tests were performed according to ASTM D2049, indicating an average maximum of 1.756 Mg/m³ and an average minimum of 1.412 Mg/m³.

4.3.3.5. Source 5

In this study, consolidated undrained triaxial tests were performed on three remoulded and eight relatively undisturbed specimens of tailings sand. The remoulded sand used was from a previously obtained composite sample from the following boreholes:

BHF-07N-87-01 @ 12.2m

BHF-26N-87-01 @.13.7m

BHF-23N-87-01 @ 29.0m

BHF-23N-87-03 @ 29.0m

The composition of the sample is described by a D_{50} of 0.140 mm, a fines content of 13.5% and a C_u of approximately 3.0 (using an estimated D_{10} of 0.05 mm). No representative max/min density determination was made for this soil. Two of the remoulded specimens (T-31 and T-32) were formed by a moist compaction method in which the wetted soil was placed in 10 mm lifts, rodded with a razor knife and levelled with a 110 gram flat disc. Scarification of the top 3 mm of each lift was done prior to the placement of each subsequent lift. The specimen was frozen and then weighed and measured prior to being set up in the triaxial cell. The dry weight was determined after the test to determine the initial dry density of the specimen.

The third remoulded specimen (T-33) was prepared using a dry pluviation method, in which a pre-determined mass of oven dried sand was allowed to flow through a funnel into a specimen former (set up on the triaxial base pedestal). The funnel was moved in a circular motion and raised as the sand flowed in, creating a loose structure. Vibration was used to create the desired density and water was then added to the specimen before freezing. A weight and measurement of the specimen was taken prior to set up to allow for the calculation of the initial dry density. The specimen was then allowed to thaw under an isotropic confining pressure of 10 kPa.

The undisturbed specimens were trimmed from four frozen fixed piston samples taken from borehole B11A-20F-87-12 at depths ranging from 30.8 to 41.5 m. Some disturbance prior to and during freezing may have occurred, but the centers of the samples were deemed relatively undisturbed. Two specimens were then taken from the center

portion of each sample. After mounting in the triaxial apparatus, an isotropic confining pressure of 13.8 kPa was applied during thaw. All remoulded and undisturbed specimens were nominally 75 mm in diameter by 150 mm in height.

A significant effort was made to ensure that the samples remained undisturbed during saturation. A procedure was developed by which the specimen was flushed completely and, over a period of several days, brought up to a back pressure of 827.4 kPa while ensuring the effective confining pressure never exceeded 13.8 kPa. All remoulded specimens (T-31, T-32 and T-33) and four of the undisturbed specimens (1-B, 2-B, 3-B, 4-B) were consolidated isotropically, while the remaining undisturbed samples were anisotropically consolidated with σ_1'/σ_3' equal to 1.39. Specimens were then loaded undrained in compression at a rate of 0.12 mm per minute (corresponding to 0.1% per minute). Specimen void ratios were determined using a special dismantling technique at the end of the test, described at the end of the report.

Leaks developed through the membrane in tests on specimens 1-A, 1-B, and 2-B, therefore these results were not considered in the present analysis. Only the isotropically consolidated specimens were used in the comparisons made in Section 4.4.

4.3.4. Summary of Testing Programs

A summary of the laboratory testing programs discussed above is shown in Table 4.2 which outlines the method of specimen preparation, the 'state' of the specimen prior to shear, material characteristics from grain size analyses and the type of stress-strain curve exhibited during shear. The specimen state is described by its pre-shear dry density and the initial effective confining pressure (p_o') exerted on the specimen just prior to shear. The

C_u , D_{50} and fines content were taken from grain size analyses performed on individual specimens or from the source material used to prepare the specimens.

A summary of the testing conditions under which each program was performed is presented in Table 4.3. The major differences among the previous programs and the present study (other than the method of specimen preparation) are the specimen size and the use of lubricated ends.

The difference in void ratio between that measured prior to thaw (initial) and that determined after shear (equivalent to the pre-shear void ratio) was compared with the initial void ratio as shown in Figure 4.14 for the present study and other source data. Frozen and unfrozen specimen preparation techniques are shown separately. A strong trend of increasing change (reduction) in void ratio with increasing initial void ratio is evident, regardless of the effective confining pressure chosen. The highest initial void ratios were observed in the unfrozen specimens from the other source data, with relative density changes greater than 100% occurring during the set-up, saturation and consolidation stages of the test.

The present study data generally shows a slightly higher void ratio reduction than the other source data at the same initial void ratio. This may be due to specimen size effects, as the other source specimens were generally larger than those of the present study. As shown in Figure 4.14, within the present study data the single unfrozen specimen falls as expected for the frozen test results. As well, the five frozen test results are scattered among the unfrozen test results within the other source data. The freezing of the specimens prior to test set-up therefore does not appear to adversely affect the volume change characteristics during the pre-shear phase of the triaxial test.

4.3.4.1. Potential Sources of Error

The difference in specimen size among testing programs is not expected to significantly affect the steady state test results. Source 3 concluded that a specimen diameter change from 7.6 cm to 15.2 cm had a negligible effect on the location of the steady state line for this material. Also, Johnson (1982) reports that comparative results from testing 3.6 cm and 7.1 cm diameter specimens of Ottawa (Banding) sand with a D_{50} of about 0.17 mm and a C_u of 1.58 indicate a negligible effect on the steady state line as determined from contractive stress-controlled triaxial tests.

However, membrane penetration has been shown to affect the pore pressure response during testing, and this effect may be accentuated by differing specimen sizes among the testing programs. Kiekbusch and Schuppener (1977) determined that the action of the membrane either into or out of the interstitial spaces at the perimeter of the specimen causes a higher dilative (or lower contractive) pore pressure response to be measured than would be experienced under undrained conditions in the field for a 'dense' or 'loose' sand, respectively. In their paper, the authors determine that the D_{50} grain size must be in the order of 0.1 mm or less for the membrane penetration effect on pore pressure response to be negligible. As the average D_{50} for the material investigated in the present study is about 0.18 mm, the membrane penetration effect may be noticeable. With a smaller specimen size, the perimeter area of the specimen is larger with respect to the overall volume, hence a larger error in pore pressure measurement due to membrane penetration would be expected in smaller specimens. As discussed in the paper, no correction is available for sands with D_{50} greater than 0.1 mm. The authors suggest that membrane penetration should be reduced by the use of a liquid rubber coating applied just before specimen assembly to allow the measurement of accurate pore pressures. No measures were taken to reduce the membrane penetration effect in the present study or the five source studies described above.

The influence of lubricated ends on the test results was not investigated but may be significant, especially for the pore pressure determination. When lubricated ends were not used, a length to diameter ratio of at least 1.5 was used for specimen preparation, as determined necessary for accurate strength determination in drained sands and undrained clays by Taylor (1941). However, the effects of non-lubricated end platens on the accurate determination of the pore pressure response are unknown.

4.4. Results

The present study test results are provided in Appendix C in the form of the stress-strain and pore pressure response curves, and the stress path (p' - q) plot. Also included is a summary sheet of measured and calculated values for each test. The test results for each of the five sources described above are included in their respective reports.

The results of the present study and the other testing programs outlined above were analyzed using two approaches. In the first approach (direct comparison), seven characteristics from each of the measured stress-strain curves were determined. These characteristics were compared among tests grouped according to similar pre-shear state (dry density and initial effective confining pressure, p_0') to determine if a consistent trend was apparent linking the fabric differences to the observed mechanical behaviour during triaxial shear. This includes both an examination of how the characteristics investigated vary when specimens with different sample preparation histories are compared, and how these parameters vary within the same sample preparation method (control group).

In the second approach (normalized comparison), the pre-shear state of the specimen is compared with the observed stress-strain test result, allowing the delineation of a 'behavioural boundary' between the contractive and dilative test results for this material.

Steady state characterization of the material is investigated, and a comparison is made between the dry density and relative density presentations of the steady state data. The concepts of relative density and state parameter are then used in relation with the behavioural boundary to analyze the data in a way that attempts to reduce the effect of small gradational differences in the material used in the testing programs on the moderate and large strain mechanical behaviour, thereby allowing fabric difference effects (if any) to be more easily isolated.

4.4.1. Direct Comparison

A number of tests are compared at the 'elbow' of the stress path plot (found in Appendix C for the present study tests). This point is chosen because of its uniqueness along the stress path, and is shown idealized in Figure 4.15 for both the contractive and dilative cases. In the contractive case, the elbow corresponds to the highest deviatoric stress encountered during shear, whereas in the dilative case, the elbow relates to the inflection point observed in the stress-strain response and the corresponding peak pore pressure response observed.

Variables compared at the elbow include the strain developed, deviatoric stress ($\sigma_1 - \sigma_3$), the change in pore pressure response, the pore pressure parameter 'A', the effective stress ratio (σ_1' / σ_3'), and the effective normal stress component ($p' = (\sigma_1' + \sigma_3') / 2$). As well, general characteristics of the stress-strain and pore pressure response curves were examined. These included the initial tangent modulus of the stress-strain curve and the initial modulus of pore pressure generation (foreslope modulus), defined as the slope of the initial portion of the pre-peak pore pressure-strain curve. The derivation of these parameters is shown in Figure 4.15.

Three tables are presented which display the results of the testing programs (Tables 4.4, 4.5, and 4.6). Table 4.4 shows the comparison of the above parameters measured at the elbow from tests performed at similar dry density conditions and p_o' levels but using different depositional methods. The results are ranked by increasing p_o' . Actual values of the test conditions and the parameters investigated are presented, along with the range observed in each condition or parameter. The data in this table were examined to determine if differences in the method of deposition are reflected in variations observed in the parameters studied.

In general, a wide scatter of the elbow data is observed with no specific trend observed with differing deposition techniques. Figures 4.16 to 4.19 allow a visual comparison of the parameters investigated among tests performed at similar initial effective confining pressures and dry densities. The results were ranked in terms of magnitude with respect to the other test(s) performed in that density and pressure range. In all cases, except in the case of the comparison of deviatoric stress (Figure 4.16a), no trend is obvious when the tests within each nominal p_o' range are compared. As well, the ranked order of the results (with respect to method of deposition) are not consistent across the parameters investigated within their respective p_o' ranges. In the case of the deviatoric stress (Figure 4.16a), a trend is observed up to $p_o'=500$ kPa where the stress level at the elbow consistently increases through the deposition methods in the order of compacted (lowest deviatoric stress), pluviated and flume (highest deviatoric stress). The single field result compared at the $p_o'=500$ kPa level is higher than that of the compacted sample. No physical explanation for this trend can be given at this time.

The above scatter of results are to be expected when an examination of Tables 4.5 and 4.6 is made. Table 4.5 is a comparison of tests performed at similar density and p_o' conditions, but this time with the same depositional method used to prepare the specimens.

This group of data acts as a control group to determine the expected scatter in the results and, when compared with ranges observed in Table 4.4, allows the determination of the relevance of the comparisons made among depositional methods. Table 4.6 compares directly the ranges observed in both the comparison group (Table 4.4) and the control group (Table 4.5). Even though the control group generally has a smaller range of test conditions (dry density and p_o'), observed ranges in the parameters are the same or larger than those of the comparison group. Since the control group is as variable as the comparison group, no meaningful comparison can be made with respect to the depositional method using this technique.

The above results are thought to be due to a combination of two phenomena. First, the effects of method of deposition on the observed parameters may be too small to be picked up with the triaxial test. Errors in measurement of load, pressure, and the determination of dry density could combine to be larger than the actual differences due to differing methods of deposition. However, the error due to testing is expected to be small in comparison to the ranges of the observed parameters outlined in Tables 4.4 to 4.6, especially since the rather large magnitude of observed differences in the control group are found both in comparisons of tests performed within laboratories as well as among laboratories.

The second phenomenon may be subtle material differences among compared specimens. As shown in Castro et. al. (1982), very small changes in the gradation and angularity of a sand have large effects on the steady state condition measured. Poulos (1971) found that the material characteristics of a sand have some influence on the stress-strain behaviour during triaxial shear, but the extent to which relatively small material changes (previously thought to be inconsequential) have on this behaviour is not well documented. If the minor material differences are important, a means to normalize the

behaviour in terms of these differences is necessary to effectively compare the results of the tests to better understand the effect of the placement technique (or fabric) on the stress-strain behaviour of this tailings sand.

4.4.2. Normalized Comparison

The pre-shear state of each specimen in relation to the type of stress-strain curve observed is first investigated for all testing programs (including the present study and Sources 1 through 5). The test results are grouped into three categories depending on the level of dilatancy exhibited, and a 'behavioural boundary' defined in terms relative density and initial effective confining pressure is determined between the observed contractive and dilative behaviour.

Secondly, the steady state characteristics of the material tested are studied in terms of dry density and relative density. The latter density format is found to 'tighten' the data closer to a line as expected by steady state theory for a single material. The behavioural boundary as determined from the pre-shear conditions is overlaid for comparison to the steady state condition.

Finally, the Relative Density (RD) parameter is developed, melding the concepts of relative density and state parameter. This parameter is used to analyze the data in a way that attempts to reduce the effect of small gradational differences in the material used in the testing programs on the moderate and large strain mechanical behaviour, thereby allowing fabric difference effects (if any) to be more easily isolated. The moderate strain parameters of initial tangent modulus, foreslope modulus, and the stress ratio and pore pressure parameter A at the elbow are compared with the RD parameter. Also compared is the steady state shear strength, revealing a strong correlation with the RD parameter.

4.4.2.1. Pre-Shear Conditions

The observed stress-strain curves were divided into three categories; contractive, contractive-dilative, and dilative (c, cd and d). These three idealized cases are represented in Figure 4.20, along with their respective pore pressure response and stress path curves, and are analogous to the conditions of liquefaction, limited liquefaction and dilation as described by Castro (1969). The distinction is made from Castro's terms to reinforce the fact that these terms (c, cd and d) are merely groupings of similar observed stress-strain/pore pressure response behaviour, and not initially linked to liquefaction or steady state behaviour.

The results of the testing programs were analyzed and grouped according to their likeness to one of the idealized cases. When the pre-shear state of each specimen is plotted in terms of dry density and effective confining pressure (p_o') with reference to the stress-strain curve type (Figure 4.21), two distinct regions are revealed. The boundary between these regions is relatively linear, and represents a delineation of the pre-shear state at which, after testing, a specimen will have behaved neither contractive nor dilative. This boundary is termed the behavioural boundary.

The data in Figure 4.21 does not exhibit a clean break between contractive and dilative tests. As well, the data that is borderline (contractive-dilative) is found completely within the scatter of contractive data. Ideally, three distinct zones should be apparent, with the contractive-dilative/dilative border falling above the steady state line for the material. This condition is observed in Figure 4.22 (adapted from Castro, 1969) and is eluded to in Poulos (1971, 1981) and Been and Jefferies (1985). One possible reason for three distinct zones not being apparent is small changes in material characteristics (such as D_{50} and C_u) among test specimens, which are known to have a significant effect on both the maximum

and minimum density determination and the steady state characteristics of the Syncrude tailings sand.

Figure 4.23 is a reproduction of the data found in Figure 4.21, except plotted in terms of relative density. The relative density is calculated using the maximum and minimum values determined from tests on the material used in each specific testing program as reported by the laboratories. A shift in the contractive-dilative data to a more central location between the contractive and dilative groups is apparent. It is possible that the relative density normalizes the data in terms of the differences in material among individual tests. This gives an indication that the relative density versus p_o' presentation may assist in comparing test specimens with slight material differences since these differences may be accounted for by the relative density determination.

4.4.2.2. Steady State Characterization

The effect of normalizing with relative density was observed above with the more rational characterization of stress-strain behaviour in terms of pre-shear specimen state. In this vein, the steady state condition (dry density versus effective stress during steady state deformation) was determined for the tailings sand studied, and compared with the same data analyzed in terms of relative density (Figures 4.24 and 4.25). Although it is recognized that the use of results of dilative tests to determine the steady state condition is considered less reliable than those of contractive tests taken to the steady state condition because of a higher likelihood of uneven distribution of void ratio and strains in the specimen (Poulos, 1971), the dilative results are plotted as well. Only those results that exhibited a constant effective stress and pore pressure response in the later stages of shear were used in the steady state characterization, and since specimens deformed uniformly to a large strain, errors due to uneven distribution of stress are likely to be small. As seen in

these figures, the present study results appear to tie in reasonably well with the data from the other sources. Some non-linearity of the steady state line in the higher stress ranges (greater than 1000 kPa) is apparent.

The relative density for each test was calculated using the reported maximum and minimum (max/min) densities determined for each source of material. Sources 2 and 5 did not report max/min density determinations for the tested material. However, Source 2 data plots similarly to Source 1 data in terms of dry density (similar slope and location of steady state line in Figure 4.24) and both testing programs were performed at the same laboratory, therefore the same max/min density determination was used for the relative density characterization of the data. The data from Source 5 was left out of the discussion, as was the field data from the present study, because of their highly variable gradational properties and hence no single set of max/min densities to represent them.

Plotting in terms of relative density had the effect of leaving the spatial relationship of the test data within each source group the same (except Source 3), but moved the groups of data around in relation to each other. In the case of the Source 3 program, max/min densities were reported for five different bag samples, from which the test specimens were created. The value used for each specific test result corresponded to the max/min densities determined for the bag of tailings sand from which the specimen was prepared, not an average of the reported values. Max/min tests for all other sources were performed on material pre-mixed prior to testing and use in specimen preparation, therefore an average value for the maximum and minimum densities was used. A list of the reported gradational characteristics, max/min densities and the method used to determine these values for the present and Source 1 to 5 studies is presented in Table 4.7.

To allow the direct comparison of the steady state data presented in terms of dry density with that formulated with relative density, the relative density plot (Figure 4.25) was drawn such that the absolute vertical distance between any two points within the same source group (except Source 3, for the reasons outlined previously) is the same as the distance measured in the dry density plot. This allows direct comparison of the two figures because the data within individual source groups using the same max/min determination in the calculation of relative density do not change spatially with respect to one another.

As can be seen with the comparison of the data in Figures 4.24 and 4.25, a reduction in the scatter in the order of 45% is evident in the relative density presentation method, in the working stress range of 20 to 1000 kPa. It is especially evident that the data points from Sources 1 and 2 are shifted closer to the other source data. It is postulated that the material used in Sources 1 and 2 is of a somewhat different composition than that of the other source materials, and that the differing nature affects both the steady state condition and the max/min density determination in a similar way such that plotting in terms of relative density somewhat compensates for the difference. This result is again an indication that the relative density analysis may have a unifying effect on the steady state determination for materials with small but significant gradational differences.

A similar comparison is made using data published in Castro et. al. (1982). Figure 4.26a shows the steady state condition for five different gradations of Banding sand, characterized as uniform with fine subrounded quartz particles and few fines (less than 1.5% passing the #200 sieve) and having slightly different uniformity coefficients ranging from 1.35 to 1.80. Reported max/min density values for each gradation were used to re-analyze the data in terms of relative density, and are re-plotted in Figure 4.26b at a scale that allows the direct visual comparison of the scatter as outlined previously. Again a reduction in the scatter is apparent, especially among the four gradations with which the

same method of max/min density determination was used. Castro et. al. (1982) also uses the presentation method of percent compaction (in this case a percentage of the reported minimum void ratio from the maximum density test), and a similar result is obtained. While these presentation methods do not unify the steady state line completely for small variations in material characteristics, they do show a trend toward a more unified steady state condition.

This trend of the relative density towards unifying the presentation of the steady state condition is postulated to occur because changes in material characteristics such as the shape of the grain size curve, and the angularity, mineralogy, and surface texture of the constituent particles are known to affect both the location of the steady state line and the magnitudes of the maximum and minimum densities for sands.

A re-working of the data in terms of relative density was again performed on the data available for this study. In this portion of the analysis the tailings sand was characterized by means of maximum and minimum density tests performed on artificially prepared gradations of the tailings sand from material retained on sieves spanning the range of gradations observed in the testing programs. This investigation is described in detail in Kupper, 1991. In this investigation, the tailings sand max/min density determination was found to be significantly dependent on the D_{50} and C_u of the material, but only marginally dependent on the fines content and then only in the maximum density determination. It was therefore considered that a reasonable representation of the sand in terms of relative density and gradational characteristics could be made by plotting the measured maximum and minimum densities against the D_{50} for the material tested, resulting in the development of a family of curves of varying C_u . The family of curves is shown in Figure 4.27, along with the measured average values of max/min density and material characteristics reported by the other sources of data.

The trend of the present max/min representation is that of increasing max/min density determination with increasing C_u and D_{50} . Both these trends have been observed in the literature (as described in Kupper, 1991), but a link to fines content is usually observed as well. In this study, the fines content was found to be loosely related to the C_u of the soil, as is expected because of the formulation of the C_u parameter and the proximity of the D_{10} size to the #200 sieve size (0.075 mm).

As the fines content increases, D_{10} decreases substantially for gradations with similar shapes, as shown in Figure 4.28. Therefore a change in C_u is often actually representing a change in fines content as well. The marked change in max/min density with small D_{50} variations was not expected but may be explained by the recognition that the smaller particles within a mass of granular materials often display less angularity than the larger particles. This may occur due to gravitational effects on the original material during transport and deposition over geological time (Twenhofel, 1950), or during the bitumen extraction process prior to placement. This would suggest that the trend with D_{50} is actually due to differences in average particle angularity, but a change in angularity with particle size among the observed SEM samples (Chapter 3) was not apparent.

The average results of the max/min density tests performed in the previous studies (Sources 1 to 5) are plotted on Figure 4.27. Reasonable fit with the present study's maximum density representation is seen with all determinations except in tests representing Sources 1 and 2, but the results of the minimum density determination from the previous studies would indicate that little variation in minimum density with C_u is to be expected. From this plot, the material used in the investigations of Sources 1 and 2 appears to be significantly different from the other materials. This supports the premise that the differing steady state condition for the Source 1 and 2 data (as observed previously in Figure 4.24) can be explained using material variance reasoning alone. This difference in location of the

steady state points from the other data has previously been accounted for by the assumption of a systematic error in the void ratio determination (Sladen and Handford, 1987), but it is plausible that material differences and void ratio measurement errors could act together to cause the observed difference.

In an attempt to reduce the scatter of the steady state results even more, the individual max/min densities for each specimen were assumed based on the results of sieve analyses performed on each specimen after the triaxial shear was performed. Figures 4.29 and 4.30 were developed using the measured D_{50} and C_u from the gradation curve for each specimen, or an estimate of these values based on a grain size analysis performed on another specimen or proximal sample considered to be most representative of the tested specimen. Individual specimen gradations were not determined for the data of Sources 1 and 3, therefore the gradational characteristics were taken from the data available on the bulk samples. Source 5 and the present study (field) data were included for completeness.

Maximum and minimum density values were assumed from Figures 4.29 and 4.30, and used to determine a specimen specific relative density. It is noted that most of the material tested falls within the range of C_u 's and D_{50} 's used to determine the representative max/min density. These figures are useful to develop a better understanding of the variation of material characteristics within and among source groups and the data of the present study. Source 3, 4 and the present study (pluviated) results are found to be the most consistent in terms of the D_{50} , while Source 2 and the present study (flume) results show significant variation in this parameter. It is observed, however, that the variation in C_u is very similar within groups, but average C_u values vary significantly among the groups presented here.

The steady state condition in terms of relative density was re-worked again, this time using the specimen specific max/min density determination to calculate the relative density. The same relative density scale was used to allow direct comparison to the two previously developed steady state condition plots. The scatter appeared larger than that of the relative density plot using the reported max/min density values both within and among data groups. It is felt that the errors associated with the grain size analysis of individual samples (especially across laboratories), and the difference between reported and artificially represented max/min density determinations (Figure 4.27) make this method of analysis impractical for further refinement of the unification of the stress-strain behaviour (or the steady state lines) for this material. This method may have merit if better control of the determination of the grain size properties can be ensured (ie. a single technician performing all sieve analyses in a consistent manner) and if a more comprehensive study were undertaken to establish the effects of parameter variability on the maximum and minimum density for the specific material tested.

4.4.2.3. Relative Density Parameter

Test results were compared as a whole by plotting the parameter of interest against a parameter developed to attempt to normalize the expected behaviour in terms of density, effective confining pressure (p_o'), and the material differences observed among source materials. The impetus for the development of this parameter came from the desire to compare test results in a rational manner such that the differences due to fabric (if any) could be isolated. A hybrid of two existing normalizing concepts is used; relative density and the state parameter. The development of this parameter and the results of its use are described below.

To allow the comparison of the available data to determine the effects of method of preparation (or initial fabric) on the stress-strain behaviour and the pore pressure response, the Relative Density (RD) parameter was derived from the relation of p_o' to the observed stress-strain behaviour in terms of relative density (Figure 4.23). The RD parameter takes advantage of the state parameter concept developed by Been and Jefferies (1985).

The state parameter is a measure of the void ratio difference between the 'pre-shear' and 'steady' states of a specimen or soil mass, at the pre-shear effective confining pressure (p_o') as shown in Figure 4.31. The concept implies that the magnitude of the distance (in terms of void ratio) from the steady state line is in some way linked with the change in observed stress-strain behaviour, where negative values indicate dilative behaviour and positive values indicate contractive behaviour.

Numerous large strain parameters have been found to correlate well with the state parameter, as outlined in the paper, and the scatter observed is attributed partially to the lack of consideration of sand fabric and anisotropy. As the effects of fabric on the behaviour is of interest in this study, the state parameter method could possibly be used directly to determine fabric effects. This method, however, relies on the accurate knowledge of the steady state line for the particular specimen or mass of soil being analyzed. As the material differences of the specimens studied in the present program are significant, even within the individual groups of data (specifically sources 2 and 5, and the present study (flume) results shown in Figures 4.29 and 4.30), this approach is not directly applicable because of the difficulty in assigning a steady state void ratio to a particular specimen.

Castro (1987) presents a design concept to correct for differences in laboratory and in-situ conditions. Using the steady state void ratio and shear strength determined in a CU test on an undisturbed specimen, an "in-situ" steady state line is drawn parallel to that

determined from remoulded specimens, as shown in Figure 4.32. This would allow the state parameter to be determined for a particular specimen, but requires steady state testing on a large number of specimens to determine the behaviour of a large and variable volume of soil.

To attempt to circumvent this problem, the RD parameter was developed from Figure 4.23. The behavioural boundary line shown through the data is an estimate of the delineation between contractive and dilative behaviour for this material as a whole. As previously discussed, the relative density presentation of this data appears to give more clarity to this division, probably due to its normalizing effect on material differences. This behavioural boundary is overlain on the relative density steady state condition plot (Figure 4.25) to show its relation to the steady state data from each source group. Similar to the state parameter concept, the vertical distance (in terms of relative density) from the behavioural boundary line (on Figure 4.23) is used to normalize the observed stress-strain response, with a negative value corresponding to the dilative case. This approach would appear, in theory, to allow relative density to compensate for material differences while the measure from the 'balance point' of observed stress-strain behaviour would account for differences in behaviour expected due to the pre-shear state (void ratio/effective confining pressure). The steady state line was not used as the balance point because of the difficulty in assigning a single line to the data.

As an example of the expected benefit of this characterization of the data, the following hypothetical discussion is presented. The initial tangent modulus is expected to increase with a shift from contractive to dilative behaviour because of less 'compliance' in the sand skeleton due to the closer proximity of individual sand grains in the dilative specimen. If the RD parameter were to normalize the behaviour completely in terms of state and material differences, any difference observed between data grouped by

preparation method may then be attributed to differences in initial fabric. Although the RD parameter is not expected to completely normalize the data, it is possible that the scatter in the results as displayed by the control group in the direct comparison of Section 4.4.1 may be reduced using this approach.

Results of the comparison of the RD parameter with various moderate strain parameters (initial tangent and foreslope moduli, and Skempton's A parameter and the stress ratio at the elbow) are presented and discussed in Appendix E. No tight correlation of these parameters with the RD parameter appear to exist for this data set.

The steady state shear strength, defined as half of the deviatoric stress at the large strain steady state, is related to the RD parameter in Figure 4.33 for the tests in which steady state behaviour was exhibited. A strong correlation is evident, with a lower steady state shear strength occurring in specimens with higher RD parameter values, but significant scatter is present, especially for the contractive specimens. No specific trend due to method of placement is expected or observed in this plot, but this relation illustrates that a lower bound shear strength could be estimated for design or risk assessment purposes from a plot such as this with the knowledge of the in-situ relative density and its relation to the behavioural boundary, and the stress state.

4.5. Summary of Results

From the results of the present study and the other testing programs outlined above, the general conclusion is made that the mechanical behaviour as exhibited in the triaxial compression test does not appear to be affected significantly by the initial fabric or methods of specimen preparation studied herein for the tailings sand examined. It is apparent that small changes in the gradational characteristics of the tailings sand affect the steady state

behaviour of this material significantly, but this study is inconclusive as to the impact of gradational changes on the moderate strain parameters studied (initial tangent modulus, foreslope modulus, stress ratio and A parameter at the elbow).

The pre-shear state of the specimen is found to be directly related to the 'dilatancy' observed in the stress-strain and pore pressure response curves for this material during undrained triaxial testing. A behavioural boundary is determined between contractive and dilative behaviour, and this boundary is especially clear when the state is determined in terms of relative density.

The steady state condition for this material is not well defined using this data set, but a reduction in the scatter of results in the order of 45% is apparent when relative density is used to represent the state of the specimens tested. This is thought to be due to a normalizing effect of relative density on the slight gradational differences between the source materials used in the various testing programs. Refinement of the relative density to a 'per-specimen' basis by inferring individual maximum and minimum densities for each specimen based on its gradation did not further reduce the scatter of results.

Steady state characterization of this material using dilative test results is possible. Successful linkage of the contractive and dilative results is attributed to the use of lubricated ends on oversized platens, and specimens sized with a length to diameter ratio of close to unity. These test conditions allowed relatively uniform straining to occur to a point where steady state conditions were achieved (generally 15% to 30% axial strain).

The RD parameter did not correlate well with the moderate strain parameters investigated, although some of the individual data groups trended in expected directions relevant to the dilativeness of the individual specimens. A strong correlation did occur

between the RD parameter and the steady state shear strength, allowing a lower bound strength to be estimated based on the proximity of the field state to the behavioural boundary determined for this material.

DRY DENSITY (Mg/m ³)	MEASUREMENT	WAX DISPLACEMENT
MEAN	1.681	1.688
STANDARD DEVIATION	0.030	0.028
COEFFICIENT OF VARIATION (%)	1.8	1.7

- a. COMPARISON OF 14 SPECIMENS USING
TWO DENSITY PREPARATION TECHNIQUES

DRY DENSITY (Mg/m ³)	VERTICAL Positions A, B, C, D	HORIZONTAL Level 2
MEAN	1.688	1.676
STANDARD DEVIATION	0.026	0.028
COEFFICIENT OF VARIATION (%)	1.6	1.7
# OF SPECIMENS	16	15

- b. COMPARISON OF VERTICAL AND HORIZONTAL DENSITY
VARIATION USING WAX/DISPLACEMENT TECHNIQUE

**TABLE 4.1 DRY DENSITY VARIATION DUE TO
METHOD AND SPATIAL LOCATION**

Program - PRESENT STUDY										
Method of Placement	Test	Pre-shear Dry Density (Mg/m ³)	Init. Effective Con. Pressure (kPa)	Cu	D50 (mm)	Fines Content < #200 sieve (%)	Stress-Strain Curve Type			
pluviated	PL 2	1.544	194.5	1.79	0.165	5.7	dilatative			
	PL 3	1.554	54.4	1.79	0.165	5.7	dilatative			
	PL 5	1.548	17.6	1.86	0.162	6.1	dilatative			
	PL 6	1.527	15.4	1.72	0.156	4.8	dilatative			
	PL 7	1.531	22.9	1.81	0.155	5.8	dilatative			
	PL 8	1.523	23.5	1.78	0.154	-	dilatative			
	PL 9	1.567	802.8	1.88	0.160	-	contractive-dilatative			
	PL 10	1.592	423.3	2.15	0.156	8.8	dilatative			
	PL 12	1.570	1282.8	1.75	0.167	5.8	contractive-dilatative			
	PL 13	1.536	48.4	2.05	0.154	8.3	dilatative			
	PL 14	1.568	395.2	2.05	0.154	8.3	dilatative			
	PL 15	1.535	51.0	1.94	0.155	7.1	dilatative			
	PL 16	1.550	255.9	2.05	0.154	8.3	dilatative			
	PL 17	1.534	121.6	2.03	0.163	5.6	dilatative			
	PL 19	1.555	396.9	1.91	0.163	7.0	dilatative			
	flume	FL 2	1.551	199.2	1.49	0.180	1.6	dilatative		
		FL 3	1.539	40.8	1.80	0.141	8.1	dilatative		
		FL 4	1.560	14.9	1.83	0.204	3.5	dilatative		
		FL 5	1.567	15.7	1.83	0.166	5.7	dilatative		
FL 6		1.604	441.9	1.82	0.189	5.3	dilatative			
FL 7		1.570	19.4	1.90	0.173	6.6	dilatative			
FL 8		1.550	17.6	1.58	0.164	-	dilatative			
FL 9		1.525	393.6	1.63	0.193	5.4	dilatative			
FL 10		1.578	973.8	1.56	0.166	-	dilatative			
UF 1		1.545	325.5	1.72	0.155	-	dilatative			
undisturbed (field)	FD 1	1.575	1030.0	2.19	0.167	7.2	dilatative			
	FD 2	1.646	393.5	2.19	0.167	7.2	dilatative			

TABLE 4.2: SPECIMEN STATE SUMMARY

Program - SOURCES 1 AND 2

Method of Placement	Test	Pre-shear Dry Density (Mg/m ³)	Init. Effective Con. Pressure (kPa)	Qu	D50 (mm)	Fines Content < #200 sieve (%)	Stress-Strain Curve Type
SOURCE 1 compacted	R-41	1.424	588.4	2.09	0.164	7.0	contractive-dilatative
	R-42	1.414	588.4	2.09	0.164	7.0	contractive
	R-43	1.406	588.4	2.09	0.164	7.0	contractive
	R-44	1.413	588.4	2.09	0.164	7.0	contractive
	R-45	1.458	1176.7	2.09	0.164	7.0	contractive-dilatative
SOURCE 2 compacted	R-5	1.349	105.9	1.86	0.176	2.7	contractive
	R-6	1.400	105.9	1.74	0.170	4.3	contractive-dilatative
	R-10	1.360	196.1	1.63	0.138	4.8	contractive
	R-11	1.371	98.1	1.96	0.126	11.8	contractive

Program - SOURCE 3

pluviated/ tapped	R-1A	1.453	94.0	1.84	0.160	5.4	contractive-dilatative
	R-3	1.498	96.0	1.80	0.162	5.4	dilatative
	R-4A	1.422	99.0	1.83	0.162	5.4	contractive
	R-5	1.431	101.0	1.80	0.162	5.4	contractive
	R-6	1.386	106.0	1.80	0.162	5.4	contractive
	R-7	1.438	97.0	1.84	0.160	5.5	contractive
	R-8	1.459	98.0	1.84	0.160	5.5	contractive-dilatative
	R-9	1.535	93.0	1.84	0.160	5.5	dilatative
compacted	R-10	1.473	92.0	1.84	0.160	5.5	dilatative
	R-11	1.542	1001.0	1.84	0.160	5.5	dilatative
	R-12A	1.472	1000.0	1.87	0.171	5.4	contractive-dilatative
	R-13	1.477	1000.0	1.87	0.171	5.4	contractive-dilatative

TABLE 4.2: SPECIMEN STATE SUMMARY

Program - SOURCE 4

Method of Placement	Test	Pre-shear Dry Density (Mg/m ³)	Init. Effective Con. Pressure (kPa)	Qu	D50 (mm)	Fines Content < #200 sieve (%)	Stress-Strain Curve Type
compacted	CU-1	1.533	1079.3	2.30	0.173	7.8	contractive
	CU-2	1.489	1079.3	2.33	0.168	7.4	contractive
	CU-3	1.479	95.1	2.32	0.167	7.2	contractive
	CU-4	1.538	1100.0	2.43	0.178	7.6	contractive
	CU-5	1.502	500.0	2.37	0.169	6.8	contractive
	CU-6	1.521	203.4	2.50	0.173	9.1	contractive
	CU-7	1.462	255.8	2.54	0.179	9.4	contractive
	CU-8	1.471	310.3	2.44	0.167	8.2	contractive
	CU-9	1.529	1199.7	2.50	0.173	8.1	contractive-dilative
	CU-10	1.573	1199.7	2.47	0.179	7.3	dilative
	CU-11	1.514	799.8	2.40	0.172	7.4	contractive
	CU-12	1.483	299.9	2.42	0.171	7.7	contractive

Program - SOURCE 5

compacted	T-31	1.427	50.7	3.00	0.140	13.5	contractive
	T-32	1.453	201.4	3.00	0.140	13.5	contractive
	T-33	1.523	500.3	3.00	0.140	13.5	contractive-dilative
undisturbed (field)	3-B	1.586	504.9	1.60	0.135	7.5	dilative
	4-B	1.519	512.7	3.00	0.132	31.0	dilative

TABLE 4.2: SPECIMEN STATE SUMMARY

3 OF 3

SOURCE	METHOD OF PREPARATION	SPECIMEN DIMENSIONS		FRICTIONLESS ENDS	TYPE OF CONSOLID'N	STRAIN RATE† (%/min)
		HEIGHT (mm)	DIAMETER (mm)			
Present Study	pluviated flume undisturbed	42 77 (UF1)	37 51 (UF1)	yes (except UF1)	isotropic	0.6
1	compacted	108	73	yes	isotropic	0.5
2	compacted	157	73	no	isotropic*	0.2
3	pluv/tapped compacted	114 259	76 152	yes	isotropic	0.1 to 0.2
4	compacted	105 150 (CU9 & CU10)	70	yes no (CU9 & CU10)	isotropic*	0.6 to 0.8
5	pluv/vibrat'n compacted undisturbed	150	75	no	isotropic	0.1

Notes: † All tests performed undrained using strain-controlled loading.

* Some tests were consolidated anisotropically and were not used in the comparison.

TABLE 4.3: TRIAXIAL TESTING CONDITIONS SUMMARY

TEST CONDITIONS		VALUE AT ELBOW									
Method of Deposition	Test (Program)	Ave. Dry Density (Mg/m ³) [range]	Ave. Initial Con. Pressure (kPa) [range]	Strain (%) [range]	Deviatoric Stress (kPa) [range]	ΔPP (kPa) [range]	A [range]	Stress Ratio [range]	$p' = (\sigma_3)^{1/2}$ (kPa) [range]	Init. Tangent Modulus (kPa) x1000 [range]	Foreslope (kPa) x1000 [range]
pluviated flume	PL 5 (Present Study)	1.548	17.6	2.7	-	15.1	-	-	2.1	8.0	1.28
	FL 5 (Present Study)	1.567 [0.019]	15.7 [1.9]	0.8 [1.9]	-	8.5 [6.6]	-	-	5.8 [3.7]	-	1.33 [0.05]
pluviated flume	PL 15 (Present Study)	1.535	51.0	1.2	4.1	18.3	4.47	1.13	34.8	-	2.51
	FL 3 (Present Study)	1.539 [0.004]	40.8 [10.2]	1.1 [0.1]	6.1 [2.0]	19.7 [1.4]	3.23 [1.24]	1.29 [0.16]	24.4 [10.4]	-	1.81 [0.70]
pluviated compacted	R-3 (Source 3)	1.498	96.0	1.5	59.0	63.0	1.08	2.81	61.5	32.0	23.0
	CU-3 (Source 4)	1.479 [0.019]	95.1 [0.9]	0.5 [1.0]	58.3 [0.7]	21.1 [41.9]	0.37 [0.71]	1.77 [1.04]	102.5 [41.0]	19.1 [12.9]	5.3 [17.7]
pluviated compacted	R-4A (Source 3)	1.422	99.0	0.3	43.0	52.0	1.21	1.94	65.0	16.5	15.0
	R-11 (Source 2)	1.371 [0.051]	98.1 [0.9]	0.4 [0.1]	30.8 [12.2]	52.3 [0.3]	1.70 [0.49]	-	66.7 [1.7]	13.4 [3.1]	14.4 [0.6]
pluviated compacted	R-6 (Source 3)	1.386	106.0	1.0	46.0	43.0	0.95	1.71	85.0	8.3	9.2
	R-5 (Source 1)	1.349 [0.037]	105.9 [0.1]	0.7 [0.3]	46.1 [0.1]	77.3 [34.3]	1.68 [0.73]	-	75.5 [9.5]	11.5 [3.2]	9.6 [0.4]
pluviated flume compacted	PL 2 (Present Study)	1.544	194.5	0.6	130.9	62.6	0.48	1.99	197.2	27.4	9.9
	FL 2 (Present Study)	1.551	199.2	0.2	316.4	162.6	0.29	2.06	235.1	55.0	14.9
pluviated compacted	CU-6 (Source 4)	1.521 [0.030]	203.4 [8.9]	0.9 [0.7]	112.0 [204.4]	96.1 [100.0]	0.87 [0.58]	2.04 [0.07]	163.3 [71.8]	33.2 [27.6]	14.8 [5.0]
	PL 10 (Present Study)	1.592	423.3	0.6	284.1	207.3	0.73	2.33	355.9	92.8	21.0
pluviated flume	FL 6 (Present Study)	1.604 [0.012]	441.9 [18.6]	0.9 [0.1]	301.7 [17.6]	222.1 [14.8]	0.74 [0.01]	2.39 [0.08]	368.6 [12.7]	123.0 [30.2]	40.7 [19.7]
	T-33 (Source 5)	1.523	500.3	3.4	210.4	393.7	1.87	2.97	213.2	46.4	41.4
pluviated field	4-B (Source 5)	1.519 [0.004]	512.7 [12.4]	2.1 [1.3]	334.9 [124.5]	355.4 [38.3]	1.06 [0.81]	3.09 [0.12]	327.4 [114.2]	35.6 [10.8]	33.0 [8.4]
	PL 12 (Present Study)	1.570	1282.8	1.7	965.5	671.5	0.70	2.58	1095.3	347.4	67.5
pluviated compacted	CU-10 (Source 4)	1.573 [0.003]	1199.7 [83.1]	2.5 [0.8]	1098.8 [133.3]	591.6 [79.9]	0.57 [0.13]	2.81 [0.23]	1157.7 [62.4]	108.0 [239.4]	37.3 [30.2]

Table 4.4: STRESS-STRAIN/PORE PRESSURE RESPONSE PARAMETERS AT ELBOW COMPARISON AMONG METHODS OF DEPOSITION

Method of Deposition	TEST CONDITIONS			AVERAGE AT ELBOW					AVERAGE		
	Tests	Ave. Dry Density (Mg/m ³) [range]	Ave. Initial Con. Pressure (kPa) [range]	Strain (%) [range]	Deviatoric Stress (kPa) [range]	ΔPP (kPa) [range]	A [range]	Stress Ratio [range]	p'=(sigma1'+sigma3')/2 (kPa) [range]	Init. Tangent Modulus (kPa) x1000 [range]	Foreslope (kPa) x1000 [range]
flume	FL 5	1.568 [0.003]	17.6 [3.7]	0.75 [0.1]	3.9	8.3 [0.5]	2.05	1.34	9.6 [7.5]	-	1.6 [0.6]
	FL 7	1.527 [0.008]	20.6 [8.1]	0.7 [0.6]	6.6 [2.2]	7.0 [11.1]	1.07 [2.33]	1.52 [0.55]	18.1 [12.6]	-	3.0 [2.5]
pluviated	PL 6	1.536 [0.001]	49.7 [2.6]	1.2	4.1	18.3	4.47	1.13	34.8	11.6	2.5
	PL 7	1.456 [0.008]	96.0 [4.0]	0.4 [0.5]	49.0 [6.0]	28.5 [17.0]	0.56 [0.30]	1.75 [0.20]	82.5 [15.0]	22.7 [25.4]	10.7 [9.5]
pluviated	R-1A	1.435 [0.007]	99.0 [4.0]	0.4 [0.6]	43.0 [6.0]	46.0 [12.0]	1.12 [0.16]	1.81 [0.22]	72.5 [9.0]	27.5 [28.7]	27.9 [38.8]
	R-8	1.477 [0.012]	305.1 [10.4]	0.5 [0.4]	138.7 [17.6]	128.4 [6.4]	0.97 [0.05]	1.79 [0.18]	246.2 [7.9]	61.5 [40.7]	35.8 [22.0]
compacted	CU-8	1.562 [0.013]	396.1 [1.7]	1.1 [0.3]	169.7 [40.4]	179.4 [38.0]	1.09 [0.49]	1.79 [0.07]	300.8 [53.5]	110.9 [132.3]	24.2 [2.2]
	CU-12	1.414 [0.018]	588.4 [0.0]	0.8 [0.3]	289.2 [99.4]	254.1 [80.8]	0.91 [0.57]	2.19 [1.11]	429.1 [14.7]	69.8 [56.0]	40.8 [7.3]
pluviated	R-41	1.475 [0.005]	1000.0 [0.0]	1.1 [0.7]	445.0 [20.0]	489.0 [52.0]	1.11 [0.14]	1.86 [0.05]	746.5 [63.0]	125.0 [16.0]	81.8 [27.6]
	R-13	1.536 [0.005]	1069.7 [20.7]	0.8 [1.3]	547.2 [234.6]	470.9 [67.5]	0.94 [0.57]	1.88 [0.25]	892.5 [205.5]	94.2 [33.6]	42.4 [19.5]
compacted	CU-1	1.474 [0.031]	1128.0 [97.4]	1.2 [0.2]	650.6 [176.5]	374.9 [138.0]	0.60 [0.38]	1.89	906.9 [19.4]	119.5 [13.0]	39.7 [0.8]
	CU-2										

Table 4.5: STRESS-STRAIN/PORE PRESSURE RESPONSE PARAMETERS AT ELBOW CONTROL GROUP

Nominal Initial Con. Pressure (kPa)	Group	RANGE OF OBSERVED VALUES										
		Dry Density (Mg/m ³)	Initial Con. Pressure (kPa)	Strain (%)	Deviatoric Stress (kPa)	ΔPP (kPa)	A	Stress Ratio	p'=(sigma1'+ sigma3')/2 (kPa)	Init. Tangent Modulus (kPa) x1000	Foreslope (kPa) x1000	
20	Control	0.003 - 0.008	3.7 - 8.1	0.1 - 0.6	2.2	0.5 - 11.1	2.33	0.55	7.5 - 12.6	-	-	0.6-2.5
	Comparison	0.019	1.9	1.9	-	6.6	-	-	3.7	-	-	0.05
50	Control	0.001	2.6	-	-	-	-	-	-	-	-	-
	Comparison	0.004	10.2	0.1	2.0	1.4	1.24	0.16	10.4	-	-	0.7
100	Control	0.006 - 0.007	4.0	0.5 - 0.6	6.0	12.0 - 17.0	0.16 - 0.30	0.20 - 0.22	9.0 - 15.0	25.4-28.7	-	9.5-38.8
	Comparison	0.019 - 0.051	0.1 - 0.9	0.1 - 1.0	0.1 - 12.2	0.3 - 41.9	0.49 - 0.73	1.04	1.7 - 41.0	3.1-12.9	-	0.4-17.7
200	Control	-	-	-	-	-	-	-	-	-	-	-
	Comparison	0.030	8.9	0.7	204.4	100.0	0.58	0.07	71.8	27.6	-	5.0
300	Control	0.012	10.4	0.4	17.6	6.4	0.05	0.18	7.9	40.7	-	22.0
	Comparison	-	-	-	-	-	-	-	-	-	-	-
400	Control	0.013	1.7	0.3	40.4	38.0	0.49	0.07	53.5	132.3	-	2.2
	Comparison	0.012	18.6	0.1	17.6	14.8	0.01	0.06	12.7	30.2	-	19.7
500	Control	0.018	0.0	0.3	99.4	80.8	0.57	1.11	14.7	56.0	-	7.3
	Comparison	0.004	12.4	1.3	124.5	38.3	0.81	0.12	114.2	10.8	-	8.4
1000	Control	0.005	0.0	0.7	20.0	52.0	0.14	0.05	63.0	16.0	-	27.6
	Comparison	-	-	-	-	-	-	-	-	-	-	-
1200	Control	0.005	20.7	1.3	234.6	67.5	0.57	0.25	205.5	33.6	-	19.5
	Comparison	-	-	-	-	-	-	-	-	-	-	-
1200	Control	0.031	97.4	0.2	176.5	138.0	0.38	-	19.4	13.0	-	0.8
	Comparison	0.003	83.1	0.8	133.3	79.9	0.13	0.23	62.4	239.4	-	30.2

Table 4.6: STRESS-STRAIN/PORE PRESSURE RESPONSE PARAMETERS AT ELBOW
COMPARISON OF RANGES OF OBSERVED VALUES BETWEEN CONTROL AND COMPARISON GROUPS

PROGRAM	FINES CONTENT %	D 50 mm	Cu	DRY DENSITY		METHOD OF DETERMINATION OF MAXIMUM AND MINIMUM DENSITY
				Maximum Mg/m ³	Minimum Mg/m ³	
PRESENT STUDY 6 sieves (average) 10 max/min tests (average)	5.6	0.159	1.81	1.639	1.410	ASTM D4254-83 MAXIMUM - Method 1A MINIMUM - Method A
SOURCE 1 As Reported	7.0	0.160	2.06	1.616	1.280	Max ASTM D2049 (Wet) Min ASTM D2049 (Oven Dried)
SOURCE 3 BAG #1 (1 seive) 2 MAX, 3 MIN (average)	4.8	0.162	1.56	1.604	1.380	Max ASTM D2049 (Wet) Min ASTM D2049 (Oven Dried)
BAG #2 (2 sieves, average) 2 MAX, 2 MIN (average)	5.2	0.169	1.87	1.636	1.374	Max ASTM D2049 (Wet) Min ASTM D2049 (Oven Dried)
BAG #3 (2 sieves, average) 2 MAX, 2 MIN (average)	5.1	0.168	1.75	1.647	1.358	Max ASTM D2049 (Wet) Min ASTM D2049 (Oven Dried)
BAG #2-3 (1 seive) 2 MAX, 3 MIN (average)	5.4	0.162	1.83	1.647	1.398	Max ASTM D2049 (Wet) Min ASTM D2049 (Oven Dried)
BAG #5 (2 sieves, average) 3 MAX, 2 MIN (average)	5.5	0.167	1.89	1.597	1.386	Max ASTM D2049 (Wet) Min ASTM D2049 (Oven Dried)
AVERAGE	5.2	0.166	1.78	1.626	1.379	

TABLE 4.7: Average Gradational and Max/Min Properties

PROGRAM	FINES CONTENT %	D 50 mm		DRY DENSITY		METHOD OF DETERMINATION OF MAXIMUM AND MINIMUM DENSITY
				Maximum Mg/m ³	Minimum Mg/m ³	
SOURCE 4 INITIAL SAMPLE						
1	6.0	0.181	2.41	1.729	1.392	Max ASTM D2049 (Wet) Min ASTM D2049 (Oven Dried) ASTM D2049 (Air Dried)
2	5.5	0.172	2.40		1.401	
3	5.7	0.178	2.35		1.412	ASTM D2049 (Air Dried)
4	5.4	0.181	2.42		1.413	ASTM D2049 (Air Dried)
5	6.1	0.179	2.40		1.419	ASTM D2049 (Oven Dried)
6	5.8	0.181	2.42		1.413	ASTM D2049 (Oven Dried)
7	6.8	0.178	2.43		1.415	ASTM D2049 (Oven Dried)
8	5.8	0.177	2.40	1.751	1.429	Max ASTM D2049 (Wet) Kolbuszewski(1948) (Air Dried) ASTM D2049
9	5.8	0.171	2.39	1.758		
10	5.6	0.177	2.37	1.756		ASTM D2049
11	6.0	0.178	2.43	1.763		ASTM D2049
12	5.4	0.184	2.40	1.752		ASTM D2049
12	5.0	0.183	2.40	1.753		ASTM D2049
AVERAGE	5.8	0.178	2.40	1.752	1.412	

TABLE 4.7: Average Gradational and Max/Min Properties

PROGRAM	FINES CONTENT %	D50 mm	Cu	DRY DENSITY		METHOD OF DETERMINATION OF MAXIMUM AND MINIMUM DENSITY
				Maximum Mg/m ³	Minimum Mg/m ³	
SOURCE 5 BAG A 3 sieves (average) 5 min tests	5.4	0.189	1.93		1.404	ASTM D4254-83 - Method A
	5.3	0.187	2.04		1.410	ASTM D4254-83 - Method A
PAIL B B1	5.0	0.185	1.90		1.409	ASTM D4254-83 - Method A
B2	5.0	0.187	1.89		1.409	ASTM D4254-83 - Method A
B3	5.1	0.186	1.89		1.411	ASTM D4254-83 - Method A
B4	5.5	0.184	1.89		1.408	ASTM D4254-83 - Method A
B5	5.6	0.182	1.87	1.727		ASTM D4254-83 - Method 1A
B6	5.1	0.190	1.92	1.722		ASTM D4254-83 - Method 1A
B7	5.4	0.189	1.94	1.725		ASTM D4254-83 - Method 1A
B8	5.4	0.186	1.92	1.717		ASTM D4254-83 - Method 1A
B9	5.4	0.185	1.92	1.724		ASTM D4254-83 - Method 1A
B10	5.3	0.186	1.92	1.723		ASTM D4254-83 - Method 1A
AVERAGE (Pail B)					1.409	

TABLE 4.7: Average Gradational and Max/Min Properties

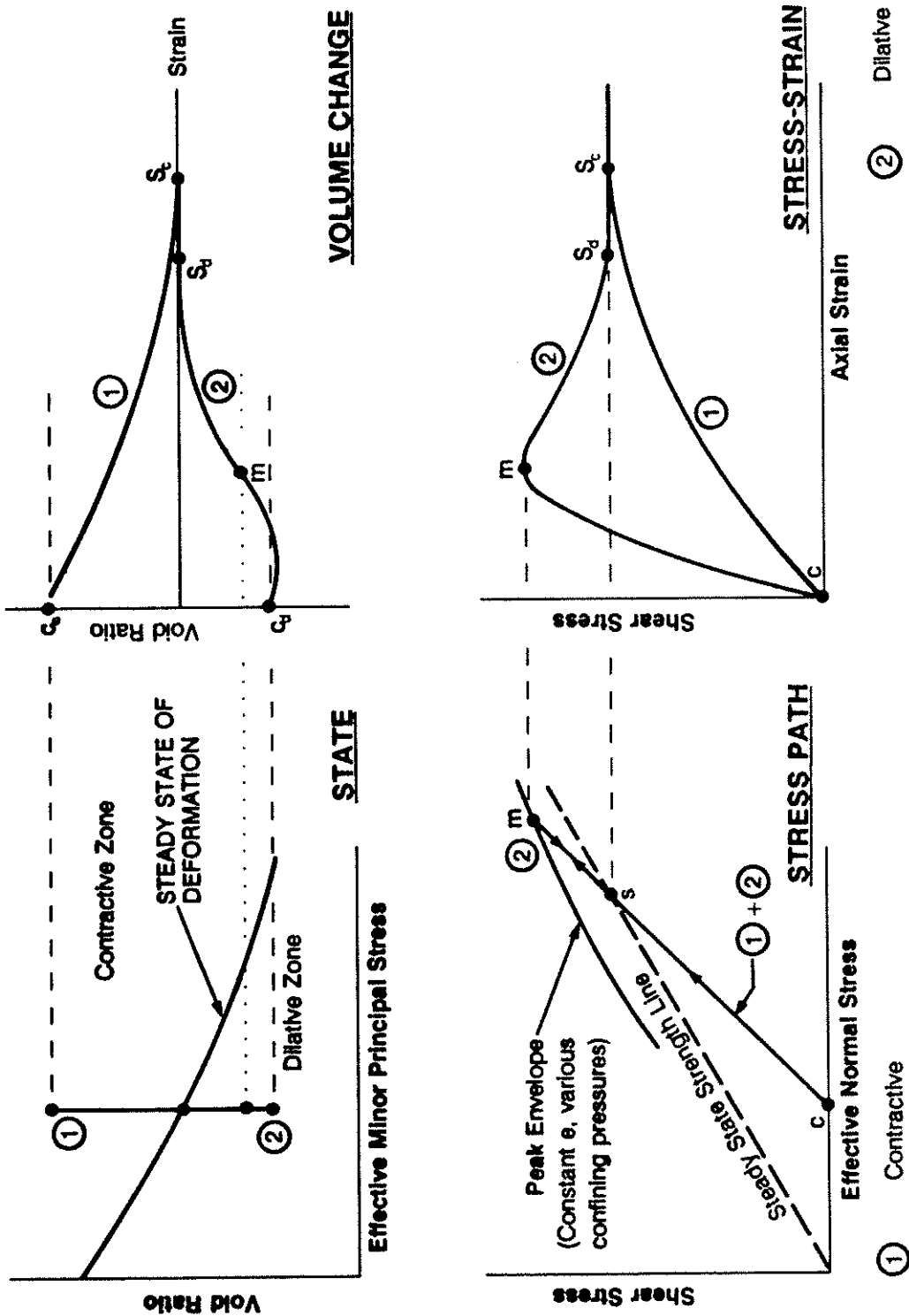


FIGURE 4.1: Idealized Triaxial Shear Results (Consolidated-Drained) Modified after Poulos, 1971

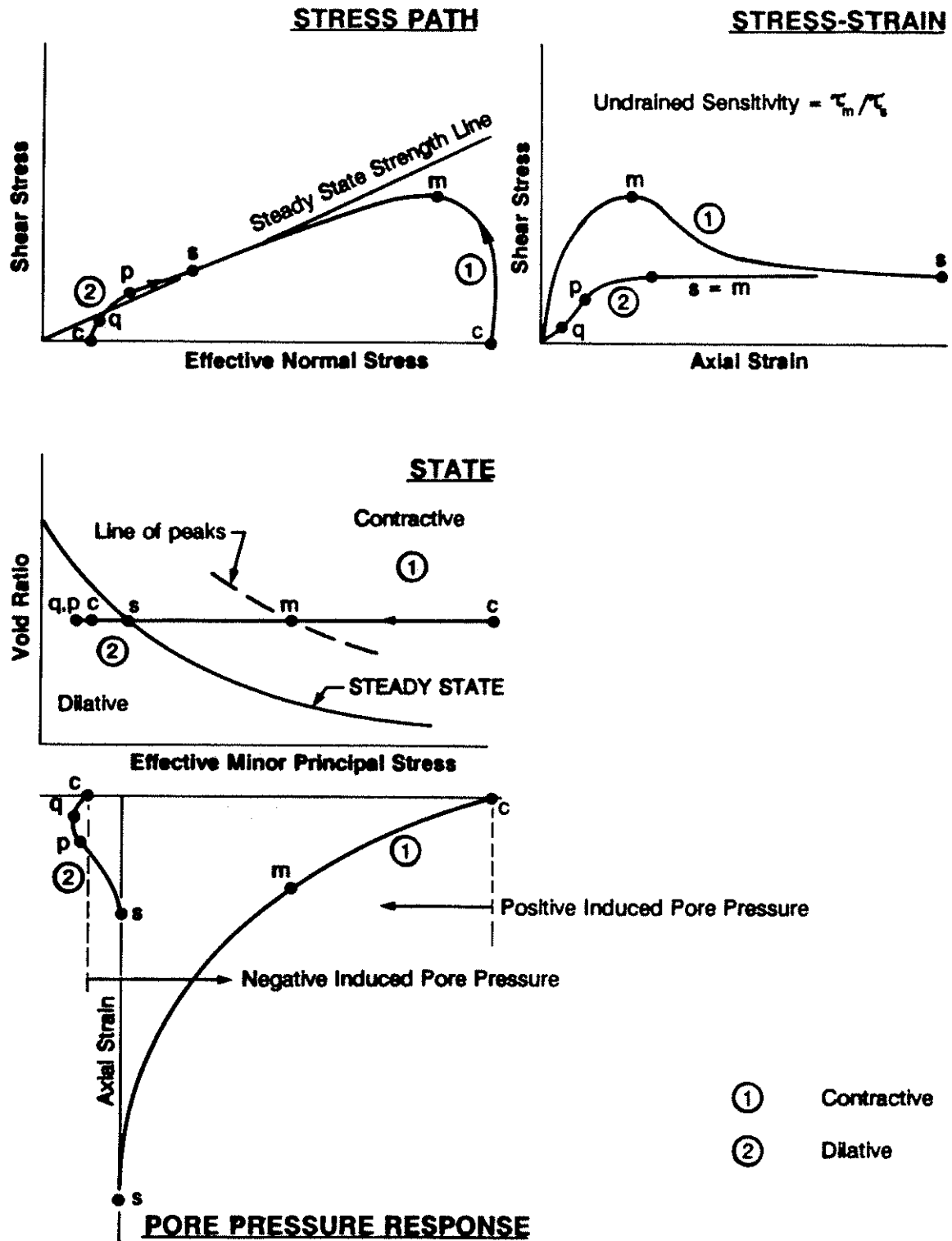


FIGURE 4.2: Idealized Triaxial Shear Results (Consolidated-Undrained) Modified after Poulos, 1971

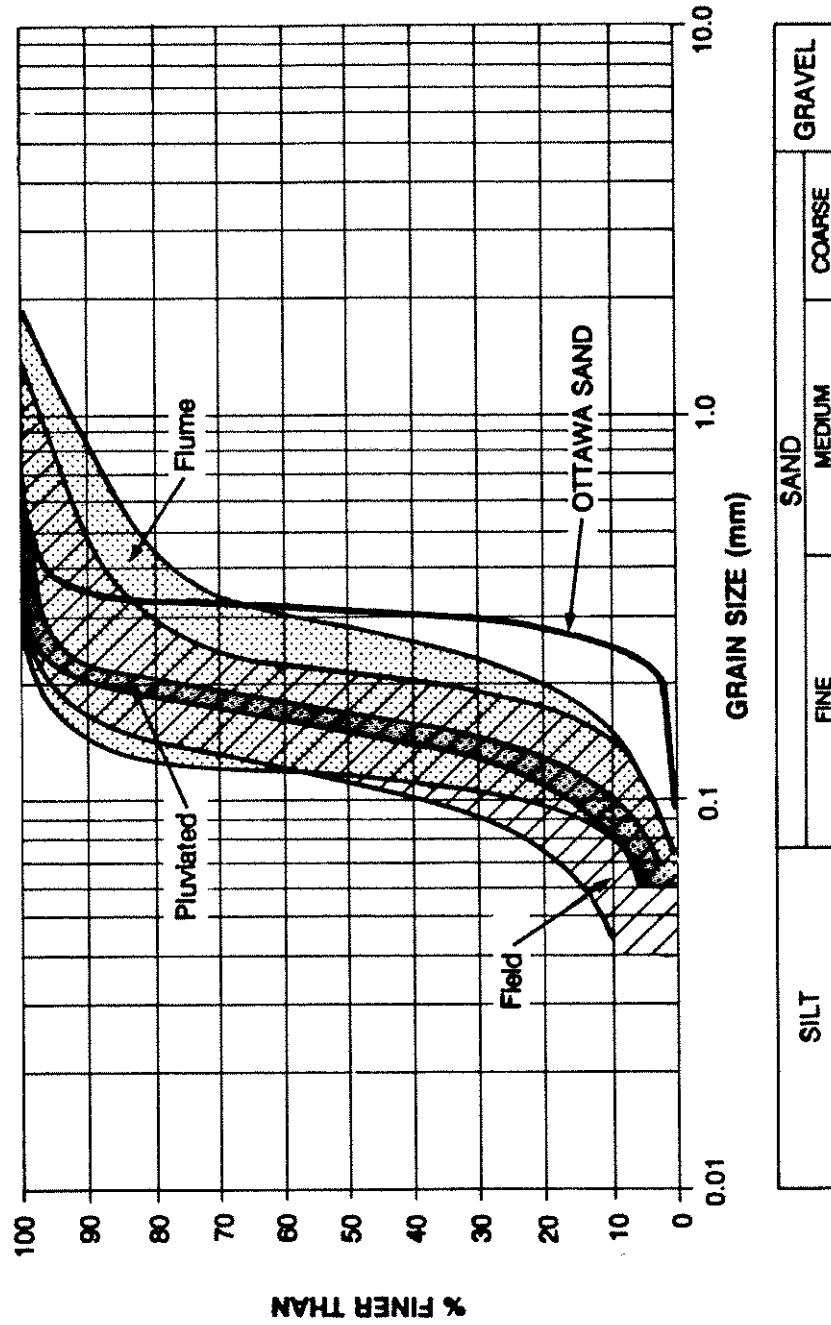
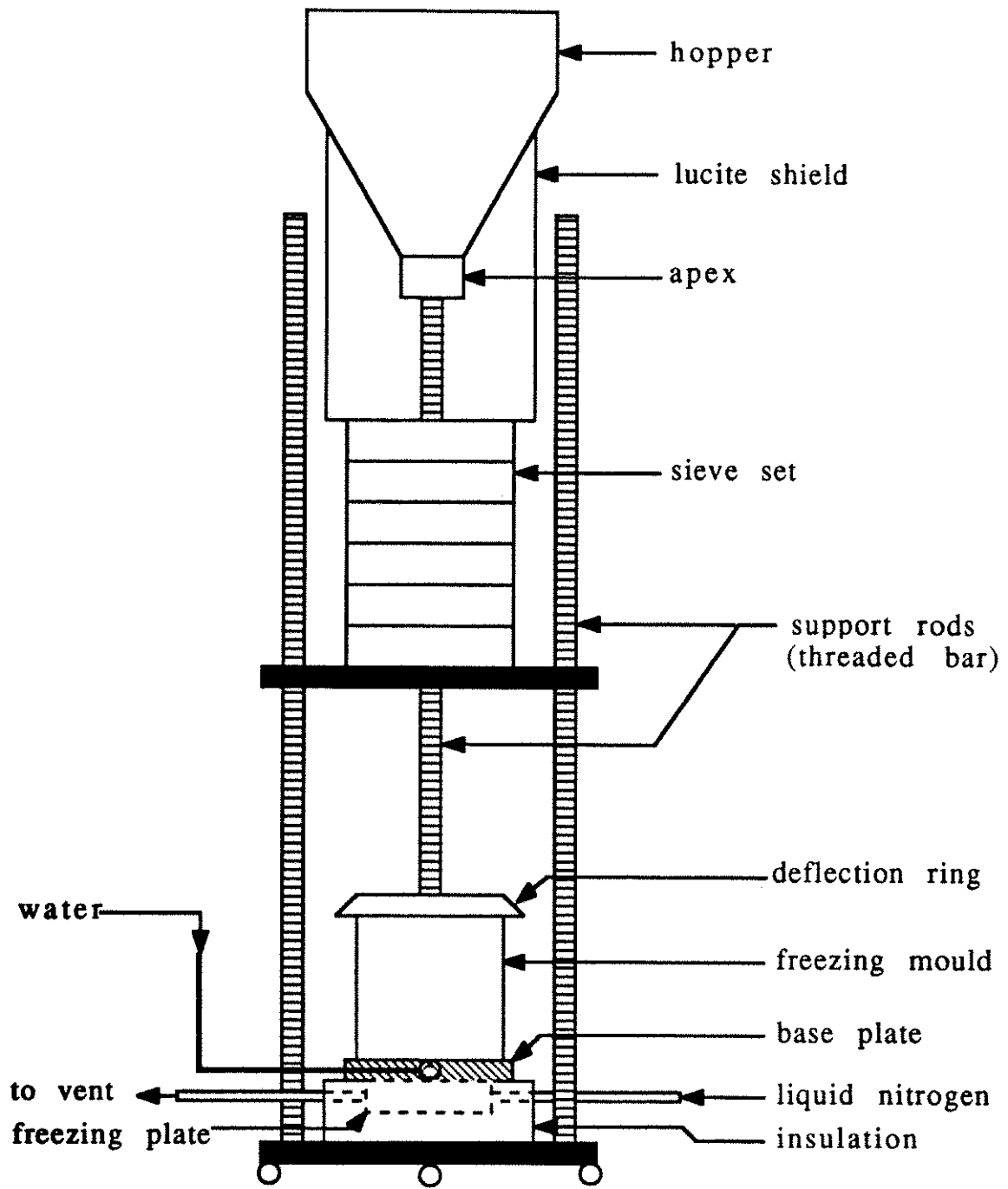


FIGURE 4.3: Range of Grain Size Distributions for Tailing Sand Investigated



Not to Scale

Figure 4.4: Multiple Sieve Pluviation Device

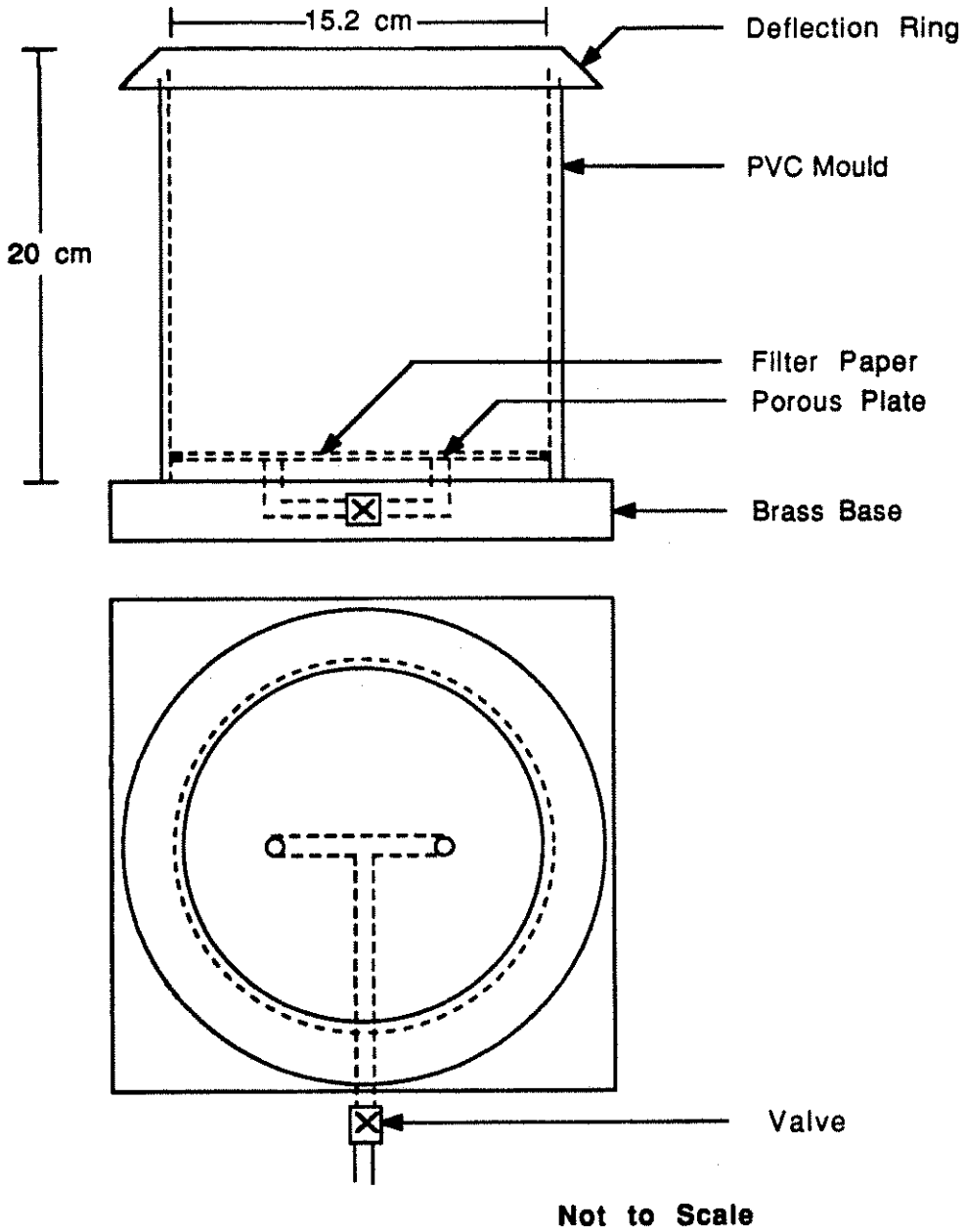
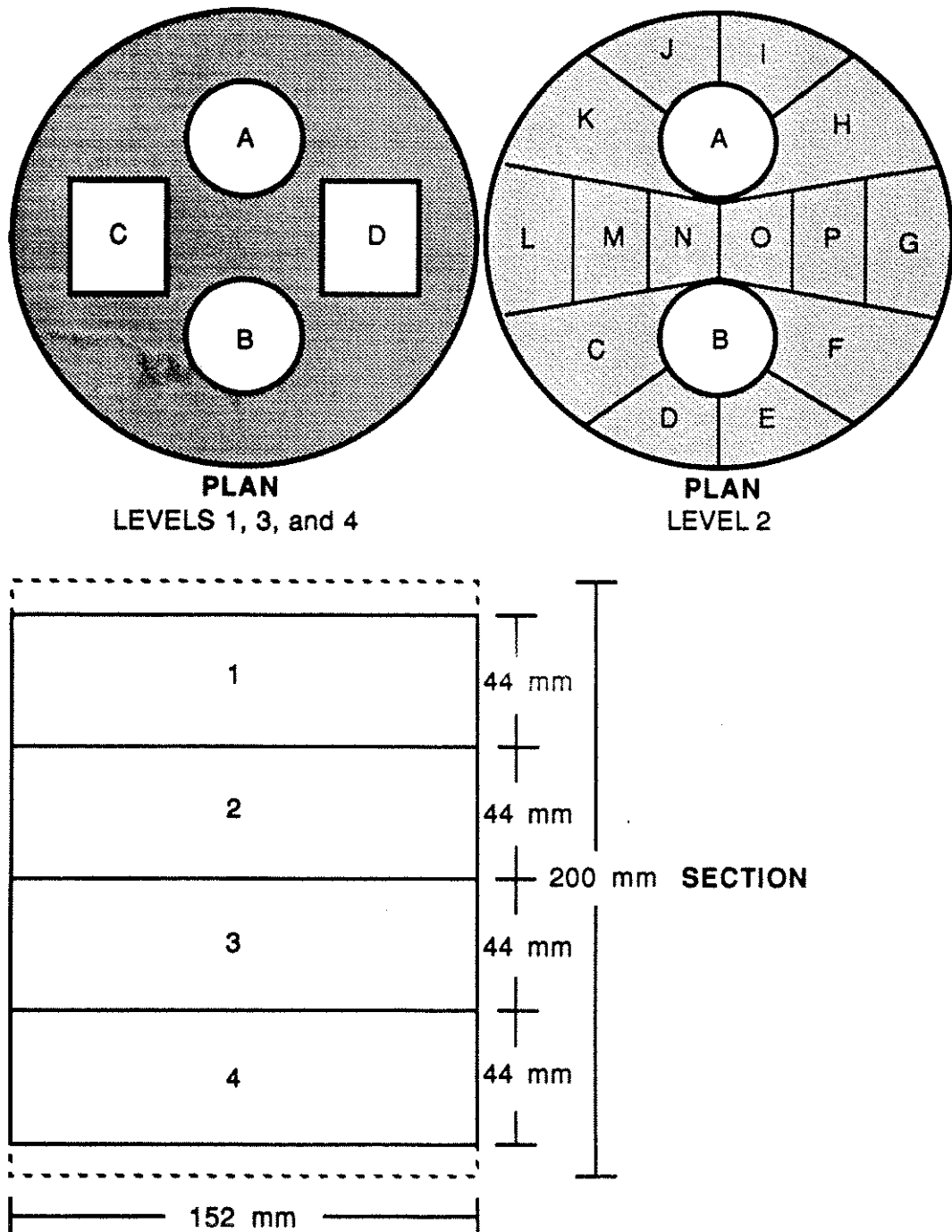


FIGURE 4.5: Pluviation Mould



**FIGURE 4.6: PLUVIATION TEST SPECIMEN LAYOUT
(Ottawa Sand)**

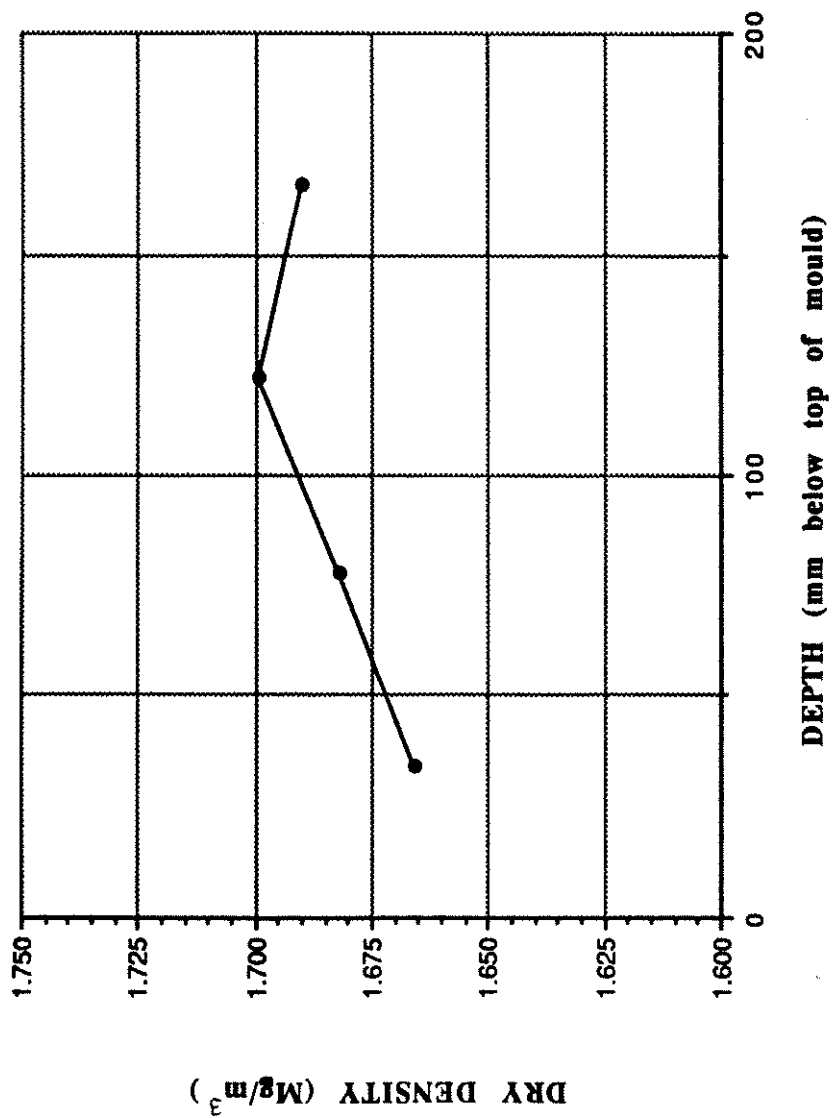


FIGURE 4.7: Average Density Variation Due To Change in Height of Drop

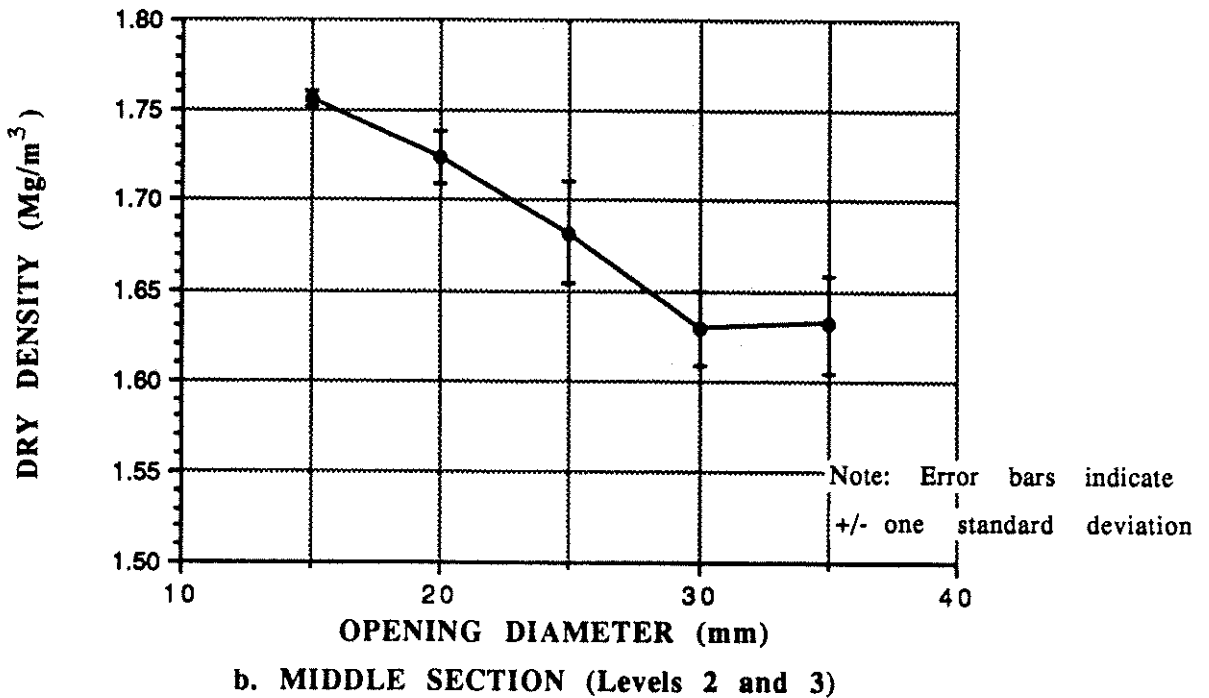
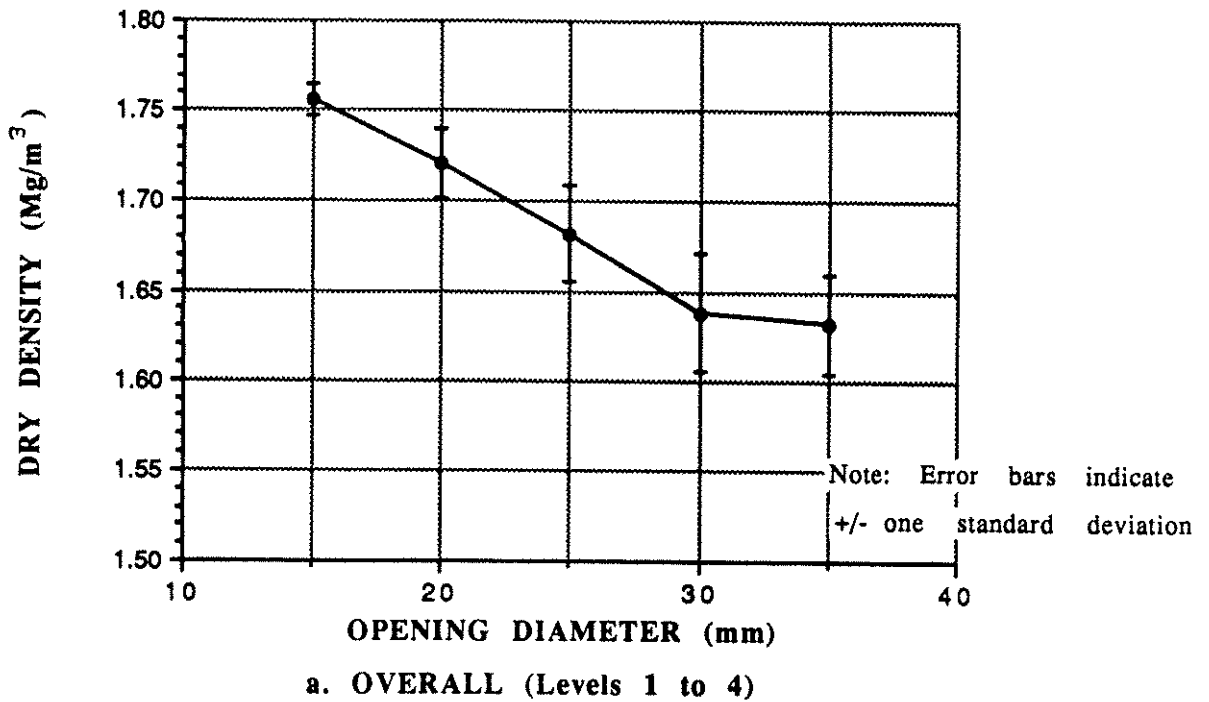
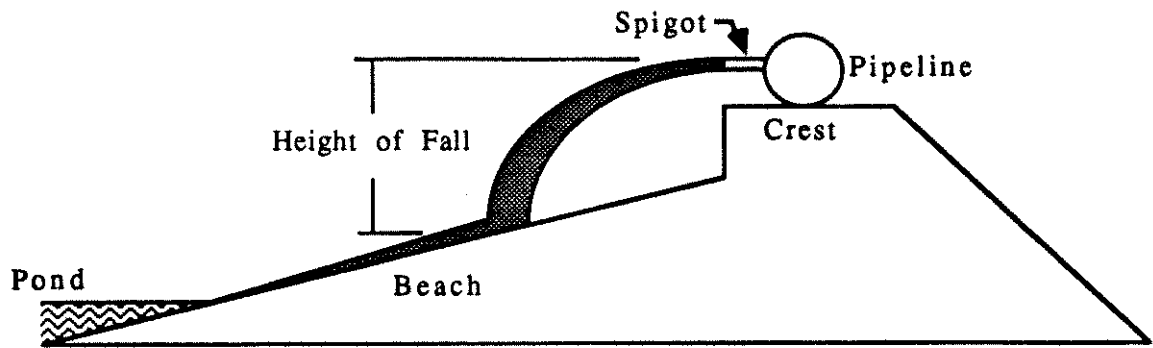
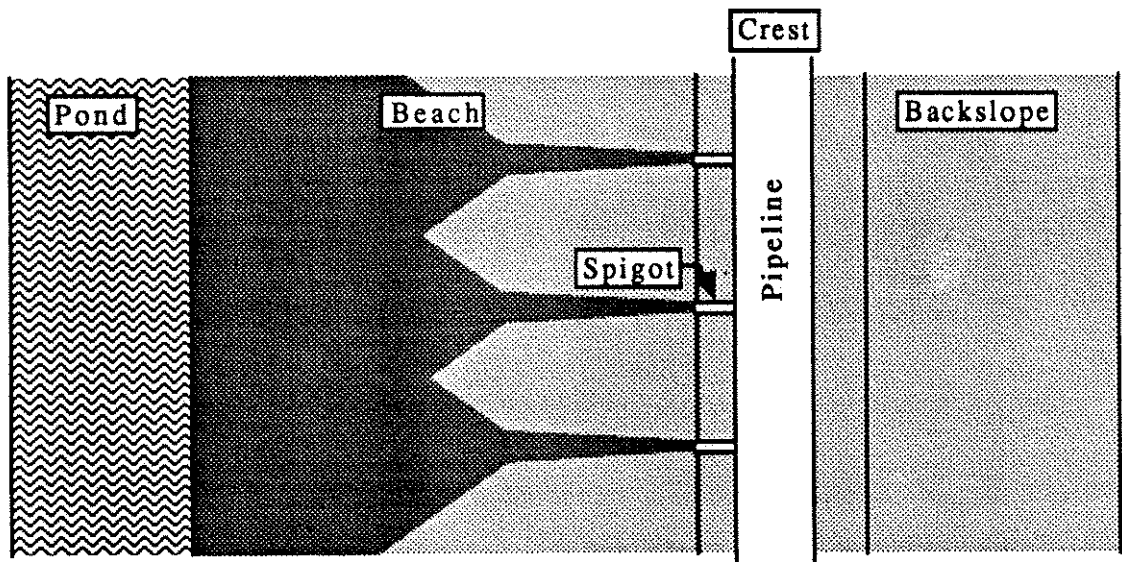


FIGURE 4.8: Variation in Density With Opening Diameter



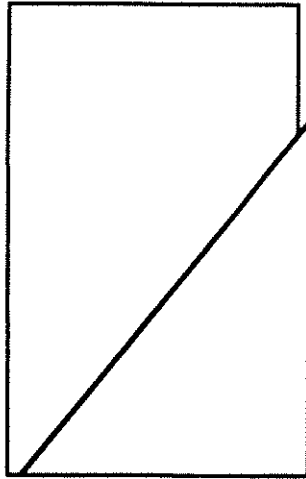
a. SECTION



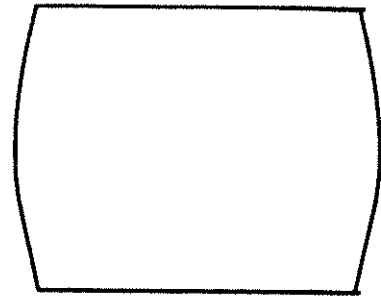
b. PLAN

(not to scale)

FIGURE 4.9: Schematic of Tailings Disposal

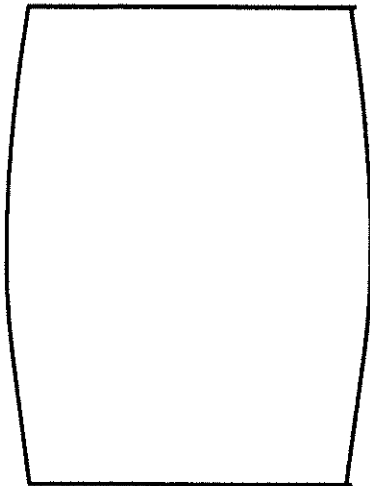


Length / Diameter ≥ 1.5

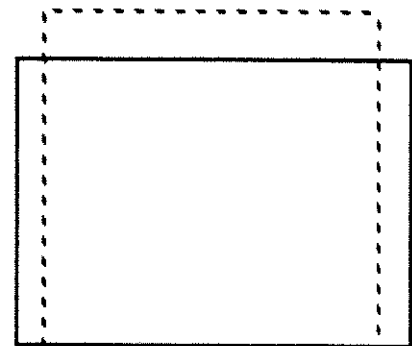


Length / Diameter ≤ 1.0

CONVENTIONAL END PLATENS



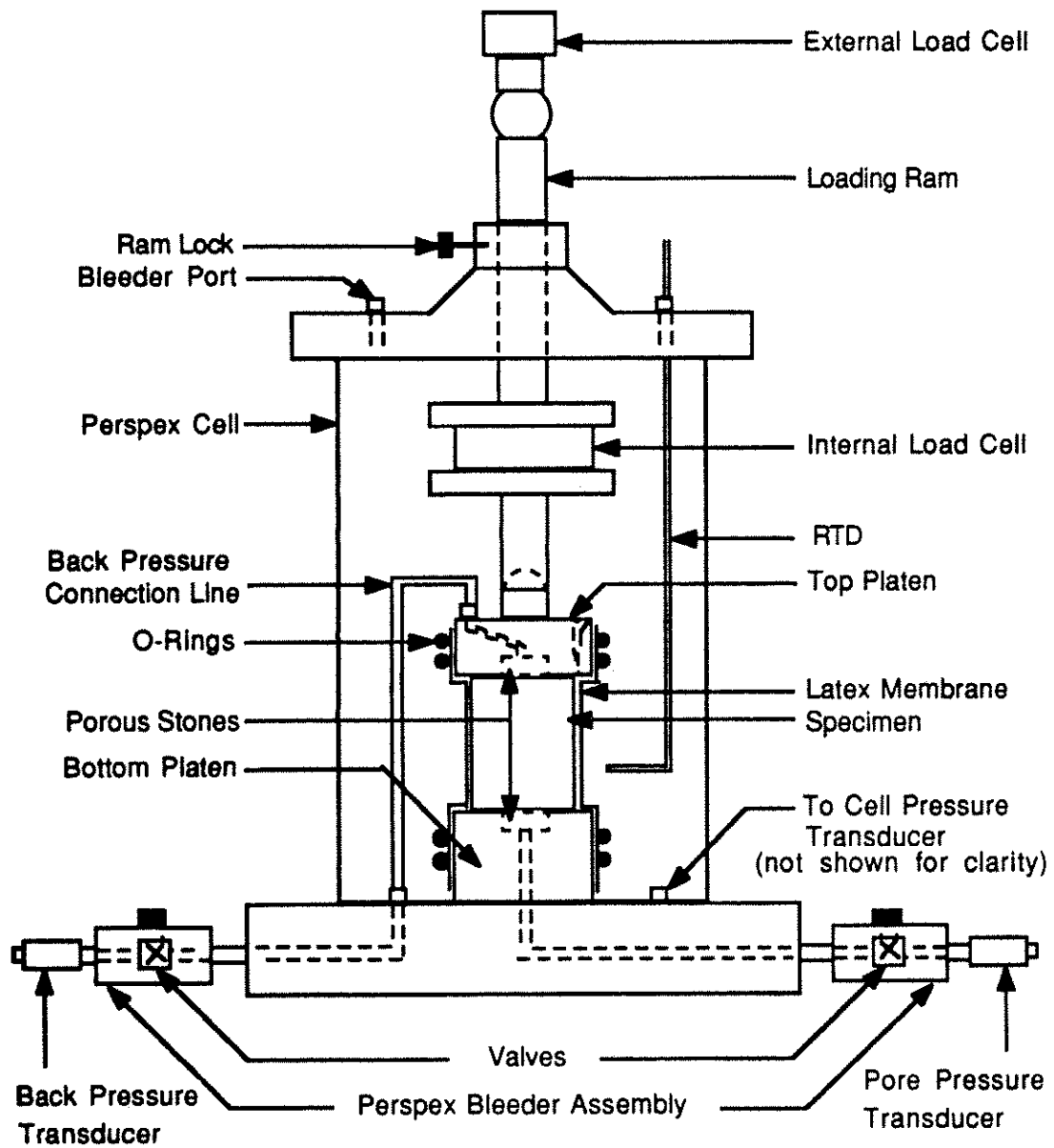
Length / Diameter ≥ 1.5



Length / Diameter ≤ 1.0

LUBRICATED END PLATENS

FIGURE 4.10: SHAPE OF TEST SPECIMENS AFTER SHEAR
(Modified after Plewes, 1987)



(not to scale)

FIGURE 4.11: Triaxial Apparatus

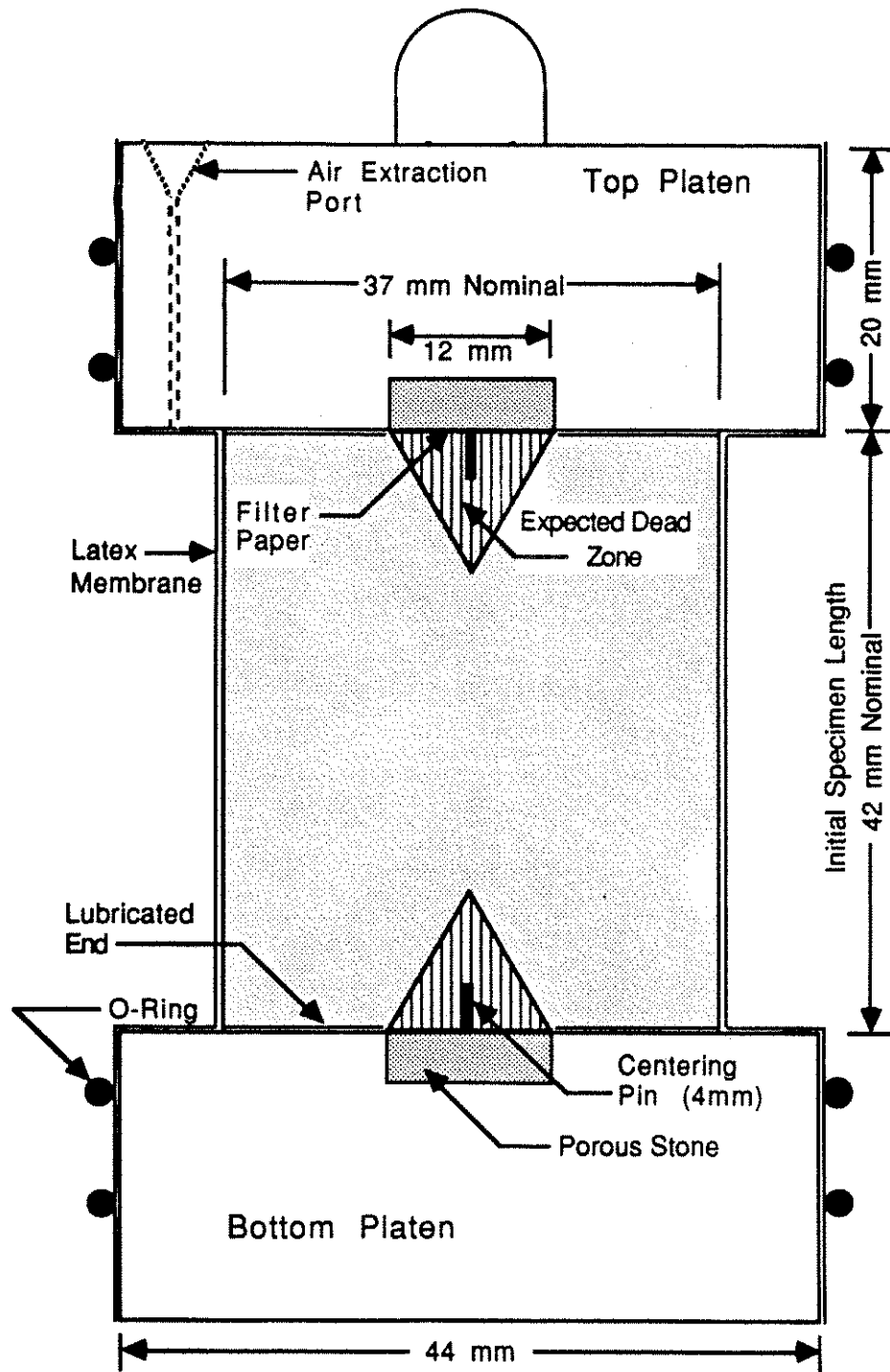


FIGURE 4.12: Platen Design and Initial Specimen Dimensions

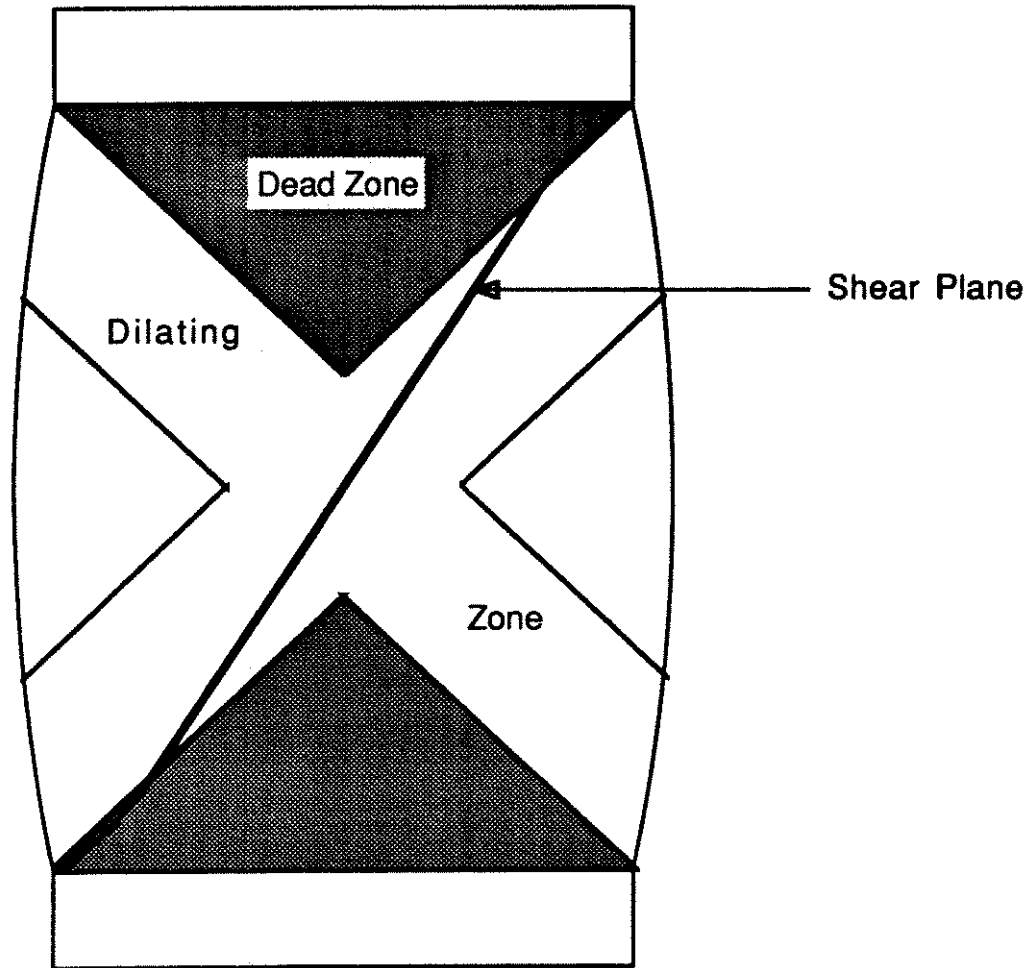


Figure 4.13: Non-Uniformity of Strains Developed During Shear Using Conventional End Platens
(Modified after Rowe and Barden, 1964)

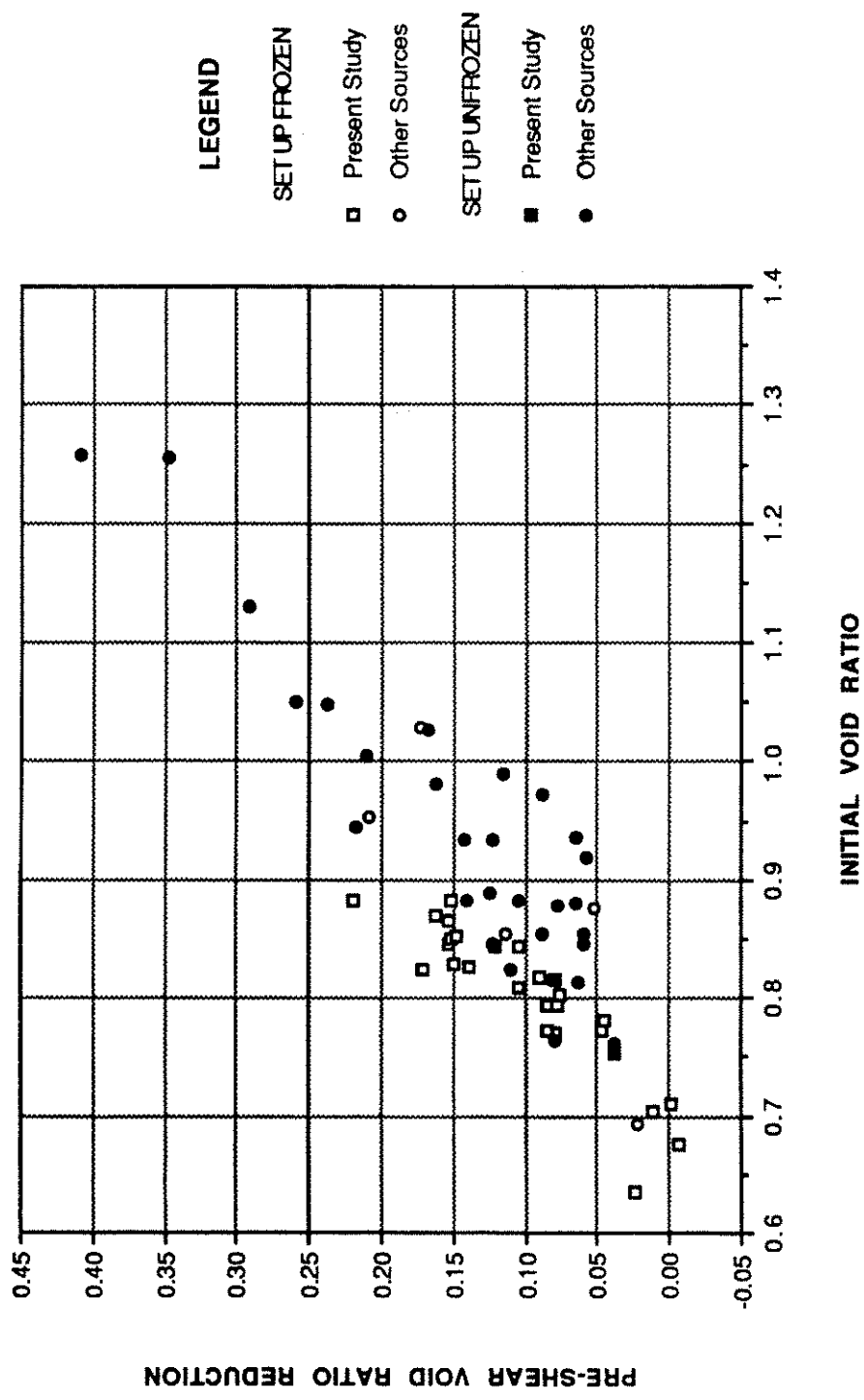


FIGURE 4.14: Pre-Shear Void Ratio Change vs Initial Void Ratio

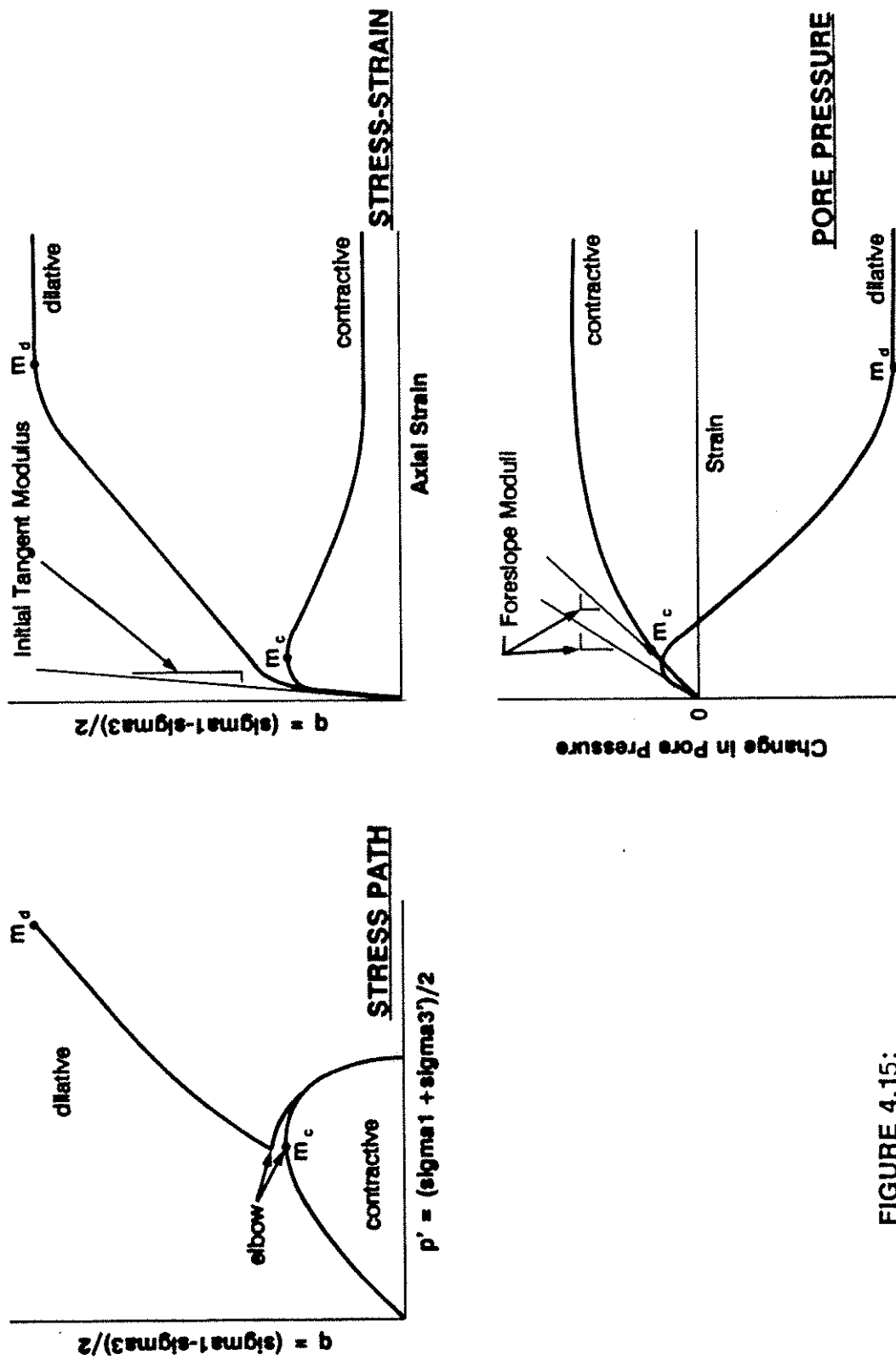
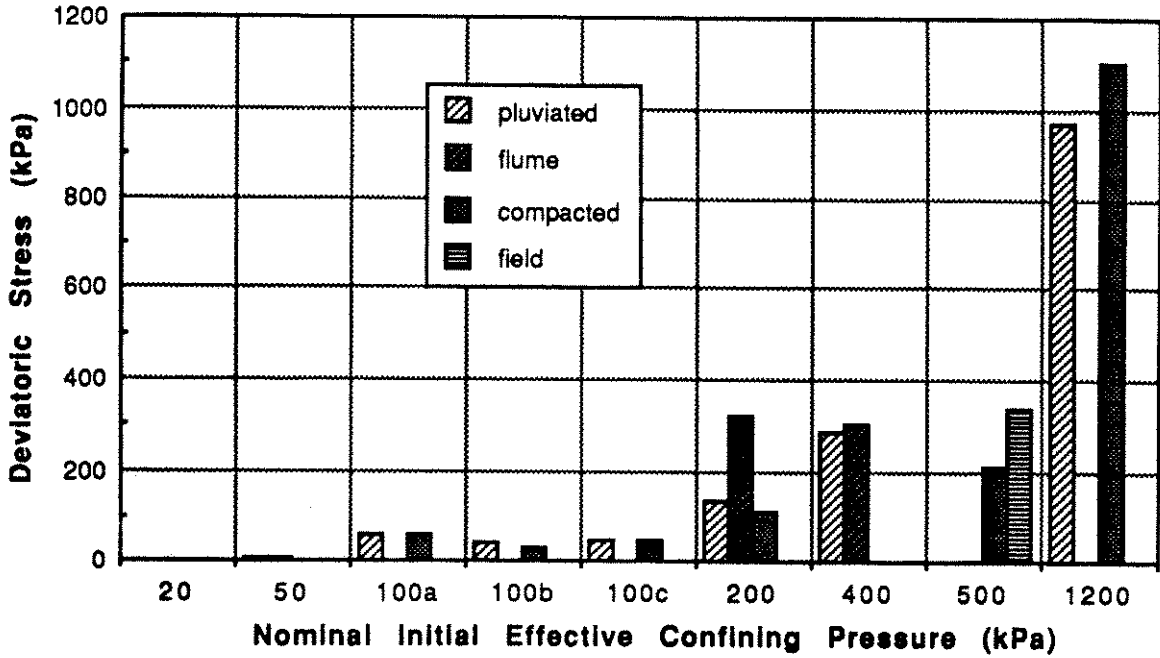
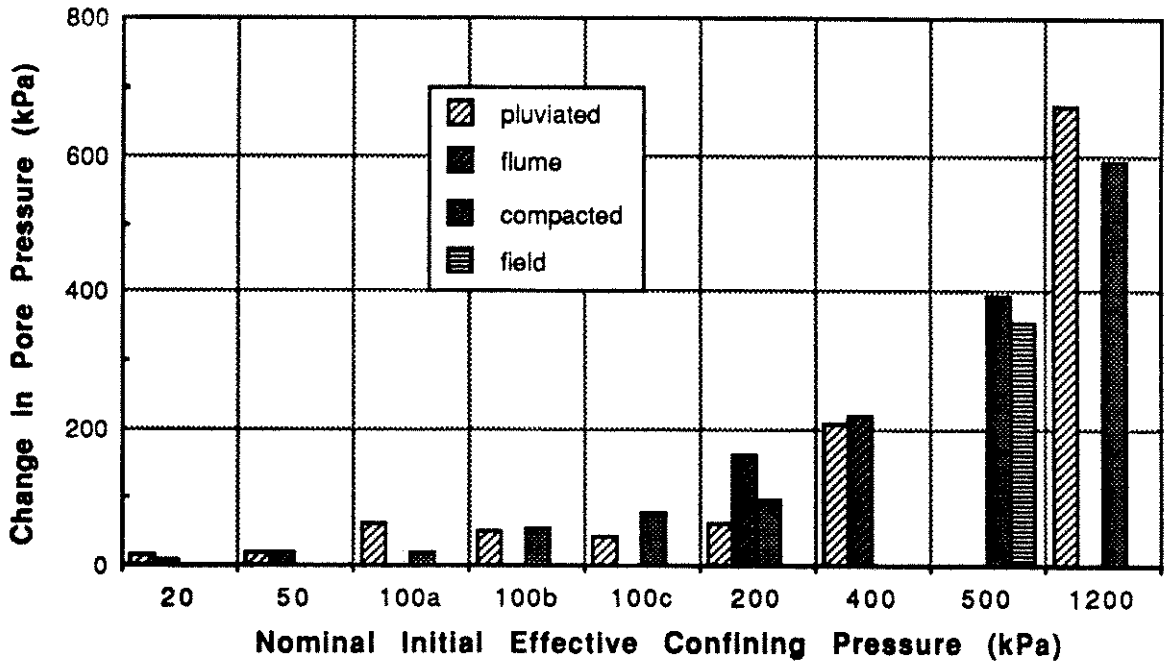


FIGURE 4.15:

Typical Stress Path, Stress-Strain and Pore Pressure Response Results

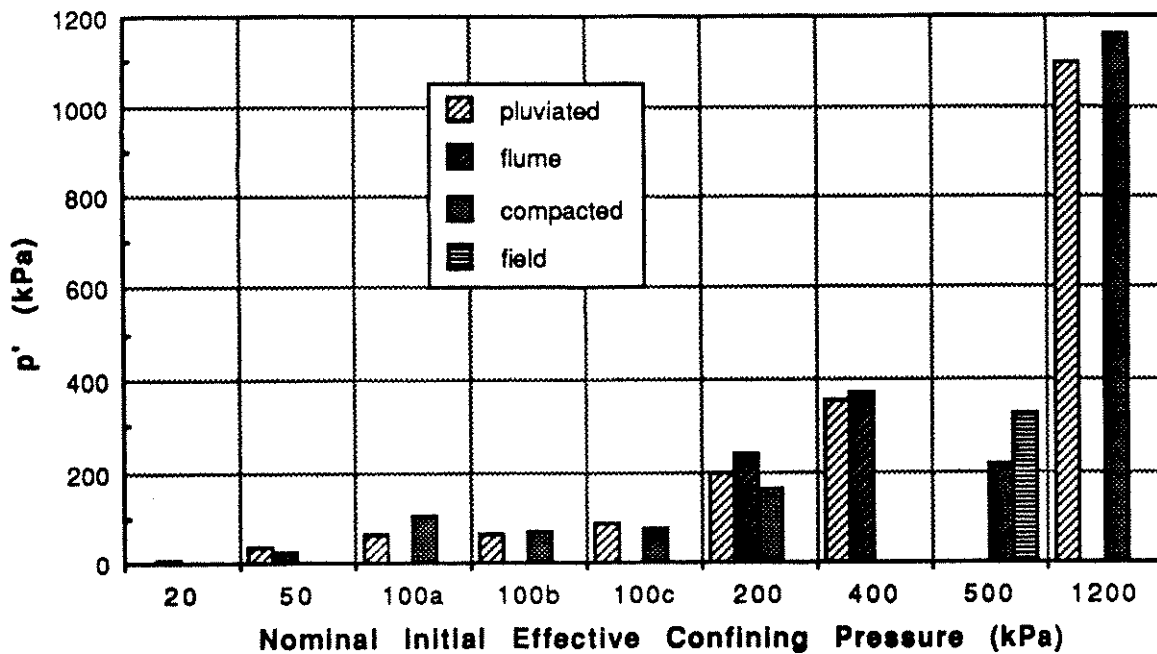


a. Deviatoric Stress

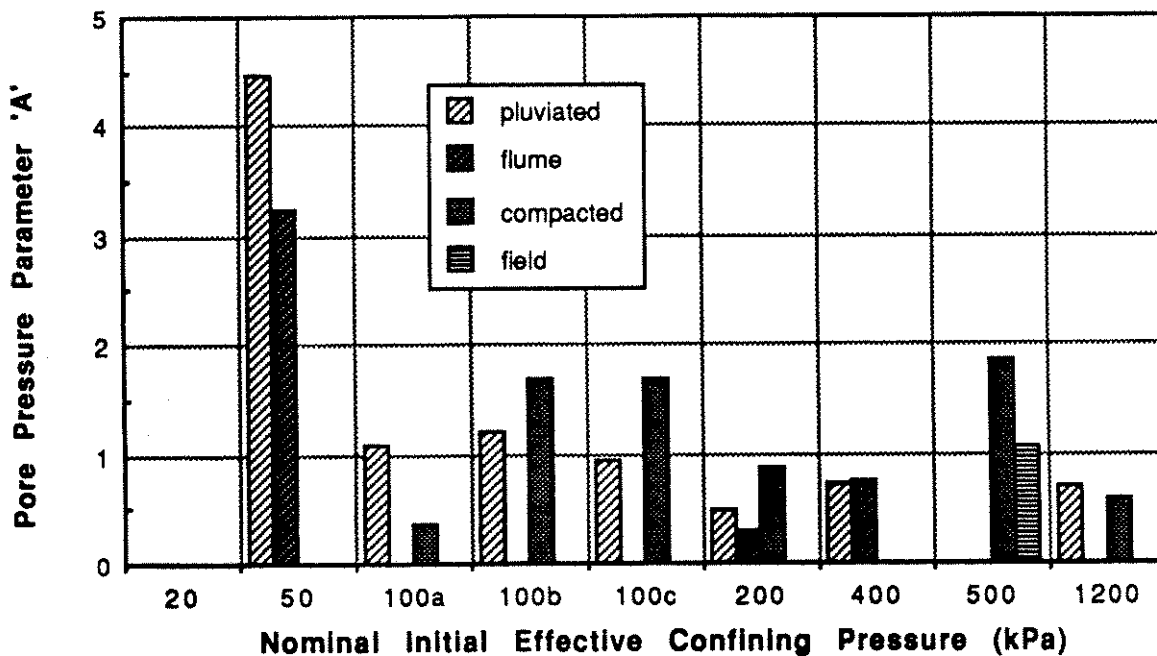


b. Δ Pore Pressure

FIGURE 4.16: Behaviour Comparison at Elbow

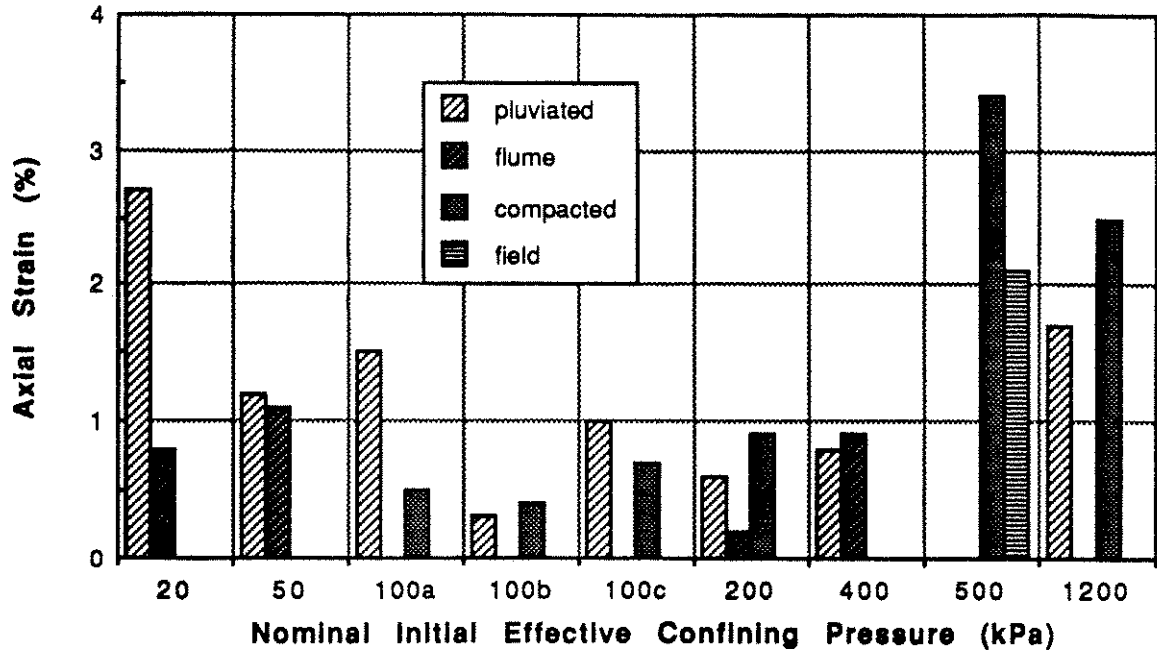


a. $p' = (\sigma_1' + \sigma_3') / 2$

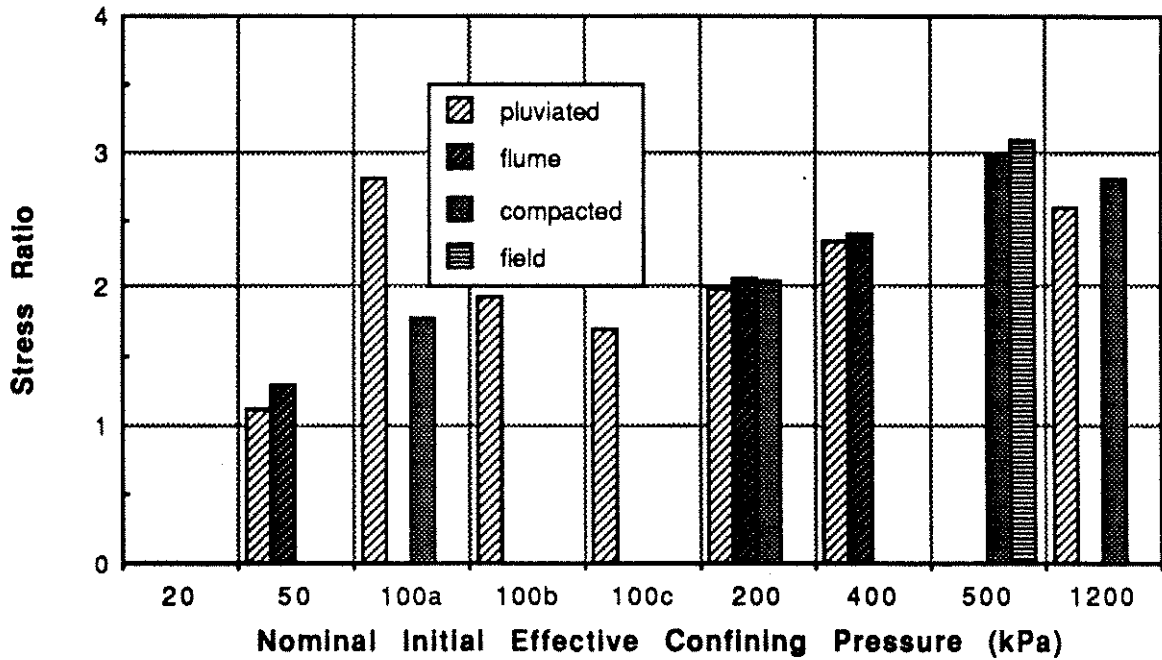


b. Pore Pressure Parameter 'A'

FIGURE 4.17: Behaviour Comparison at Elbow

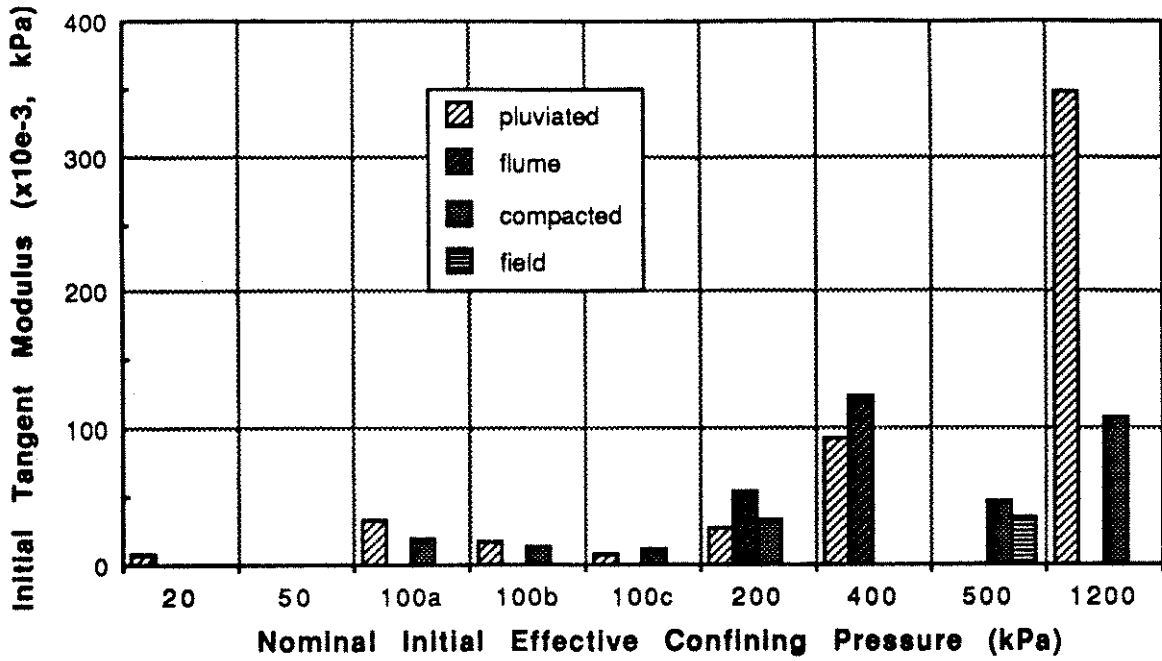


a. Strain

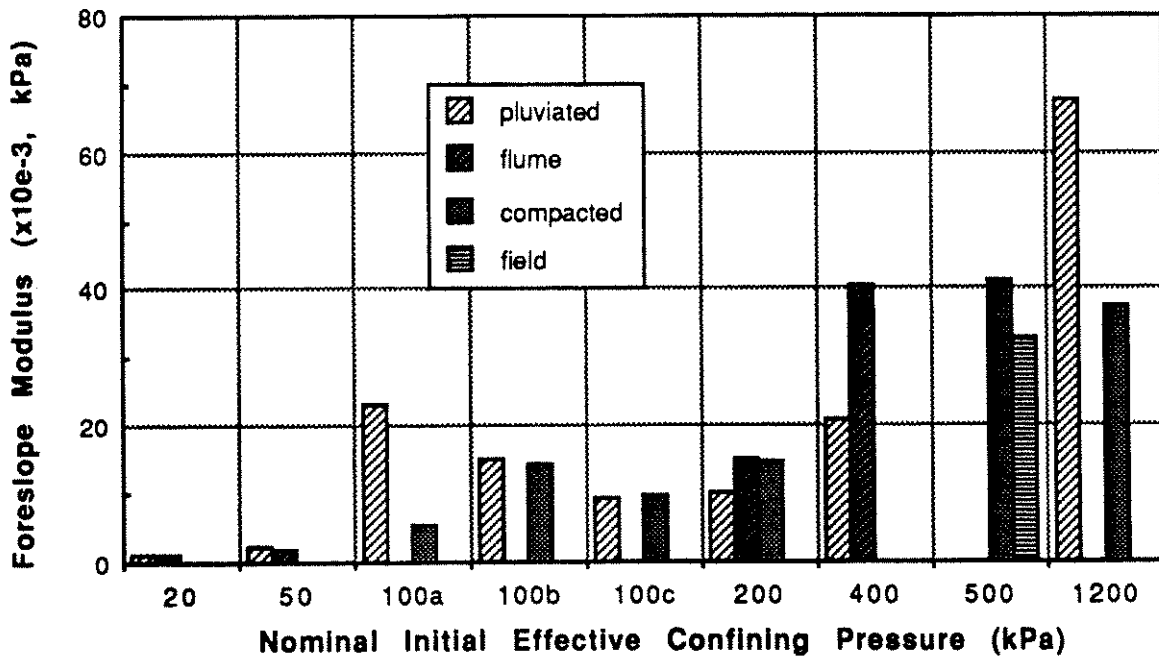


b. Stress Ratio

FIGURE 4.18: Behaviour Comparison at Elbow

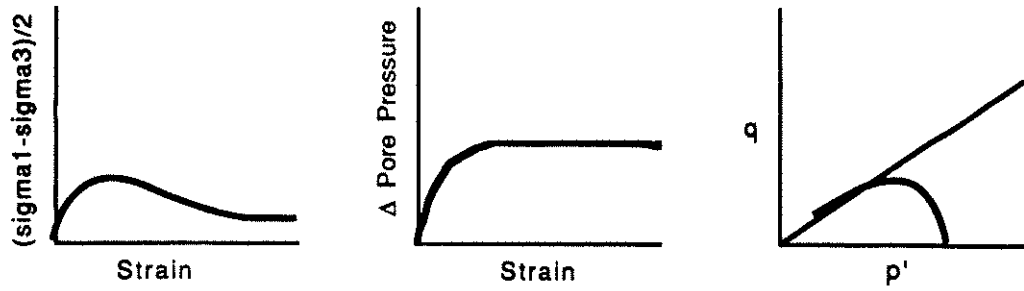


a. Initial Tangent Modulus

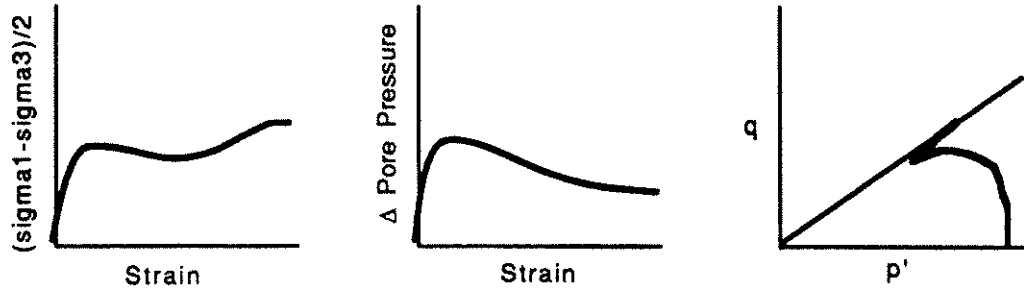


b. Forslope Modulus

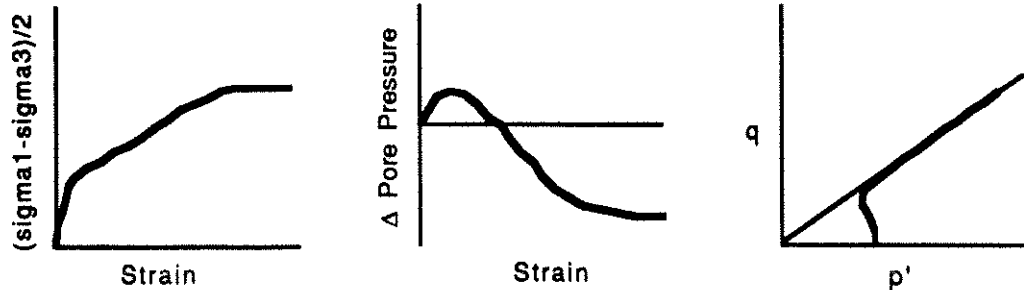
FIGURE 4.19: Behaviour Comparison at Elbow



a. Contractive



b. Contractive-Dilative



c. Dilative

FIGURE 4.20: Typical Stress-Strain, Pore Pressure and Stress Path Response

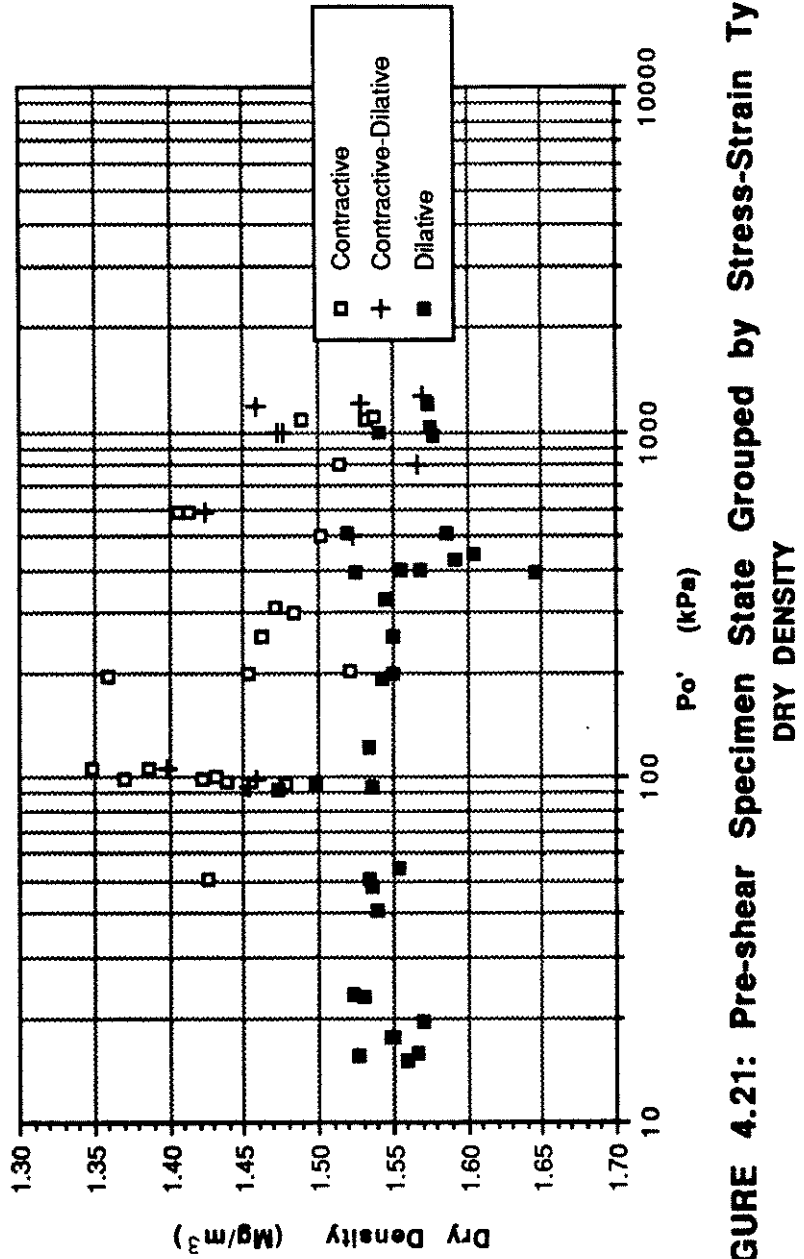


FIGURE 4.21: Pre-shear Specimen State Grouped by Stress-Strain Type

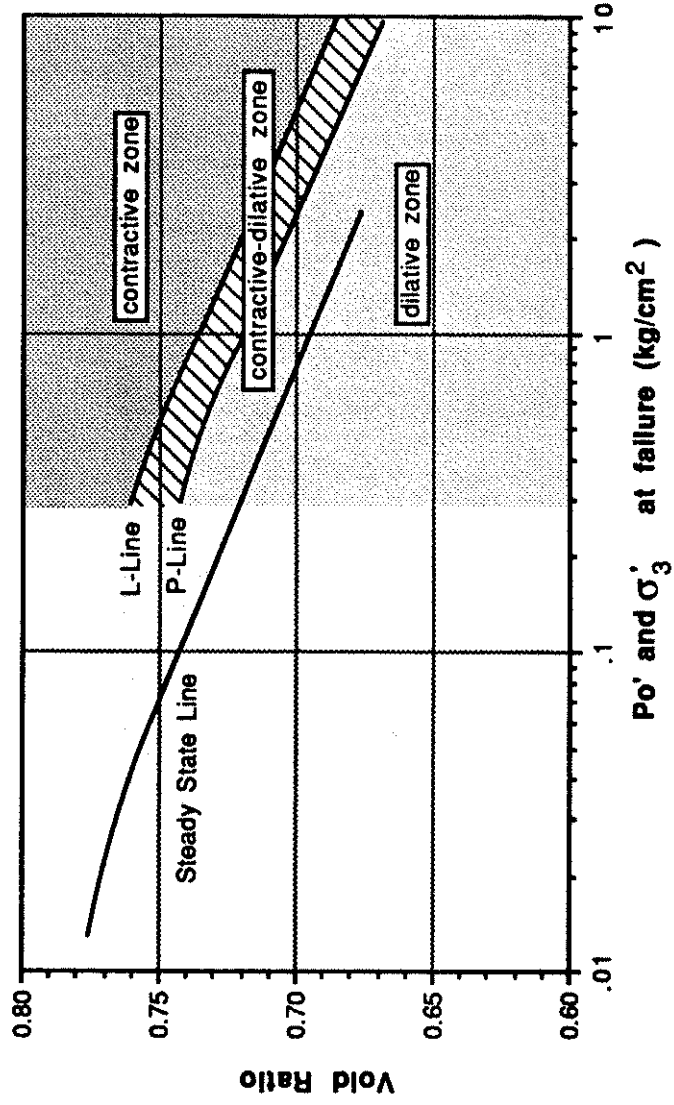


FIGURE 4.22: Pre-Shear and Steady State Relationship
Modified after Castro (1969)

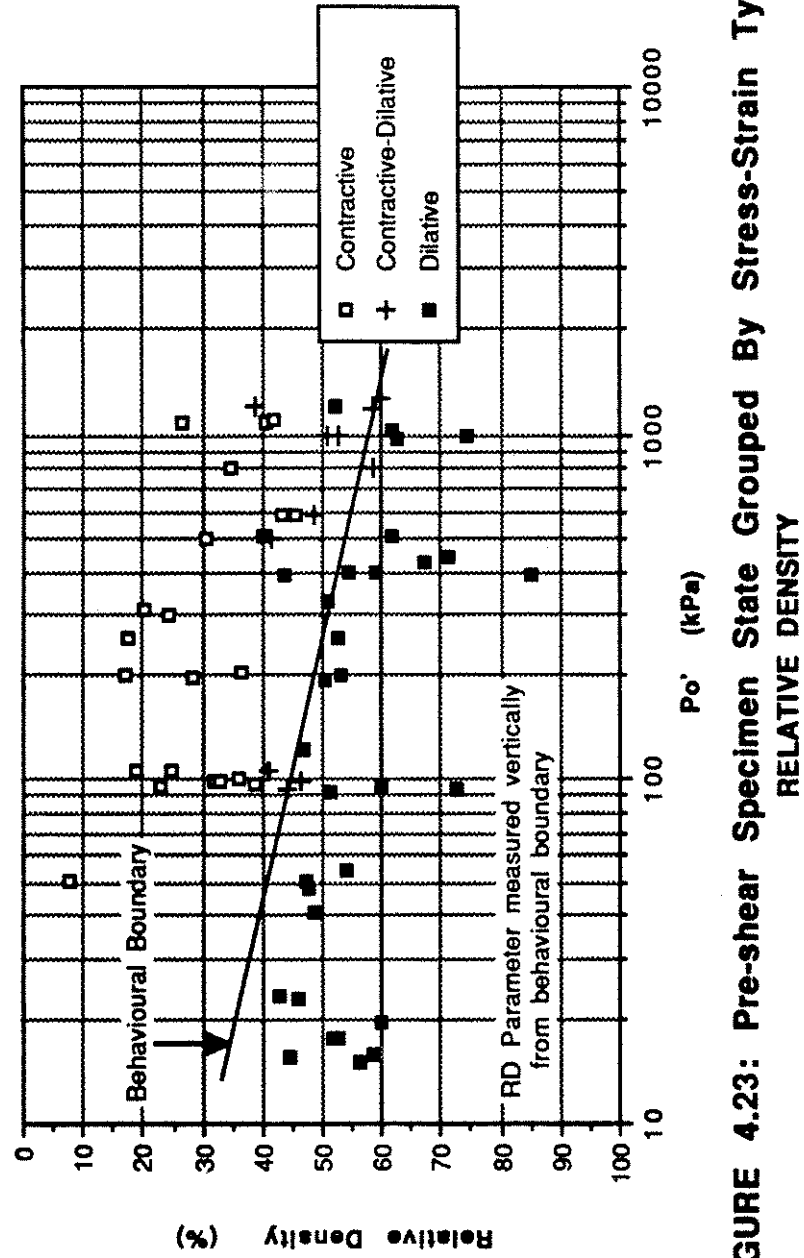


FIGURE 4.23: Pre-shear Specimen State Grouped By Stress-Strain Type

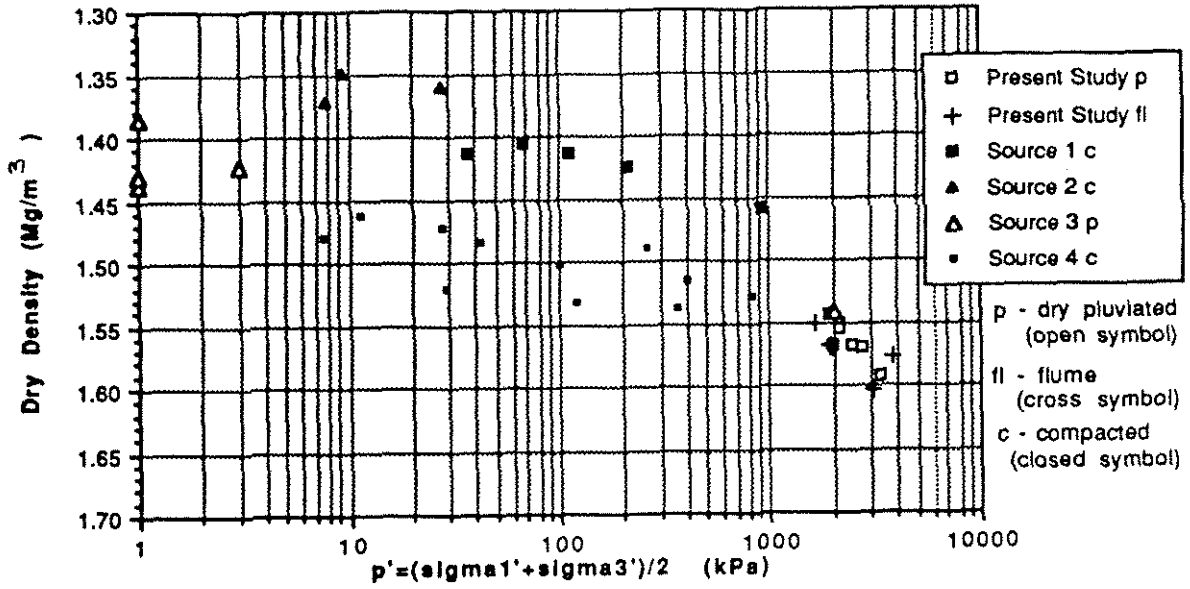


FIGURE 4.24: STEADY STATE CONDITIONS
Dry Density

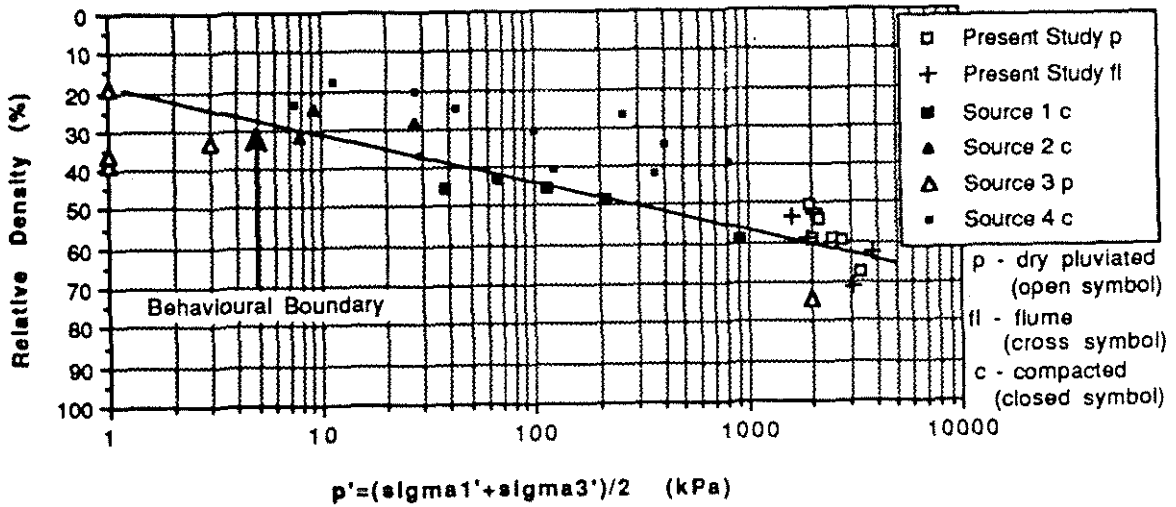
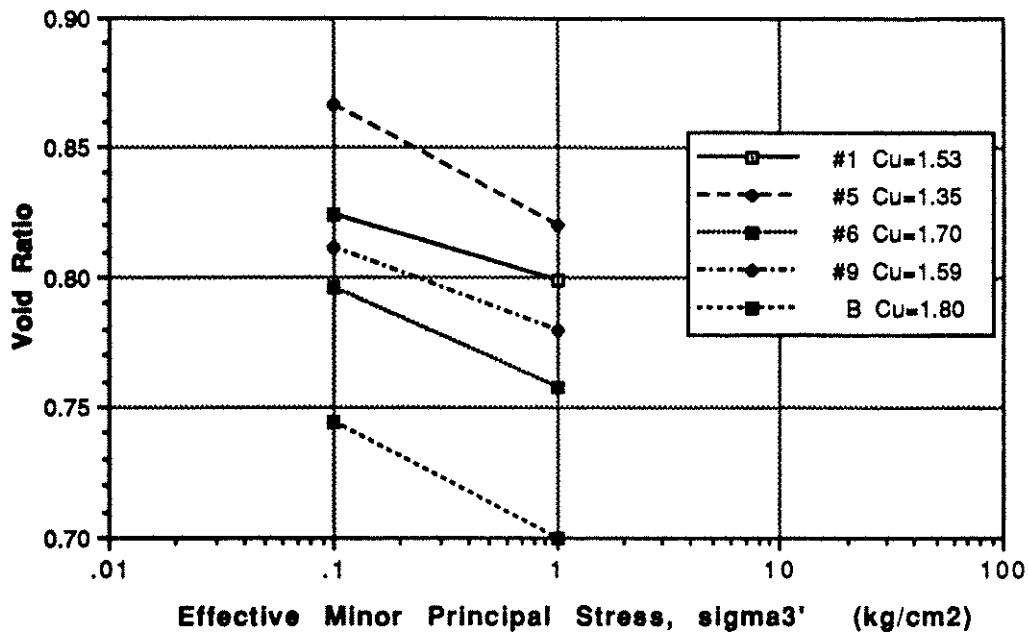
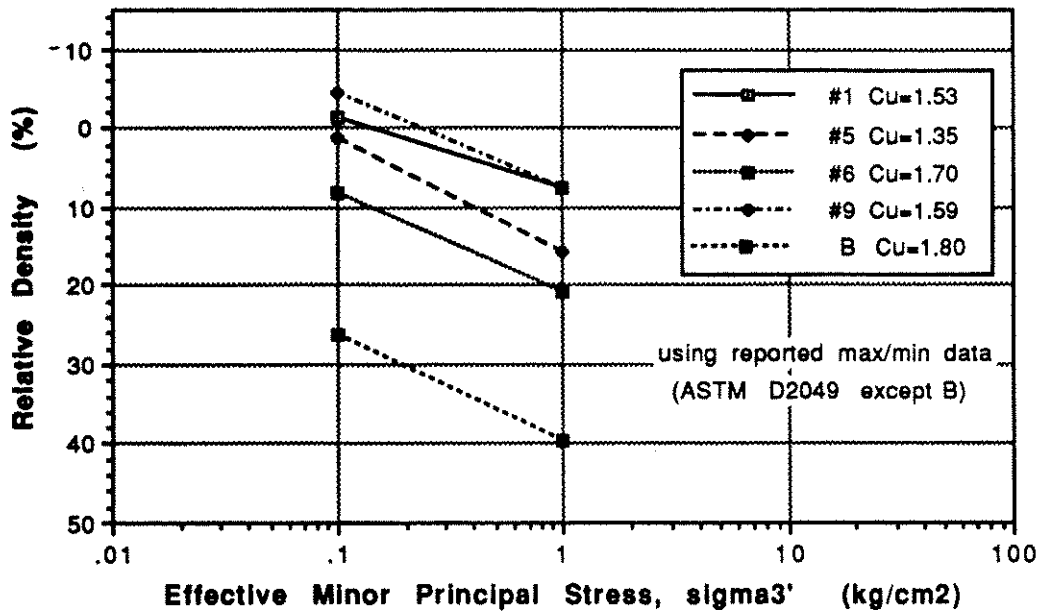


FIGURE 4.25: STEADY STATE CONDITIONS
Relative Density



a. Steady State Condition for Banding Sand
(Modified after Castro et. al., 1982)



b. Steady State Condition for Banding Sand
(Calculated from data presented in Castro et. al., 1982)

FIGURE 4.26: Relative Density Representation of Steady State Condition

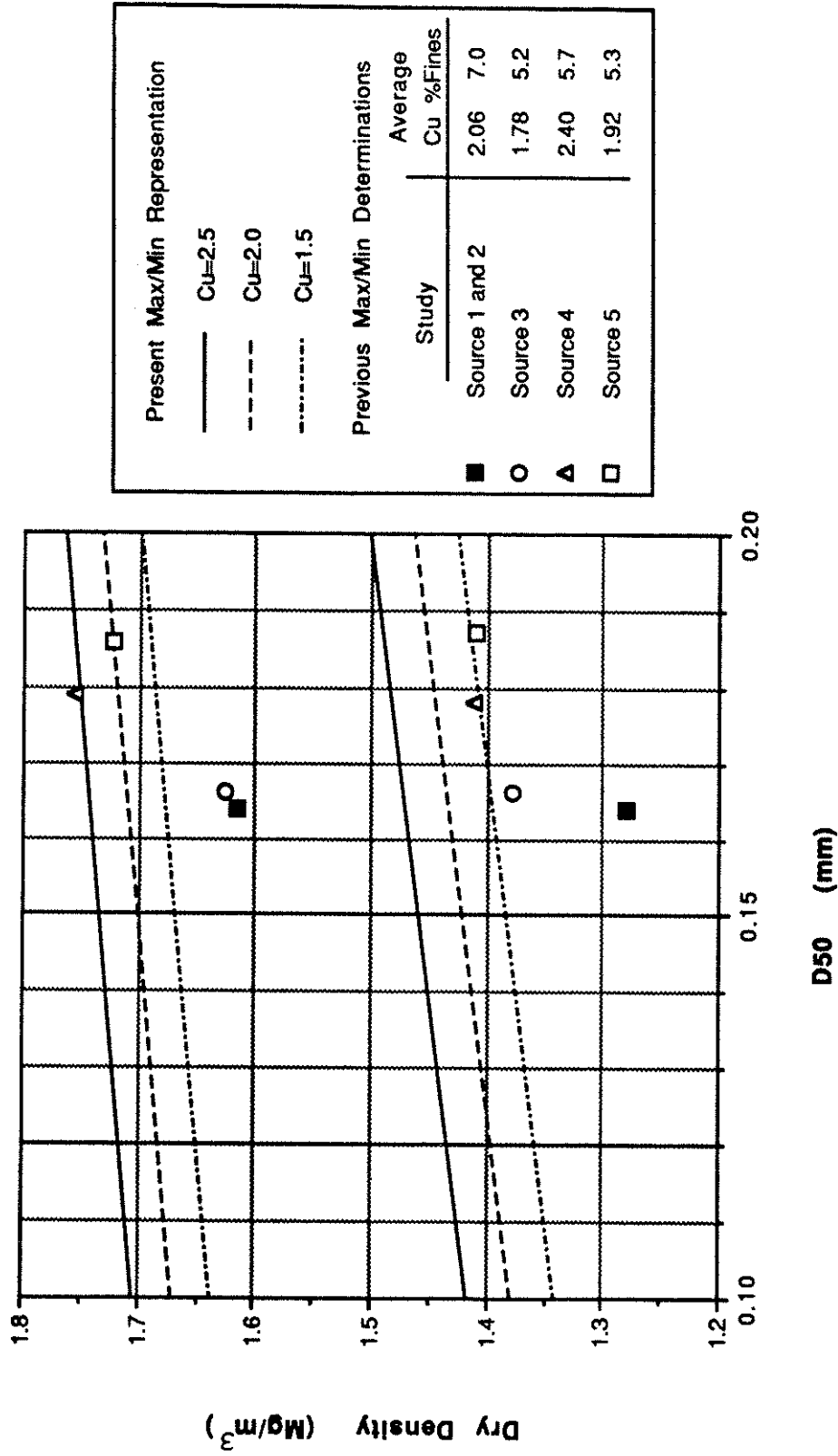


FIGURE 4.27: Effect of D50 and Cu on Maximum and Minimum Density

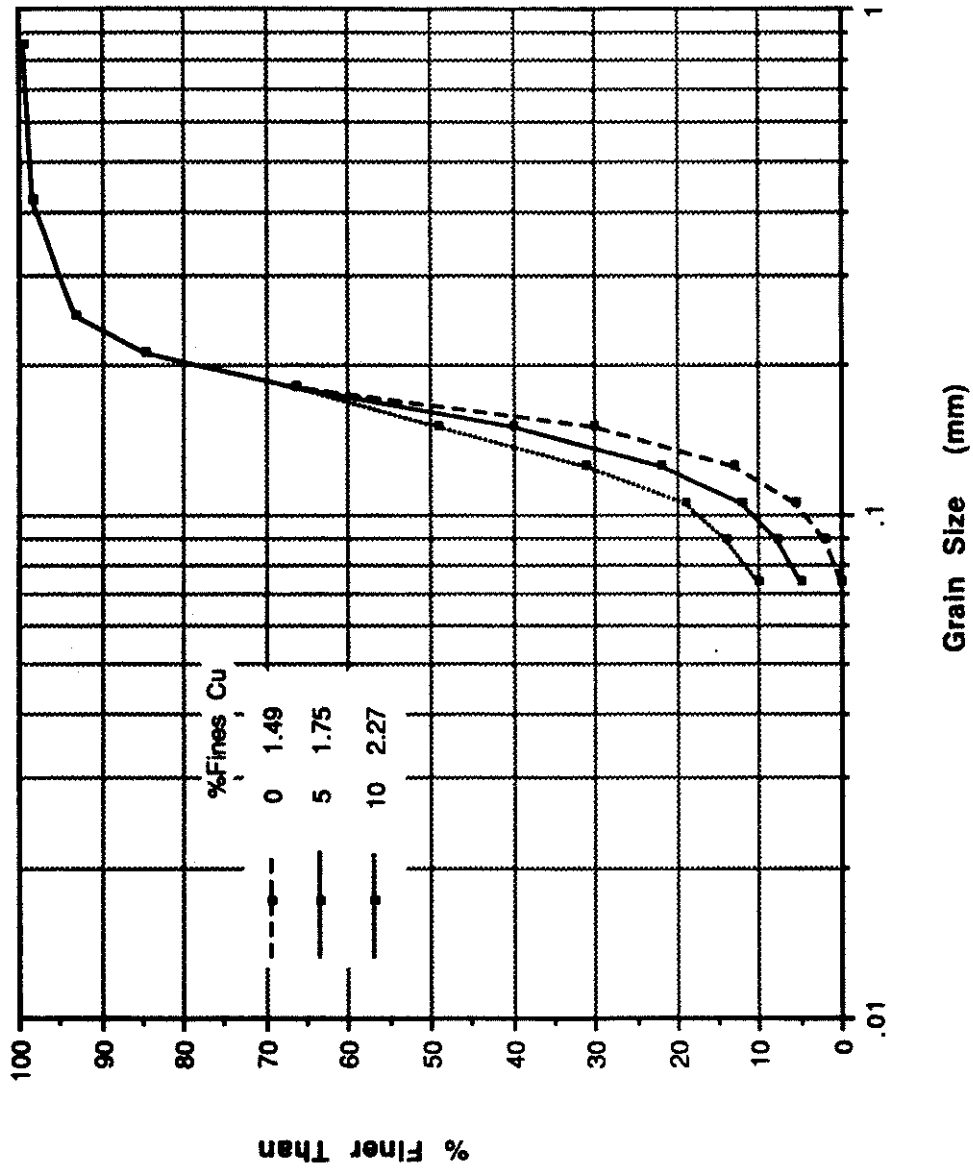


FIGURE 4.28: Effect of Fines Content on Cu for Similar Gradations

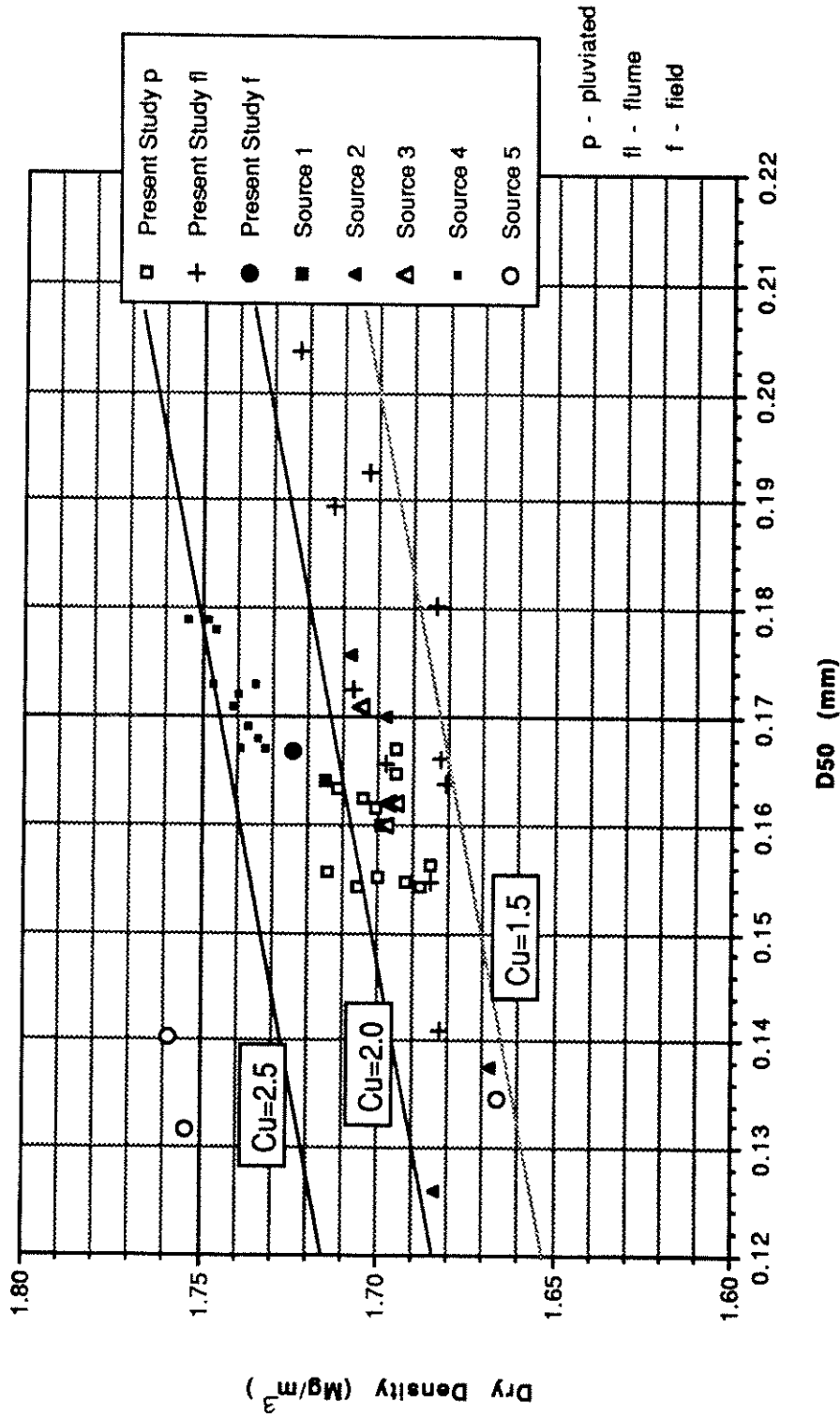


FIGURE 4.29: Maximum Dry Density Corresponding to Measured D50 and C_u

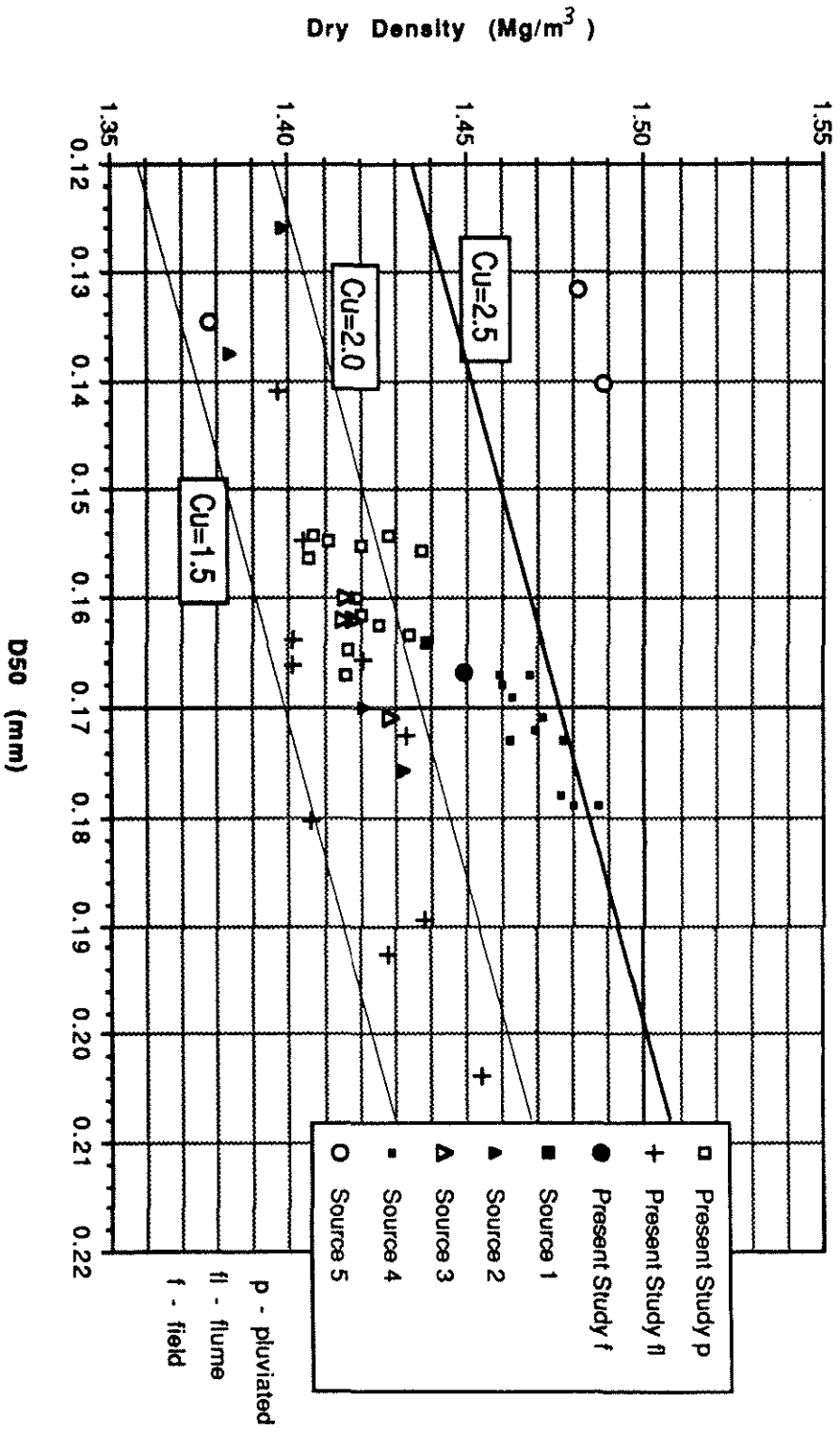


FIGURE 4.30: Minimum Dry Density Corresponding to Measured D50 and Cu

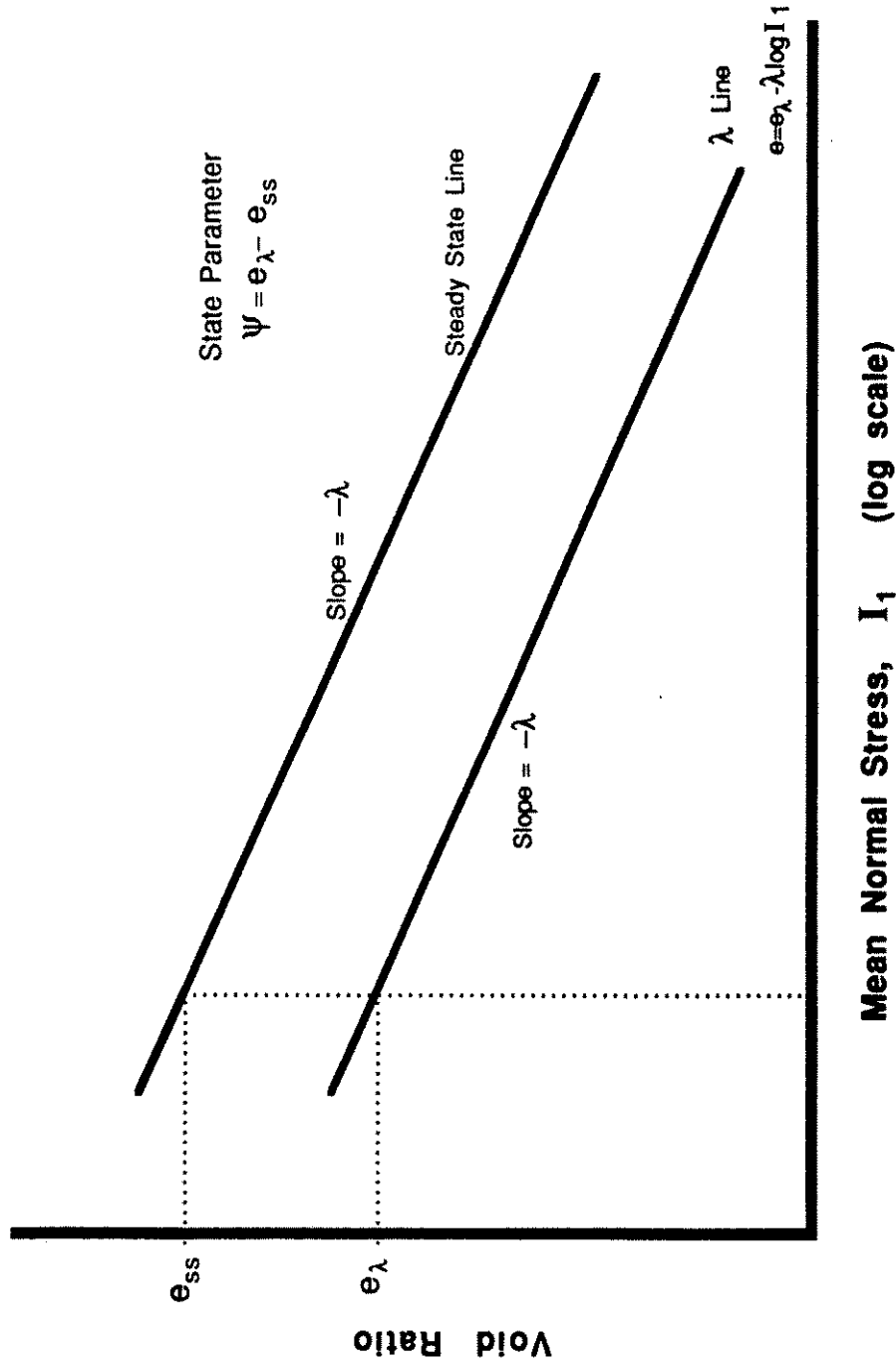


FIGURE 4.31: State Parameter Definition

Adapted from Been and Jefferies (1985)

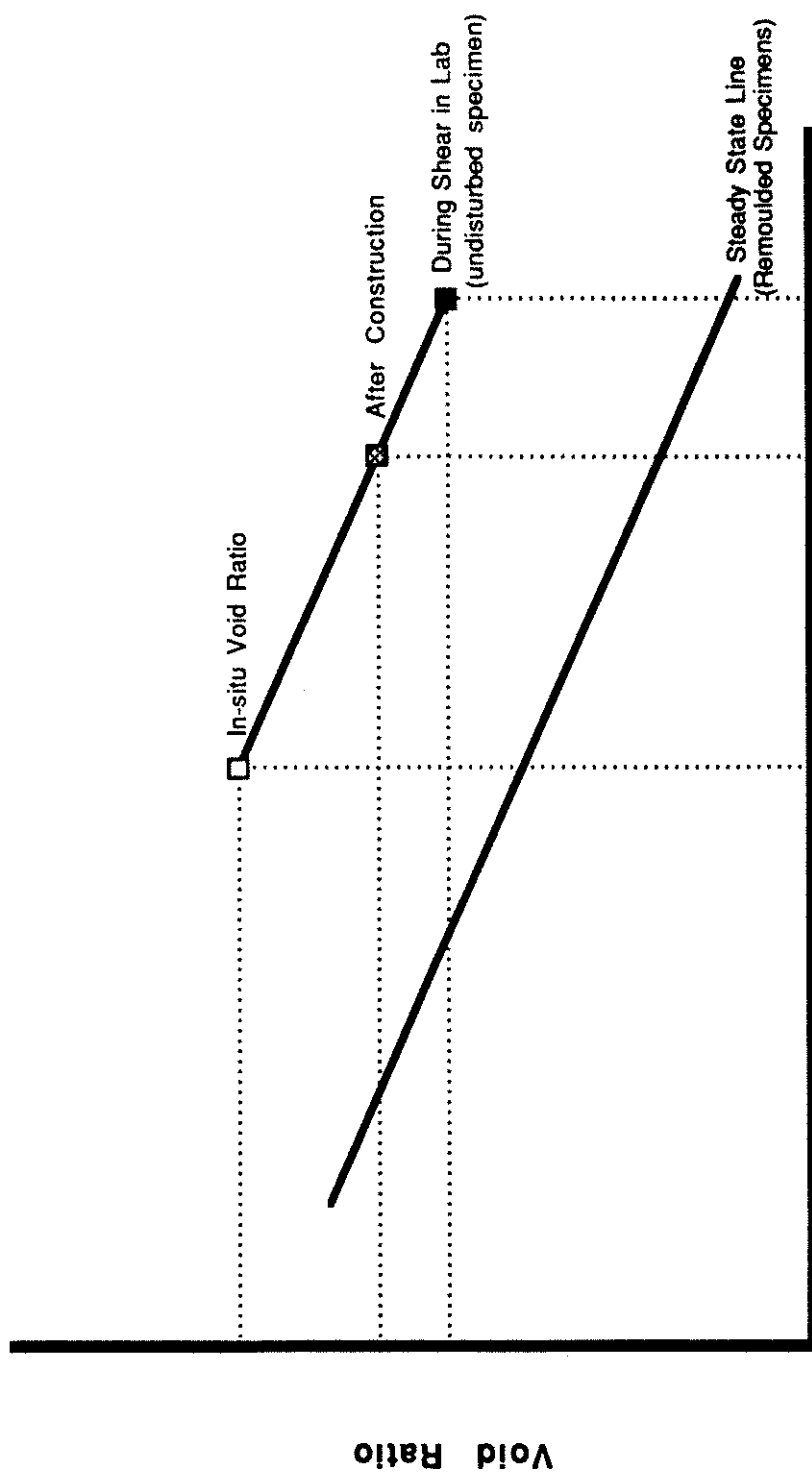


FIGURE 4.32: Steady State Diagram Showing Correction of S_{us}
Adapted from Castro (1985)

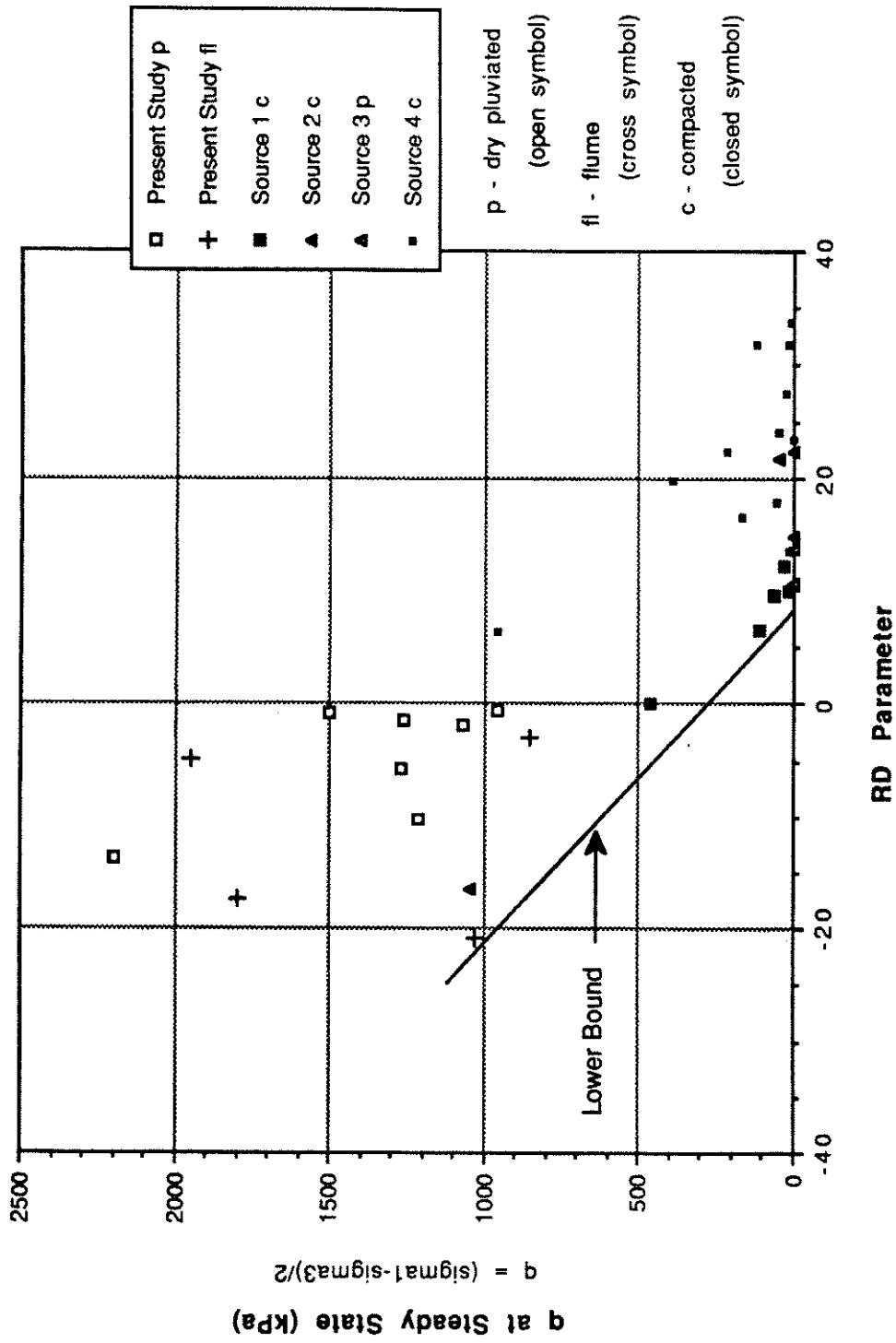


FIGURE 4.33: Steady State Shear Strength vs RD Parameter

5. CONCLUSIONS

5.1. General

The analysis of fabric as determined by the qualitative and quantitative techniques outlined in Chapter 3 failed to show a significant difference in fabric among the three depositional methods studied (pluviation, flume and field deposition). A technique was developed to allow the viewing of undisturbed tailings sand in the Scanning Electron microscope, and a practical method of obtaining and analyzing orientation data from the SEM micrographs is outlined. This quantitative analysis was compared to a visual assessment of the fabric as determined from the micrographs.

The Chapter 4 assessment of the mechanical behaviour differences due to specimen preparation differences (or inherent fabric) indicated that no specific fabric induced behavioural differences could be separated from the natural scatter of the data. The pre-shear and steady state conditions were determined for this material in terms of dry density and relative density. Less scatter was observed with the use of the relative density representation of the state conditions, likely due to the normalizing effect of relative density on the factors known to affect both the maximum and minimum density determinations and the steady state condition (including grain size distribution, grain shape and surface texture). Dilative test results were used to characterize the steady state condition above the 1000 kPa effective stress level, and the results linked well with those determined from contractive test data. For this tailings sand material, volume change characteristics in the pre-shear stage of the triaxial test do not appear to be affected by freezing the sand specimen prior to test set-up.

The Relative Density (RD) parameter was developed to attempt to normalize the observed mechanical behaviour in terms of state and small gradational differences among the tests. A weak correlation was observed with the moderate strain parameters (initial tangent modulus, foreslope modulus, stress ratio and A parameter at the elbow), but no fabric influence was evident. A strong correlation exists between the RD parameter and the steady state shear strength. From this plot a lower bound shear strength can be estimated based on the expected field state and its proximity to the behavioural boundary defined in terms of the RD parameter.

From the above results on the effect of the inherent fabric on the mechanical behaviour as observed in the undrained triaxial compression test, the method of deposition during specimen preparation was found to be relatively unimportant for this sand. Subtle differences may exist, however, that were not revealed by this study. Of more importance appears to be the understanding of the range of material differences to be expected in the volume of material investigated, and obtaining material representative of this range for testing.

5.2. Limitations Of The Study

The analysis of fabric performed in this study was by no means exhaustive. This investigation was limited to a two-dimensional quantitative study of the long axis orientations of the visible portions of the grains exposed on each face studied, coupled with a visual assessment of the fabric characteristics. A more complete study, possibly including three-dimensional grain orientation determination and the assessment of contact normal direction distributions may have allowed the statistical determination of fabric differences among the depositional methods studied. This study also focused on the

microfabric of the material. The actual field behaviour may be more dependent on a pervasive macrofabric than the general underlying microfabric analyzed in this study.

The fabric produced by the compaction method of deposition, as performed by the other testing laboratories whose results are included in the analysis, was not investigated in this study. Although no apparent mechanical behaviour differences were observed due to this placement method, the observed fabric may be different than that observed for the other methods of placement.

The data compared in this study was from six different sources performed at five different laboratories, each using somewhat different equipment and operation techniques. Some of the scatter observed in the comparison of the triaxial test results is undoubtedly due to these factors.

Membrane penetration effects on the pore pressure response are expected to be small because of the fine grained nature of the material investigated. The effects may not be negligible, however, and variation in pore pressure response due to this phenomenon is expected, especially between testing programs with different specimen sizes. The effects of membrane penetration on the foreslope modulus may be significant, and were not accounted for in the present study nor the other studies investigated. This error is expected to have added to the scatter of the triaxial test results.

In summary, a more thorough fabric analysis, consistent testing conditions and a better understanding of the material variability may have allowed the observation of subtle fabric differences among the placement methods and possibly the determination of the influence of these subtle fabric differences on the mechanical behaviour of the tailings sand material.

5.3. Recommendations For Further Study

The effect of small variations in the gradational properties on the steady state and max/min density characteristics of this material is not fully understood at this time. Further study into the effect of these variations is recommended to better understand the relationship between material differences and general behaviour during shear. A study into the macrofabric of this material as deposited on site may give insight into the differences expected between laboratory and field behaviour.

The use of the SEM to assess fabric characteristics is promising. With patience, a three-dimensional representation of the orientation fabric may be obtained. The SEM also gives the viewer a good understanding of the grain to grain contact and packing characteristics associated with the fabric of the material. Stereo photography is one possible method to convey this information to the reader. Specimen preparation and viewing using the SEM would be highly facilitated by using a cryostage on which to mount and view specimens. With a cryostage set-up, many of the difficulties involved in maintaining specimen orientation and providing for the least specimen disturbance possible would be averted.

REFERENCES

- Arthur, J. R. F. and Menzies, B. K., 1972. Inherent anisotropy in a sand. *Geotechnique*, Volume 22, No. 1, pp. 115-128.
- Baker, T. H. W., 1976. Transportation, preparation, and storage of frozen soil samples for laboratory testing. *Soil Specimen Preparation for Laboratory Testing*, ASTM STP 599, pp. 88-112.
- Been, K. and Jefferies, M. G., 1985. A state parameter for sands. *Geotechnique*, Volume 35, No. 2, pp. 99-112.
- Bishop, A. W. and Henkel, D. J., 1962. *The measurement of soil properties in the triaxial test*. Second Edition, Edward Arnold (Publishers) Ltd., London, 227 p.
- Bishop, A. and Eldin, A. K. G., 1950. Undrained triaxial tests on saturated sands and their significance in the general theory of shear strength. *Geotechnique*, Volume 2, No. 4, pp. 13-32.
- Black, D.K. and Lee, K.L., 1973. Saturating laboratory samples by back pressure. *ASCE JSMFD*, SM1, Volume 99, pp. 75-93.
- Brewer, R., 1964. *Fabric and Mineral Analysis of Soils*. J. Wiley and Sons Inc., New York.
- Campbell, D. A., 1985. Sand fabric as an indicator of stress-strain response and enhanced techniques for its measurement. Ph.D. Thesis, Univ. of Colorado, 1985, 415 p.
- Casagrande, A. and Carillo, N., 1944. Shear failure of anisotropic materials. *Proceedings of the Boston Society of Civil Engineers*, Volume 31, pp. 74-87.
- Casagrande, A., 1936. Characteristics of cohesionless soils affecting the stability of slopes and earth fills. *Journal of the Boston Society of Civil Engineers*, Reprinted in 'Contributions to Soil Mechanics 1925-1940', Boston Society of Civil Engineers (1940), pp. 257-276.
- Castro, G., 1969. Liquefaction of sands. Ph. D Thesis, Harvard University, 1969, 112 p.

- Castro, G., 1975. Liquefaction and cyclic mobility of saturated sands. ASCE JGED, Volume 101, GT6, pp. 551-569.
- Castro, G., Poulos, S. J., France, J. W., and Enos, J. L., 1982. Liquefaction induced by cyclic loading. Report to National Science Foundation by Geotechnical Engineers Inc., Winchester, Massachusetts, pp. 1-80.
- Castro, G., Poulos, S. J. and Leathers, F. D., 1985. Re- examination of the slide of Lower San Fernando dam. ASCE JGED, Volume 111, GT9, pp. 1093-1107.
- Castro, G., 1987. On the behaviour of soils during earthquakes. Liquefaction - 3rd International Conference on Soil Dynamics and Earthquake Engineering, pp. 169-204.
- Curry, J. R., 1956. The analysis of two-dimensional orientation data. Journal of Geology, Volume 64, pp. 115-131.
- Dennis, N. D., 1988. Influence of specimen preparation techniques and testing procedures on undrained steady state shear strength. Advanced Testing of Soil and Rock, ASTM STP 977, pp. 642-654.
- Dunstan, T., 1972. The influence of grading on the anisotropic strength of sand. Geotechnique, Volume 22, No. 3, pp. 529-532.
- Dusseault, M. B., 1977. The geotechnical characteristics of the Athabasca oil sands. Ph D Thesis, Department. of Civil Engineering, University of Alberta, 472 p.
- EBA Engineering Consultants Ltd., 1987. Steady state triaxial testing of Syncrude tailings sand. Report submitted to Syncrude Canada Ltd., R 0202, pp. 1-12.
- Feda, J., 1982. Mechanics of Particulate Materials; The Principles. Elsevier Scientific Publishing Co., Amsterdam, 447 p.
- Geotechnical Engineers Inc., 1978a. Report on laboratory investigation of liquefaction potential of Syncrude tar-sand tailings. Report submitted to R. M. Hardy & Associates Ltd. for Syncrude Canada Ltd., R 0023, pp. 1-17.

- Geotechnical Engineers Inc., 1978b. Evaluation of liquefaction potential - Syncrude tar-sand tailings. Report submitted to R. M. Hardy & Associates Ltd. for Syncrude Canada Ltd., R 0027, pp. 1-9.
- Geotechnical Engineers Inc., 1981a. Liquefaction potential of tailings sand in Syncrude tailings dam. Report submitted to R. M. Hardy & Associates Ltd. for Syncrude Canada Ltd., R 0052, pp. 1-7.
- Geotechnical Engineers Inc., 1981b. Data for tests in report titled 'Liquefaction potential of tailings sand in Syncrude Tailings Dam'. Report submitted to R. M. Hardy & Associates Ltd. for Syncrude Canada Ltd., R 0168,
- Hardy BBT Ltd., 1987. Laboratory testing - Liquefaction Studies. Report submitted to Syncrude Canada Ltd., R 0184, pp. 1-5.
- Hardy BBT Ltd., 1988. Laboratory Testing - Liquefaction Studies. Report submitted to Syncrude Canada Ltd., R 0299, pp. 1-7.
- Johnson, H. V., 1982. Effects of end platens, method of loading, and specimen size in monotonic triaxial R tests. US Army Waterways Experimental Station (Vicksburg, Miss.), GL-82-10, pp. 1-122.
- Kiekbusch, M. and Schuppener, B., 1977. Membrane penetration and its effect on pore pressures. ASCE JGED, Volume 103, GT11, pp. 1267-1279.
- Kupper, A. A. G., 1991. Design of hydraulic fills. Ph. D Thesis, Department of Civil Engineering, University of Alberta.
- Ladd, R. S., 1974. Specimen preparation and liquefaction of sands. ASCE JGED, Volume 100, GT10, pp. 1180-1184.
- Lee, K. L., 1978. End restraint effects on undrained static triaxial strength of sand. ASCE JGED, Volume 140, GT6, pp. 687-704.
- Mahmood, A. and Mitchell, J. K., 1974. Fabric-property relationships in fine granular materials. Clays and Clay Minerals, Volume 22, No. 516, pp.397-408.

- Mahmood, A., Mitchell, J. K. and Lindblom, U., 1976. Effect of specimen preparation method on the grain arrangement and compressibility in sand. *Soil Specimen Preparation for Laboratory Testing*, ASTM STP 599, pp. 169-192.
- Mitchell, J. K., Chatoian, J. M. and Carpenter, G. C., 1976. The influences of sand fabric on liquefaction behavior. *Contract Report S-76-5*, US Army Waterways Experimental Station (Vicksburg, Miss.), pp. 1-79.
- Miura, S. and Toki, S., 1982. A sample preparation method and its effect on static and cyclic deformation-strength properties of sand. *Soils and Foundations*, JSSMFE, Volume 22, No. 1, pp. 61-77.
- Mohamad, R. and Dobry, R., 1986. Undrained monotonic and cyclic triaxial strength of sand. *ASCE JGED*, Volume 112, No. 10, pp. 941-958.
- Mulilis, J. P., Seed, H. B., Chan, C. K., Mitchell, J. K. and Arulanandan, K., 1977. Effects of sample preparation on sand liquefaction. *ASCE JGED*, Volume 103, GT2, pp. 91-108.
- Nemat-Nasser, S. and Tobita, Y., 1982. Influence of fabric on liquifaction and densification potential of cohesionless sand. *Mechanics of Materials*, Volume 1, pp. 43-62.
- Ochiai, H. and Lade, P. V., 1983. Three-dimensional behavior of sand with anisotropic fabric. *ASCE JGED*, Volume 109, No. 10, pp. 1313-1328.
- Oda, M., 1972a. The mechanism of fabric changes during compressional deformation of sand. *Soils and Foundations*, JSSMFE, Volume 12, No. 2, pp. 1-18.
- Oda, M., 1972b. Initial fabrics and their relations to mechanical properties of granular material. *Soils and Foundations*, JSSMFE, Volume 12, No. 1, pp. 17-36.
- Oda, M., 1972c. Deformation mechanism of sand in triaxial compression. *Soils and Foundations*, JSSMFE, Volume 12, No. 4, pp. 45-63.
- Oda, M., 1976. Fabrics and their effects on the deformation behaviours of sand. *Department of Foundation Engineering, Saitama University, Japan, Special Issue*, pp. 1-59.

- Oda, M., Konishi, J. and Nemat-Nasser, S., 1980. Some experimentally based fundamental results on the mechanical behaviour of granular materials. *Geotechnique*, Volume 30, No. 4, pp. 479-495.
- Phillips, A. B. and May, P. H., 1967. A form of anisotropy in granular media. Special Task Report, Department of Civil and Municipal Engineering, University College, London.
- Pincus, H. J., 1953. The analysis of aggregates of orientation data in the earth sciences. *Journal of Geology*, Volume 61, No. 6, pp. 482-509.
- Plewes, H. D., 1987. Undrained strength of Athabasca oil sand. M. Sc. Thesis, Department of Civil Engineering, University of Alberta, 428 p.
- Poulos, S. J., 1971. The stress-strain curves of soils. *Geotechnical Engineers Inc.*, Winchester, Massachusetts, pp. 1-80.
- Poulos, S. J., 1981. The steady state of deformation. *JGED ASCE*, Volume 107, GT5, pp. 553-561.
- Raju, V. S., Sadasivan, S. K. and Venkataraman, M., 1972. Use of lubricated and conventional end platens in triaxial tests on sands. *Soils and Foundations*, *JSSMFE*, Volume 12, No. 4, pp. 35-43.
- Rayleigh, Lord (Strutt, J. W.), 1894. *The theory of sound*. 2nd Edition, Vol. 1, New York, reprinted in 1945 by Dover Publications, 480 p.
- Rowe, P. W. and Barden, L., 1964. Importance of free ends in triaxial testing. *ASCE JSMFD*, Volume 90, SM1, pp. 1-27.
- Saada, A. S. and Townsend, F. C., 1981. State of the art: Laboratory strength testing of soils. *Laboratory Shear Strength of Soil*, ASTM STP 740, pp. 7-77.
- Sides, G. R., 1971. Soil microstructure and sample disturbance observations in the stereoscan electron microscope. *Proceedings of the Roscoe Memorial Symposium on Stress-Strain Behaviour of Soils*, Cambridge University, March 1971, pp. 89-98.

- Singh, S., Seed, H. B., and Chan, C. H., 1982. Undisturbed sampling of saturated sands by freezing. ASCE JGED, GT2, Volume 108, pp. 247-264.
- Sladen, J. A. and Handford, G., 1987. A potential systematic error in laboratory testing of very loose sands. Canadian Geotechnical Journal, Volume 24, pp.462-466.
- Smart, P., 1973. Microstructure analysis methods using electron microscopy. Proceedings of the International Symposium on Soil Structure, Gothenburg, Sweden, pp. 69-76.
- Taylor, D. W., 1941. Cylindrical compression research program on stress deformation and strength characteristics of soils. Seventh Progress Report to U.S Corps of Engineers, M.I.T.
- Thurber Consultants Ltd., 1985. Steady state testing of tailings sand - Laboratory Investigation. Report submitted to Syncrude Canada Ltd., R 0151, pp. 1-10.
- Tovey, N. K., 1973. Quantitative analysis of electron micrographs of soil structure. Proceedings of the International Symposium on Soil Structure, Gothenburg, Sweden, pp. 50-57.
- Tovey, N. K. and Yan, W. K., 1973. The preparation of soils and other geological materials for the S. E. M. Proceedings of the International Symposium on Soil Structure, Gothenburg, Sweden, pp. 59-67.
- Twenhofel, W. H., 1950. Principles of Sedimentation. McGraw-Hill Book Co. Inc., New York, pp. 303-313.
- Wong, R. K. S. and Arthur, J. R. F., 1985. Induced and inherent anisotropy in sand. Geotechnique, Volume 35, No. 4, pp. 478-481.
- Yano, L. T. and Handford, G. T., 1988. Tailings Engineering at Syncrude. Paper No. 181, Presented at the Canadian Institute of Mining Annual General Meeting, May 1988, Edmonton, Alberta, pp. 1-5.

**APPENDIX A - Selected SEM Micrographs and Rose
Diagrams**

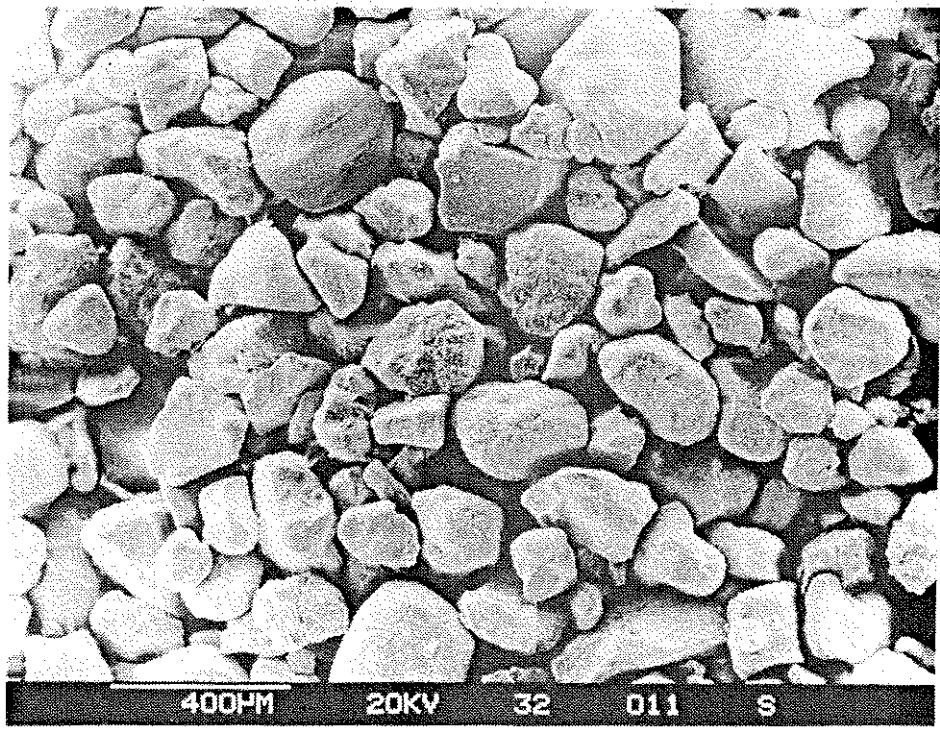
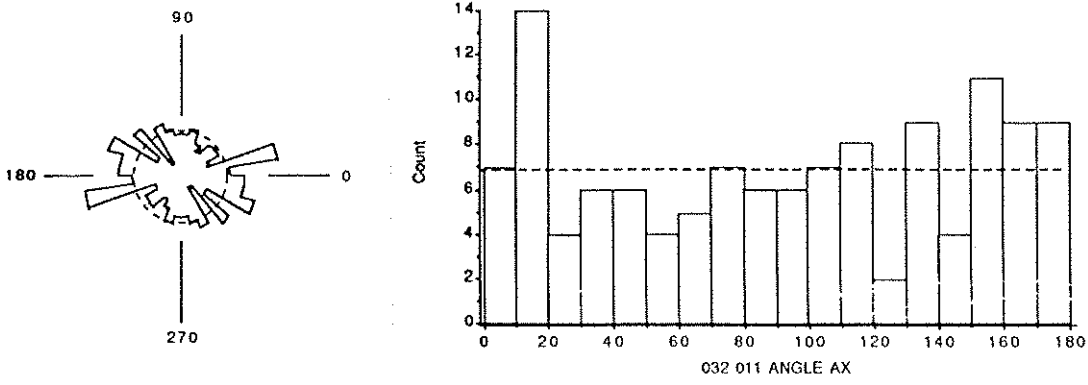


**PLATE A-1: Histogram and Rose Diagram
Micrograph 32 011 (Pluviated)**

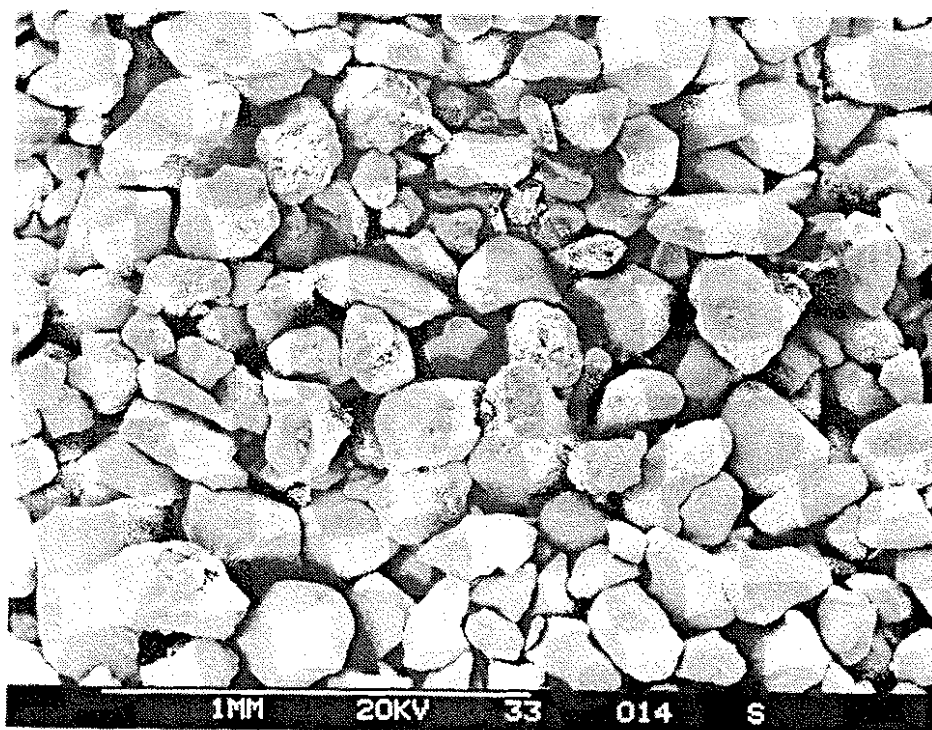
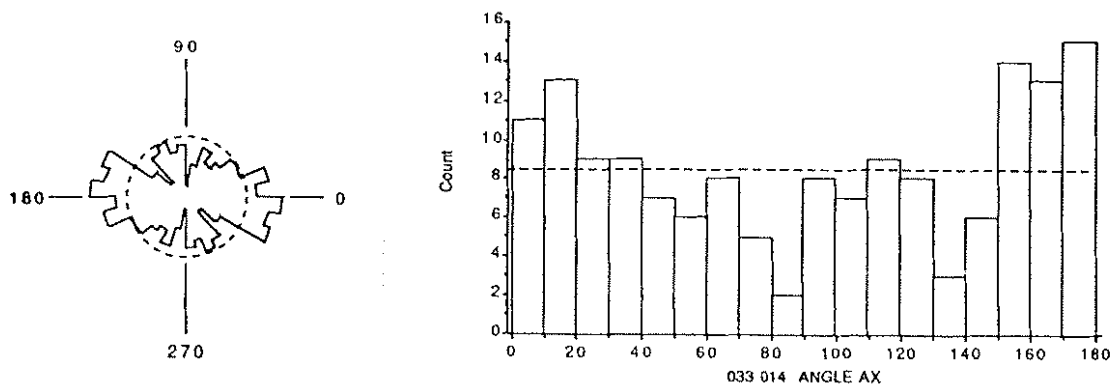


**PLATE A-2: Histogram and Rose Diagram
Micrograph 33 014 (Pluviated)**

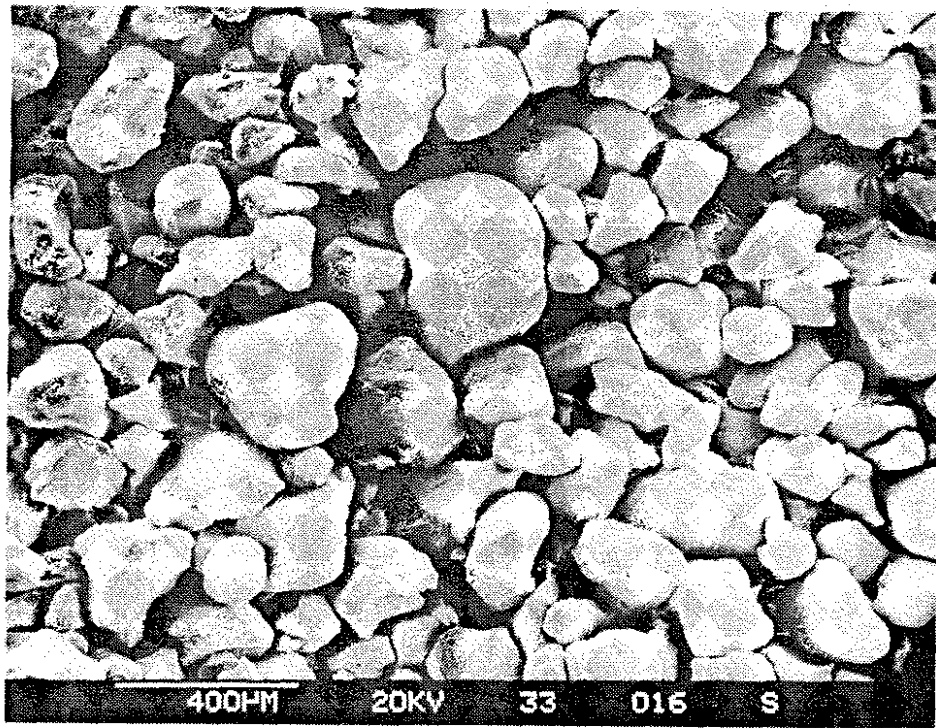
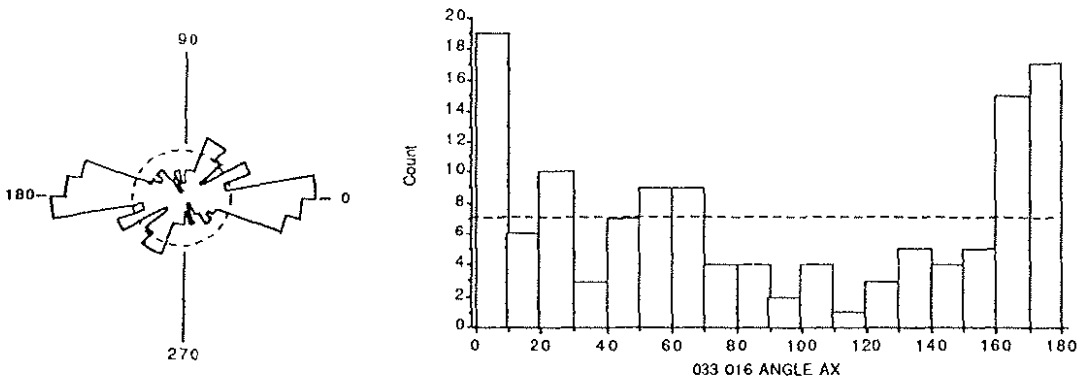


**PLATE A-3: Histogram and Rose Diagram
Micrograph 33 016 (Pluviated)**

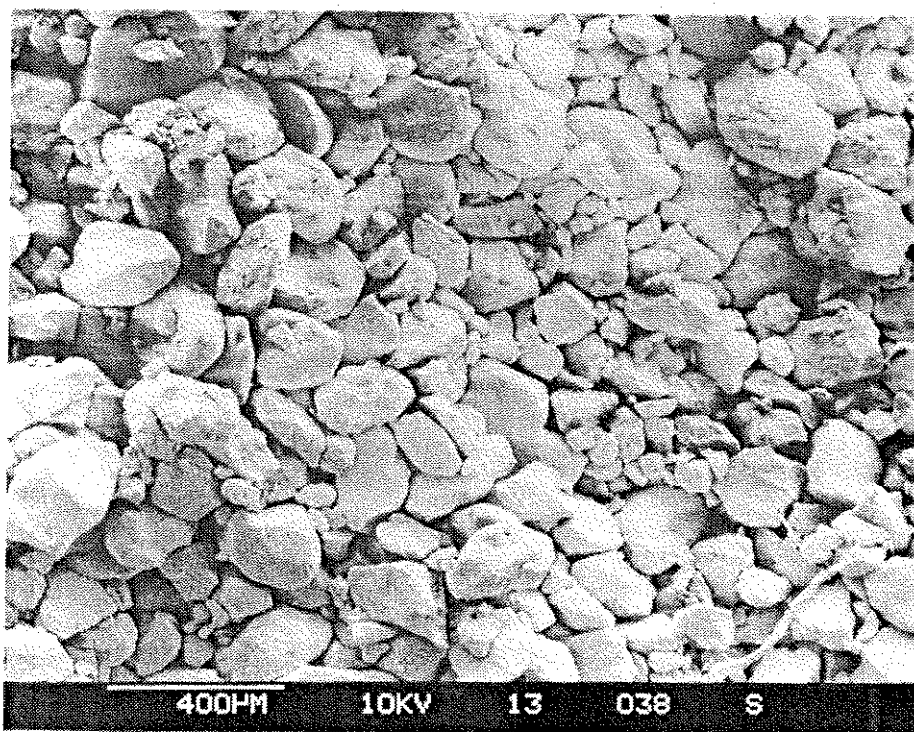
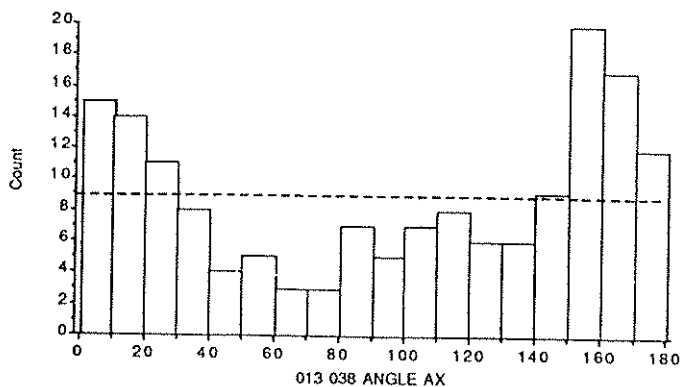
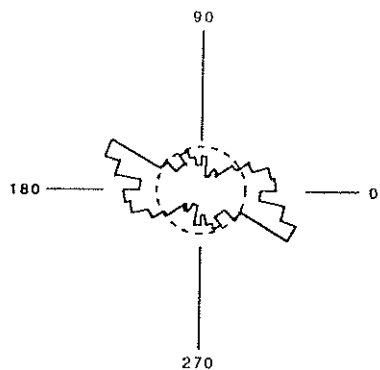


**PLATE A-4: Histogram and Rose Diagram
Micrograph 13 038 (Flume)**

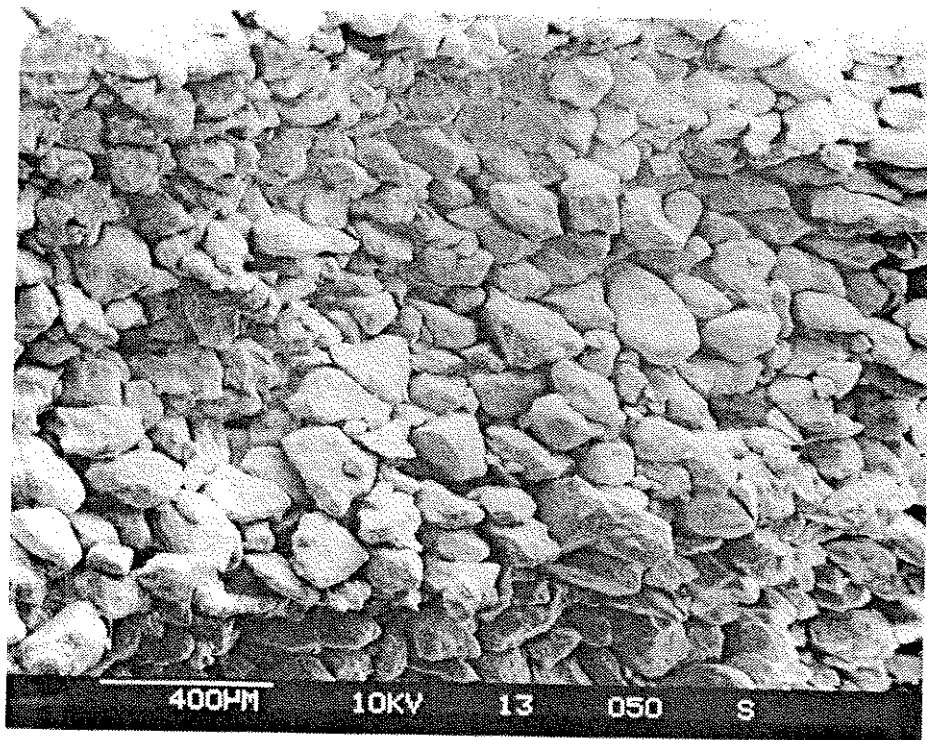
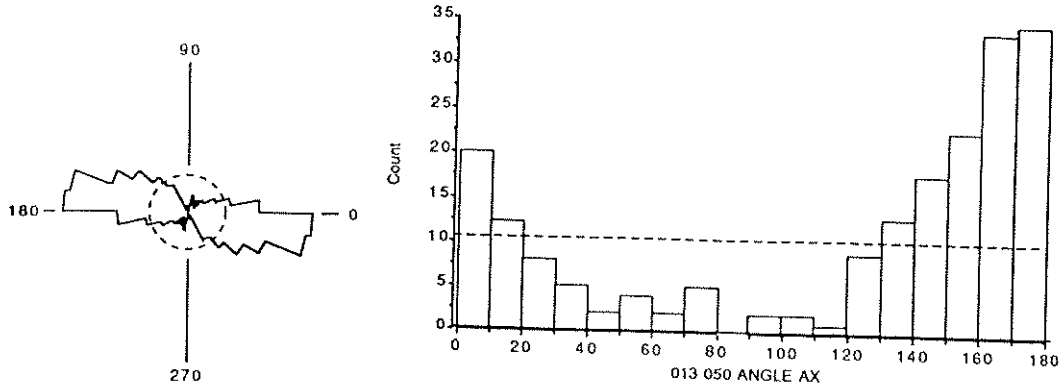


**PLATE A-5: Histogram and Rose Diagram
Micrograph 13 050 (Flume)**

MICROGRAPH 013 054

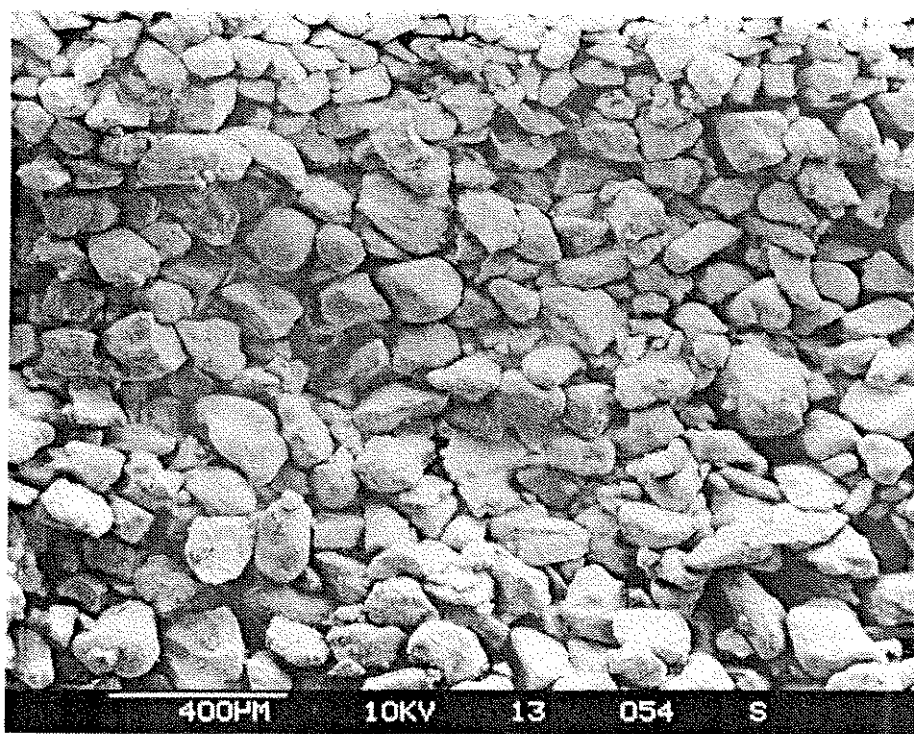
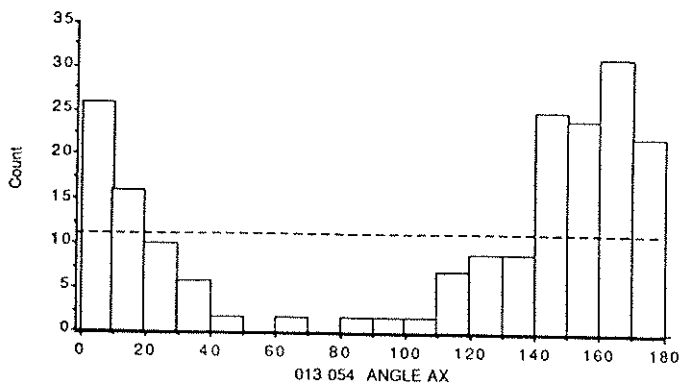
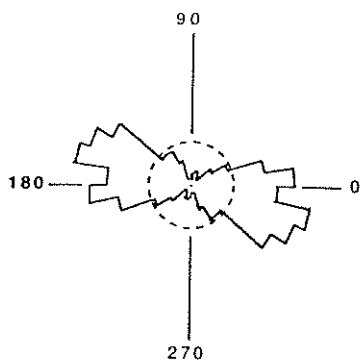
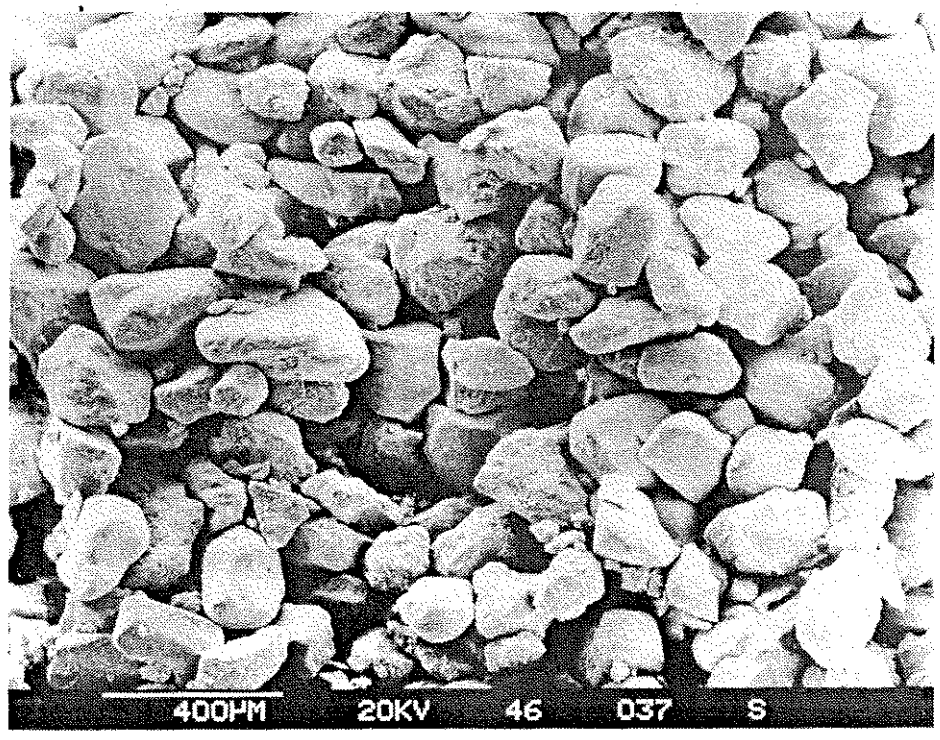
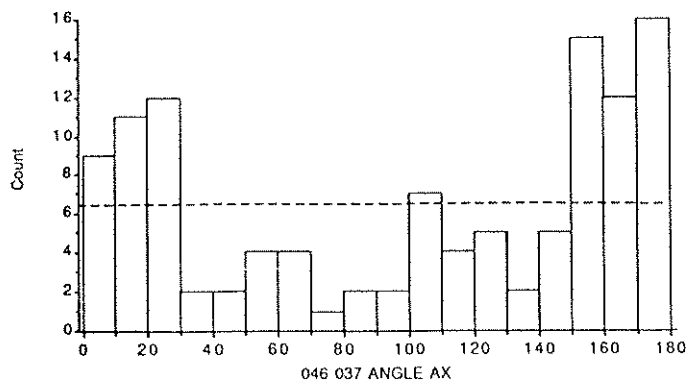
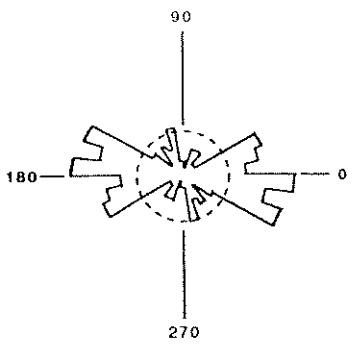
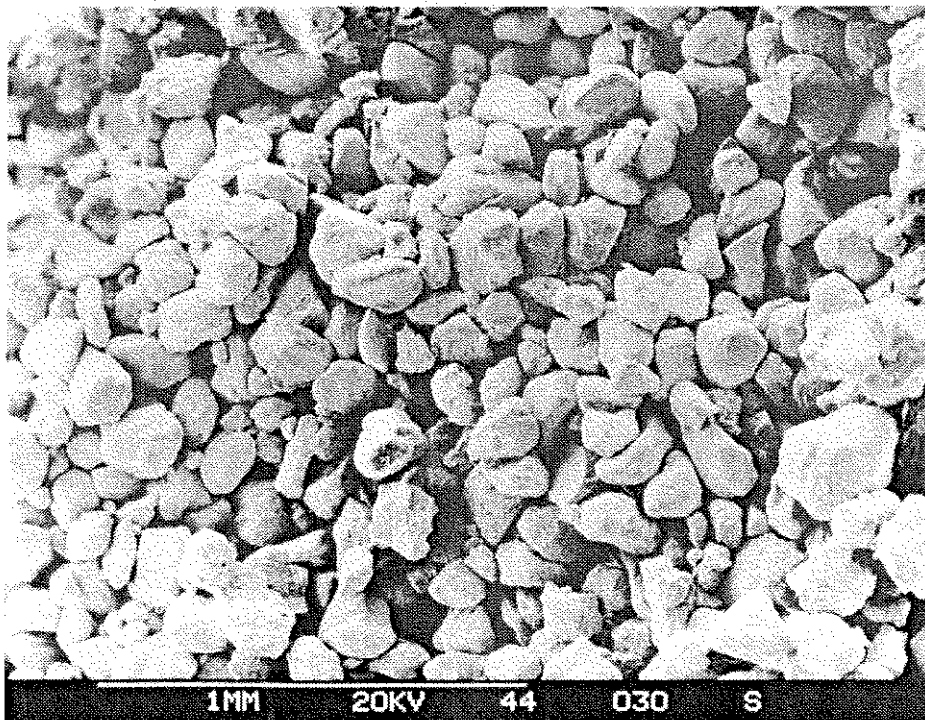
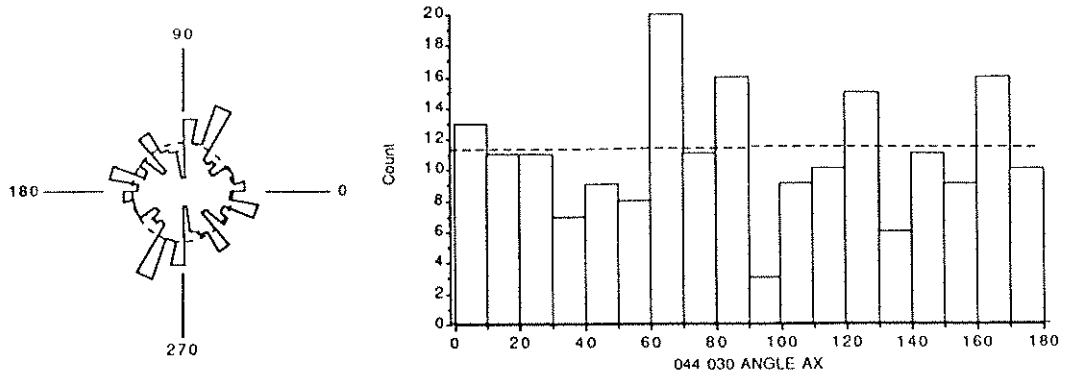


PLATE A-6: Histogram and Rose Diagram
Micrograph 13 054 (Flume)



**PLATE A-7: Histogram and Rose Diagram
Micrograph 46 037 (Flume)**



**PLATE A-8: Histogram and Rose Diagram
Micrograph 44 030 (Flume)**

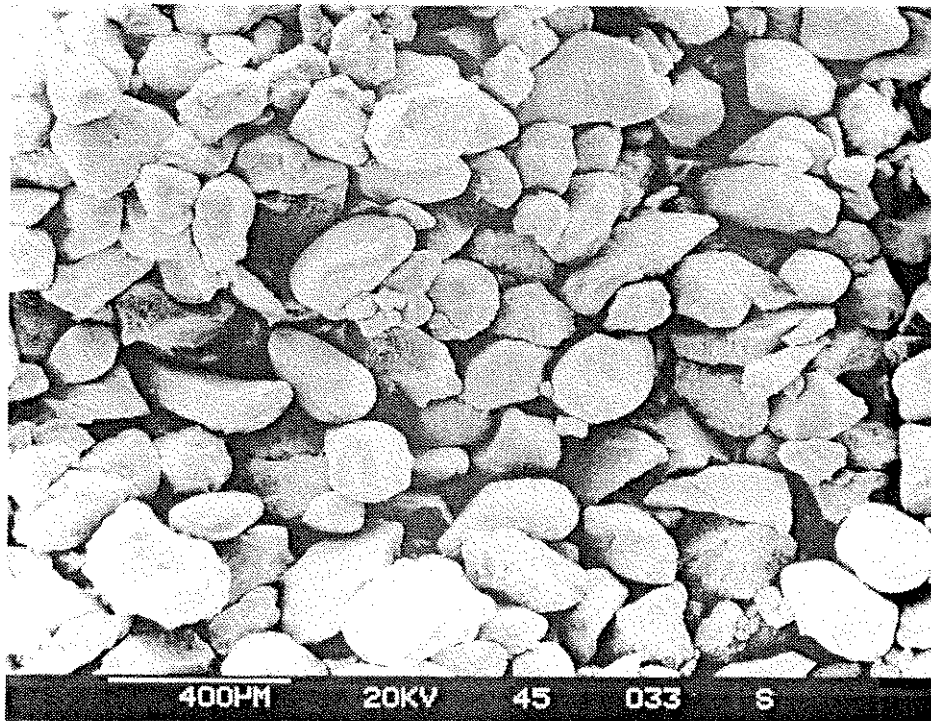
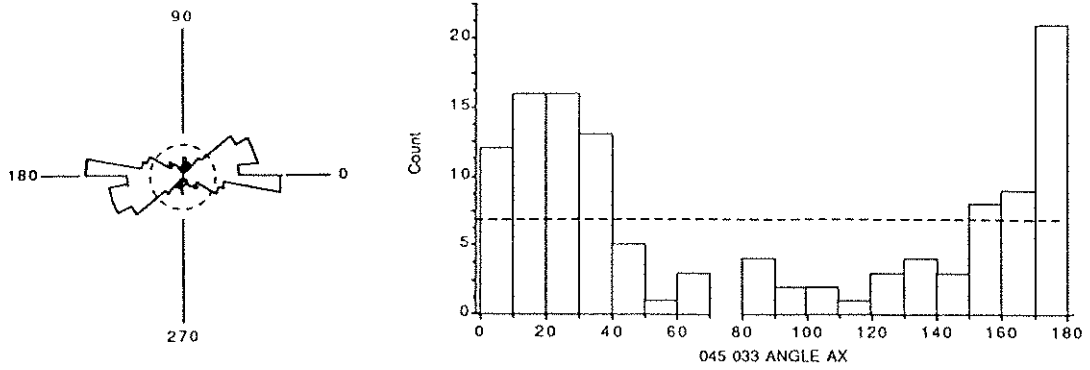


**PLATE A-9: Histogram and Rose Diagram
Micrograph 45 033 (Flume)**

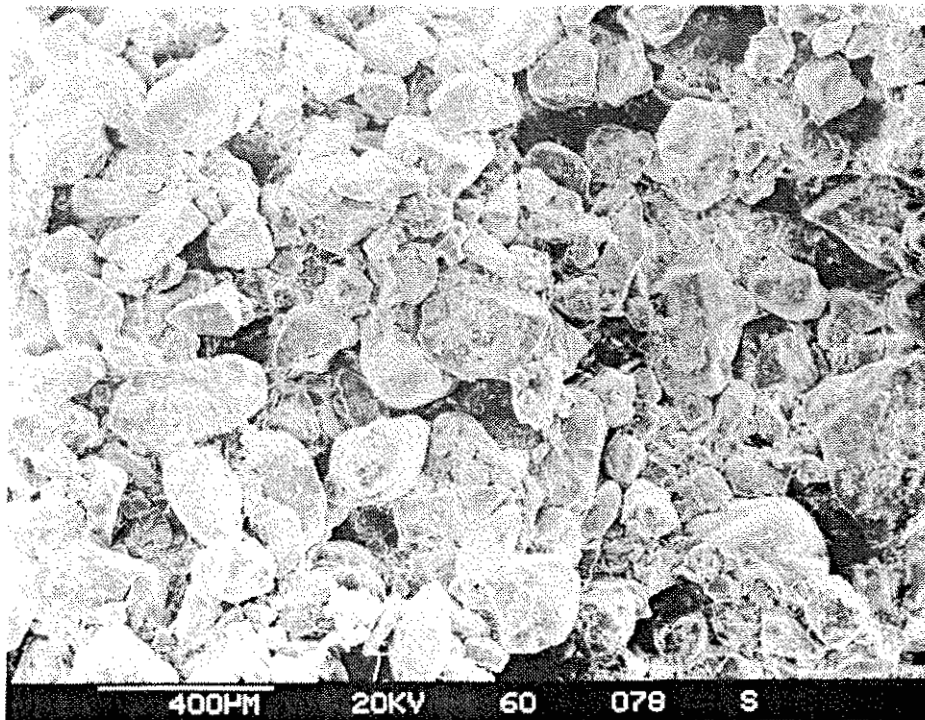
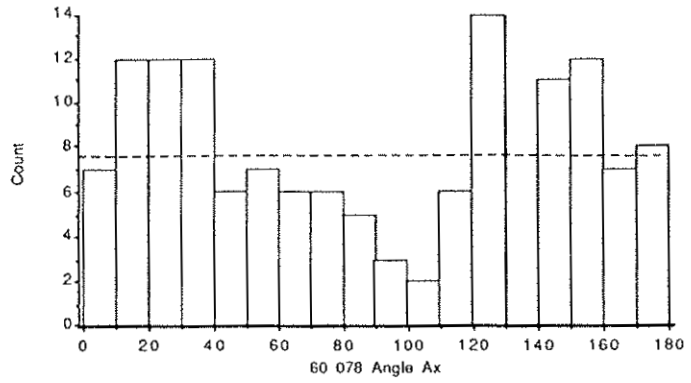
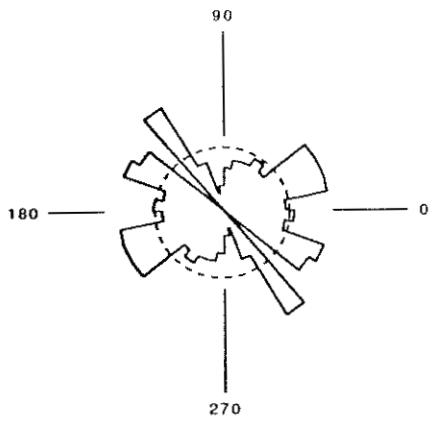


**PLATE A-10: Histogram and Rose Diagram
Micrograph 60 078 (Field)**

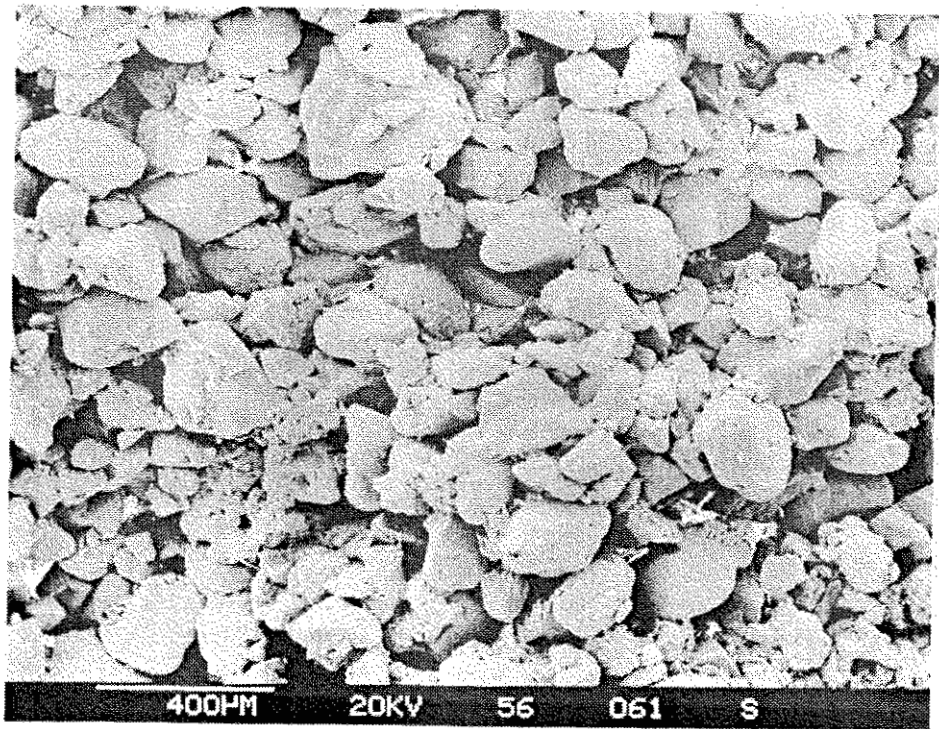
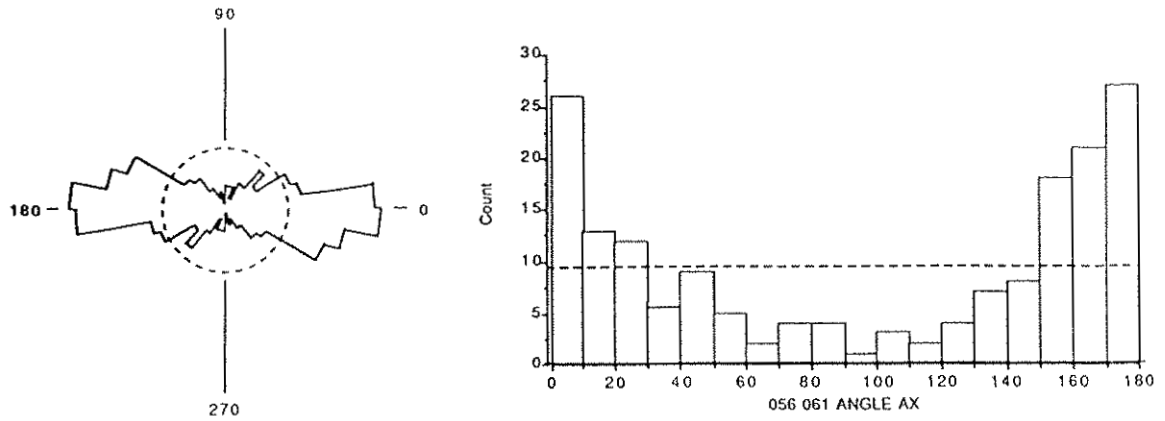


**PLATE A-11: Histogram and Rose Diagram
Micrograph 56 061 (Field)**

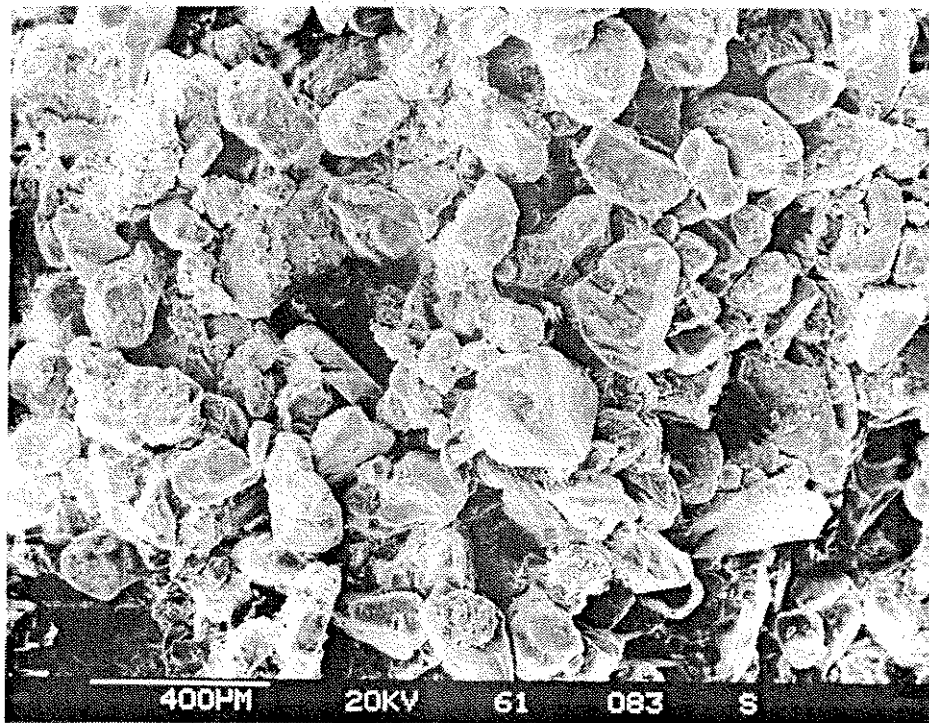
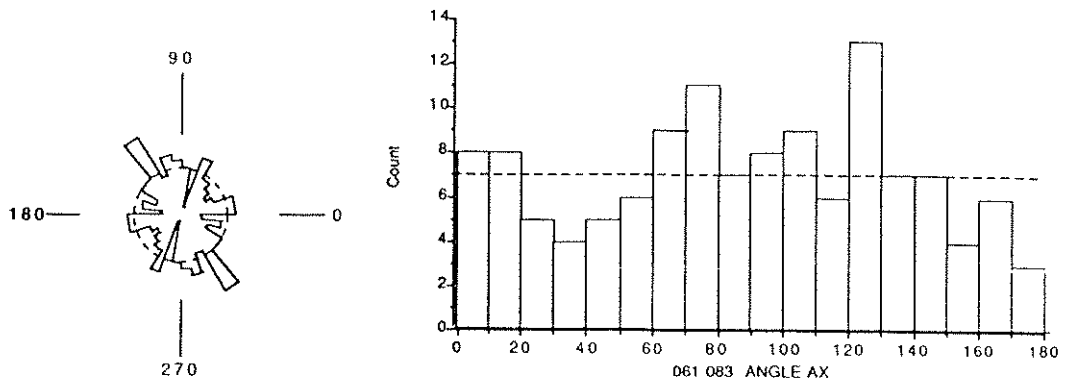


**PLATE A-12: Histogram and Rose Diagram
Micrograph 61 083 (Field)**

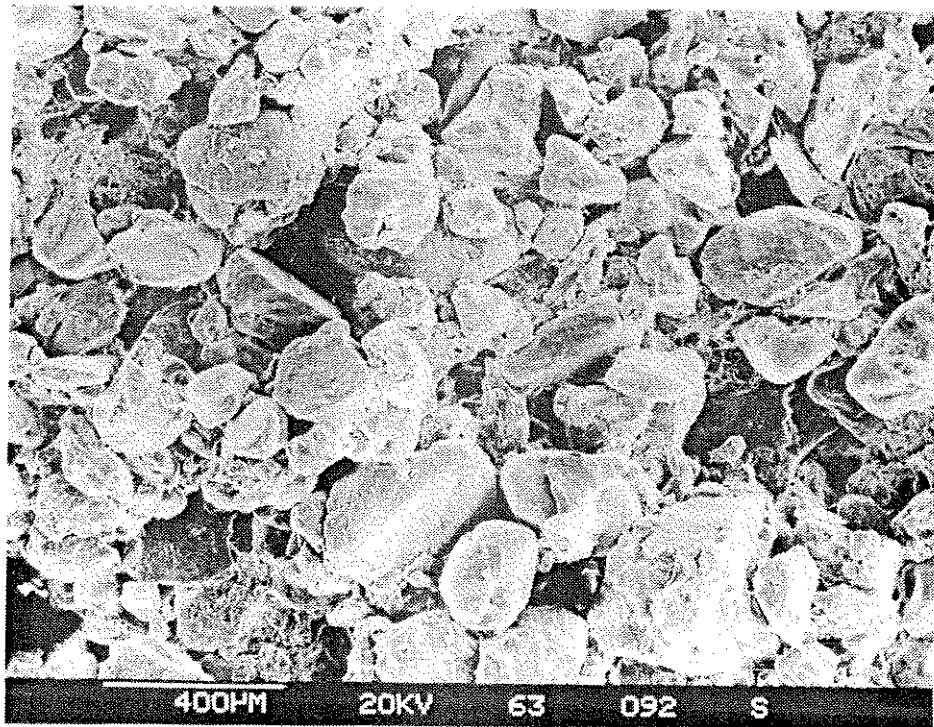
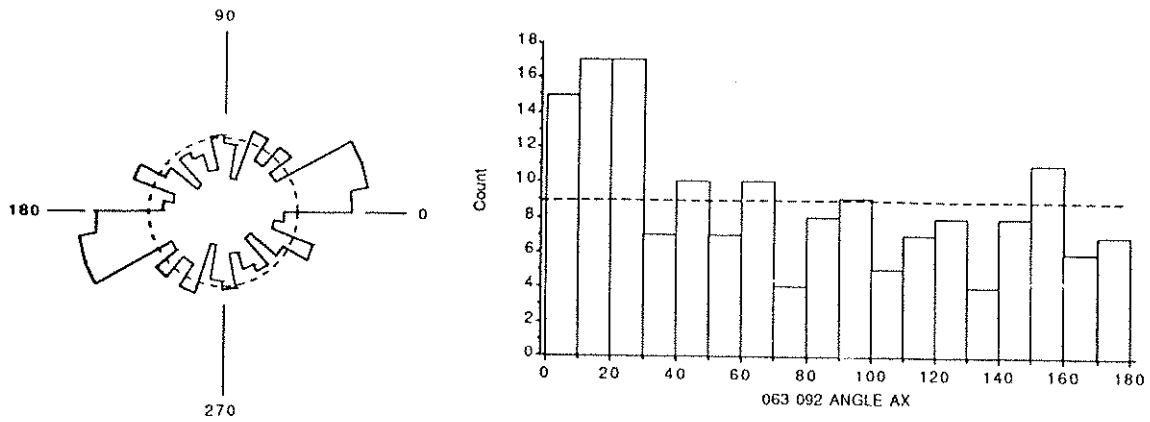


**PLATE A-13: Histogram and Rose Diagram
Micrograph 63 092 (Field)**

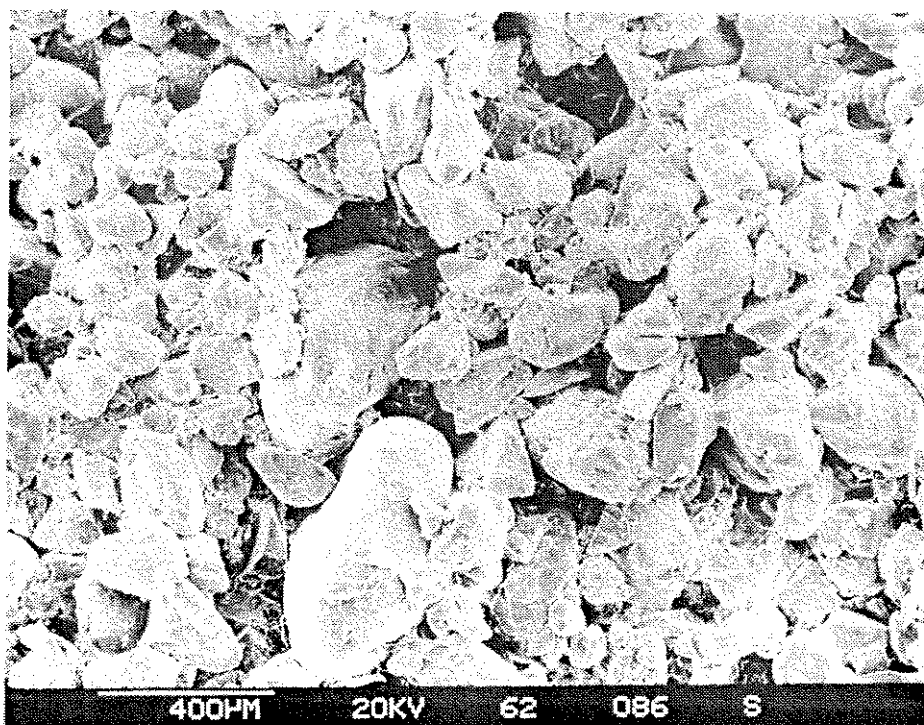
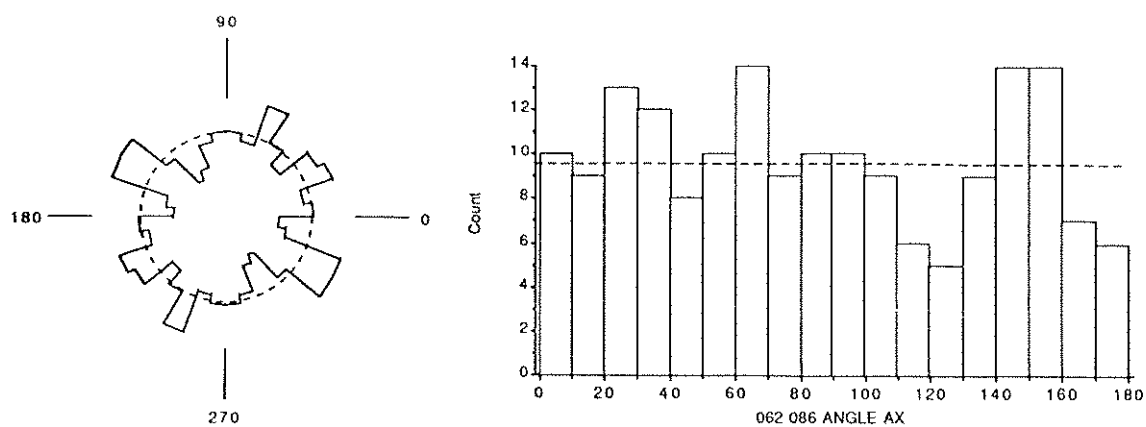
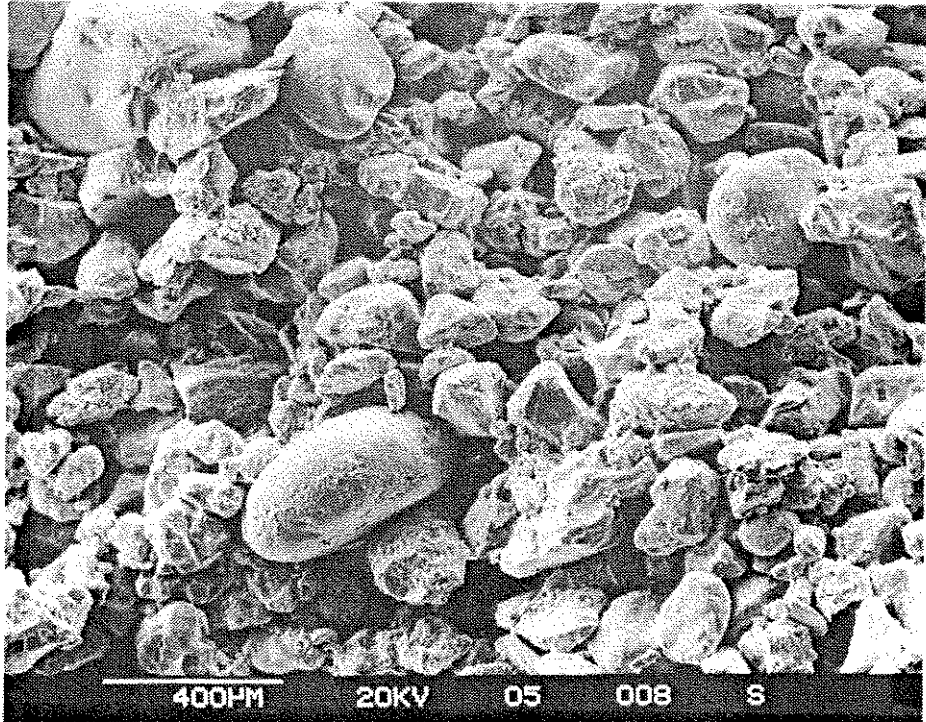
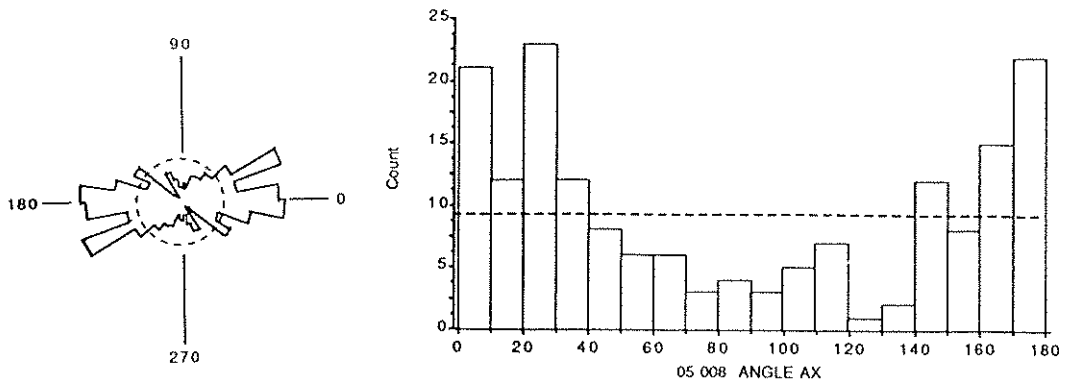
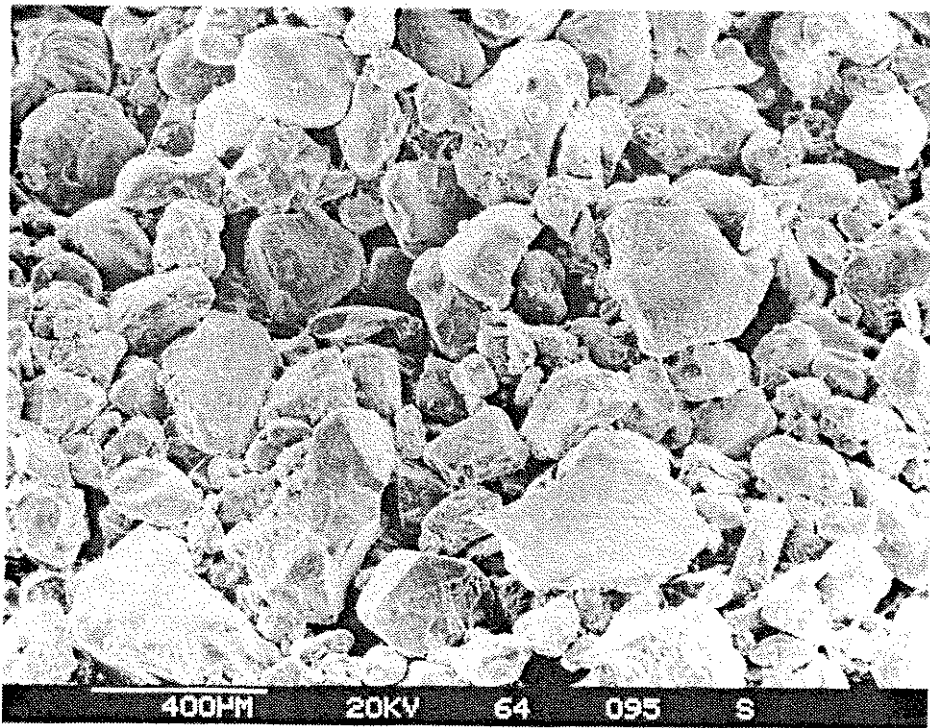
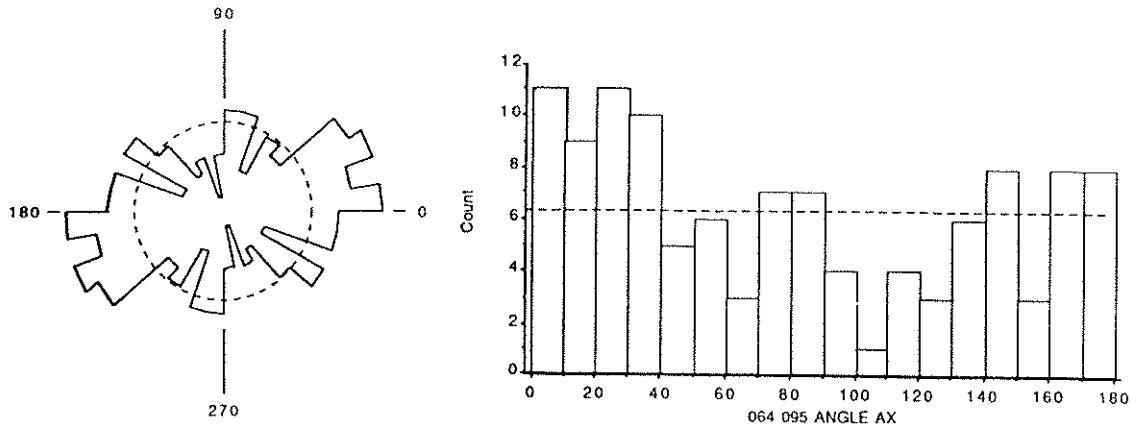


PLATE A-14: Histogram and Rose Diagram
Micrograph 62 086 (Field)



**PLATE A-15: Histogram and Rose Diagram
Micrograph 05 008 (Field)**



**PLATE A-16: Histogram and Rose Diagram
Micrograph 64 095 (Field)**

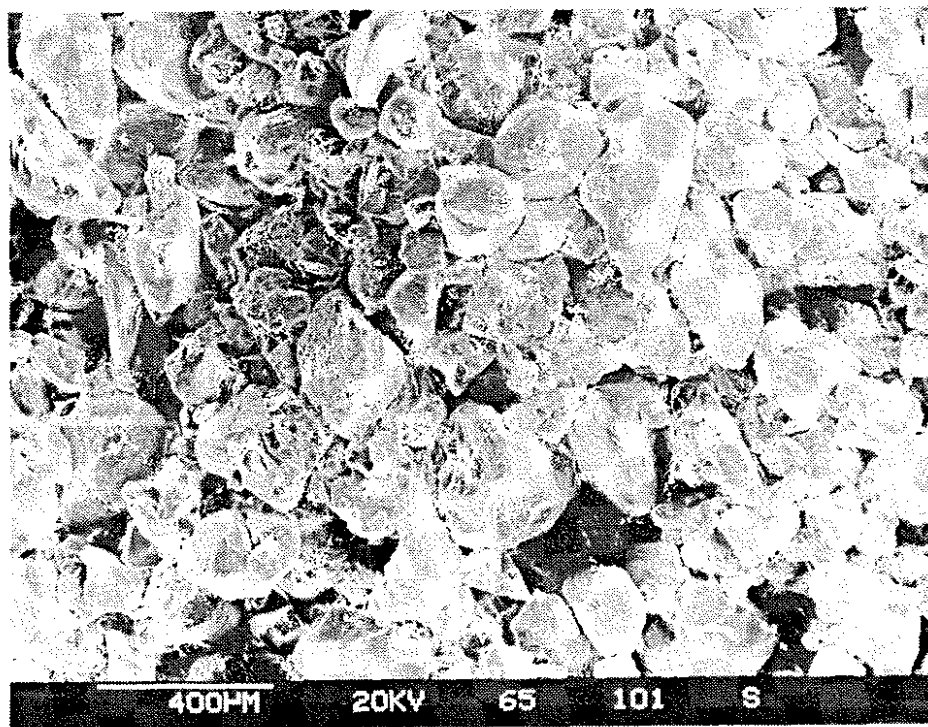
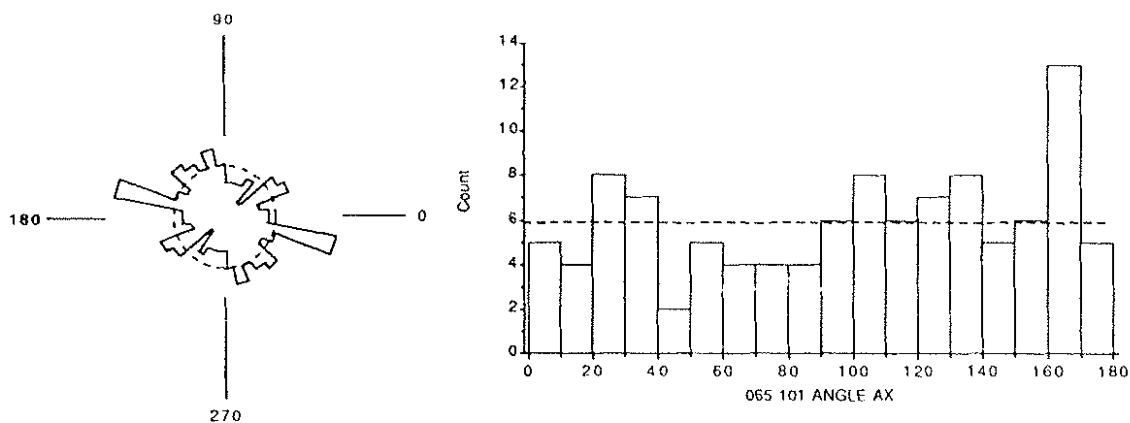


**PLATE A-17: Histogram and Rose Diagram
Micrograph 65 101 (Field)**

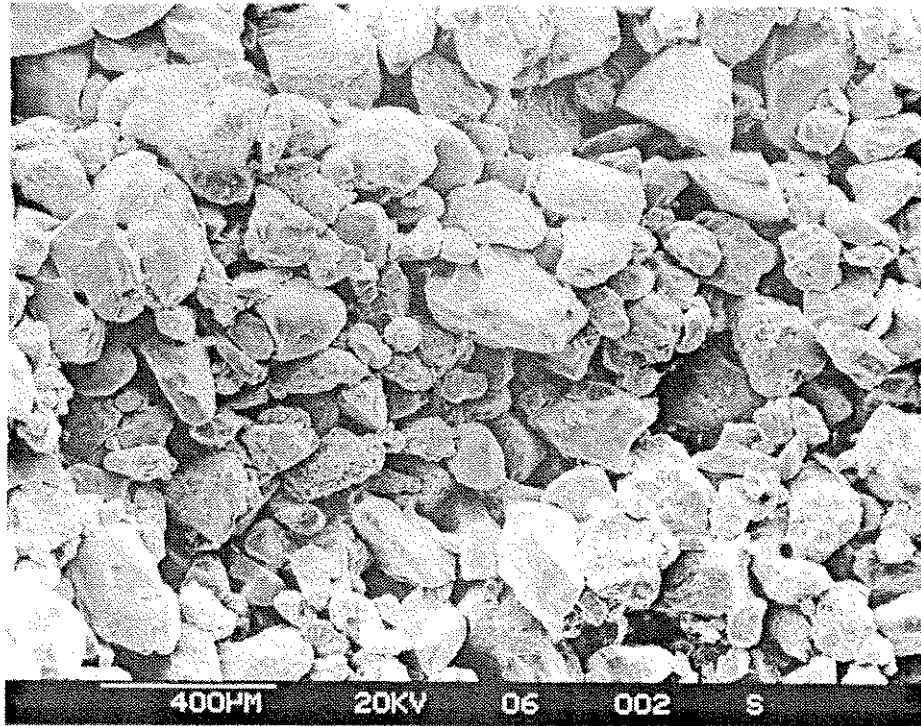
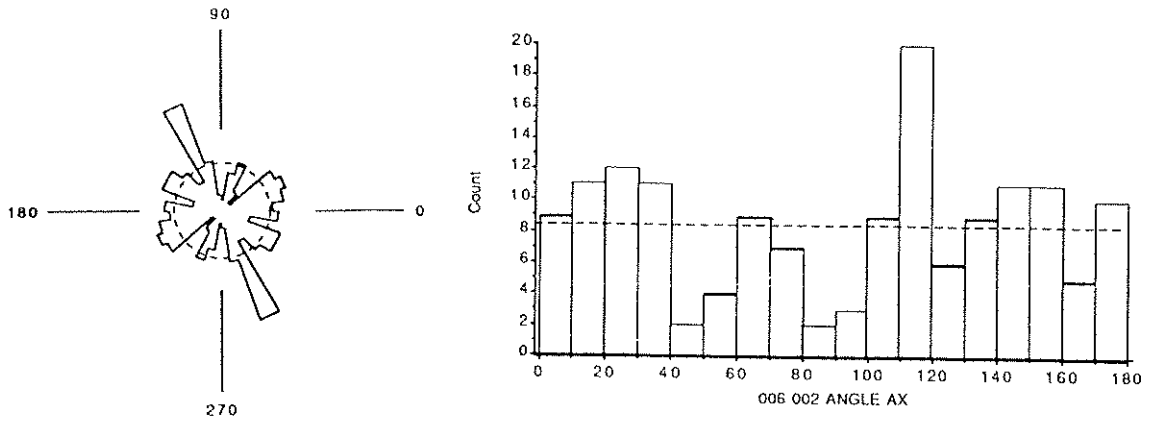


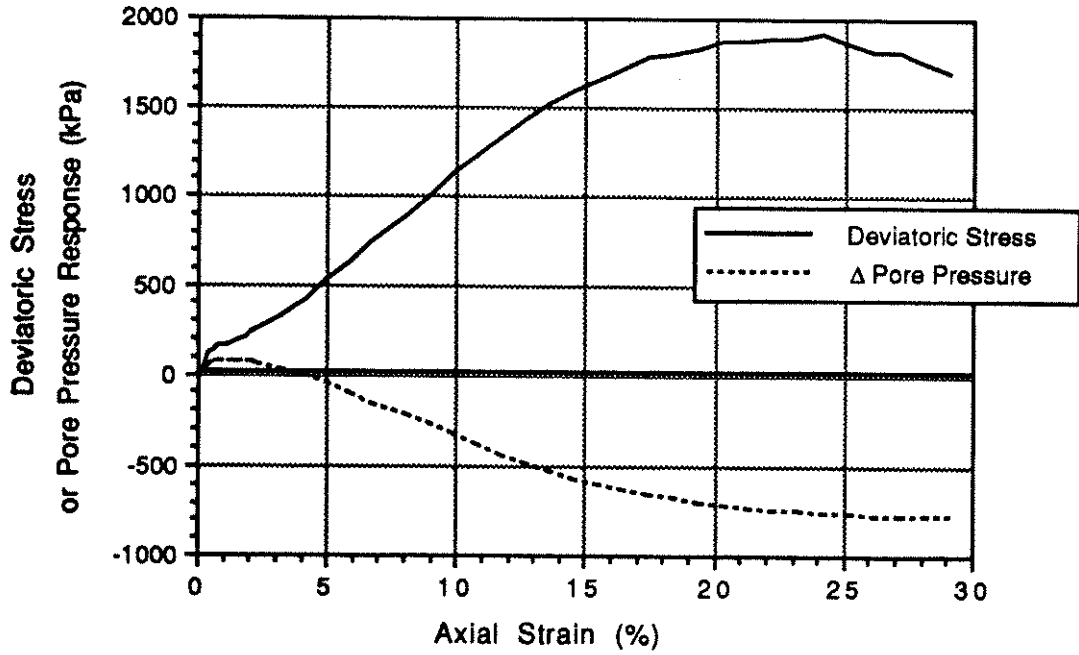
**PLATE A-18: Histogram and Rose Diagram
Micrograph 06 002 (Field)**

APPENDIX B - Triaxial Apparatus Calibrations

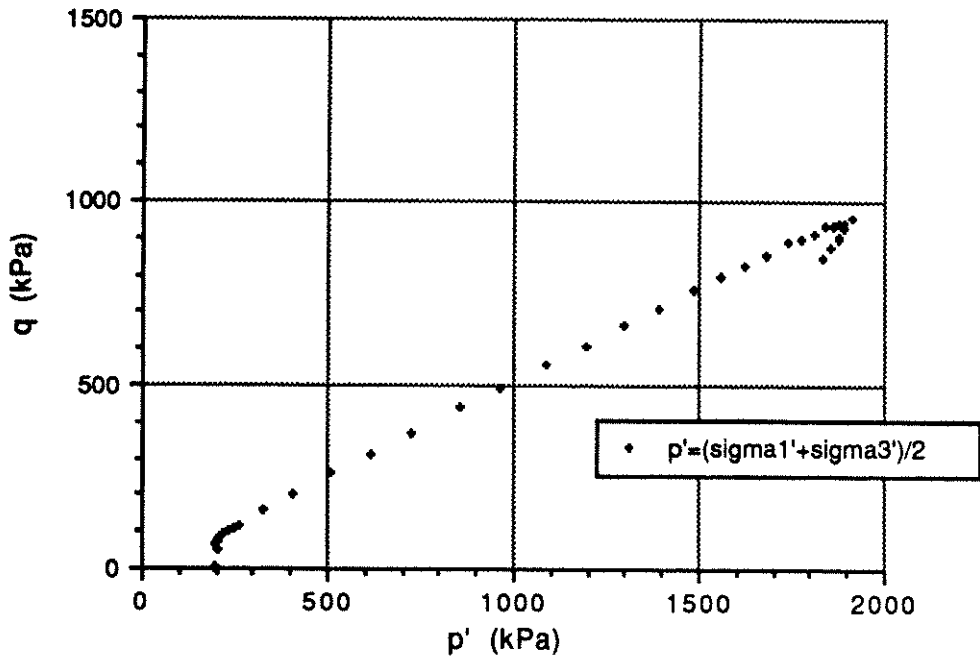
TABLE B-1: CALIBRATION DATA

DEVICE	SERIAL NUMBER	CALIBRATION	RANGE	PRECISION
Pressure Transducers	4444	21.221 kPa/mV	2068.5 kPa	±0.5% of range
	8414	21.796 kPa/mV	2068.5 kPa	±0.5% of range
	35574	70.181 kPa/mV	1723.8 kPa	±0.5% of range
	36545	70.285 kPa/mV	1723.8 kPa	±0.5% of range
	8413	21.298 kPa/mV	2068.5 kPa	±0.5% of range
	2599	14.220 kPa/mV	1379.0 kPa	±0.5% of range
	8415	21.256 kPa/mV	2068.5 kPa	±0.5% of range
	1111	14.137 kPa/mV	1379.0 kPa	±0.5% of range
Volume Change Devices	3058	UP 6.1359 cc/V DOWN -6.1523 cc/V	55 cc/stroke	-
	3059	UP 5.976 cc/V DOWN -6.014 cc/V	55 cc/stroke	-
	#8	UP 6.1219 cc/V DOWN -6.1237 cc/V	55 cc/stroke	-
	#9	UP 6.4354 cc/V DOWN -6.4141 cc/V	55 cc/stroke	-
Load Cells	#1 (Internal)	-1.0521 kN/mV	250 kg	-
	#2 (Internal)	0.6917 kN/mV	250 kg	-
	49677 (External)	-0.1194 kN/mV	227 kg	±0.01% of range
	87632 (External)	-0.1180 kN/mV	227 kg	±0.01% of range
	04135 (External)	-0.4581 kN/mV	909 kg	±0.01% of range
	04129 (External)	-0.4582 kN/mV	909 kg	±0.01% of range
LVTD's	2554	-3.1696 mm/V	25 mm	±0.5% of range
	#2	-0.8319 mm/V	25 mm	±0.5% of range
RTD's	#1	0.39 mV/°C	-	-
	#2	0.39 mV/°C	-	-

APPENDIX C - Present Study Triaxial Test Results



DEVIATORIC STRESS AND Δ PORE PRESSURE



STRESS PATH (p'-q)

FIGURE C-1: TEST PL 2 (PLUVIATED)

Specimen FM 9 C1 Test PL 2 Set-up # 2 Load Cell Internal

A. INITIAL CONDITION

Gs=2.65

Dry Density	1.477 Mg/m ³	Void ratio	0.794	Dry Wt.	74.14 g
Relative Density	25.4 %	Saturation	87.9 %		
Max Density	1.695 Mg/m ³	Min Density	1.415 Mg/m ³		

B. PRE-SHEAR CONDITIONS

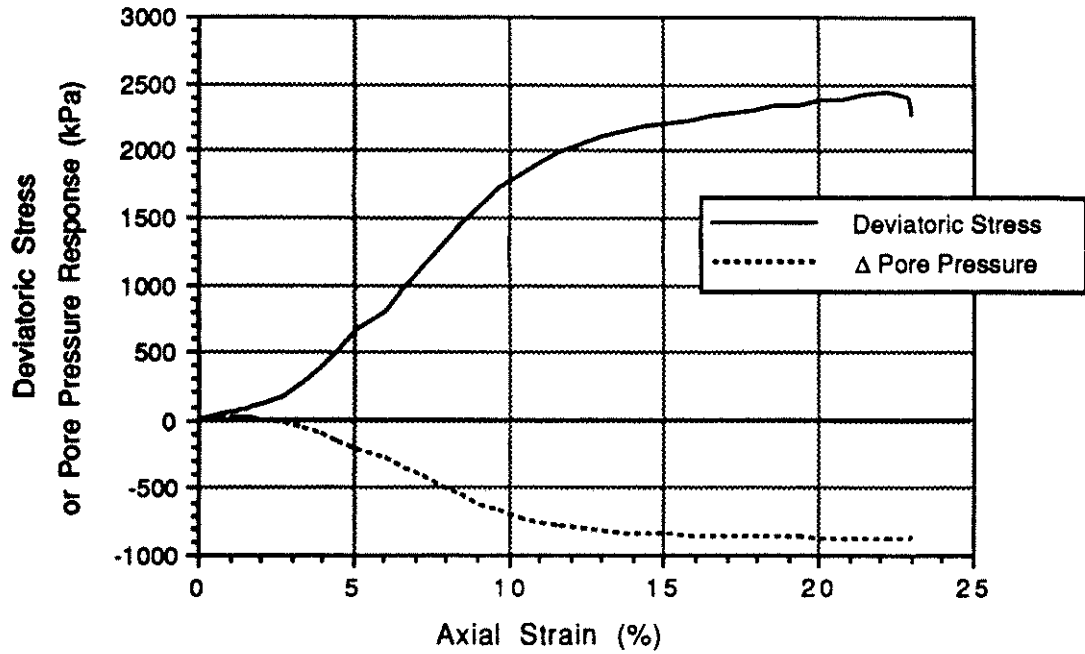
Dry Density	1.544 Mg/m ³	B	0.998	Volume	48.0 cc
Void ratio	0.716	Con. Pressure	186.2 kPa		
Rel Density	50.6 %	Con. Volume	0.65 cc		
Init. Effective Con. Pressure	194.5 kPa	Applied Back Pressure	843.1 kPa		

C. DURING SHEAR

Deviatoric Stress (kPa)			Δ Pore Pressure (kPa)			Stress Ratio	
Break/			Peak	72.5 @ 1.1 %	Break	2.43	
Peak	106.9 @ 0.4 %		10%	-332.0	@	1.3 %	
10%	1114.8		Elbow	62.6	10%	3.12	
Elbow	130.9		Break	-439.7 @ 11.7 %	Elbow	1.99	
Initial Tangent Modulus	2.741E4 kPa/Strain		Foreslope	9.930E3 kPa/Strain			
			Backslope1	-2.010E3 kPa/Strain			
			Backslope2	-5.560E3 kPa/Strain			

PP Parameter "A"			p' (kPa)			q (kPa)	
Peak ΔPP	0.45 @ 1.1 %		(σ' ₁ +σ' ₃)/2		(σ' ₁ -σ' ₃)/2		
10%	-0.30		Elbow	197.2 @ 0.6 %	Elbow	65.4	
Elbow	0.48		10%	1084.0	10%	557.4	
Break ΔPP	-0.33		Steady State	1915.6 @ 24.2 %	Steady State	959.2	
			(σ' ₁ +2σ' ₃)/3		(P _o '/P _{ss} ')/Dr		
SS Reached? yes			Elbow	175.4		0.201	
dilative			10%	898.2	Ø'	30.7 °	
			Steady State	1595.8	SS Type	dilative reversal below	

TABLE C-1: TEST PL 2 (pluviated)



DEVIATORIC STRESS AND Δ PORE PRESSURE

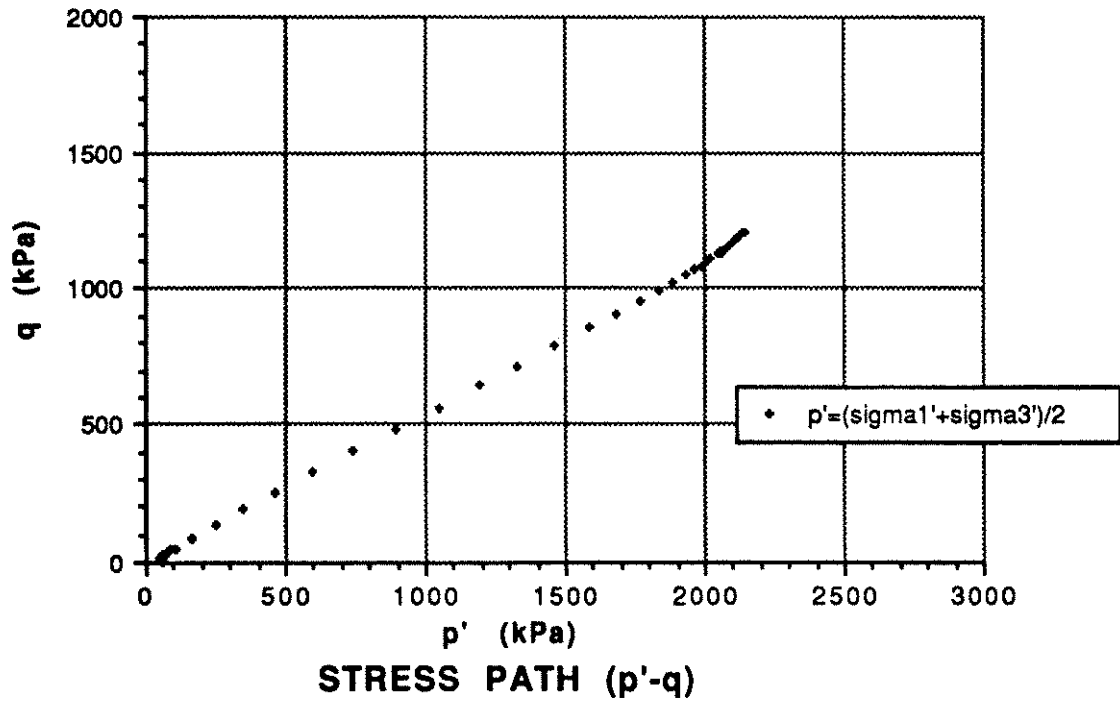


FIGURE C-2: TEST PL 3 (PLUVIATED)

Specimen FM 9 C2 Test PL 3 Set-up # 2 Load Cell Internal

A. INITIAL CONDITION

G_s=2.65

Dry Density	1.431 Mg/m ³	Void ratio	0.852	Dry Wt.	70.00 g
Relative Density	6.8 %	Saturation	88.6 %		
Max Density	1.695 Mg/m ³	Min Density	1.415 Mg/m ³		

B. PRE-SHEAR CONDITIONS

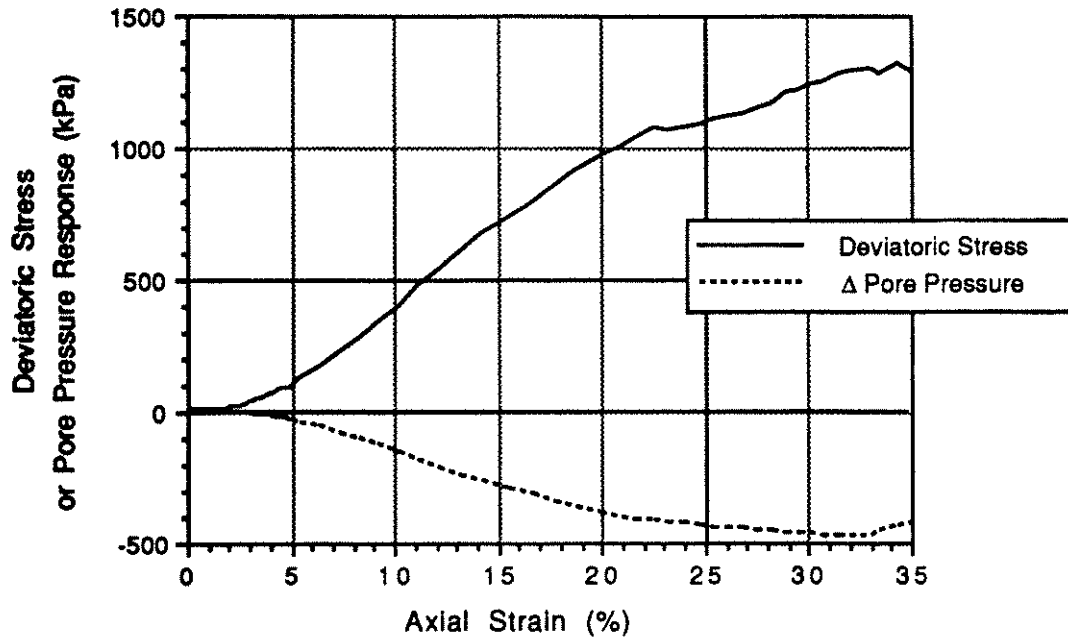
Dry Density	1.554 Mg/m ³	B	0.998	Volume	45.0 cc
Void ratio	0.705	Con. Pressure	50.0 kPa		
Rel Density	54.1 %	Con. Volume	cc		
Init. Effective Con. Pressure	54.4 kPa	Applied Back Pressure	841.4 kPa		

C. DURING SHEAR

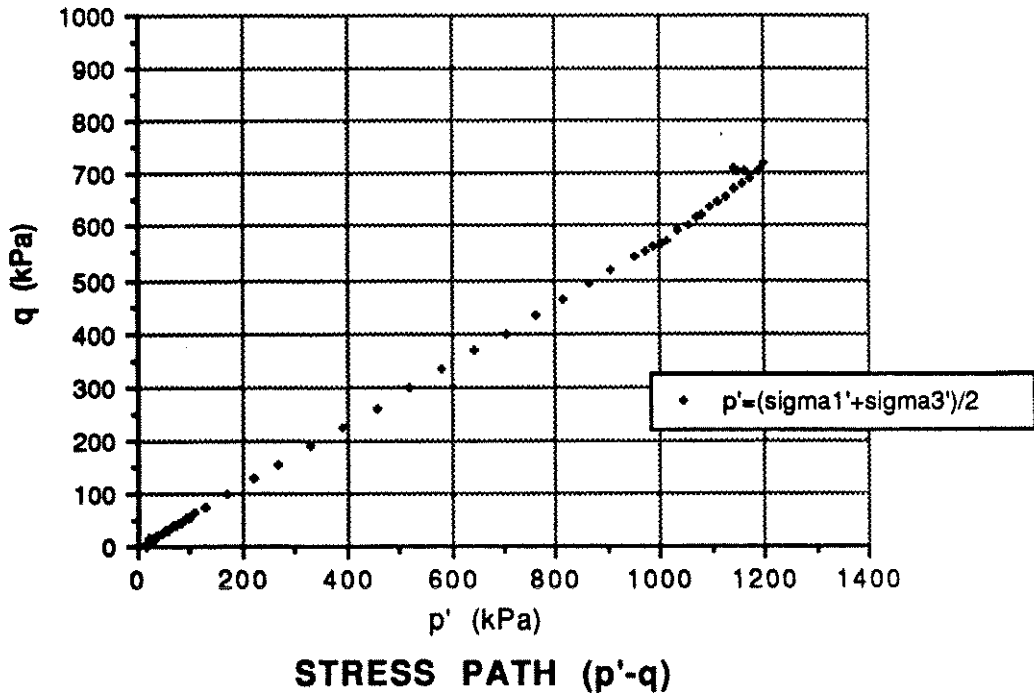
Deviatoric Stress (kPa)			Δ Pore Pressure (kPa)			Stress Ratio	
Break/ Peak	@	%	Peak	23.7 @	0.7 %	Break	2.80
10%	1764.4		10%	-698.2		@	1.4 %
Elbow	40.4		Elbow	23.7		10%	3.34
Initial Tangent Modulus	4.890E3 kPa/Strain		Break	-621.3 @	9.1 %	Elbow	2.32
			Foreslope	3.390E3 kPa/Strain			
			Backslope1	-1.760E3 kPa/Strain			
			Backslope2	-9.950E3 kPa/Strain			

PP Parameter "A"			p' (kPa)			q (kPa)	
Peak ΔPP	0.59 @	0.7 %	(σ ₁ ' + σ ₃ ')/2			(σ ₁ ' - σ ₃ ')/2	
10%	-0.40		Elbow	50.8 @	0.7 %	Elbow	20.2
Elbow	0.59		10%	1634.8		10%	882.3
Break ΔPP	-0.39		Steady State	2140.7 @	22.2 %	Steady State	1212.4
			(σ ₁ ' + 2σ ₃ ')/3			(P _o '/P _{ss} ')/D _r	
SS Reached? yes			Elbow	44.1			0.047
dilative			10%	1340.8		Ø'	32.1 °
			Steady State	1736.6		SS Type	dilative reversal above

TABLE C-2: TEST PL 3 (pluviated)



DEVIATORIC STRESS AND Δ PORE PRESSURE



STRESS PATH (p'-q)
FIGURE C-3: TEST PL 6 (PLUVIATED)

Specimen FM 10 4A Test PL 6 Set-up # 2 Load Cell Internal

A. INITIAL CONDITION

G_s=2.65

Dry Density	1.460 Mg/m ³	Void ratio	0.815	Dry Wt.	71.88 g
Relative Density	18.7 %	Saturation	89.3 %		
Max Density	1.695 Mg/m ³	Min Density	1.415 Mg/m ³		

B. PRE-SHEAR CONDITIONS

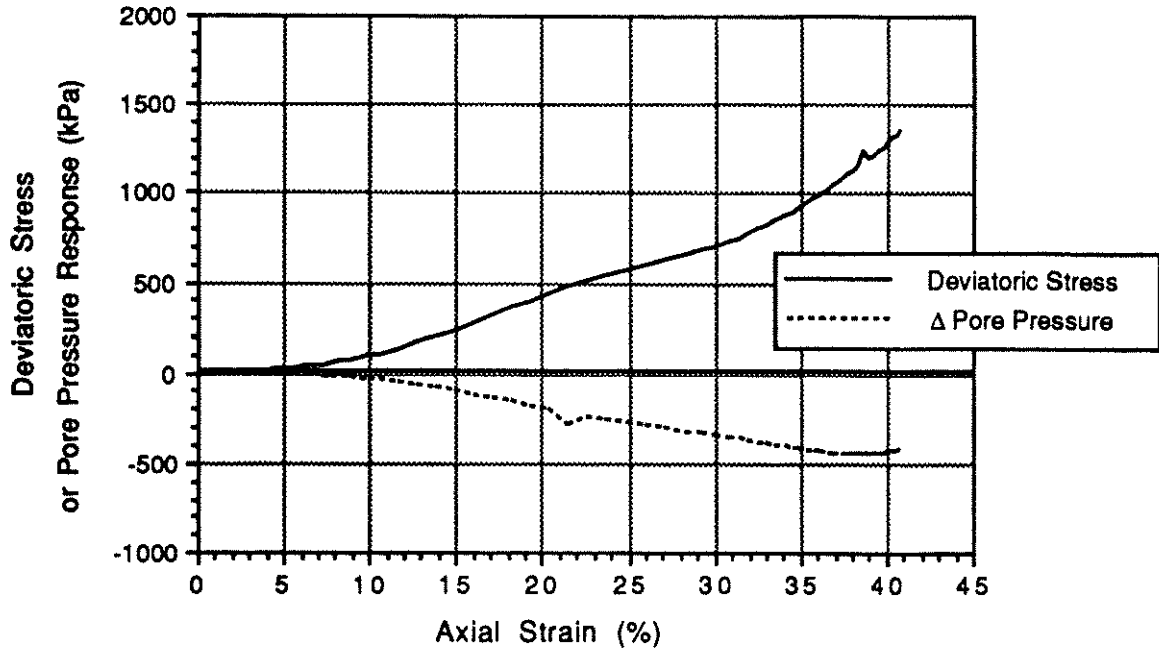
Dry Density	1.527 Mg/m ³	B	1.000	Volume	47.1 cc
Void ratio	0.736	Con. Pressure	15.0 kPa		
Rel Density	44.4 %	Con. Volume	cc		
Init. Effective Con. Pressure	15.4 kPa	Applied Back Pressure	821.9 kPa		

C. DURING SHEAR

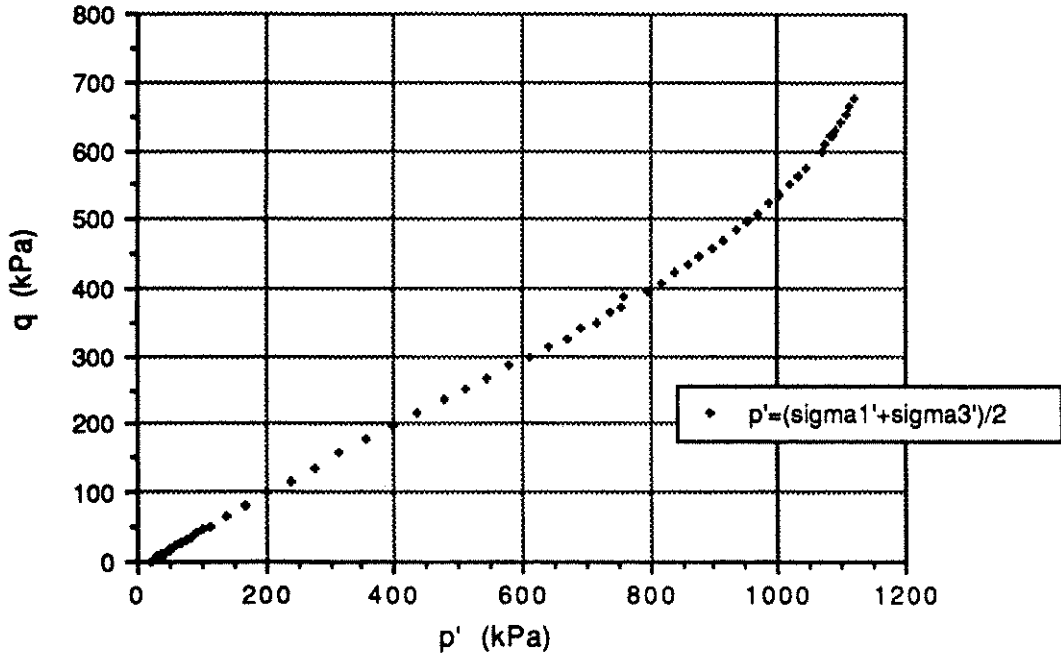
Deviatoric Stress (kPa)			Δ Pore Pressure (kPa)			Stress Ratio	
Break/ Peak	@	%	Peak	7.1 @	0.9 %	Break	3.46
10%	424.1		10%	-143.3		@	1.8 %
Elbow	8.1		Elbow	6.5		10%	3.67
Initial Tangent Modulus	0.000E0 kPa/Strain		Break	-365.4 @	19.2 %	Elbow	1.86
			Foreslope	1.770E3 kPa/Strain			
			Backslope1	-9.700E2 kPa/Strain			
			Backslope2	-2.870E3 kPa/Strain			

PP Parameter "A"			p' (kPa)			q (kPa)	
Peak ΔPP	0.64 @	0.9 %	(σ' ₁ +σ' ₃)/2			(σ' ₁ -σ' ₃)/2	
10%	-0.34		Elbow	13.6 @	0.5 %	Elbow	4.1
Elbow	0.80		10%	370.7		10%	212.0
Break ΔPP	-0.37		Steady State	1128.5 @	32.8 %	Steady State	649.3
			(σ' ₁ +2σ' ₃)/3			(P _o '/P _{ss} ')/D _r	
SS Reached?	no		Elbow	12.2			0.031
dilative			10%	300.0		Ø'	33.6 °
			Steady State	912.1		SS Type	dilative reversal above

TABLE C - 3 TEST PL 6 (pluviated)



DEVIATORIC STRESS AND Δ PORE PRESSURE



STRESS PATH (p' - q)

FIGURE C-4: TEST PL 7 (PLUVIATED)

Specimen FM 10 C1 Test PL 7 Set-up # 1 Load Cell External

A. INITIAL CONDITION

Gs=2.65

Dry Density	1.407 Mg/m ³	Void ratio	0.883	Dry Wt.	70.27 g
Relative Density	-3.4 %	Saturation	88.4 %		
Max Density	1.695 Mg/m ³	Min Density	1.415 Mg/m ³		

B. PRE-SHEAR CONDITIONS

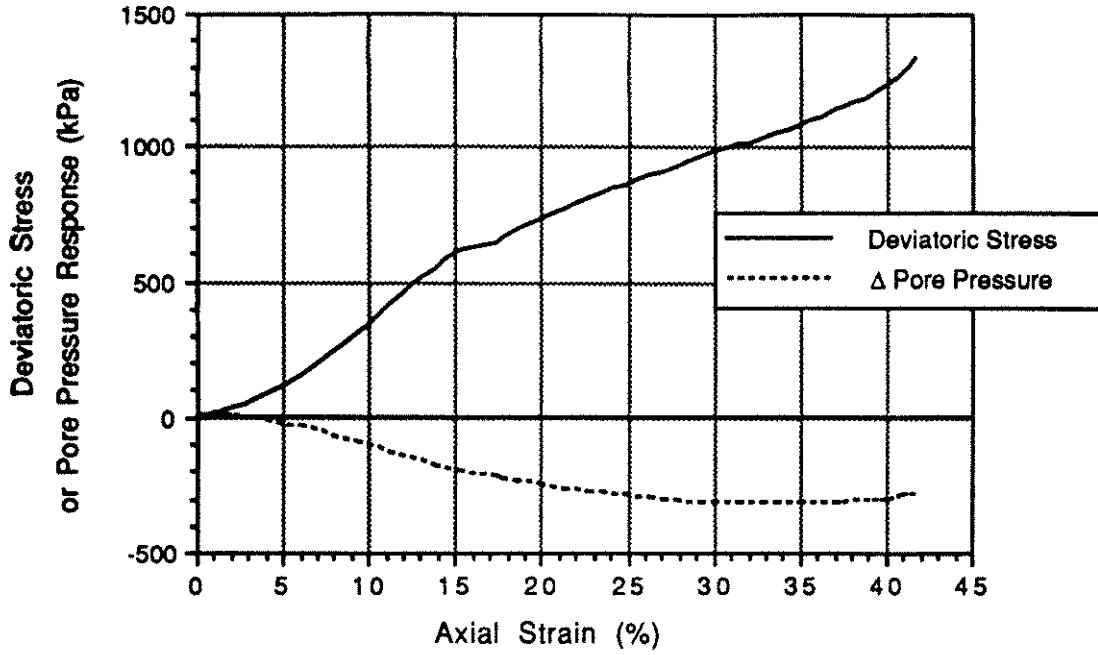
Dry Density	1.531 Mg/m ³	B	1.000	Volume	45.9 cc
Void ratio	0.731	Con. Pressure	20.0 kPa		
Rel Density	45.9 %	Con. Volume	cc		
Init. Effective Con. Pressure	22.9 kPa	Applied Back Pressure	820.8 kPa		

C. DURING SHEAR

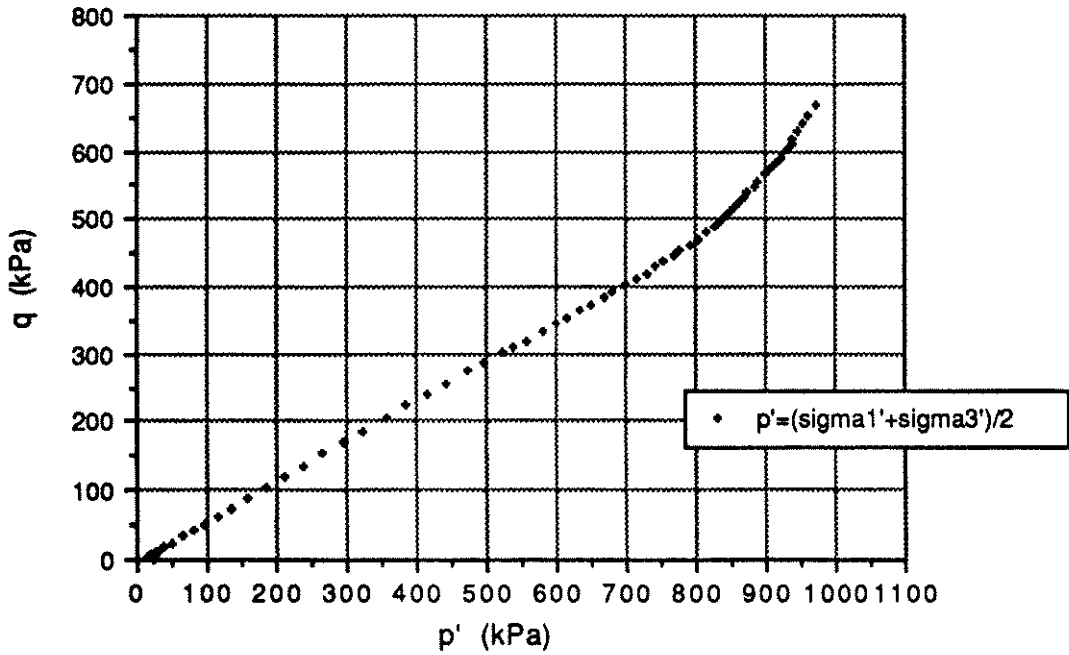
Deviatoric Stress (kPa)			Δ Pore Pressure (kPa)			Stress Ratio	
Break/Peak	@	%	Peak	0.3 @	1.1 %	Break	2.81
10%	92.7		10%	-33.1		@	11.7 %
Elbow	7.0		Elbow	0.3		10%	2.67
Initial Tangent Modulus	0.000E0 kPa/Strain		Break	-433.3 @	36.2 %	Elbow	1.31
			Foreslope	4.000E1 kPa/Strain			
			Backslope1	-1.400E2 kPa/Strain			
			Backslope2	-1.570E3 kPa/Strain			

PP Parameter "A"			p' (kPa)			q (kPa)	
Peak ΔPP	0.04 @	1.1 %	$(\sigma' + \sigma_3')/2$			$(\sigma' - \sigma_3')/2$	
10%	-0.36		Elbow	26.2 @	1.1 %	Elbow	3.5
Elbow	0.04		10%	102.0		10%	46.3
Break ΔPP	-0.44		Steady State	1043.6 @	38.4 %	Steady State	574.7
			$(\sigma' + 2\sigma_3')/3$			$(P_o'/P_{ss}')/D_r$	
SS Reached? no			Elbow	25.0			0.048
dilative			10%	86.5			
			Steady State	852.0		Ø'	30.0 °
						SS Type	dilative bunching

TABLE C-4: TEST PL 7 (pluviated)



DEVIATORIC STRESS AND Δ PORE PRESSURE



STRESS PATH (p'-q)

FIGURE C-5: TEST PL 8 (PLUVIATED)

Specimen FM 10 C3 Test PL 8 Set-up # 2 Load Cell Internal

A. INITIAL CONDITION

Gs=2.65

Dry Density	1.437 Mg/m ³	Void ratio	0.844	Dry Wt.	73.95 g
Relative Density	9.3 %	Saturation	89.2 %		
Max Density	1.695 Mg/m ³	Min Density	1.415 Mg/m ³		

B. PRE-SHEAR CONDITIONS

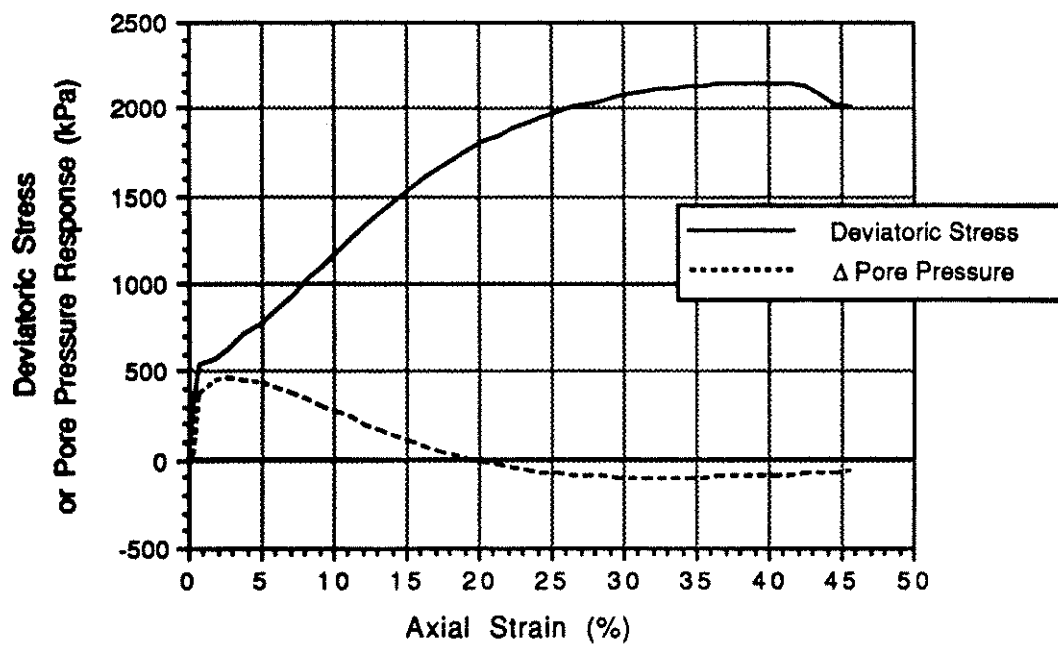
Dry Density	1.523 Mg/m ³	B	1.000	Volume	48.6 cc
Void ratio	0.740	Con. Pressure	15.0 kPa		
Rel Density	42.9 %	Con. Volume	cc		
Init. Effective Con. Pressure	23.5 kPa	Applied Back Pressure	824.3 kPa		

C. DURING SHEAR

Deviatoric Stress (kPa)			Δ Pore Pressure (kPa)			Stress Ratio	
Break/			Peak	11.7 @	0.7 %	Break	1.40
Peak	@	%	10%	-101.2		@	0.5 %
10%	342.8		Elbow	11.4		10%	3.73
Elbow	4.8		Break	-196.1 @	15.2 %	Elbow	1.40
Initial Tangent Modulus	0.000E0 kPa/Strain		Foreslope	4.250E3 kPa/Strain			
			Backslope1	-4.300E2 kPa/Strain			
			Backslope2	-1.790E3 kPa/Strain			

PP Parameter "A"			p' (kPa)			q (kPa)		
Peak ΔPP	1.64 @	0.7 %	($\sigma_1' + \sigma_3'$)/2	Elbow	14.5 @	0.5 %	($\sigma_1' - \sigma_3'$)/2	
10%	-0.30		Elbow	296.8			Elbow	2.4
Elbow	2.37		Steady State	791.3 @	30.2 %	Steady State	461.6	
Break ΔPP	-0.32		($\sigma_1' + 2\sigma_3'$)/3	Elbow	13.7		(Po'/Pss')/Dr	
SS Reached? no			Elbow	239.7			0.069	
dilative			Steady State	637.5		Ø'	35.3 °	
						SS Type	dilative bunching	

TABLE C-5: TEST PL 8 (pluviated)



DEVIATORIC STRESS AND Δ PORE PRESSURE

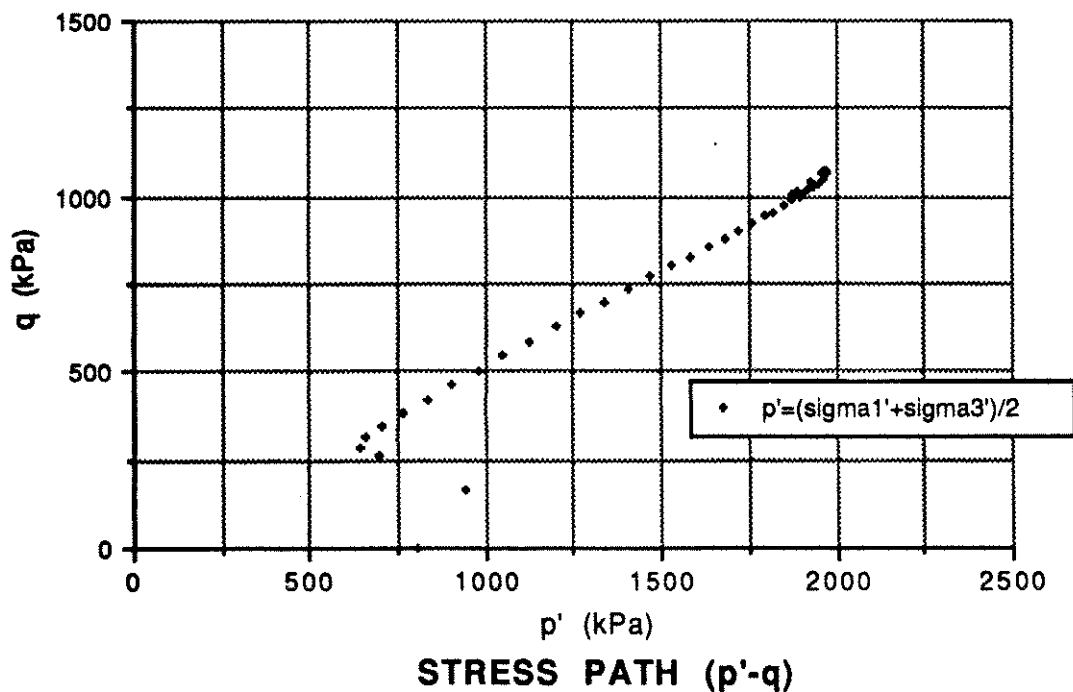


FIGURE C-6: TEST PL 9 (PLUVIATED)

Specimen FM 10 C4 Test PL 9 Set-up # 1 Load Cell External

A. INITIAL CONDITION

Gs=2.65

Dry Density	1.436 Mg/m ³	Void ratio	0.845	Dry Wt.	70.52 g
Relative Density	8.9 %	Saturation	89.5 %		
Max Density	1.695 Mg/m ³	Min Density	1.415 Mg/m ³		

B. PRE-SHEAR CONDITIONS

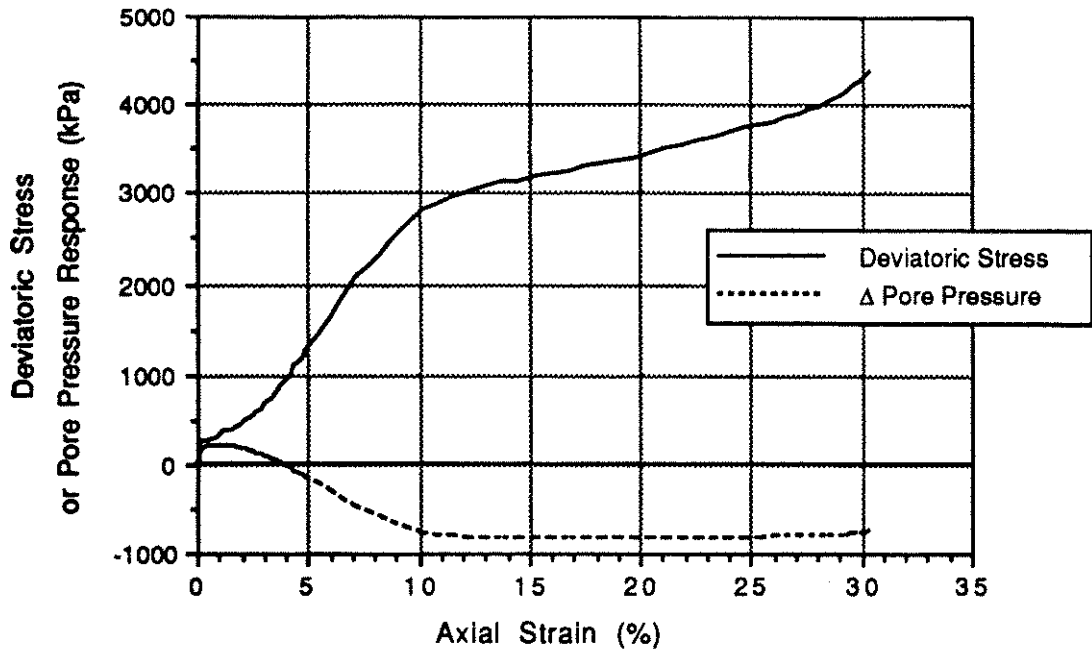
Dry Density	1.567 Mg/m ³	B	0.950	Volume	45.0 cc
Void ratio	0.691	Con. Pressure	746.1 kPa		
Rel Density	58.7 %	Con. Volume	0.98 cc		
Init. Effective Con. Pressure	802.8 kPa	Applied Back Pressure	184.2 kPa		

C. DURING SHEAR

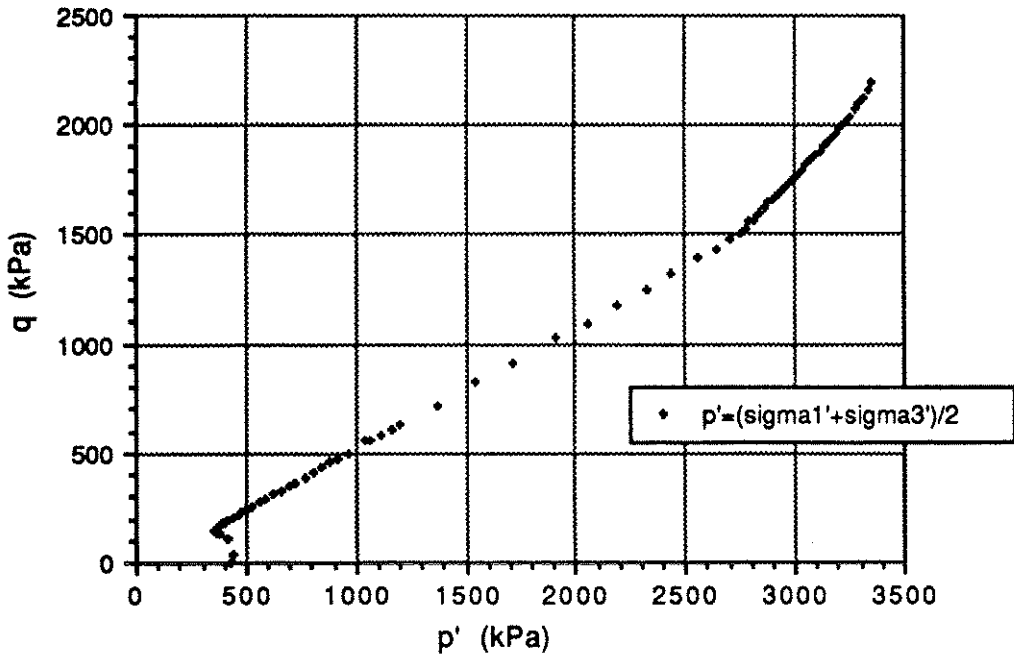
Deviatoric Stress (kPa)			Δ Pore Pressure (kPa)			Stress Ratio	
Break/			Peak	458.8 @	2.8 %	Break	2.83
Peak	529.2 @	0.8 %	10%	274.1		@	2.8 %
10%	1150.5		Elbow	448.5		10%	3.18
Elbow	569.5		Break	72.4 @	15.3 %	Elbow	2.61
Initial Tangent Modulus	6.963E4 kPa/Strain		Foreslope	4.941E4 kPa/Strain			
			Backslope1	-1.640E3 kPa/Strain			
			Backslope2	-3.220E3 kPa/Strain			

PP Parameter "A"			p' (kPa)			q (kPa)	
Peak ΔPP	0.77 @	2.8 %	(sigma' + sigma3')/2			(sigma' - sigma3')/2	
10%	0.25		Elbow	639.0 @	1.8 %	Elbow	284.7
Elbow	0.83		10%	1104.1		10%	575.2
Break ΔPP	0.05		Steady State	1973.1 @	37.6 %	Steady State	1070.3
			(sigma' + 2sigma3')/3			(Po'/Pss')/Dr	
SS Reached? yes			Elbow	544.1			0.693
dilative			10%	912.4		Ø'	30.8 °
			Steady State	1616.4		SS Type	dilative reversal above

TABLE C-6: TEST PL 9 (pluviated)



DEVIATORIC STRESS AND Δ PORE PRESSURE



STRESS PATH (p'-q)

FIGURE C-7: TEST PL 10 (PLUVIATED)

Specimen FM 11 C1 Test PL 10 Set-up # 2 Load Cell Internal

A. INITIAL CONDITION

G_s=2.65

Dry Density	1.407 Mg/m ³	Void ratio	0.883	Dry Wt.	61.97 g
Relative Density	-3.4 %	Saturation	87.3 %		
Max Density	1.695 Mg/m ³	Min Density	1.415 Mg/m ³		

B. PRE-SHEAR CONDITIONS

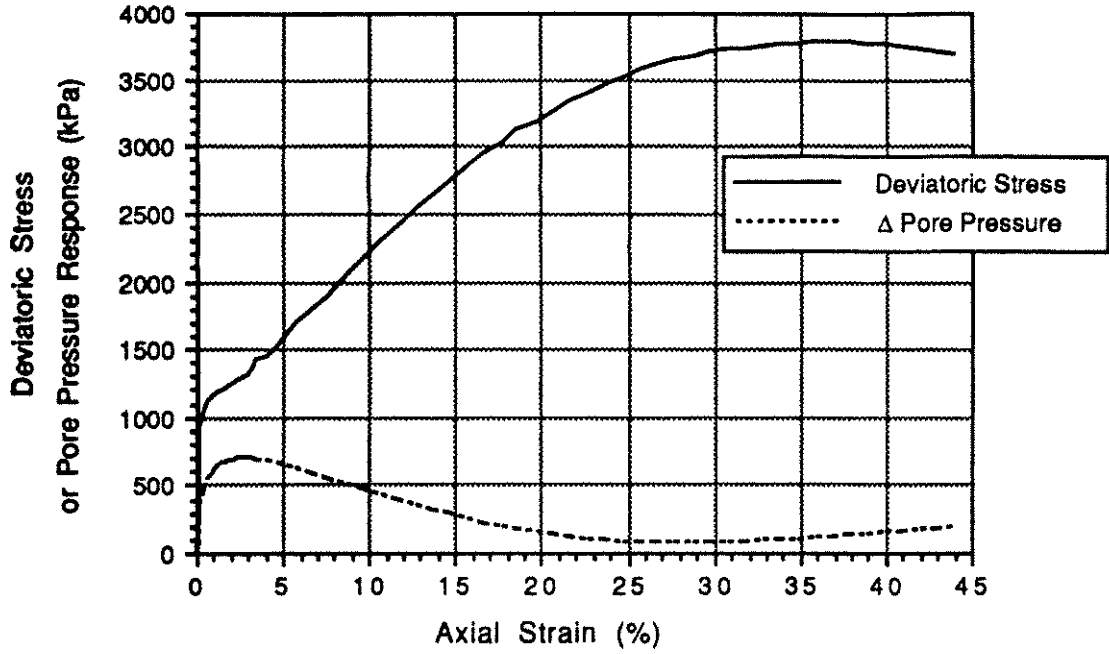
Dry Density	1.592 Mg/m ³	B	1.000	Volume	38.9 cc
Void ratio	0.664	Con. Pressure	420.3 kPa		
Rel Density	67.3 %	Con. Volume	0.65 cc		
Init. Effective Con. Pressure	423.3 kPa	Applied Back Pressure	785.9 kPa		

C. DURING SHEAR

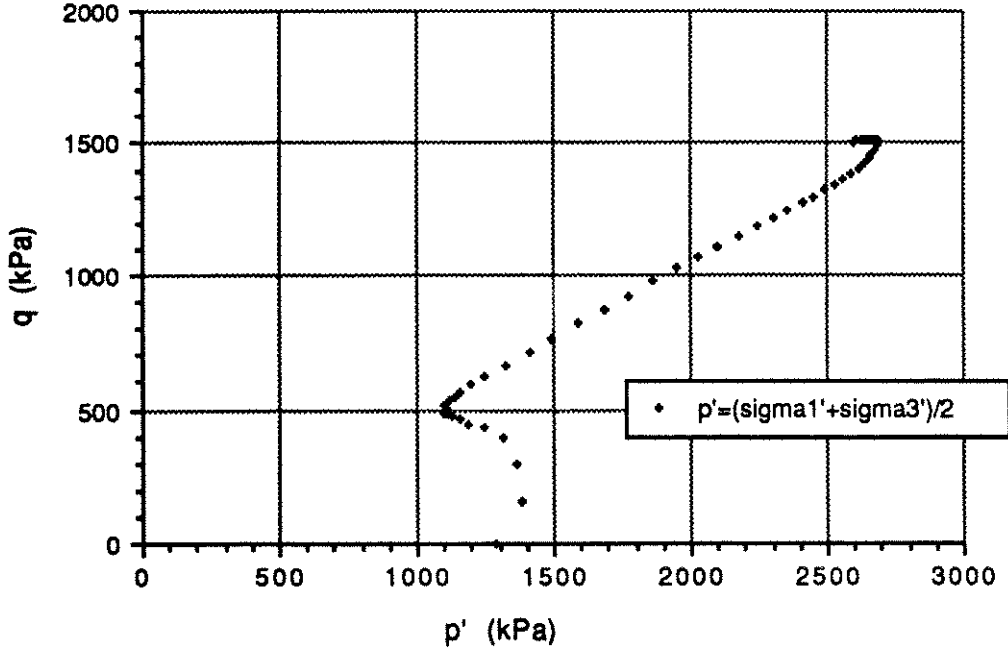
Deviatoric Stress (kPa)			Δ Pore Pressure (kPa)			Stress Ratio	
Break/			Peak	213.9 @ 1.0 %	Break	2.52	
Peak	259.7 @ 0.3 %		10%	-746.6	@	1.0 %	
10%	2756.2		Elbow	207.3	10%	3.39	
Elbow	284.1		Break	-653.4 @ 8.9 %	Elbow	2.33	
Initial Tangent Modulus	9.275E4 kPa/Strain		Foreslope	2.097E4 kPa/Strain			
			Backslope1	-5.180E3 kPa/Strain			
			Backslope2	-1.401E4 kPa/Strain			

PP Parameter "A"			p' (kPa)			q (kPa)	
Peak ΔPP	0.68 @ 1.0 %		(σ ₁ ' + σ ₃ ')/2		(σ ₁ ' - σ ₃ ')/2		
10%	-0.27		Elbow	355.9 @ 0.8 %	Elbow	142.0	
Elbow	0.73		10%	2530.4	10%	1378.1	
Break ΔPP	-0.26		Steady State	3347.9 @ 30.4 %	Steady State	2193.0	
			(σ ₁ ' + 2σ ₃ ')/3		(P _o '/P _{ss} ')/D _r		
SS Reached? no			Elbow	308.6		0.188	
dilative			10%	2071.0	Ø'	32.4 °	
			Steady State	2616.9	SS Type	dilative end point	

TABLE C-7: TEST PL 10 (pluviated)



DEVIATORIC STRESS AND Δ PORE PRESSURE



STRESS PATH (p'-q)

FIGURE C-8: TEST PL 12 (PLUVIATED)

Specimen FM 11 C3 Test PL 12 Set-up # HP Load Cell External

A. INITIAL CONDITION

Gs=2.65

Dry Density	1.451 Mg/m ³	Void ratio	0.826	Dry Wt. 72.85 g
Relative Density	15.0 %	Saturation	86.7 %	
Max Density	1.695 Mg/m ³	Min Density	1.415 Mg/m ³	

B. PRE-SHEAR CONDITIONS

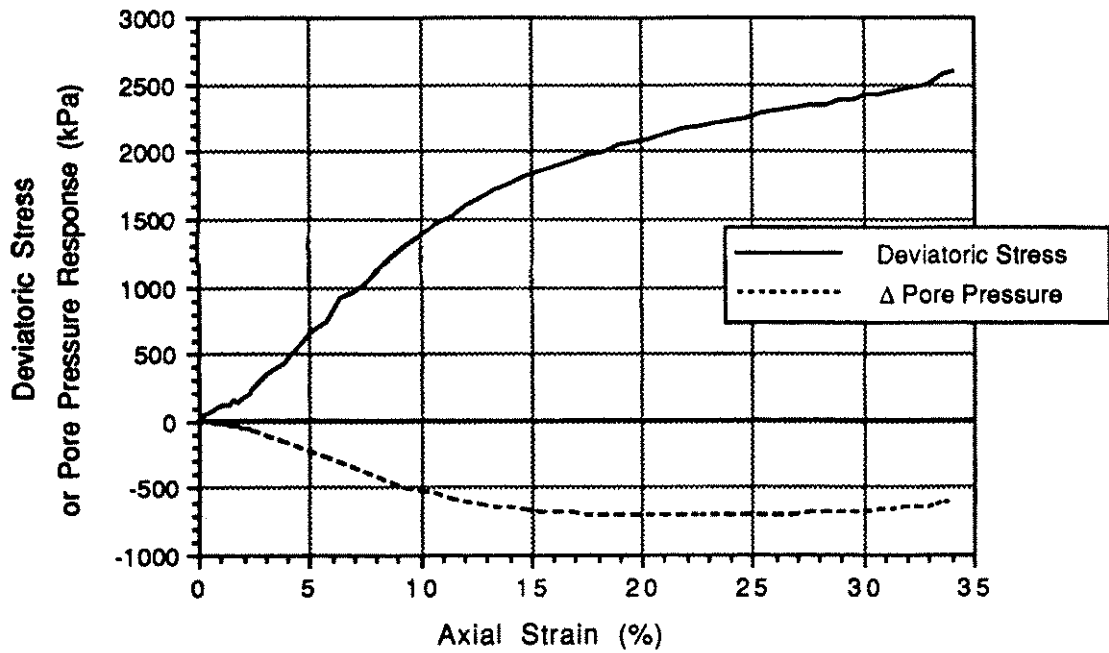
Dry Density	1.570 Mg/m ³	B	0.996	Volume	46.4 cc
Void ratio	0.688	Con. Pressure	1271.5 kPa		
Rel Density	59.8 %	Con. Volume	1.54 cc		
Init. Effective Con. Pressure	1282.8 kPa	Applied Back Pressure	595.3 kPa		

C. DURING SHEAR

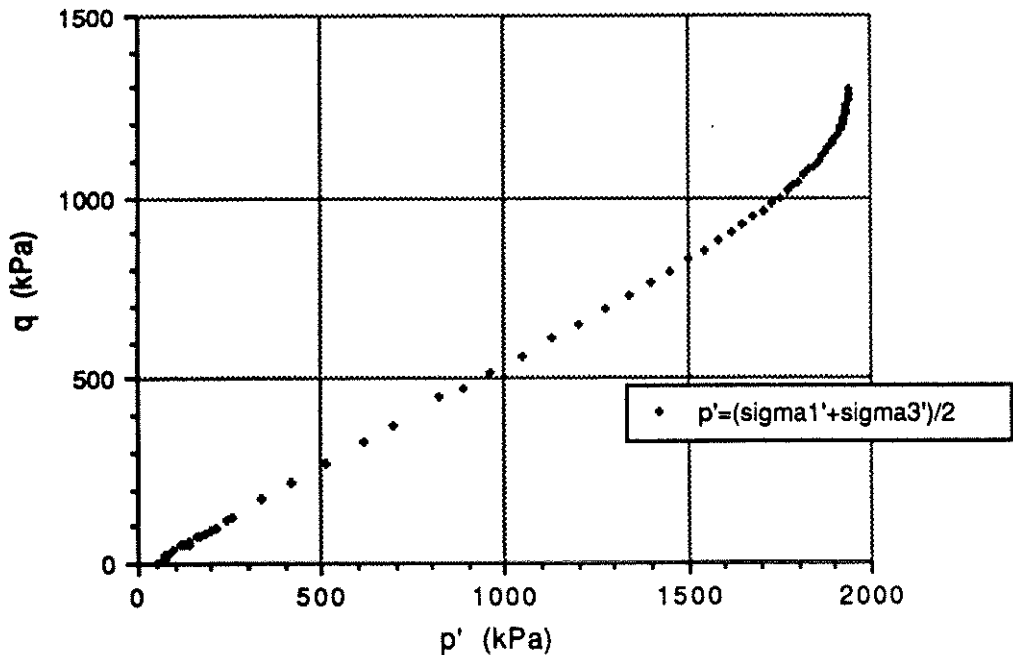
Deviatoric Stress (kPa)			Δ Pore Pressure (kPa)			Stress Ratio	
Break/ Peak	792.0 @ 0.2 %		Peak	695.7 @ 2.7 %	Break	2.54	
10%	1782.7		10%	464.3	@	1.4 %	
Elbow	965.5		Elbow	671.5	10%	3.17	
			Break	166.3 @ 18.9 %	Elbow	2.58	
Initial Tangent Modulus	3.474E5 kPa/Strain		Foreslope	6.745E4 kPa/Strain			
			Backslope1	-1.850E3 kPa/Strain			
			Backslope2	-3.630E3 kPa/Strain			

PP Parameter "A"			p' (kPa)			q (kPa)	
Peak ΔPP	0.67 @ 2.7 %		(sigma1'+sigma3')/2		(sigma1'-sigma3')/2		
10%	0.26		Elbow	1095.3 @ 1.7 %	Elbow	482.7	
Elbow	0.70		10%	1712.7	10%	891.4	
Break ΔPP	0.05		Steady State	2684.5 @ 34.1 %	Steady State	1501.0	
			(sigma1'+2sigma3')/3		(Po'/Pss')/Dr		
SS Reached? yes			Elbow	934.4		0.799	
dilative			10%	1415.6	Ø'	33.2 °	
			Steady State	2184.2	SS Type	dilative reversal above	

TABLE C-8: TEST PL 12 (pluviated)



DEVIATORIC STRESS AND Δ PORE PRESSURE



STRESS PATH (p'-q)

FIGURE C-9: TEST PL 13 (PLUVIATED)

Specimen FM 12 A4 Test PL 13 Set-up # 2 Load Cell Internal

A. INITIAL CONDITION

Gs=2.65

Dry Density	1.494 Mg/m ³	Void ratio	0.773	Dry Wt.	69.56 g
Relative Density	32.0 %	Saturation	89.6 %		
Max Density	1.695 Mg/m ³	Min Density	1.415 Mg/m ³		

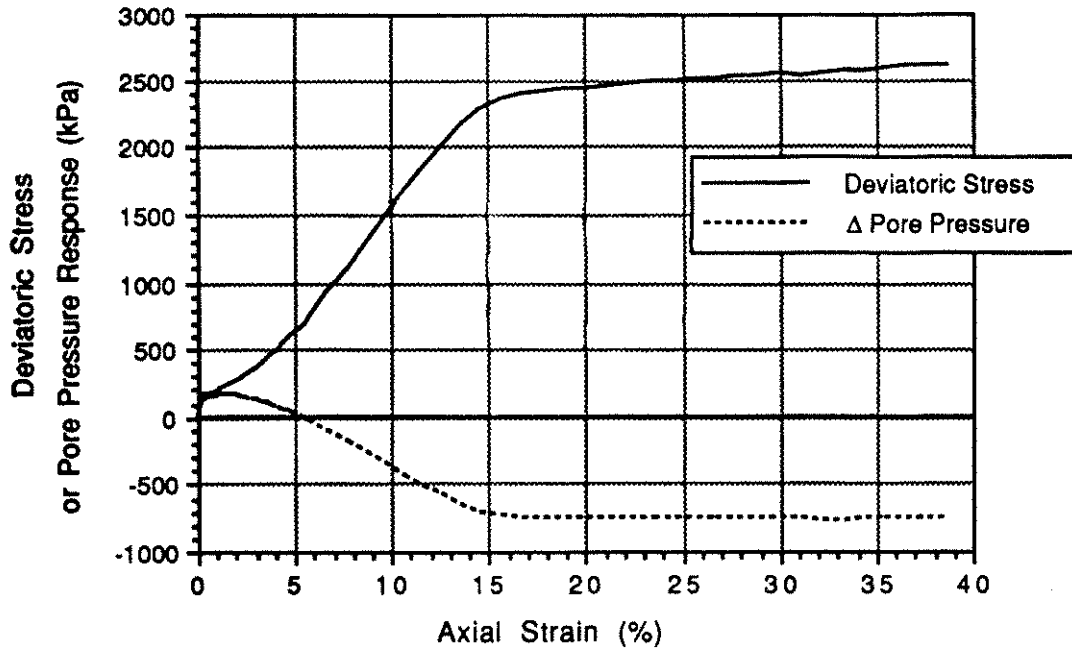
B. PRE-SHEAR CONDITIONS

Dry Density	1.536 Mg/m ³	B	0.985	Volume	45.3 cc
Void ratio	0.725	Con. Pressure	46.9 kPa		
Rel Density	47.7 %	Con. Volume	0.23 cc		
Init. Effective Con. Pressure	48.4 kPa	Applied Back Pressure	900.4 kPa		

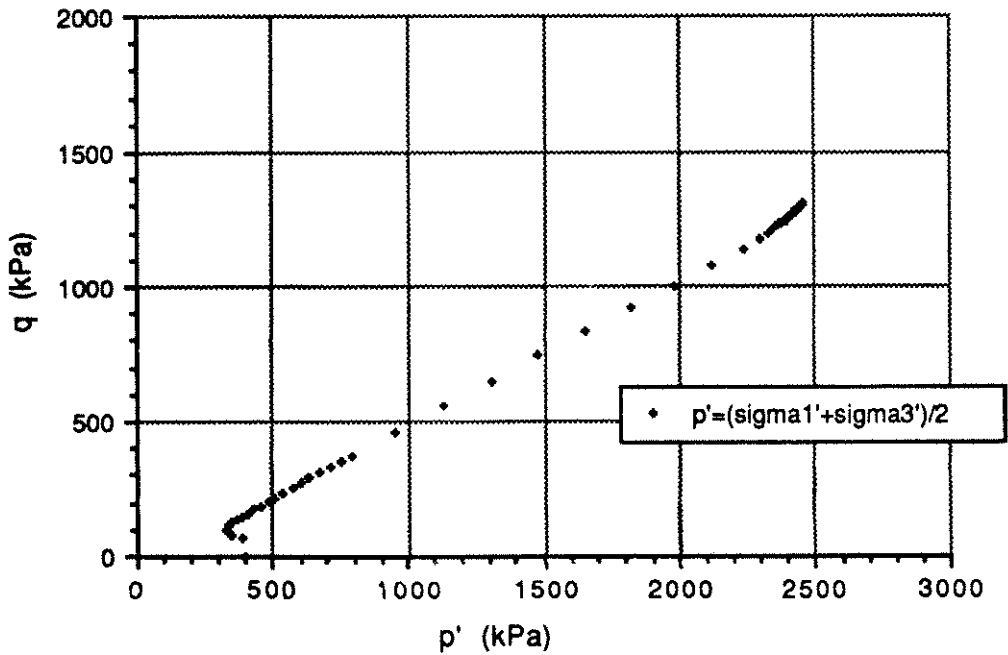
C. DURING SHEAR

Deviatoric Stress (kPa)			Δ Pore Pressure (kPa)			Stress Ratio	
Break/ Peak	39.4 @	0.3 %	Peak	@	%	Break	2.54
10%	1363.1		10%	-526.5		@	1.6 %
Elbow			Elbow			10%	3.37
Initial Tangent Modulus	1.159E4 kPa/Strain		Break	-560.0 @	10.8 %	Elbow	
			Foreslope	0.000E0 kPa/Strain			
			Backslope1	-2.800E3 kPa/Strain			
			Backslope2	-6.300E3 kPa/Strain			
PP Parameter "A"			p' (kPa)			q (kPa)	
Peak ΔPP	@	%	$(\sigma_1' + \sigma_3')/2$			$(\sigma_1' - \sigma_3')/2$	
10%	-0.40		Elbow	@	%	Elbow	
Elbow			10%	1257.3		10%	681.6
Break ΔPP	-0.39		Steady State	1922.1 @	29.6 %	Steady State	1192.3
			$(\sigma_1' + 2\sigma_3')/3$			$(P_o'/P_{ss}')/Dr$	
SS Reached? no dilative			Elbow				0.053
			10%	1030.1		Ø'	32.5 °
			Steady State	1524.6		SS Type	dilative reversal above

TABLE C-9: TEST PL 13 (pluviated)



DEVIATORIC STRESS AND Δ PORE PRESSURE



STRESS PATH (p'-q)

FIGURE C-10: TEST PL 14 (PLUVIATED)

Specimen FM 12 A1 Test PL 14 Set-up # 1 Load Cell External

A. INITIAL CONDITION

estimate

G_s=2.65

Dry Density	1.497 Mg/m ³	Void ratio	0.770	Dry Wt.	67.57 g
Relative Density	33.2 %	Saturation	%		
Max Density	1.695 Mg/m ³	Min Density	1.415 Mg/m ³		

B. PRE-SHEAR CONDITIONS

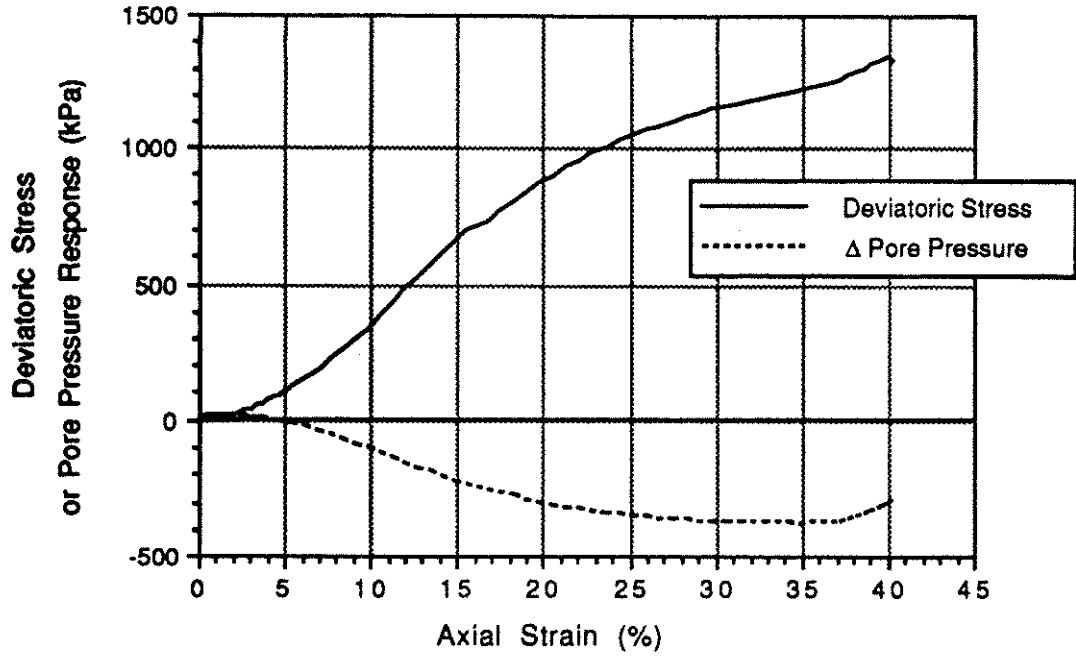
Dry Density	1.568 Mg/m ³	B	1.000	Volume	43.1 cc
Void ratio	0.690	Con. Pressure	395.0 kPa		
Rel Density	59.1 %	Con. Volume	cc		
Init. Effective Con. Pressure	395.2 kPa	Applied Back Pressure	738.2 kPa		

C. DURING SHEAR

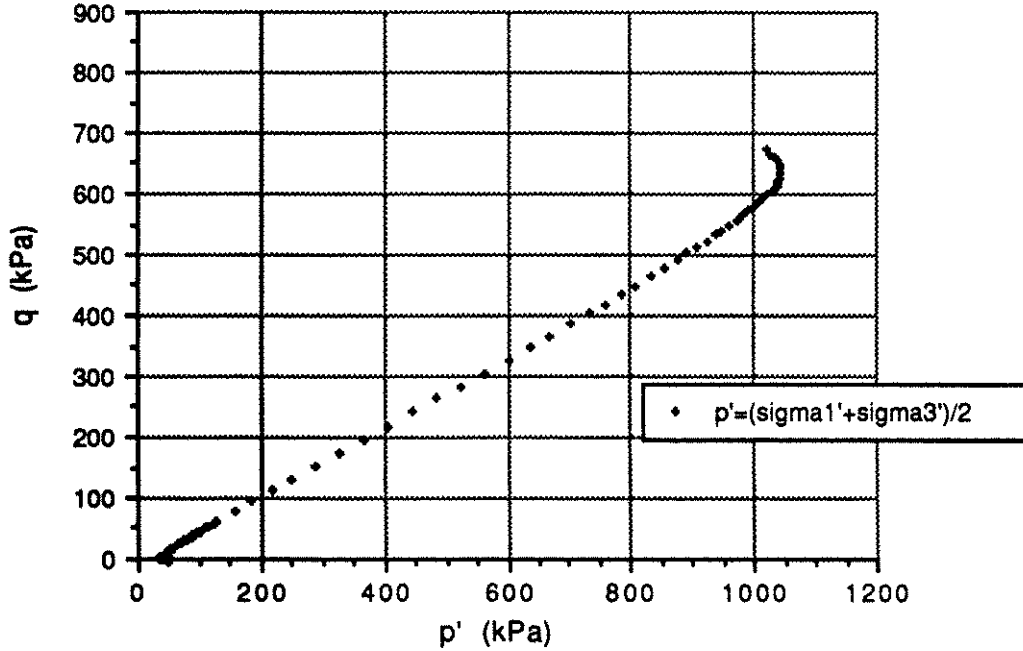
Deviatoric Stress (kPa)			Δ Pore Pressure (kPa)			Stress Ratio	
Break/			Peak	167.4 @ 1.4 %	Break	2.08	
Peak	141.5 @ 0.1 %		10%	-372.9	@	1.7 %	
10%	1546.6		Elbow	160.4	10%	3.02	
Elbow	189.9		Break	-702.2 @ 14.6 %	Elbow	1.82	
Initial Tangent Modulus	1.769E5 kPa/Strain		Foreslope	2.531E4 kPa/Strain			
			Backslope1	-3.000E3 kPa/Strain			
			Backslope2	-8.030E3 kPa/Strain			

PP Parameter "A"			p' (kPa)			q (kPa)	
Peak ΔPP	0.74 @ 1.4 %		(σ ₁ ' + σ ₃ ')/2		(σ ₁ ' - σ ₃ ')/2		
10%	-0.24		Elbow	327.5 @ 0.9 %	Elbow	95.0	
Elbow	0.84		10%	1539.7	10%	773.3	
Break ΔPP	-0.31		Steady State	2420.9 @ 31.1 %	Steady State	1270.7	
			(σ ₁ ' + 2σ ₃ ')/3		(P _o '/P _{ss} ')/Dr		
SS Reached? yes			Elbow	295.8		0.276	
dilative			10%	1281.8	Ø'	31.3 °	
			Steady State	1997.4	SS Type	dilative reversal above	

TABLE C-10: TEST PL 14 (pluviated)



DEVIATORIC STRESS AND Δ PORE PRESSURE



STRESS PATH (p'-q)

FIGURE C-11: TEST PL 15 (PLUVIATED)

Specimen FM 11 A3 Test PL 15 Set-up # 2 Load Cell External

A. INITIAL CONDITION

estimate

Gs=2.65

Dry Density	1.470 Mg/m ³	Void ratio	0.802	Dry Wt.	64.38 g
Relative Density	22.6 %	Saturation	%		
Max Density	1.695 Mg/m ³	Min Density	1.415 Mg/m ³		

B. PRE-SHEAR CONDITIONS

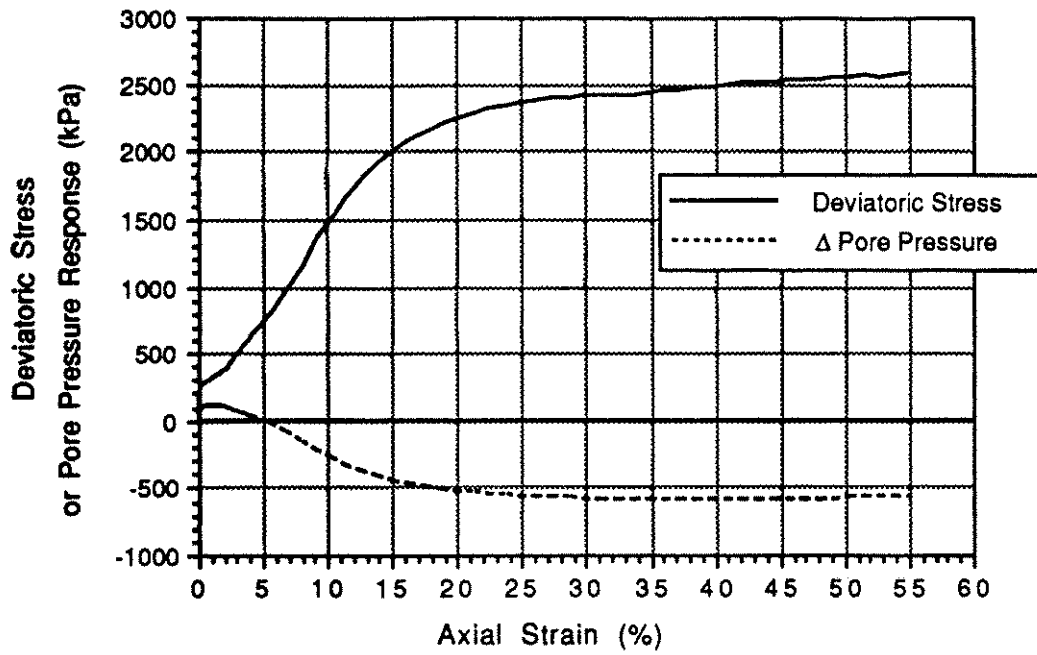
Dry Density	1.535 Mg/m ³	B	0.990	Volume	41.9 cc
Void ratio	0.727	Con. Pressure	70.3 kPa		
Rel Density	47.3 %	Con. Volume	0.33 cc		
Init. Effective Con. Pressure	51.0 kPa	Applied Back Pressure	808.7 kPa		

C. DURING SHEAR

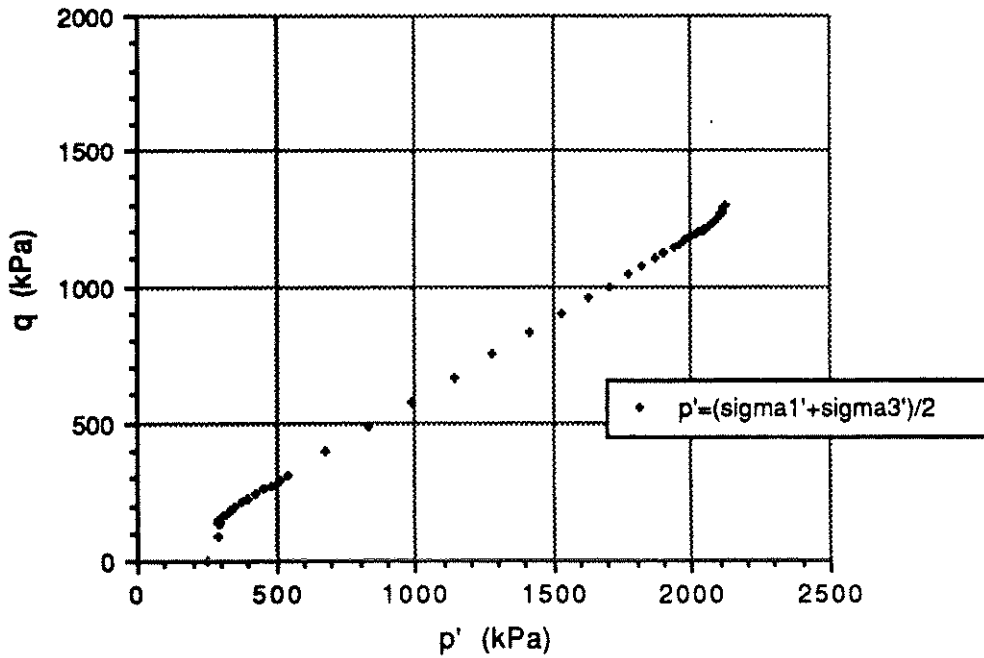
Deviatoric Stress (kPa)			Δ Pore Pressure (kPa)			Stress Ratio	
Break/ Peak	@	%	Peak	18.3 @	1.2 %	Break	3.04
10%	343.7		10%	-103.7		@	6.2 %
Elbow	4.1		Elbow	18.3		10%	3.24
Initial Tangent Modulus	0.000E0 kPa/Strain		Break	-291.5 @	19.0 %	Elbow	1.13
			Foreslope	2.510E3 kPa/Strain			
			Backslope1	-8.500E2 kPa/Strain			
			Backslope2	-2.290E3 kPa/Strain			

PP Parameter "A"			p' (kPa)			q (kPa)	
Peak ΔPP	4.47 @	1.2 %	$(\sigma_1' + \sigma_3')/2$			$(\sigma_1' - \sigma_3')/2$	
10%	-0.30		Elbow	34.8 @	1.2 %	Elbow	2.1
Elbow	4.47		10%	325.2		10%	171.9
Break ΔPP	-0.35		Steady State	1044.7 @	37.7 %	Steady State	636.1
			$(\sigma_1' + 2\sigma_3')/3$			$(P_o'/P_{ss}')/D_r$	
SS Reached? no			Elbow	34.1			0.103
dilative			10%	267.9			
			Steady State	832.7		Ø'	33.7 °
						SS Type dilative reversal above	

TABLE C-11: TEST PL 15 (pluviated)



DEVIATORIC STRESS AND Δ PORE PRESSURE



STRESS PATH (p'-q)

FIGURE C-12: TEST PL 16 (PLUVIATED)

Specimen FM 12 A2 Test PL 16 Set-up # 1 Load Cell Internal

A. INITIAL CONDITION

Gs=2.65

Dry Density	1.477 Mg/m ³	Void ratio	0.794	Dry Wt.	60.43 g
Relative Density	25.4 %	Saturation	88.9 %		
Max Density	1.695 Mg/m ³	Min Density	1.415 Mg/m ³		

B. PRE-SHEAR CONDITIONS

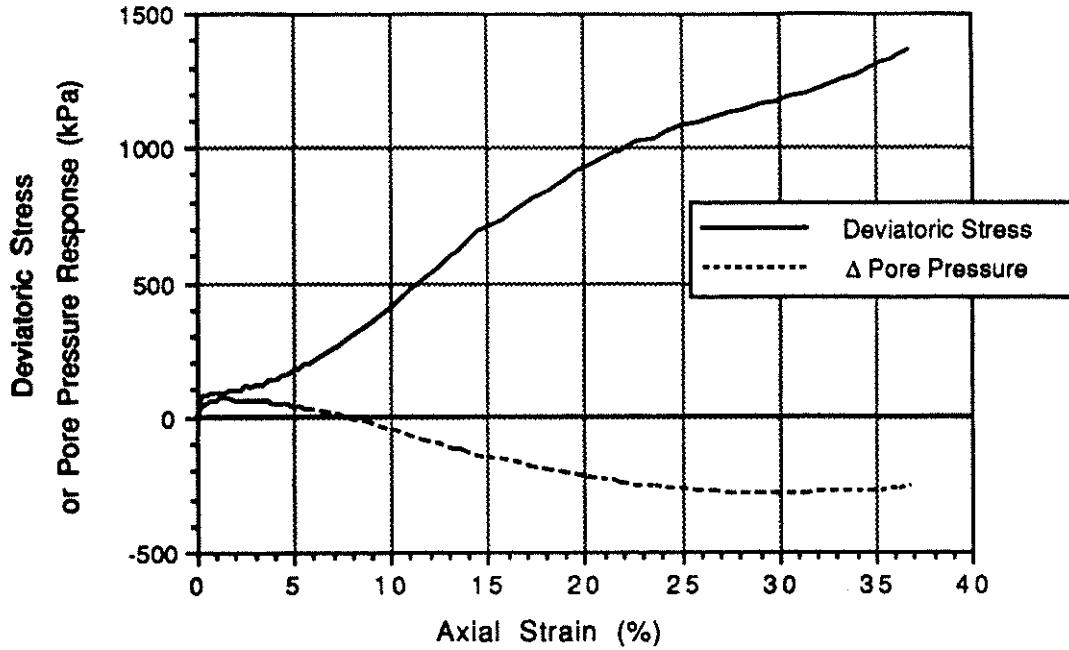
Dry Density	1.550 Mg/m ³	B	0.998	Volume	39.0 cc
Void ratio	0.710	Con. Pressure	53.5 kPa		
Rel Density	52.7 %	Con. Volume	0.21 cc		
Init. Effective Con. Pressure	255.9 kPa	Applied Back Pressure	599.5 kPa		

C. DURING SHEAR

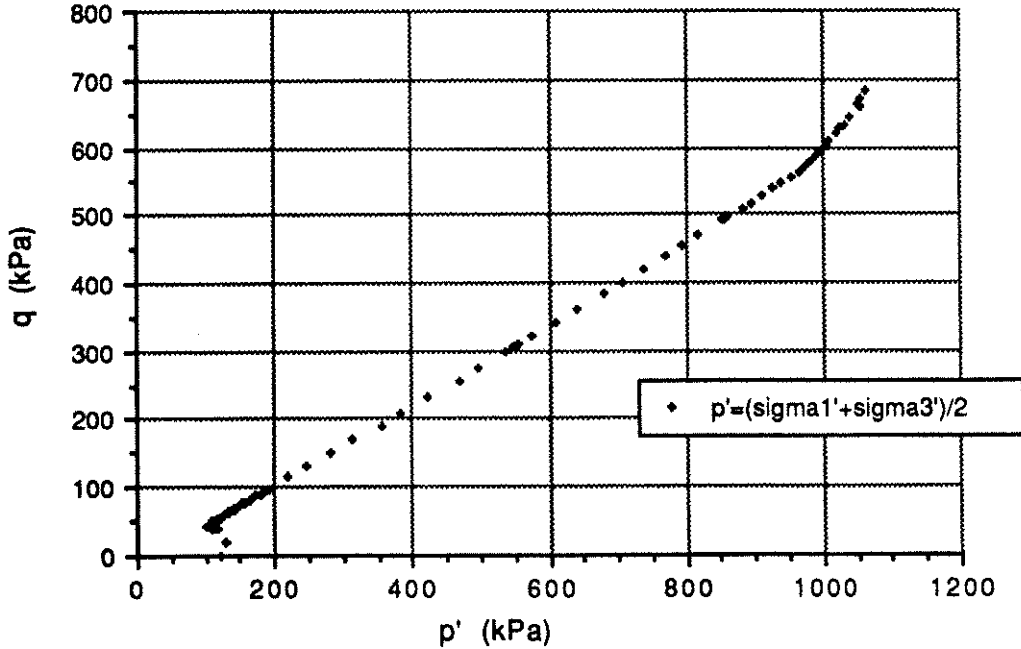
Deviatoric Stress (kPa)			Δ Pore Pressure (kPa)			Stress Ratio	
Break/			Peak	111.8 @	1.3 %	Break	3.38
Peak	297.7 @	1.0 %	10%	-259.5		@	1.9 %
10%	1450.4		Elbow	105.6		10%	3.81
Elbow	279.3		Break	-416.4 @	13.9 %	Elbow	2.86
Initial Tangent Modulus	4.297E4 kPa/Strain		Foreslope	1.625E4 kPa/Strain			
			Backslope1	-3.940E3 kPa/Strain			
			Backslope2	-5.160E3 kPa/Strain			

PP Parameter "A"			p' (kPa)		q (kPa)		
Peak ΔPP	0.35 @	1.3 %	($\sigma_1' + \sigma_3'$)/2		($\sigma_1' - \sigma_3'$)/2		
10%	-0.18		Elbow	289.9 @	0.6 %	Elbow	139.7
Elbow	0.38		10%	1240.5		10%	725.2
Break ΔPP	-0.22		Steady State	2104.7 @	46.9 %	Steady State	1264.9
			($\sigma_1' + 2\sigma_3'$)/3		(P_o'/P_{ss}')/Dr		
SS Reached? yes			Elbow	243.4			0.231
dilative			10%	998.7		Ø'	35.5 °
			Steady State	1683.1		SS Type	dilative reversal above

TABLE C-12: TEST PL 16 (pluviated)



DEVIATORIC STRESS AND Δ PORE PRESSURE



STRESS PATH (p'-q)

FIGURE C-13: TEST PL 17 (PLUVIATED)

Specimen FM 11 A4 Test PL 17 Set-up # 2 Load Cell Internal

A. INITIAL CONDITION

G_s=2.65

Dry Density	1.458 Mg/m ³	Void ratio	0.817	Dry Wt.	62.40 g
Relative Density	17.9 %	Saturation	90.5 %		
Max Density	1.695 Mg/m ³	Min Density	1.415 Mg/m ³		

B. PRE-SHEAR CONDITIONS

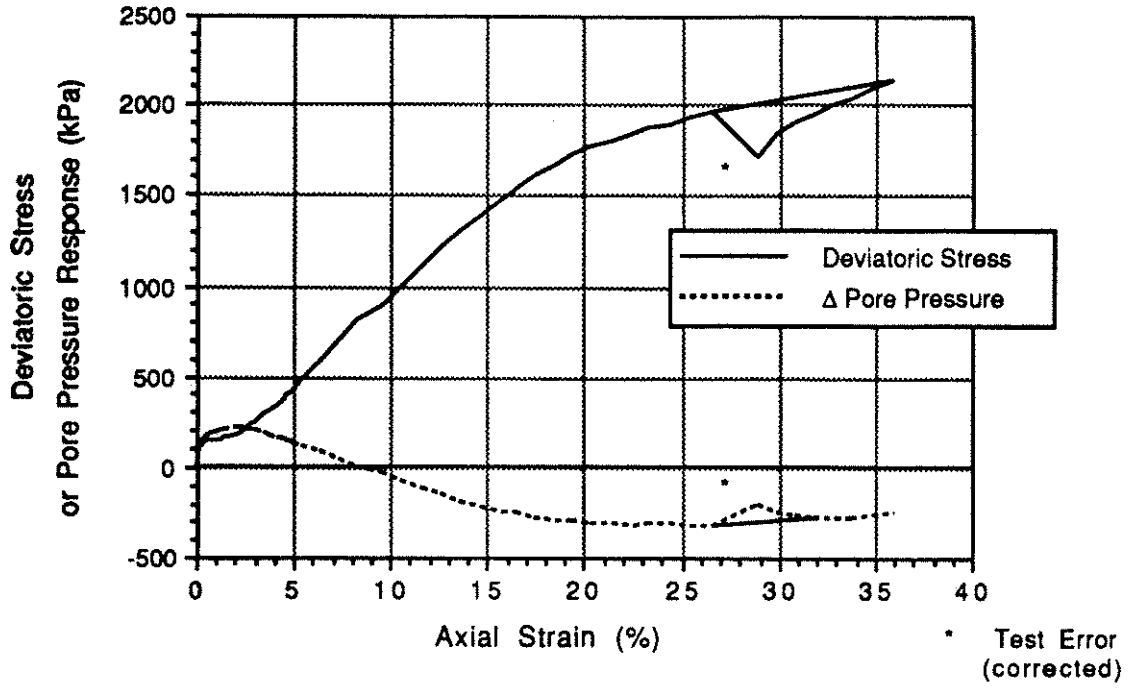
Dry Density	1.534 Mg/m ³	B	0.897	Volume	40.7 cc
Void ratio	0.727	Con. Pressure	124.3 kPa		
Rel Density	47.0 %	Con. Volume	0.37 cc		
Init. Effective Con. Pressure	121.6 kPa	Applied Back Pressure	858.2 kPa		

C. DURING SHEAR

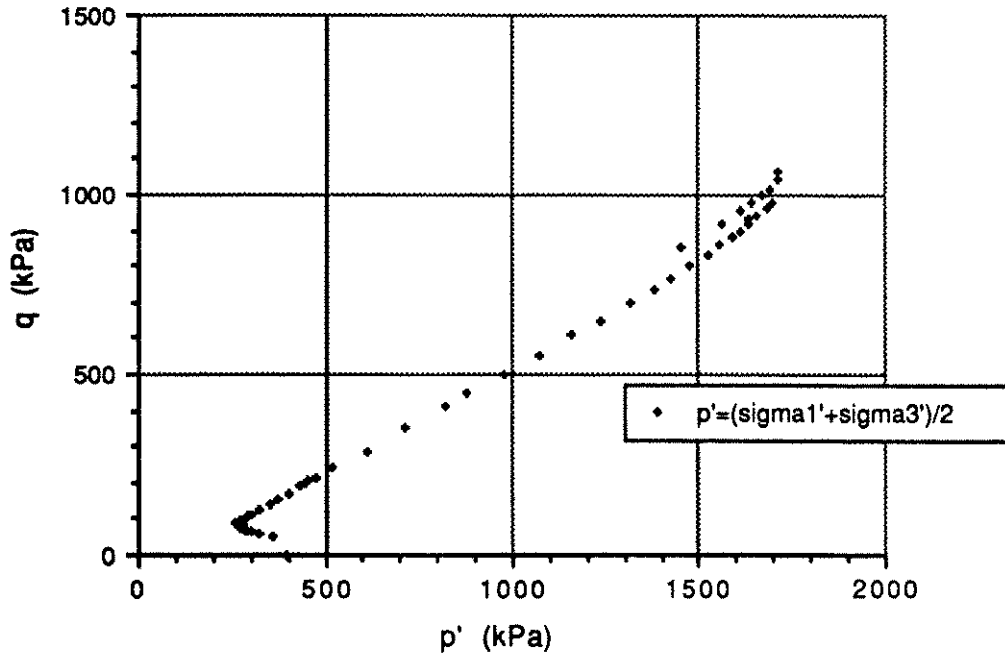
Deviatoric Stress (kPa)			Δ Pore Pressure (kPa)			Stress Ratio	
Break/			Peak	61.4 @ 1.7 %	Break	2.57	
Peak	75.1 @ 0.3 %		10%	-50.1	@	1.9 %	
10%	407.6		Elbow	61.2	10%	3.37	
Elbow	85.0		Break	-218.5 @ 19.6 %	Elbow	2.41	
Initial Tangent Modulus	2.423E4 kPa/Strain		Foreslope	1.322E4 kPa/Strain			
			Backslope1	-9.900E2 kPa/Strain			
			Backslope2	-1.950E3 kPa/Strain			

PP Parameter "A"			p' (kPa)			q (kPa)	
			$(\sigma_1' + \sigma_3')/2$			$(\sigma_1' - \sigma_3')/2$	
Peak ΔPP	0.75 @ 1.7 %		Elbow	102.9 @ 1.3 %	Elbow	42.5	
10%	-0.13		10%	375.5	10%	203.9	
Elbow	0.80		Steady State	1051.9 @ 35.8 %	Steady State	663.5	
Break ΔPP	-0.27		$(\sigma_1' + 2\sigma_3')/3$			$(\sigma_1'/\sigma_3')/Dr$	
			Elbow	88.7		0.246	
SS Reached? no			10%	307.5	Ø'	35.0 °	
dilative			Steady State	830.7	SS Type	dilative reversal above	

TABLE C-13: TEST PL 17 (pluviated)



DEVIATORIC STRESS AND Δ PORE PRESSURE



STRESS PATH (p'-q)

FIGURE C-14: TEST PL 19 (PLUVIATED)

Specimen FM 11 C4 Test PL 19 Set-up # 2 Load Cell Internal

A. INITIAL CONDITION

Gs=2.65

Dry Density	1.465 Mg/m ³	Void ratio	0.809	Dry Wt.	68.66 g
Relative Density	20.7 %	Saturation	89.0 %		
Max Density	1.695 Mg/m ³	Min Density	1.415 Mg/m ³		

B. PRE-SHEAR CONDITIONS

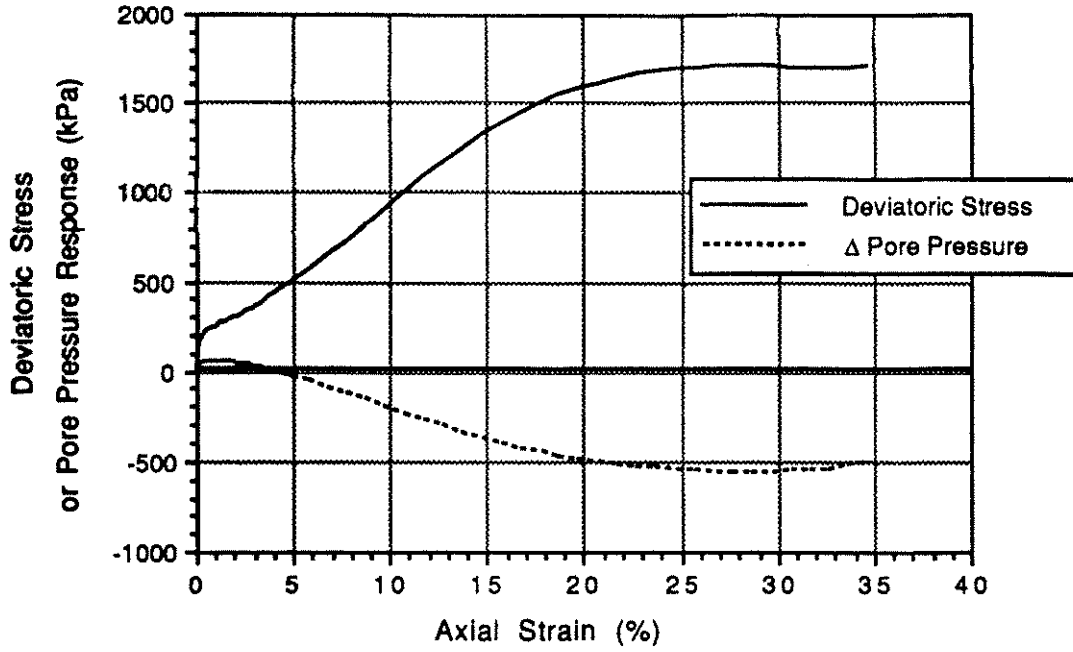
Dry Density	1.555 Mg/m ³	B	1.000	Volume	44.2 cc
Void ratio	0.704	Con. Pressure	401.5 kPa		
Rel Density	54.5 %	Con. Volume	1.03 cc		
Init. Effective Con. Pressure	396.9 kPa	Applied Back Pressure	783.1 kPa		

C. DURING SHEAR

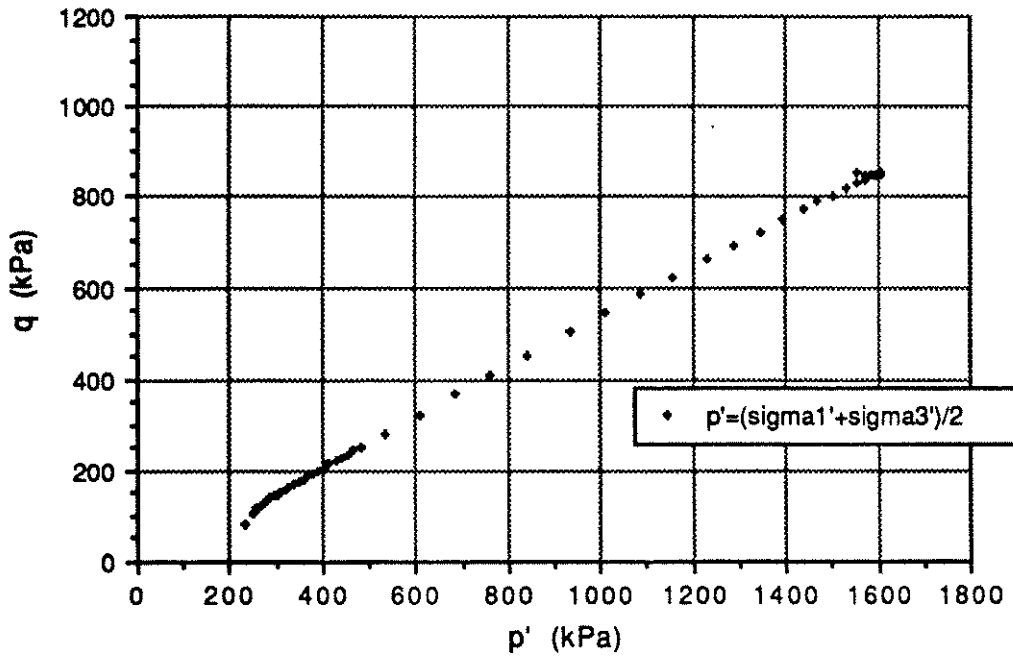
Deviatoric Stress (kPa)			Δ Pore Pressure (kPa)			Stress Ratio	
Break/			Peak	275.2 @ 1.8 %	Break	1.94	
Peak	120.8 @ 0.3 %		10%	-59.3	@	1.7 %	
10%	943.6		Elbow	198.4	10%	3.07	
Elbow	149.5		Break	-244.7 @ 15.8 %	Elbow	1.75	
Initial Tangent Modulus	4.474E4 kPa/Strain		Foreslope	2.306E4 kPa/Strain			
			Backslope1	0.000E0 kPa/Strain			
			Backslope2	-3.890E3 kPa/Strain			

PP Parameter "A"			p' (kPa)			q (kPa)	
Peak ΔPP	@ %		(σ' ₁ +σ' ₃)/2		(σ' ₁ -σ' ₃)/2		
10%	-0.06		Elbow	274.0 @ 1.2 %	Elbow	74.7	
Elbow	1.33		10%	927.3	10%	471.8	
Break ΔPP	-0.17		Steady State	1708.8 @ 35.2 %	Steady State	1047.6	
			(σ' ₁ +2σ' ₃)/3		(P _o '/P _{ss} ')/D _r		
SS Reached? no			Elbow	249.1		0.426	
dilative			10%	770.1	Ø'	32.5 °	
			Steady State	1359.6	SS Type	dilative reversal above	

TABLE C-14: TEST PL 19 (pluviated)



DEVIATORIC STRESS AND Δ PORE PRESSURE



STRESS PATH (p'-q)

FIGURE C-15: TEST FL 2 (FLUME)

Specimen TS1 4/T1 B Test FL 2 Set-up # 2 Load Cell Internal

A. INITIAL CONDITION

$G_s=2.65$

Dry Density	1.417 Mg/m ³	Void ratio	0.870	Dry Wt.	64.08 g
Relative Density	0.9 %	Saturation	82.5 %		
Max Density	1.695 Mg/m ³	Min Density	1.415 Mg/m ³		

B. PRE-SHEAR CONDITIONS

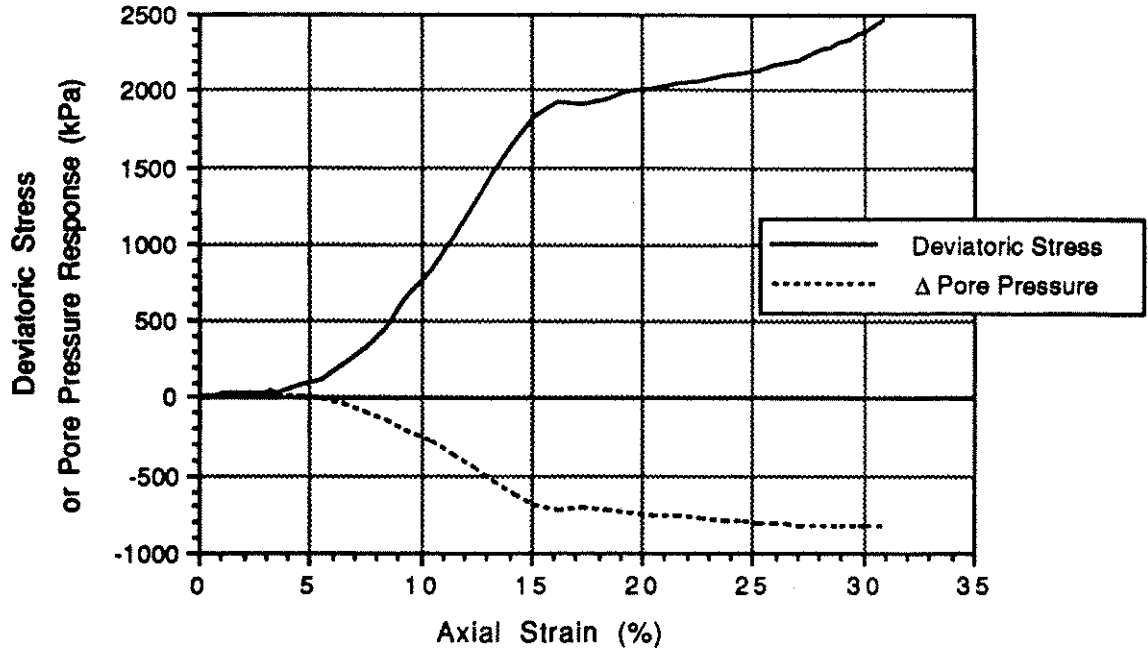
Dry Density	1.551 Mg/m ³	B	0.966	Volume	41.3 cc
Void ratio	0.708	Con. Pressure	200.0 kPa		
Rel Density	53.1 %	Con. Volume	cc		
Init. Effective Con. Pressure	199.2 kPa	Applied Back Pressure	885.5 kPa		

C. DURING SHEAR

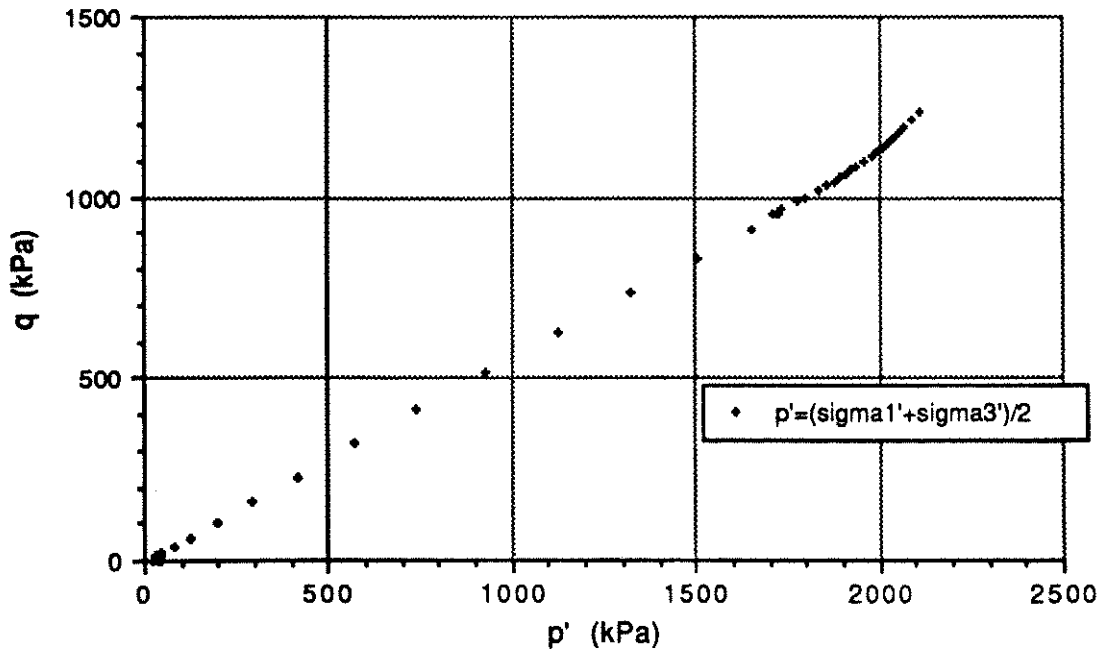
Deviatoric Stress (kPa)			Δ Pore Pressure (kPa)			Stress Ratio	
Break/			Peak	59.7 @ 0.8 %	Break	2.84	
Peak	209.1 @ 0.4 %		10%	-204.9	@	1.1 %	
10%	936.9		Elbow	162.6	10%	3.32	
Elbow	316.4		Break	-422.0 @ 16.6 %	Elbow	2.06	
Initial Tangent Modulus	5.503E4 kPa/Strain		Foreslope	1.489E4 kPa/Strain			
			Backslope1	-1.700E3 kPa/Strain			
			Backslope2	-3.500E3 kPa/Strain			

PP Parameter "A"			p' (kPa)			q (kPa)	
			$(\sigma' + \sigma_3')/2$			$(\sigma' - \sigma_3')/2$	
Peak ΔPP	0.26 @ 0.8 %		Elbow	235.1 @ 0.2 %	Elbow	81.3	
10%	-0.23		10%	872.6	10%	468.5	
Elbow	0.29		Steady State	1610.9 @ 27.6 %	Steady State	853.0	
Break ΔPP	-0.30		$(\sigma' + 2\sigma_3')/3$			$(P_o'/P_{ss}')/D_r$	
			Elbow	207.9		0.233	
			10%	716.5	ϕ'	31.2 °	
			Steady State	1326.6	SS Type dilative reversal		
SS Reached? yes							
dilative							

TABLE C-15: TEST FL 2 (flume)



DEVIATORIC STRESS AND Δ PORE PRESSURE



STRESS PATH (p'-q)

FIGURE C-16: TEST FL 3 (FLUME)

Specimen TS1 4/T2 A Test FL 3 Set-up # 1 Load Cell Internal

A. INITIAL CONDITION

Gs=2.65

Dry Density	1.438 Mg/m ³	Void ratio	0.843	Dry Wt.	68.56 g
Relative Density	9.7 %	Saturation	92.3 %		
Max Density	1.695 Mg/m ³	Min Density	1.415 Mg/m ³		

B. PRE-SHEAR CONDITIONS

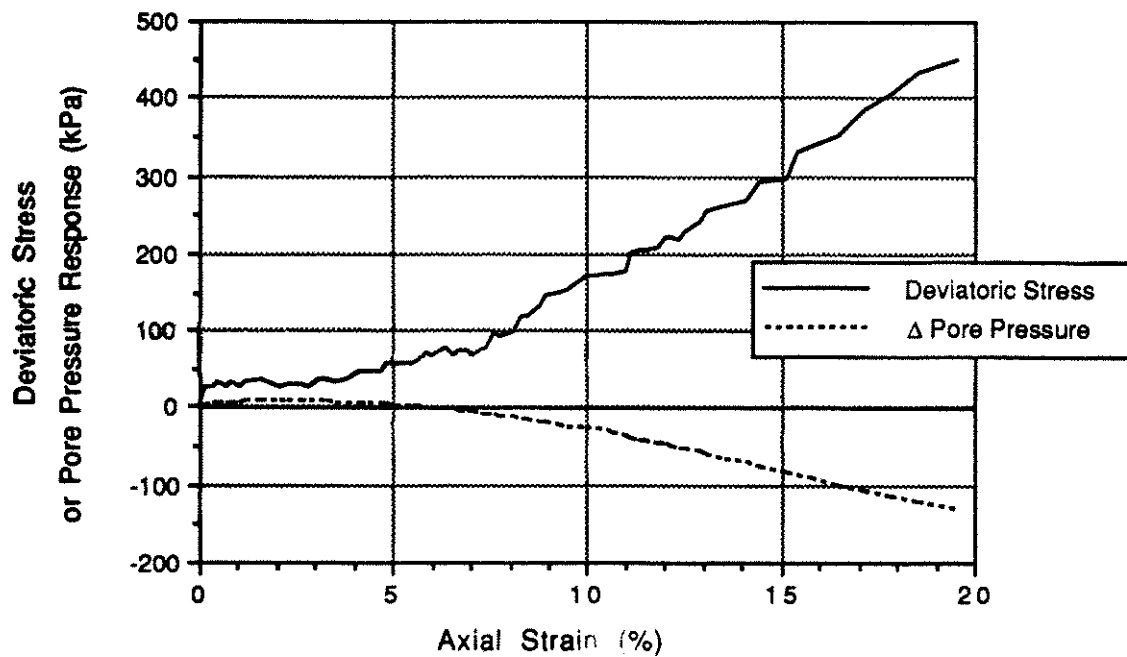
Dry Density	1.539 Mg/m ³	B	1.000	Volume	44.5 cc
Void ratio	0.722	Con. Pressure	42.1 kPa		
Rel Density	48.8 %	Con. Volume	0.89 cc		
Init. Effective Con. Pressure	40.8 kPa	Applied Back Pressure	833.8 kPa		

C. DURING SHEAR

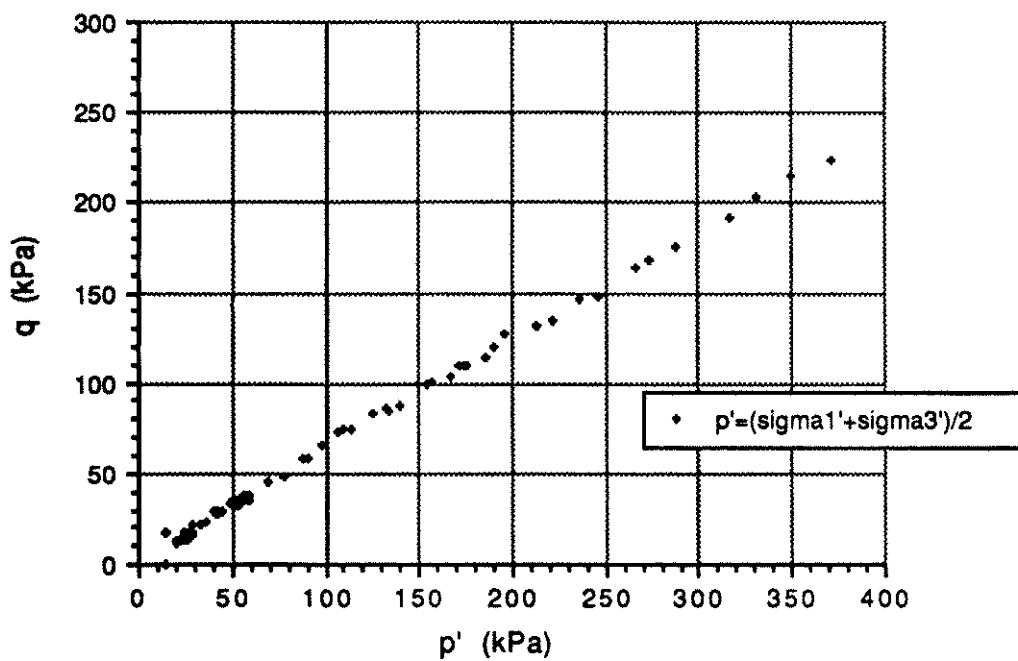
Deviatoric Stress (kPa)			Δ Pore Pressure (kPa)			Stress Ratio	
Break/ Peak	@	%	Peak	22.5 @	1.9 %	Break	3.31
10%	739.3		10%	-250.4		@	6.6 %
Elbow	6.1		Elbow	19.7		10%	3.52
Initial Tangent Modulus	0.000E0 kPa/Strain		Break	-727.8 @	16.2 %	Elbow	1.29
			Foreslope	1.810E3 kPa/Strain			
			Backslope1	-7.900E2 kPa/Strain			
			Backslope2	-9.390E3 kPa/Strain			

PP Parameter "A"			p' (kPa)			q (kPa)	
Peak ΔPP	1.01 @	1.9 %	$(\sigma_1' + \sigma_3')/2$			$(\sigma_1' - \sigma_3')/2$	
10%	-0.34		Elbow	24.4 @	1.1 %	Elbow	3.1
Elbow	3.23		10%	632.5		10%	369.7
Break ΔPP	-0.38		Steady State	2110.9 @	31.0 %	Steady State	1234.4
			$(\sigma_1' + 2\sigma_3')/3$			$(P_o'/P_{ss}')/D_r$	
SS Reached? no			Elbow	23.4			0.040
dilative			10%	539.3			
			Steady State	1699.5		Ø'	32.9 °
						SS Type dilative bunching	

TABLE C-16: TEST FL 3 (flume)



DEVIATORIC STRESS AND Δ PORE PRESSURE



STRESS PATH (p' - q)

FIGURE C-17: TEST FL 4 (FLUME)

Specimen TS1 4/T2 C Test FL 4 Set-up # 2 Load Cell Internal

A. INITIAL CONDITION

G_s=2.65

Dry Density	1.432 Mg/m ³	Void ratio	0.850	Dry Wt.	68.78 g
Relative Density	7.2 %	Saturation	78.0 %		
Max Density	1.695 Mg/m ³	Min Density	1.415 Mg/m ³		

B. PRE-SHEAR CONDITIONS

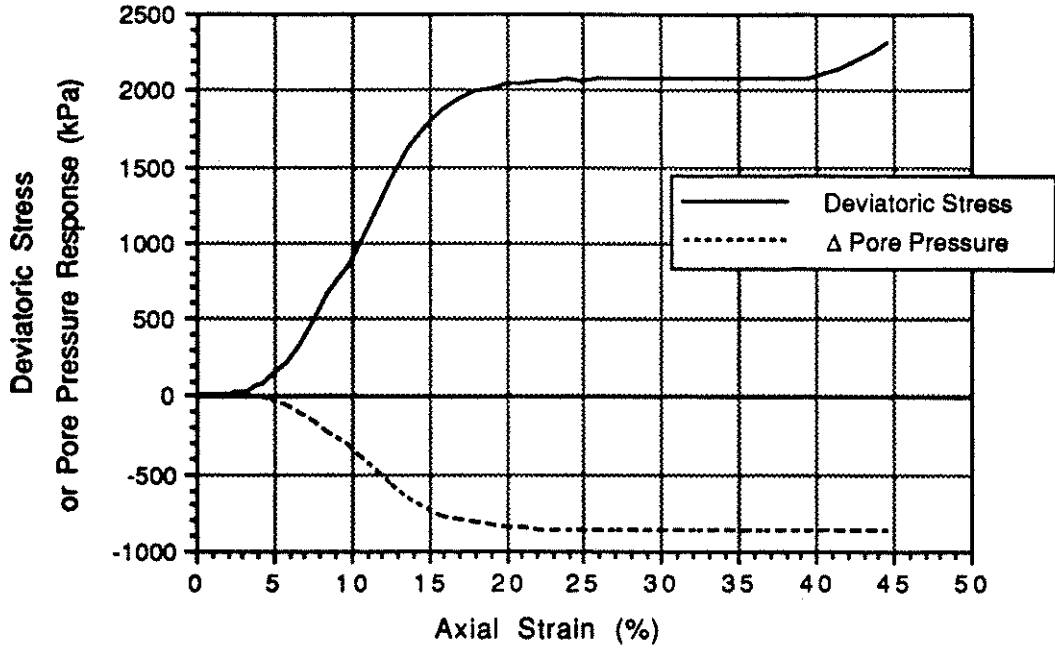
Dry Density	1.560 Mg/m ³	B	1.000	Volume	44.1 cc
Void ratio	0.699	Con. Pressure	20.0 kPa		
Rel Density	56.3 %	Con. Volume	cc		
Init. Effective Con. Pressure	14.9 kPa	Applied Back Pressure	821.6 kPa		

C. DURING SHEAR

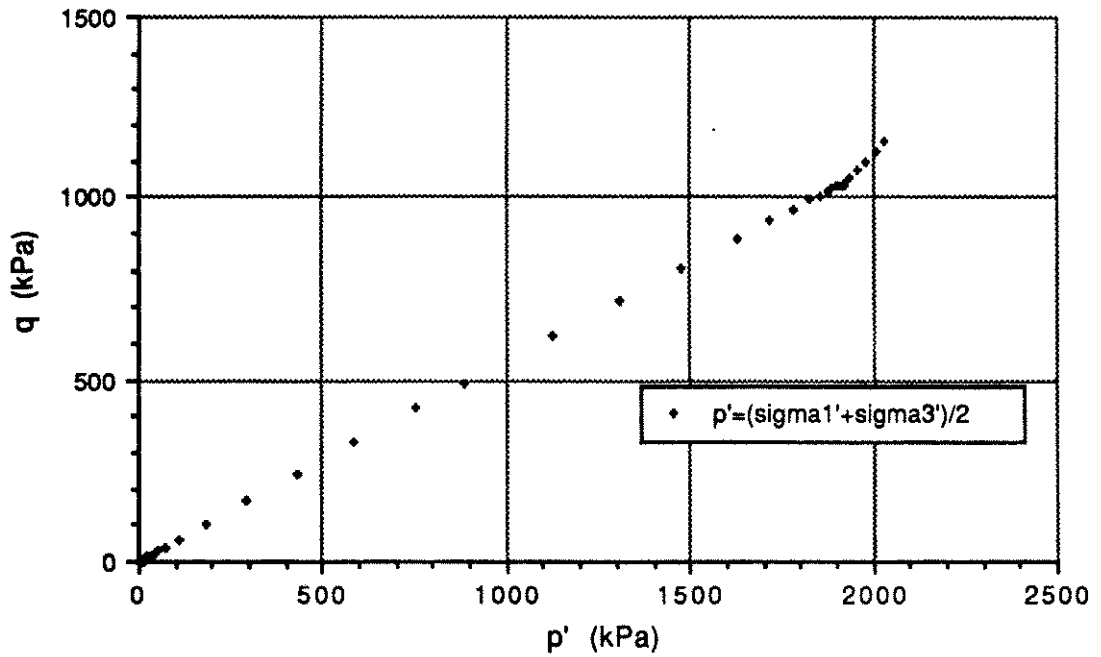
Deviatoric Stress (kPa)		Δ Pore Pressure (kPa)		Stress Ratio	
Break/ Peak	@ %	Peak	8.5 @ 3.3 %	Break	%
10%		10%	-27.3	@	
Elbow		Elbow		10%	
Initial Tangent Modulus	0.000E0 kPa/Strain	Break	@ %	Elbow	
		Foreslope	8.060E2 kPa/Strain		
		Backslope1	-3.403E2 kPa/Strain		
		Backslope2	-1.115E3 kPa/Strain		

PP Parameter "A"		p' (kPa)		q (kPa)	
Peak ΔPP	@ %	$(\sigma_1' + \sigma_3')/2$		$(\sigma_1' - \sigma_3')/2$	
10%		Elbow	@ %	Elbow	
Elbow		10%		10%	
Break ΔPP		Steady State	@ %	Steady State	
		$(\sigma_1' + 2\sigma_3')/3$		$(\sigma_1' - \sigma_3')/3$	
SS Reached? no		Elbow			NA
dilative		10%			
		Steady State		Ø'	°
				SS Type dilative no SS	

TABLE C-17: TEST FL 4 (flume)



DEVIATORIC STRESS AND Δ PORE PRESSURE



STRESS PATH (p'-q)

FIGURE C-18: TEST FL 5 (FLUME)

Specimen TS 3 P2D A Test FL 5 Set-up # 1 Load Cell Internal

A. INITIAL CONDITION

Gs=2.65

Dry Density	1.555 Mg/m ³	Void ratio	0.704	Dry Wt.	74.25 g
Relative Density	54.5 %	Saturation	87.3 %		
Max Density	1.695 Mg/m ³	Min Density	1.415 Mg/m ³		

B. PRE-SHEAR CONDITIONS

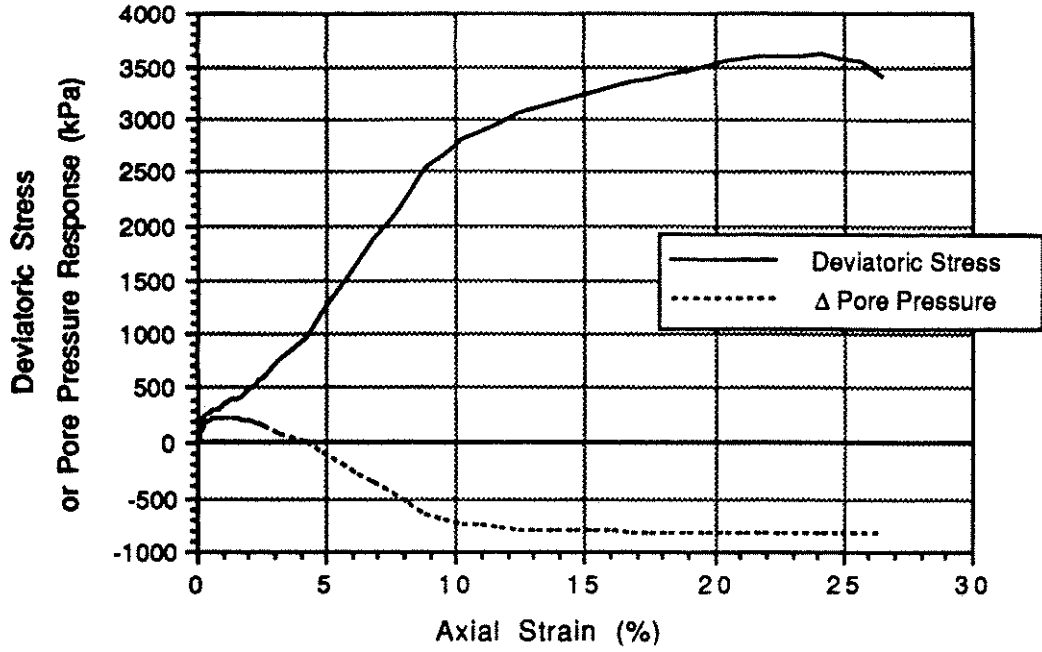
Dry Density	1.567 Mg/m ³	B	1.000	Volume	47.4 cc
Void ratio	0.692	Con. Pressure	15.0 kPa		
Rel Density	58.7 %	Con. Volume	cc		
Init. Effective Con. Pressure	15.7 kPa	Applied Back Pressure	825.1 kPa		

C. DURING SHEAR

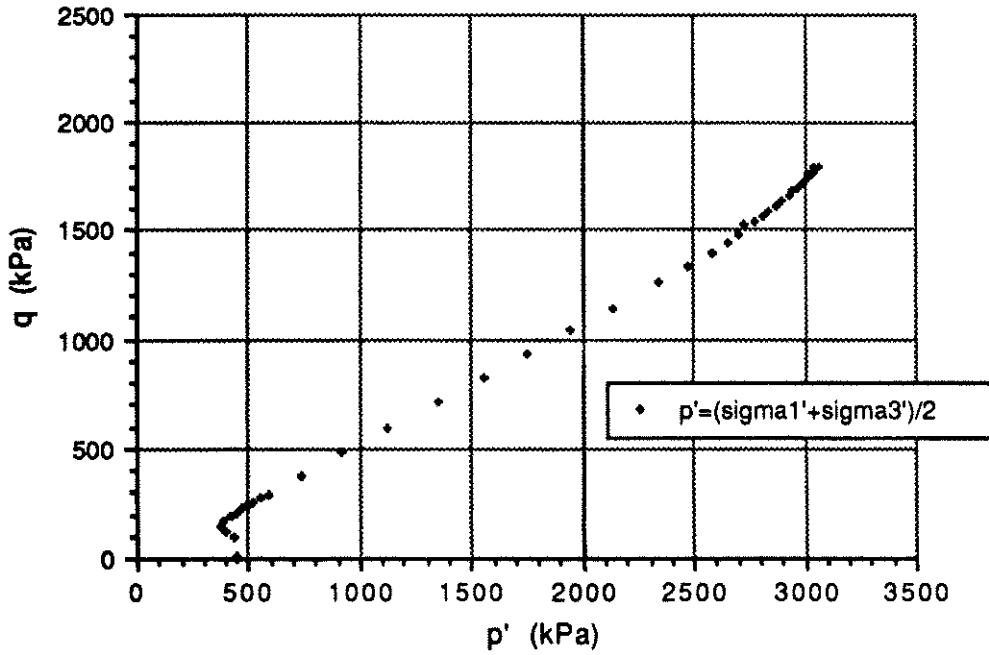
Deviatoric Stress (kPa)			Δ Pore Pressure (kPa)			Stress Ratio	
Break/ Peak	@	%	Peak	9.8 @	1.4 %	Break	3.24
10%	843.3		10%	-316.7		@	3.8 %
Elbow			Elbow	8.5		10%	3.54
Initial Tangent Modulus	0.000E0 kPa/Strain		Break	-653.6 @	13.7 %	Elbow	
			Foreslope	1.330E3 kPa/Strain			
			Backslope1	-5.500E2 kPa/Strain			
			Backslope2	-9.050E3 kPa/Strain			

PP Parameter "A"			p' (kPa)			q (kPa)	
Peak ΔPP	0.93 @	1.4 %	($\sigma_{1'} + \sigma_{3'}$)/2			($\sigma_{1'} - \sigma_{3'}$)/2	
10%	-0.38		Elbow	5.8 @	0.8 %	Elbow	6.4
Elbow			10%	754.3		10%	421.7
Break ΔPP	-0.41		Steady State	1903.2 @	22.9 %	Steady State	1030.4
			($\sigma_{1'} + 2\sigma_{3'}$)/3			(Po'/Pss')/Dr	
SS Reached? yes			Elbow				0.014
dilative			10%	613.7		Ø'	33.9 °
			Steady State	1559.7		SS Type	dilative reversal

TABLE C-18: TEST FL 5 (flume)



DEVIATORIC STRESS AND Δ PORE PRESSURE



STRESS PATH (p'-q)

FIGURE C-19: TEST FL 6 (FLUME)

Specimen TS3 P2D D Test FL 6 Set-up # 2 Load Cell Internal

A. INITIAL CONDITION

Gs=2.65

Dry Density	1.453 Mg/m ³	Void ratio	0.824	Dry Wt.	64.48 g
Relative Density	15.8 %	Saturation	83.4 %		
Max Density	1.695 Mg/m ³	Min Density	1.415 Mg/m ³		

B. PRE-SHEAR CONDITIONS

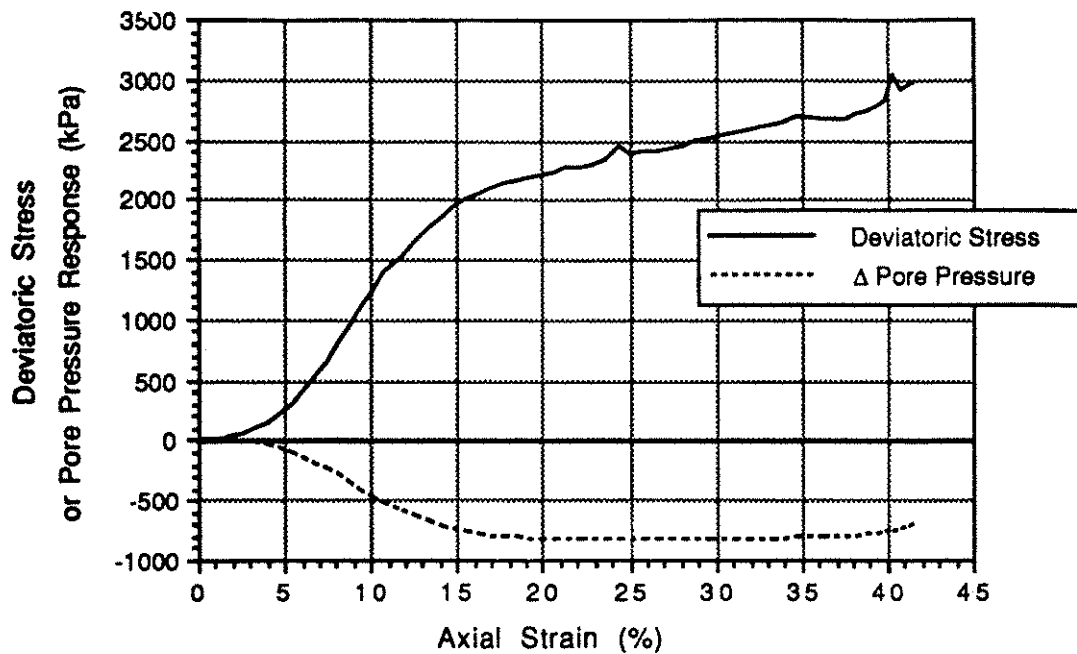
Dry Density	1.604 Mg/m ³	B	1.000	Volume	40.2 cc
Void ratio	0.653	Con. Pressure	442.3 kPa		
Rel Density	71.3 %	Con. Volume	0.83 cc		
Init. Effective Con. Pressure	441.9 kPa	Applied Back Pressure	808.7 kPa		

C. DURING SHEAR

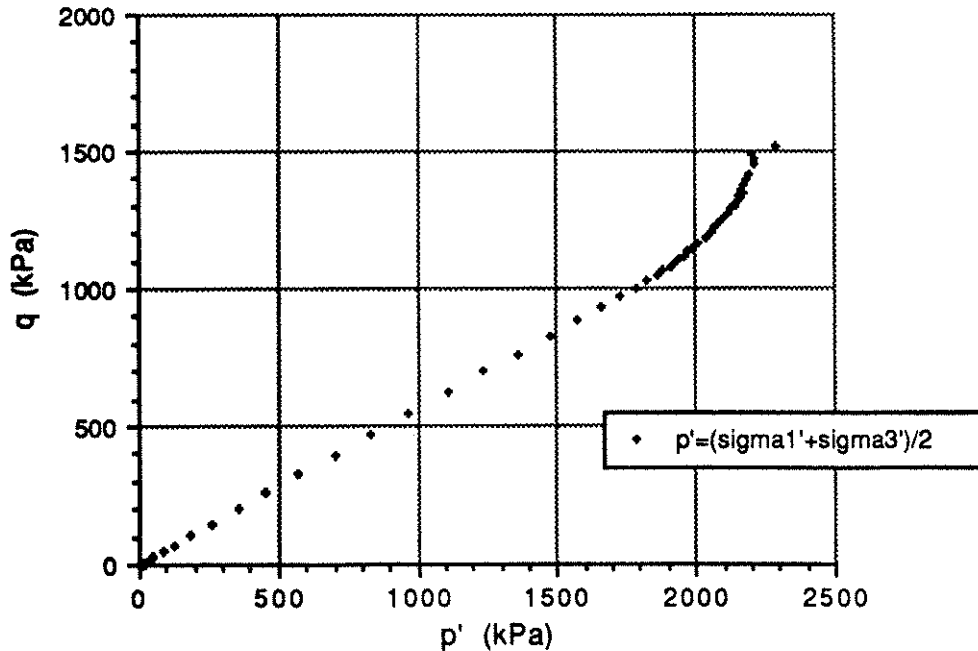
Deviatoric Stress (kPa)		Δ Pore Pressure (kPa)		Stress Ratio	
Break/		Peak	222.1 @ 0.9 %	Break	2.73
Peak	196.4 @ 0.2 %	10%	-729.8	@	1.6 %
10%	2750.9	Elbow	222.1	10%	3.35
Elbow	301.7	Break	-701.9 @ 9.5 %	Elbow	2.39
Initial Tangent Modulus	1.228E5 kPa/Strain	Foreslope	4.067E4 kPa/Strain		
		Backslope1	-6.220E3 kPa/Strain		
		Backslope2	-1.434E4 kPa/Strain		

PP Parameter "A"			p' (kPa)		q (kPa)	
Peak ΔPP	0.74 @ 0.9 %		(sigma1'+sigma3')/2		(sigma1'-sigma3')/2	
10%	-0.27		Elbow	368.6 @ 0.9 %	Elbow	150.9
Elbow	0.74		10%	2546.4	10%	1375.4
Break ΔPP	-0.26		Steady State	3068.6 @ 22.7 %	Steady State	1796.6
			(sigma1'+2sigma3')/3		(Po'/Pss')/Dr	
SS Reached? yes			Elbow	318.3		0.202
dilative			10%	2088.0	Ø'	32.4 °
			Steady State	2469.7	SS Type	dilative reversal above

TABLE C-19: TEST FL 6 (flume)



DEVIATORIC STRESS AND Δ PORE PRESSURE



STRESS PATH (p' - q)

FIGURE C-20: TEST FL 7 (FLUME)

Specimen TS1 4/T3 A Test FL 7 Set-up # 2 Load Cell Internal

**A. INITIAL
CONDITION**

Gs=2.65

Dry Density	1.495 Mg/m ³	}	Void ratio	0.773	}	Dry Wt.	65.49 g
Relative Density	32.4 %		Saturation	89.9 %			
Max Density	1.695 Mg/m ³		Min Density	1.415 Mg/m ³			

B. PRE-SHEAR CONDITIONS

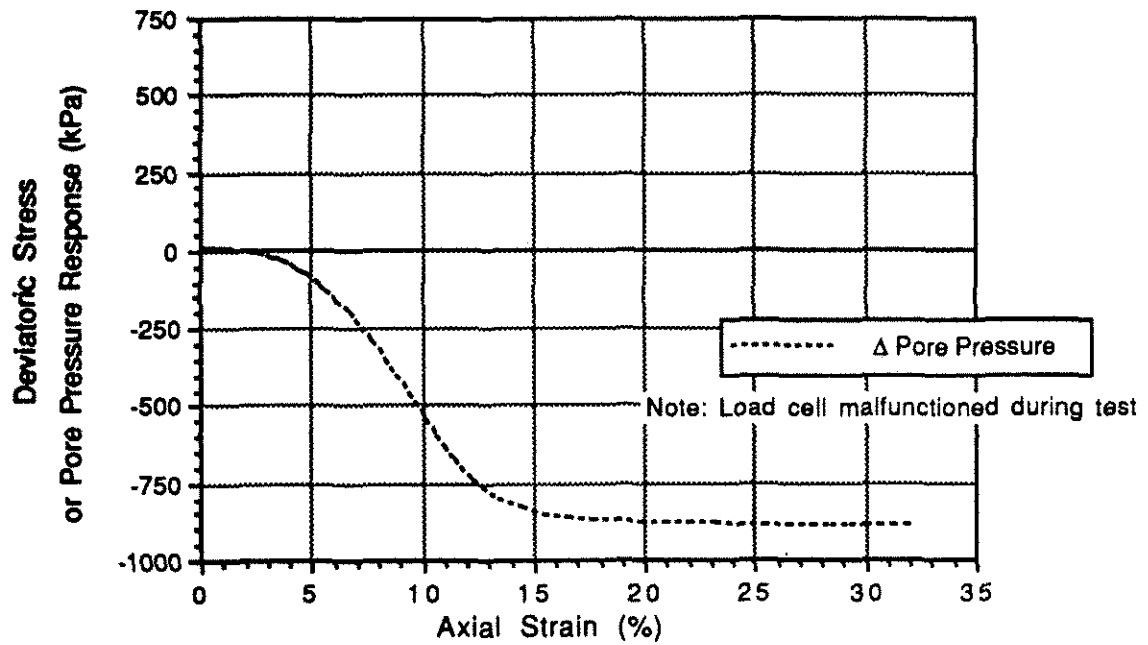
Dry Density	1.570 Mg/m ³	}	B	1.000	}	Volume	41.7 cc
Void ratio	0.688		Con. Pressure	15.0 kPa			
Rel Density	59.8 %		Con. Volume	cc			
Init. Effective Con. Pressure	19.4 kPa	}	Applied Back Pressure	815.8 kPa			

C. DURING SHEAR

Deviatoric Stress (kPa)			Δ Pore Pressure (kPa)			Stress Ratio	
Break/ Peak	@	%	Peak	8.0 @	0.7 %	Break	2.92
10%	1247.3		10%	-464.3		@	2.6 %
Elbow	3.9		Elbow	8.0		10%	3.58
Initial Tangent Modulus	0.000E0	kPa/ Strain	Break	-673.9 @	13.4 %	Elbow	1.34
			Foreslope	1.940E3	kPa/Strain		
			Backslope1	-1.070E3	kPa/Strain		
			Backslope2	-7.500E3	kPa/Strain		

PP Parameter "A"				p' (kPa)		q (kPa)	
				$(\sigma_1' + \sigma_3')/2$		$(\sigma_1' - \sigma_3')/2$	
Peak Δ PP	2.05 @	0.7 %	Elbow	13.3 @	0.7 %	Elbow	2.0
10%	-0.37		10%	1106.6		10%	623.6
Elbow	2.05		Steady State	2191.7 @	39.9 %	Steady State	1411.0
Break Δ PP	-0.38		$(\sigma_1' + 2\sigma_3')/3$		$(\sigma_1' - \sigma_3')/3$		
			Elbow	12.7			0.015
			10%	898.7		ϕ'	35.0 °
SS Reached? no			Steady State	1721.3		SS Type dilative reversal above	
dilative							

TABLE C-20: TEST FL 7 (flume)

**DEVIATORIC STRESS AND Δ PORE PRESSURE****FIGURE C-21: TEST FL 8 (FLUME)**

Specimen TS1 4/T3 C Test FL 8 Set-up # 1 Load Cell External

A. INITIAL CONDITION

Gs=2.65

Dry Density	1.550 Mg/m ³	Void ratio	0.709	Dry Wt.	69.52 g
Relative Density	52.7 %	Saturation	91.6 %		
Max Density	1.695 Mg/m ³	Min Density	1.415 Mg/m ³		

B. PRE-SHEAR CONDITIONS

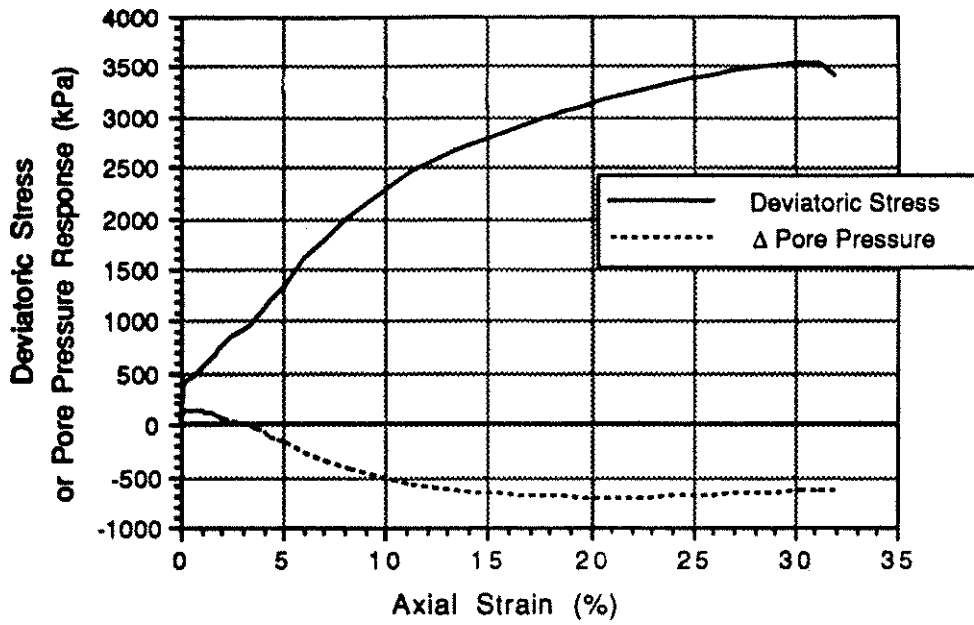
Dry Density	1.550 Mg/m ³	B	1.000	Volume	44.9 cc
Void ratio	0.710	Con. Pressure	15.0 kPa		
Rel Density	52.7 %	Con. Volume	cc		
Init. Effective Con. Pressure	17.6 kPa	Applied Back Pressure	828.5 kPa		

C. DURING SHEAR

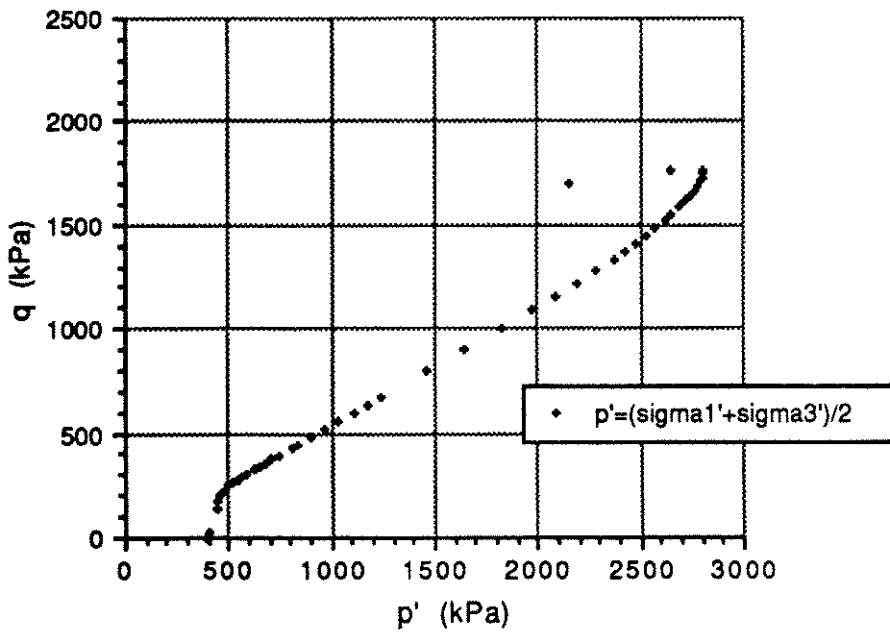
Deviatoric Stress (kPa)		Δ Pore Pressure (kPa)		Stress Ratio	
Break/ Peak	@ %	Peak	7.2 @ 0.8 %	Break	
10%		10%	-518.7	@	%
Elbow		Elbow		10%	
Initial Tangent Modulus	0.000E0 kPa/Strain	Break	-799.7 @ 13.4 %	Elbow	
		Foreslope	1.430E3 kPa/Strain		
		Backslope1	-1.320E3 kPa/Strain		
		Backslope2	-1.035E4 kPa/Strain		

PP Parameter "A"		p' (kPa)		q (kPa)	
Peak ΔPP	@ %	$(\sigma_1' + \sigma_3')/2$		$(\sigma_1' - \sigma_3')/2$	
10%		Elbow	@ %	Elbow	
Elbow		10%		10%	
Break ΔPP		Steady State	@ %	Steady State	
		$(\sigma_1' + 2\sigma_3')/3$		$(\sigma_1' - \sigma_3')/3$	
SS Reached? no		Elbow			NA
dilative		10%			
		Steady State		Ø'	o
				SS Type dilative no SS	

TABLE C-21: TEST FL 8 (flume)



DEVIATORIC STRESS AND Δ PORE PRESSURE



STRESS PATH (p'-q)

FIGURE C-22: TEST FL 9 (FLUME)

Specimen TS1 4/T3 D Test FL 9 Set-up # 2 Load Cell Internal

A. INITIAL CONDITION

Gs=2.65

Dry Density	1.487 Mg/m ³	Void ratio	0.782	Dry Wt.	66.16 g
Relative Density	29.3 %	Saturation	88.6 %		
Max Density	1.695 Mg/m ³	Min Density	1.415 Mg/m ³		

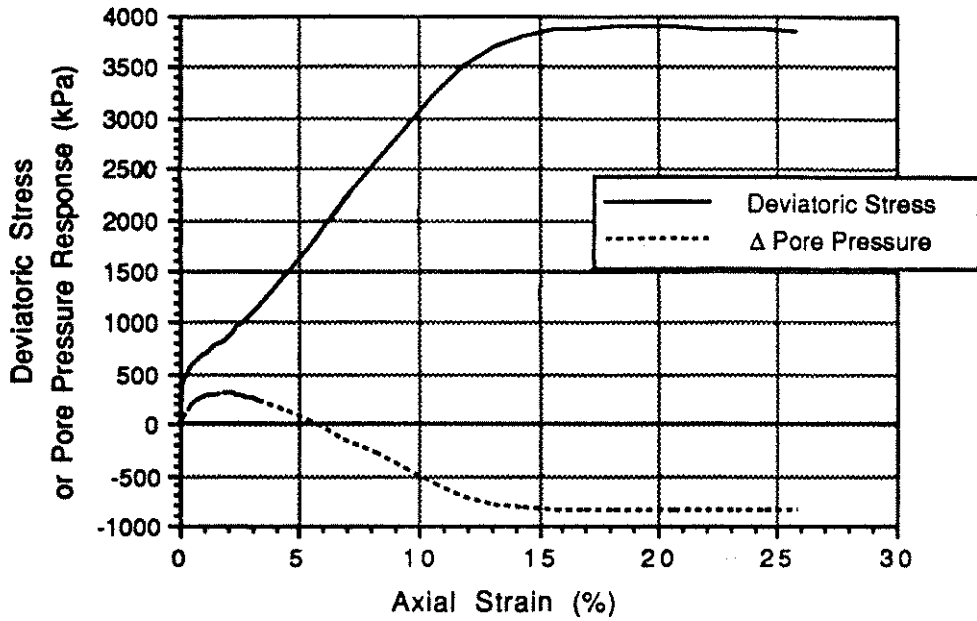
B. PRE-SHEAR CONDITIONS

Dry Density	1.525 Mg/m ³	B	1.000	Volume	43.4 cc
Void ratio	0.737	Con. Pressure	392.9 kPa		
Rel Density	43.7 %	Con. Volume	1.15 cc		
Init. Effective Con. Pressure	393.6 kPa	Applied Back Pressure	792.5 kPa		

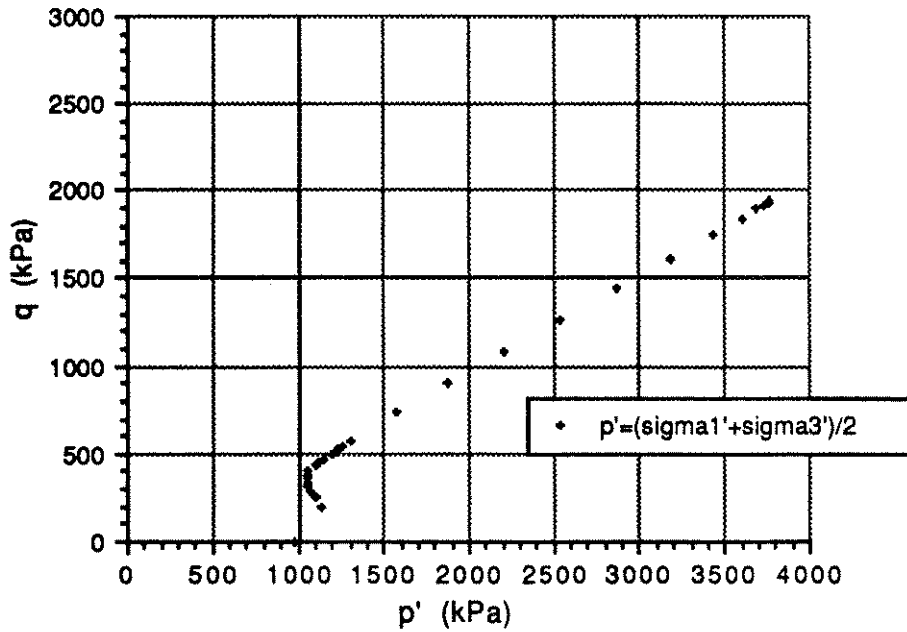
C. DURING SHEAR

Deviatoric Stress (kPa)			Δ Pore Pressure (kPa)			Stress Ratio	
Break/ Peak	364.6 @	0.2 %	Peak	146.0 @	0.5 %	Break	3.03
10%	2269.8		10%	-521.9		@	0.9 %
Elbow	364.6		Elbow	128.3		10%	3.48
Initial Tangent Modulus	2.279E5	kPa/ Strain	Break	-514.3 @	9.8 %	Elbow	2.37
			Foreslope	8.019E4	kPa/Strain		
			Backslope1	-3.350E3	kPa/Strain		
			Backslope2	-8.820E3	kPa/Strain		
PP Parameter "A"			p' (kPa)			q (kPa)	
			$(\sigma_1' + \sigma_3')/2$			$(\sigma_1' - \sigma_3')/2$	
Peak Δ PP	0.33 @	0.5 %	Elbow	448.3 @	0.2 %	Elbow	182.3
10%	-0.23		10%	2051.1		10%	1134.9
Elbow	0.35		Steady State	2801.3 @	27.7 %	Steady State	1738.7
Break Δ PP	-0.23		$(\sigma_1' + 2\sigma_3')/3$			$(\sigma_1'/\sigma_3')/D_r$	
			Elbow	387.6			0.322
SS Reached? no			10%	1672.8		ϕ'	33.2 °
dilative			Steady State	2221.8		SS Type dilative reversal above	

TABLE C-22: TEST FL 9 (flume)



DEVIATORIC STRESS AND Δ PORE PRESSURE



STRESS PATH (p'-q)

FIGURE C-23: TEST FL 10 (FLUME)

Specimen TS4 M2R B Test FL 10 Set-up # HP Load Cell External

A. INITIAL CONDITION

Gs=2.65

Dry Density	1.449 Mg/m ³	Void ratio	0.829	Dry Wt. 60.65 g
Relative Density	14.2 %	Saturation	86.7 %	
Max Density	1.695 Mg/m ³	Min Density	1.415 Mg/m ³	

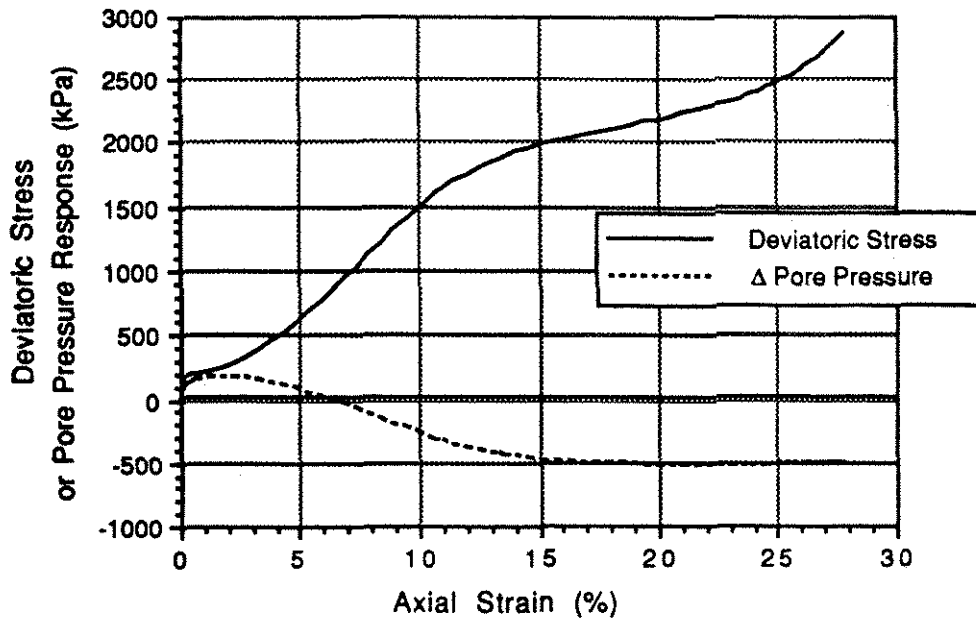
B. PRE-SHEAR CONDITIONS

Dry Density	1.578 Mg/m ³	B	0.996	Volume 38.4 cc
Void ratio	0.679	Con. Pressure	981.9 kPa	
Rel Density	62.5 %	Con. Volume	0.46 cc	
Init. Effective Con. Pressure	973.8 kPa	Applied Back Pressure	784.8 kPa	

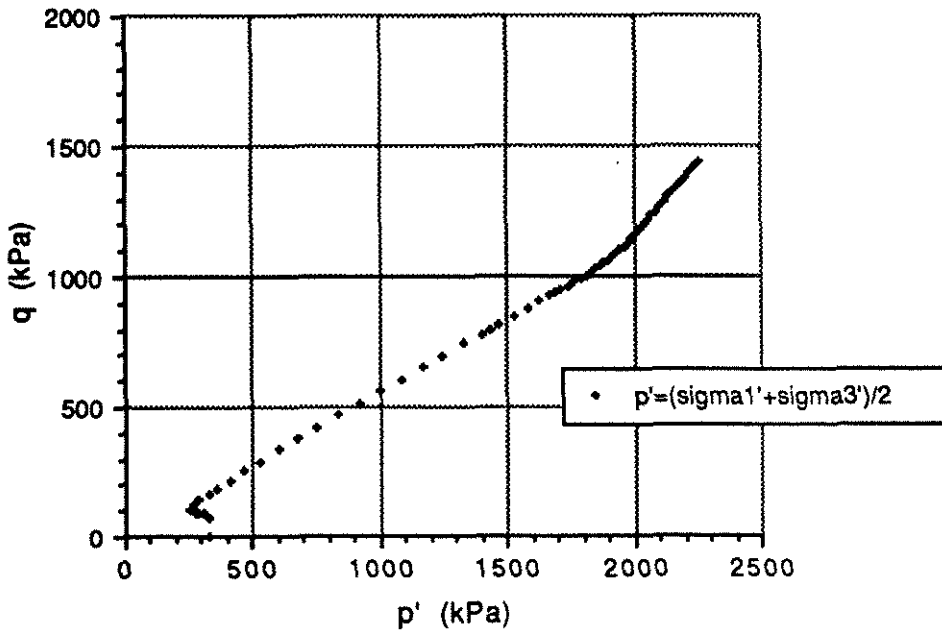
C. DURING SHEAR

Deviatoric Stress (kPa)			Δ Pore Pressure (kPa)			Stress Ratio	
Break/			Peak	322.4 @ 1.8 %	Break	2.30	
Peak	509.0 @ 0.3 %		10%	-508.1	@	2.0 %	
10%	3054.0		Elbow	308.4	10%	3.06	
Elbow	743.6		Break	-785.9 @ 13.1 %	Elbow	2.12	
Initial Tangent Modulus	1.885E5 kPa/Strain		Foreslope	3.290E4 kPa/Strain			
			Backslope1	-5.780E3 kPa/Strain			
			Backslope2	-1.147E4 kPa/Strain			
PP Parameter "A"			p' (kPa)			q (kPa)	
Peak Δ PP	0.07 @ 1.8 %		($\sigma_1' + \sigma_3'$)/2		($\sigma_1' - \sigma_3'$)/2		
10%	-0.17		Elbow	1037.4 @ 1.7 %	Elbow	371.8	
Elbow	0.42		10%	3010.3	10%	1527.0	
Break Δ PP	-0.21		Steady State	3766.4 @ 19.5 %	Steady State	1947.8	
			($\sigma_1' + 2\sigma_3'$)/3		(P_o'/P_{ss}')/Dr		
SS Reached? yes			Elbow	913.4		0.414	
dilative			10%	2501.3	ϕ'	31.5 °	
			Steady State	3117.1	SS Type	dilative reversal	

TABLE C-23: TEST FL 10 (flume)



DEVIATORIC STRESS AND Δ PORE PRESSURE

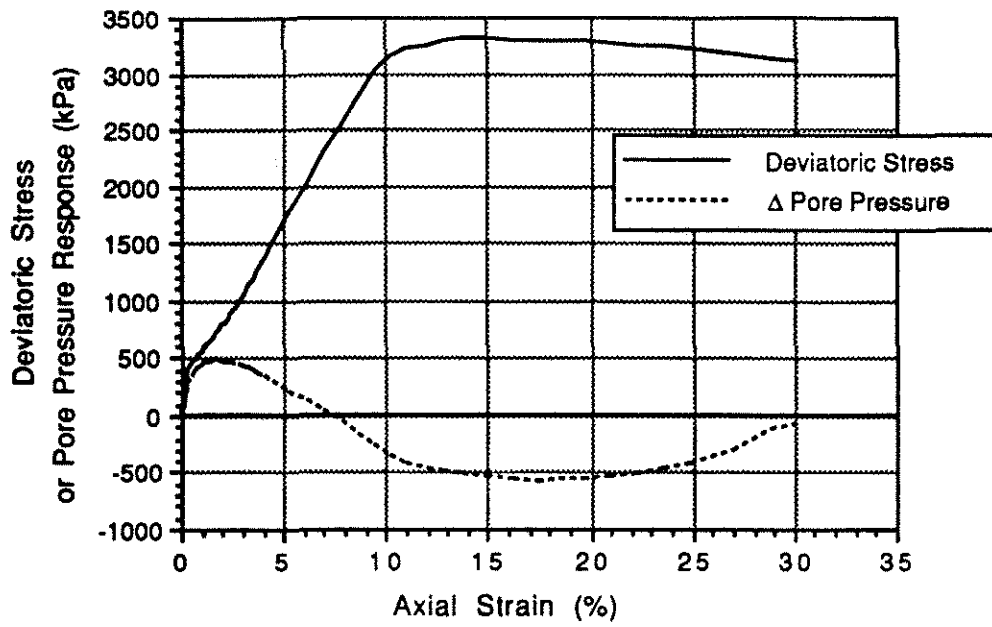


STRESS PATH (p'-q)

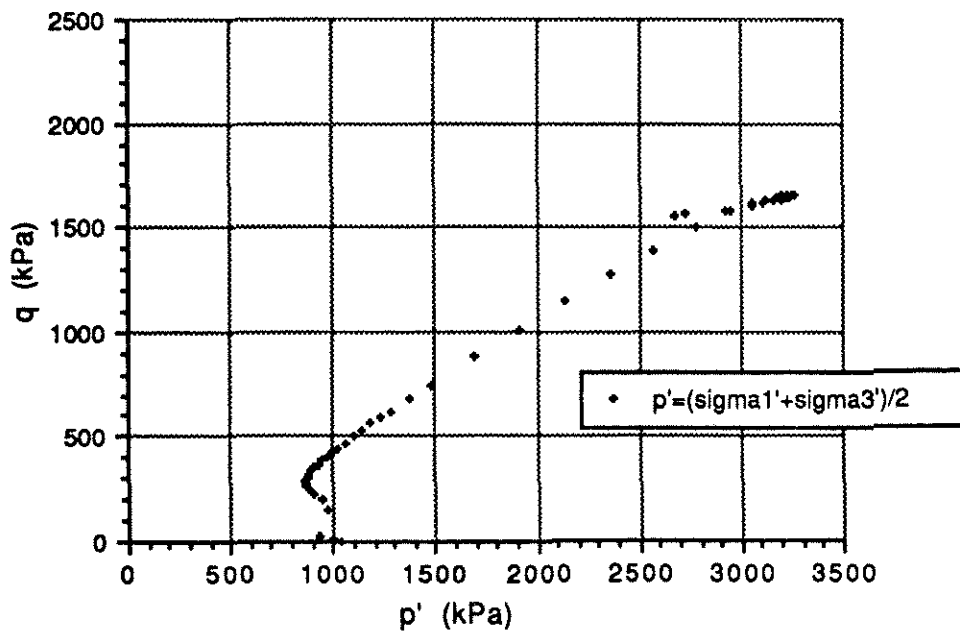
FIGURE C-24: TEST UF 1 (FLUME)

Specimen	TS35 P2	Test	UF 1	Set-up #	2	Load Cell	Internal
A. INITIAL CONDITION		no f. ends	Gs=2.65				
Dry Density	1.511 Mg/m ³	Void ratio	0.754	Dry Wt. 184.75 g			
Relative Density	38.5 %	Saturation	57.9 %				
Max Density	1.695 Mg/m ³	Min Density	1.415 Mg/m ³				
B. PRE-SHEAR CONDITIONS							
Dry Density	1.545 Mg/m ³	B	0.970	Volume 119.6 cc			
Void ratio	0.715	Con. Pressure	320.1 kPa				
Rel Density	50.9 %	Con. Volume	1.31 cc				
Init. Effective Con. Pressure	325.5 kPa	Applied Back Pressure	837.4 kPa				
C. DURING SHEAR							
Deviatoric Stress (kPa)		Δ Pore Pressure (kPa)		Stress Ratio			
Break/		Peak	183.3 @ 1.7 %	Break	2.67		
Peak	178.3 @ 0.3 %	10%	-260.5	@	1.7 %		
10%	1480.0	Elbow	181.2	10%	3.53		
Elbow	207.5	Break	-400.4 @ 12.6 %	Elbow	2.43		
Initial Tangent Modulus	6.369E4 kPa/Strain	Foreslope	2.720E4 kPa/Strain				
		Backslope1	-2.950E3 kPa/Strain				
		Backslope2	-6.610E3 kPa/Strain				
PP Parameter "A"		p' (kPa)		q (kPa)			
Peak ΔPP	0.79 @ 1.7 %	$(\sigma' + \sigma_3')/2$		$(\sigma' - \sigma_3')/2$			
10%	-0.19	Elbow	248.8 @ 1.2 %	Elbow	103.8		
Elbow	0.90	10%	1324.6	10%	740.0		
Break ΔPP	-0.23	Steady State	2252.3 @ 27.8 %	Steady State	1435.6		
		$(\sigma' + 2\sigma_3')/3$		$(\sigma' - \sigma_3')/Dr$			
SS Reached? no		Elbow	214.2	0.284			
dilative		10%	1077.9	Ø' 33.5 °			
		Steady State	1773.8	SS Type dilative end pt above			

TABLE C-24: TEST UF 1 (flume)



DEVIATORIC STRESS AND Δ PORE PRESSURE



STRESS PATH (p' - q)

FIGURE C-25: TEST FD 1 (FIELD)

Specimen T1 SG4 2/3B Test FD 1 Set-up # HP Load Cell External

A. INITIAL CONDITION

Gs=2.65

Dry Density	1.581 Mg/m ³	Void ratio	0.676	Dry Wt. 71.31 g
Relative Density	63.6 %	Saturation	86.0 %	
Max Density	1.695 Mg/m ³	Min Density	1.415 Mg/m ³	

B. PRE-SHEAR CONDITIONS

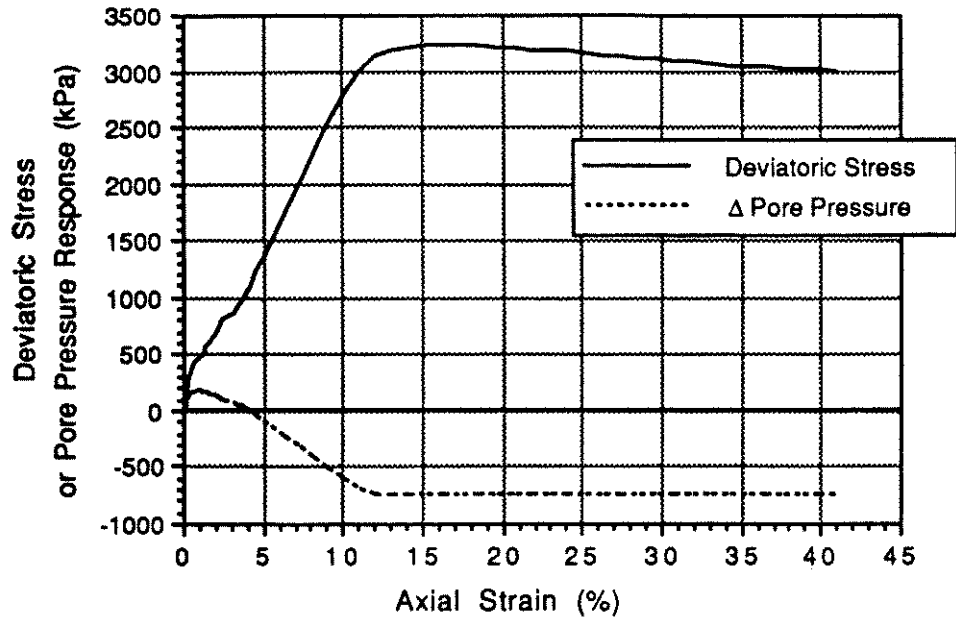
Dry Density	1.575 Mg/m ³	B	0.990	Volume 45.3 cc
Void ratio	0.682	Con. Pressure	1040.0 kPa	
Rel Density	61.5 %	Con. Volume	0.66 cc	
Init. Effective Con. Pressure	1030.0 kPa	Applied Back Pressure	969.7 kPa	

C. DURING SHEAR

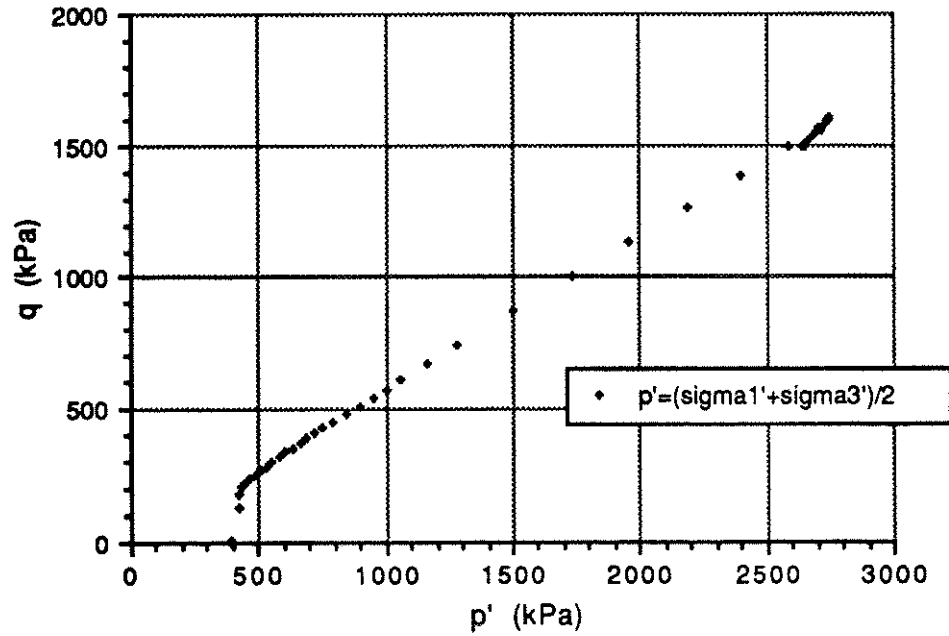
Deviatoric Stress (kPa)		Δ Pore Pressure (kPa)		Stress Ratio	
Break/Peak	396.8 @ 0.3 %	Peak	476.5 @ 1.7 %	Break	2.62
10%	3128.0	10%	-342.9	@	2.7 %
Elbow	552.0	Elbow	422.9	10%	3.32
Initial Tangent Modulus	1.202E5 kPa/Strain	Break	-464.1 @ 12.0 %	Elbow	1.94
		Foreslope	5.690E4 kPa/Strain		
		Backslope1	-3.970E3 kPa/Strain		
		Backslope2	-1.105E4 kPa/Strain		

PP Parameter "A"		p' (kPa)		q (kPa)	
Peak ΔPP	0.68 @ 1.7 %	(σ ₁ ' + σ ₃ ')/2		(σ ₁ ' - σ ₃ ')/2	
10%	-0.10	Elbow	865.3 @ 1.0 %	Elbow	276.0
Elbow	0.81	10%	2914.1	10%	1564.0
Break ΔPP	-0.14	Steady State	3258.9 @ 17.4 %	Steady State	1650.1
		(σ ₁ ' + 2σ ₃ ')/3		(P _o '/P _{ss} ')/Dr	
SS Reached? no		Elbow	773.3		0.514
dilative		10%	2292.7	Ø'	33.2 °
		Steady State	2708.9	SS Type dilative reversal below	

TABLE C-25: TEST FD 1 (field)



DEVIATORIC STRESS AND Δ PORE PRESSURE



STRESS PATH (p'-q)

FIGURE C-26: TEST FD 2 (FIELD)

Specimen T1 SG4 2/3C Test FD 2 Set-up # 2 Load Cell Internal

A. INITIAL CONDITION

G_s=2.65

Dry Density	1.622 Mg/m ³	Void ratio	0.634	Dry Wt.	75.93 g
Relative Density	77.3 %	Saturation	85.9 %		
Max Density	1.695 Mg/m ³	Min Density	1.415 Mg/m ³		

B. PRE-SHEAR CONDITIONS

Dry Density	1.646 Mg/m ³	B	0.998	Volume	46.1 cc
Void ratio	0.610	Con. Pressure	394.3 kPa		
Rel Density	85.0 %	Con. Volume	0.94 cc		
Init. Effective Con. Pressure	393.5 kPa	Applied Back Pressure	687.8 kPa		

C. DURING SHEAR

Deviatoric Stress (kPa)			Δ Pore Pressure (kPa)			Stress Ratio	
Break/			Peak	172.3 @ 1.0 %	Break	3.37	
Peak	267.6 @ 0.4 %		10%	-612.5	@	1.6 %	
10%	2778.2		Elbow	152.3	10%	3.76	
Elbow	356.8		Break	-742.5 @ 12.1 %	Elbow	2.48	
Initial Tangent Modulus	7.042E4 kPa/Strain		Foreslope	2.820E4 kPa/Strain			
			Backslope1	-6.370E3 kPa/Strain			
			Backslope2	-1.011E4 kPa/Strain			
PP Parameter "A"			p' (kPa)			q (kPa)	
			$(\sigma_1' + \sigma_3')/2$			$(\sigma_1' - \sigma_3')/2$	
Peak ΔPP	0.38 @ 1.0 %		Elbow	419.3 @ 0.5 %	Elbow	178.4	
10%	-0.22		10%	2395.5	10%	1389.1	
Elbow	0.43		Steady State	2750.5 @ 16.4 %	Steady State	1607.1	
Break ΔPP	-0.24		$(\sigma_1' + 2\sigma_3')/3$			$(P_o'/P_{ss}')/D_r$	
			Elbow	359.5		0.168	
			10%	1932.5			
			Steady State	2214.8	Ø'	36.0 °	
SS Reached? yes					SS Type dilative reversal below		
dilative							

TABLE C-26: TEST FD 2 (field)

APPENDIX D - Grain Size Analysis Summary and Results

TABLE D-1: GRAIN SIZE RESULTS PLUVIATED TESTS					
TEST/SAMPLE	D10	D50	D60	Q_i	<#200
PL 3 FM9 C2	0.0973	0.1648	0.1745	1.79	5.70
PL 5 FM10 1A	0.0926	0.1616	0.1726	1.86	6.09
PL 6 FM10 4A	0.1005	0.1564	0.1726	1.72	4.81
PL 7 FM10 C1	0.0947	0.1547	0.1716	1.81	5.79
PL 8 FM10 C3	0.0970	0.1543	0.1726	1.78	
PL 9 FM10 C4	0.0900	0.1599	0.1688	1.88	
PL 10 FM11 C1	0.0794	0.1556	0.1707	2.15	8.83
PL 12 FM11 C3	0.1033	0.1670	0.1808	1.75	5.76
PL 15 FM11 A3	0.0855	0.1552	0.1661	1.94	7.12
PL 16 FM12 A2	0.0803	0.1543	0.1648	2.05	8.28
PL 17 FM11 A4	0.0853	0.1634	0.1735	2.03	5.64
PL 19 FM11 C4	0.0904	0.1625	0.1726	1.91	7.02
SUM	1.0963	1.9097	2.0612	22.6794	65.0400
SUM2	1.2019	3.6470	4.2485	514.3544	4230.2016
AVERAGE	0.0914	0.1591	0.1718	1.8899	6.5040
S.D.	0.0076	0.0046	0.0041	0.1331	1.2783
COV.	8.4	2.9	2.4	7.0	19.7

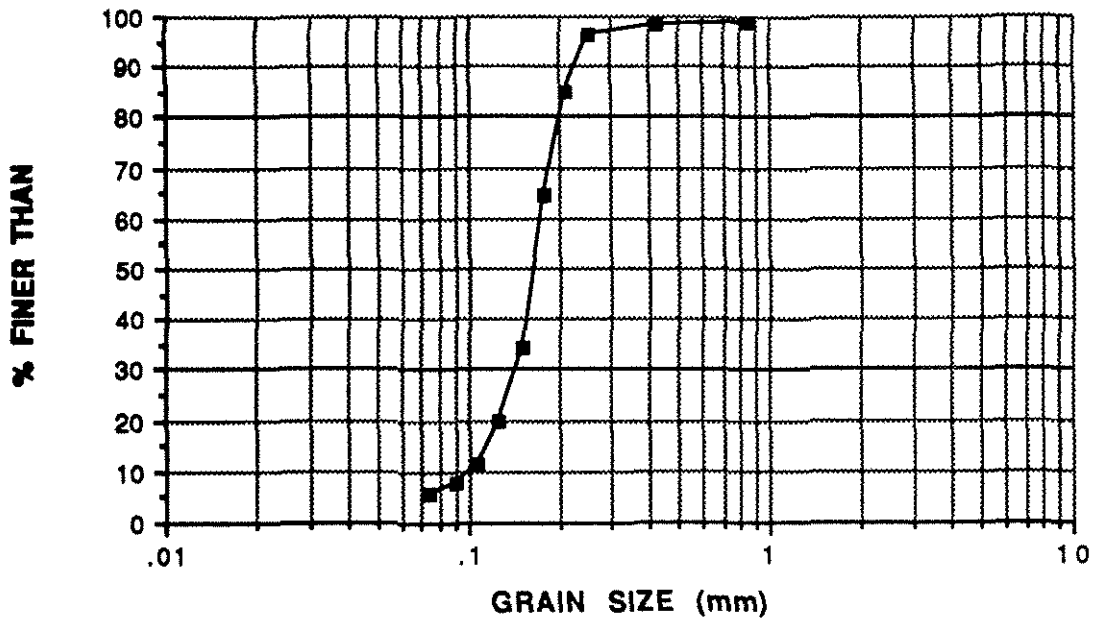
1 of 3

TABLE D-1: GRAIN SIZE RESULTS FLUME TESTS					
TEST/SAMPLE	D10	D50	D60	Q _i	<#200
FL 2 (from TS1 D2)	0.1278	0.1803	0.1909	1.49	1.58
FL 3 TS1 4/T2 A	0.0835	0.1410	0.1506	1.80	8.13
FL 4 TS1 4/T2 C	0.1251	0.2038	0.2292	1.83	3.52
FL 5 TS3 P2D A	0.1000	0.1657	0.1832	1.83	5.74
FL 6 TS3 P2D A	0.1115	0.1893	0.2033	1.82	5.33
FL 7 TS1 4/T3 A	0.1008	0.1726	0.1914	1.90	6.58
FL 8 TS1 4/T3 C	0.1094	0.1639	0.1726	1.58	
FL 9 TS1 4/T3 D	0.1244	0.1925	0.2033	1.63	5.39
FL 10 (from TS4 M2)	0.1109	0.1661	0.1735	1.56	
UF 1 TS35 P2	0.0950	0.1547	0.1634	1.72	
SUM	1.0884	1.7299	1.8614	17.1811	36.2700
SUM2	1.1845	2.9926	3.4648	295.190	1315.51
AVERAGE	0.1088	0.1730	0.1861	1.7181	5.1814
S.D.	0.0144	0.0188	0.0227	0.1406	2.1118
C.O.V.	13.2	10.9	12.2	8.2	40.8

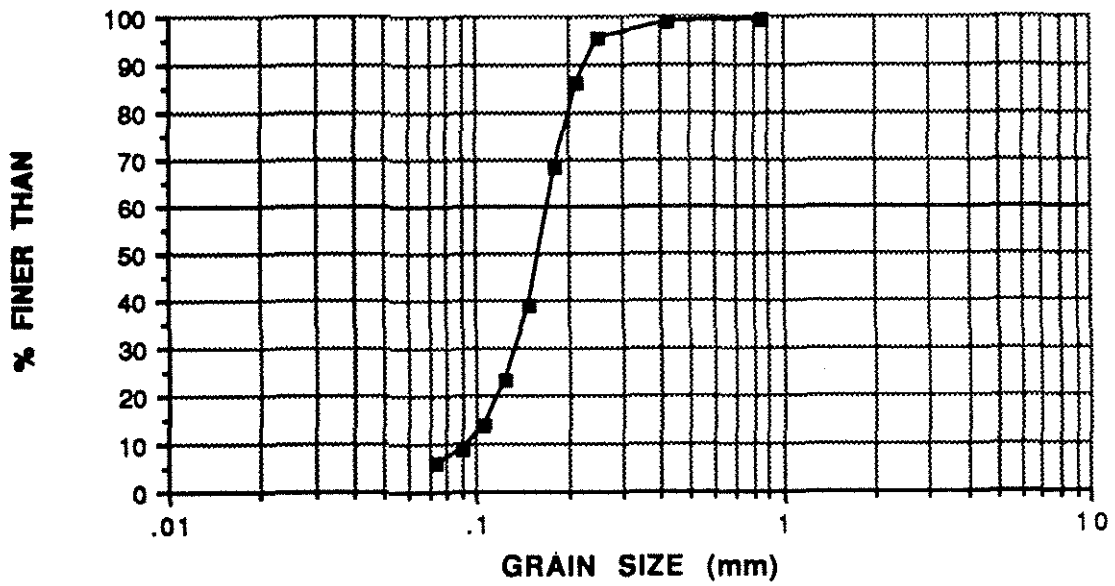
**TABLE D-1: GRAIN SIZE RESULTS
FIELD TESTS**

TEST/SAMPLE	D10	D50	D60	Cu	<#200
FD 1 T1 SG4 2/3B	0.0839	0.1670	0.1837	2.19	7.16
FD 2 (from T1 SG4 2/3B)	0.0839	0.1670	0.1837	2.19	7.16

3 of 3

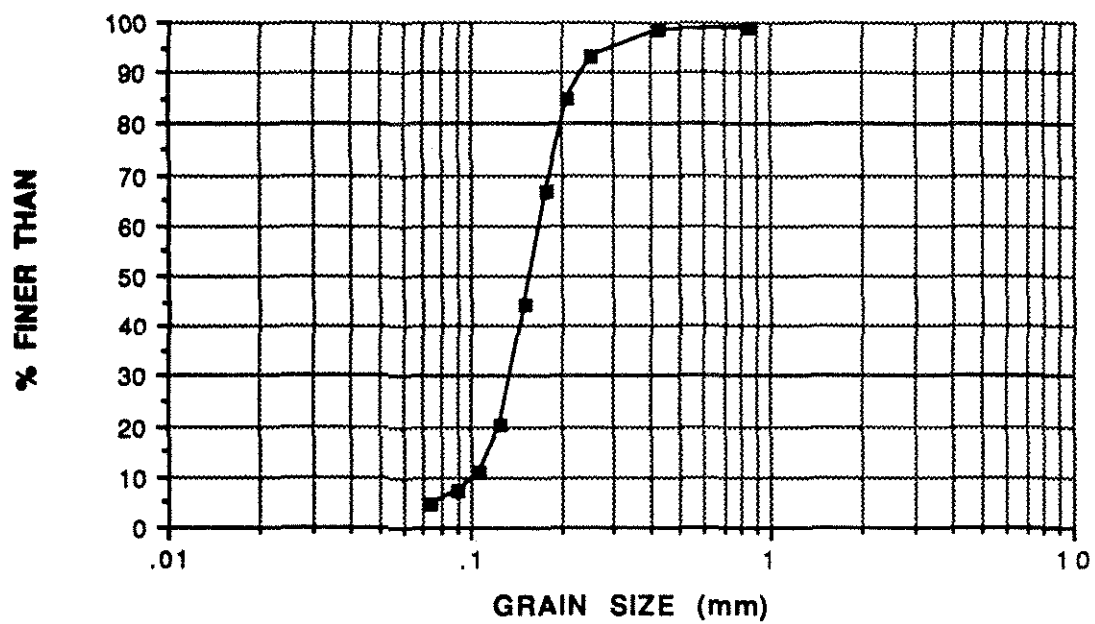


PL 3

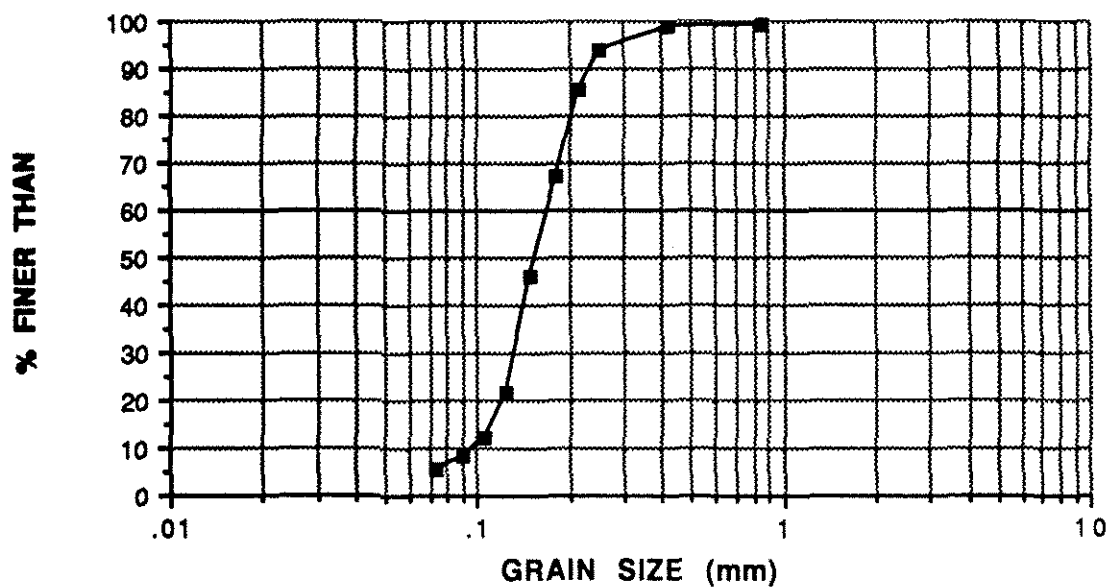


PL 5

FIGURE D-1: Grain Size Distribution for PL 3 and PL 5



PL 6



PL 7

FIGURE D-2: Grain Size Distribution for PL 6 and PL 7

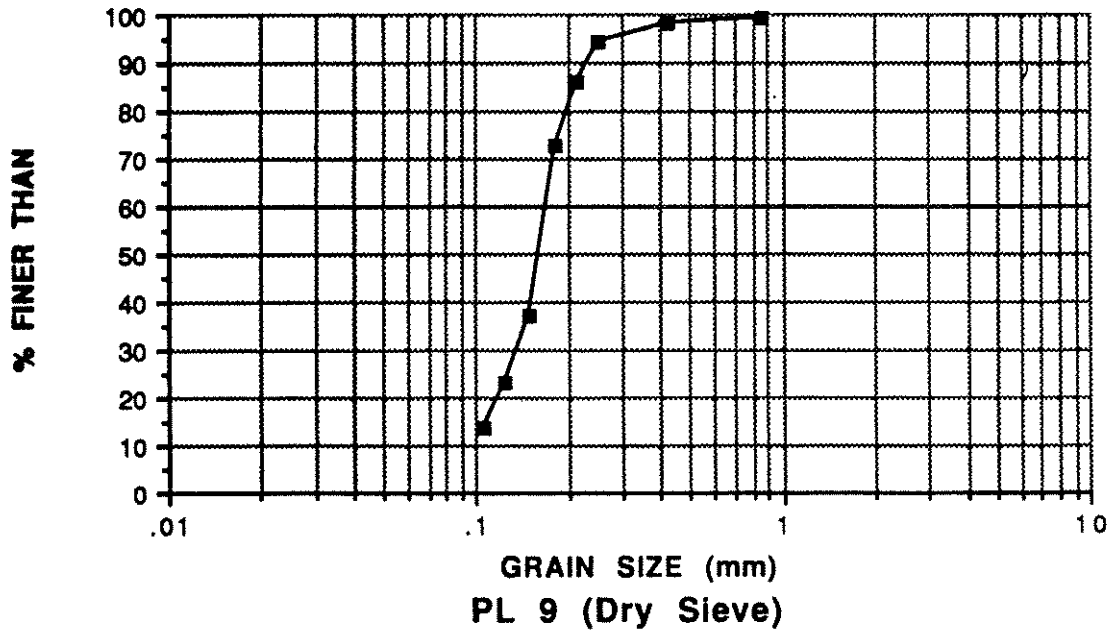
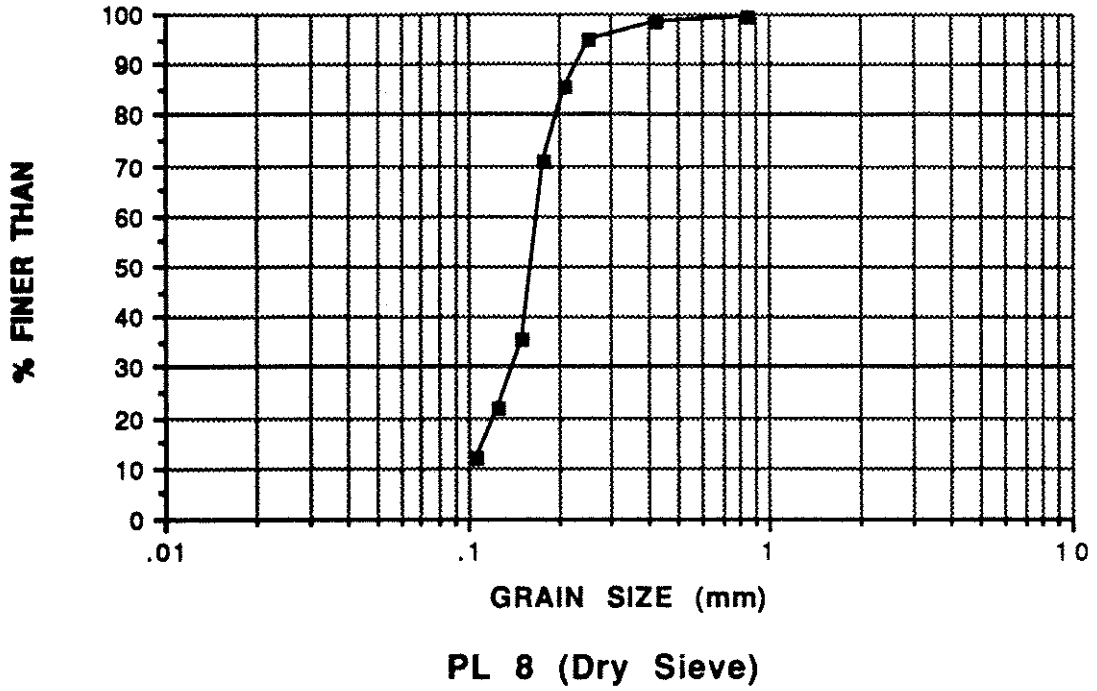
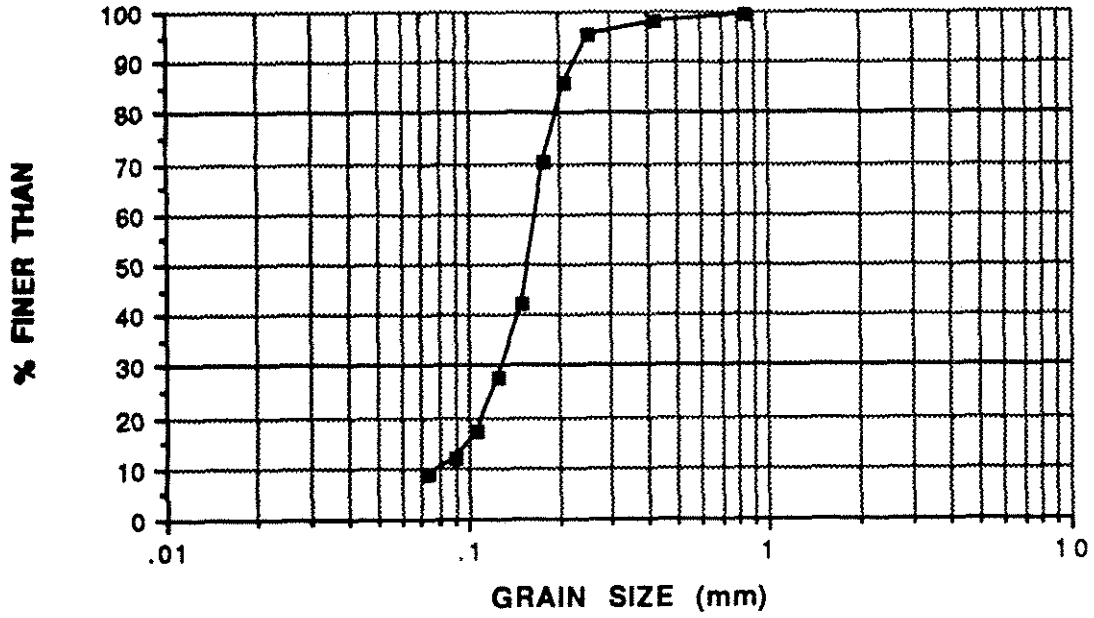
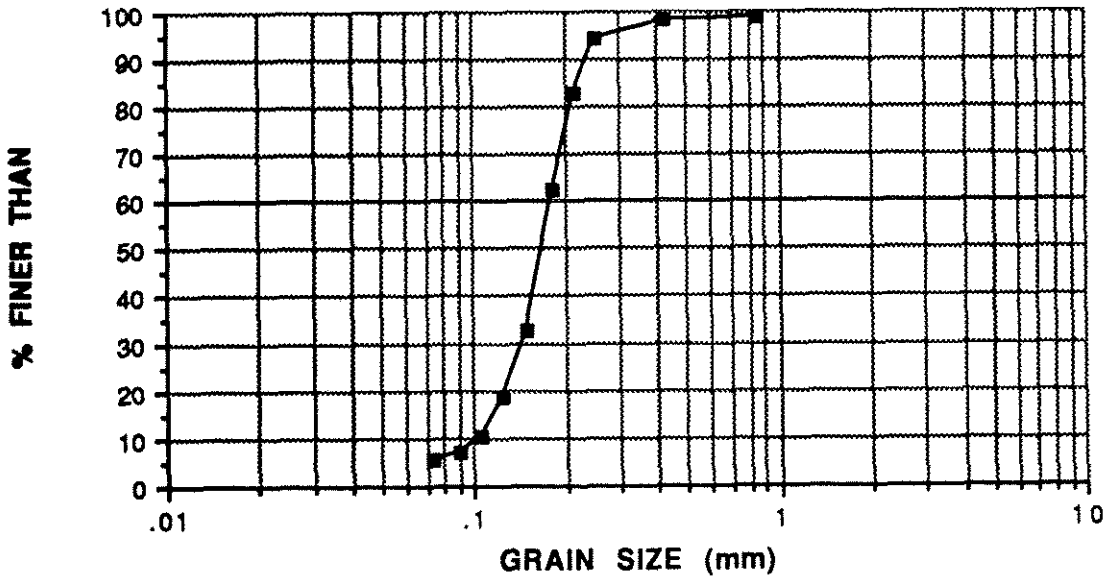


FIGURE D-3: Grain Size Distribution for PL 8 and PL 9

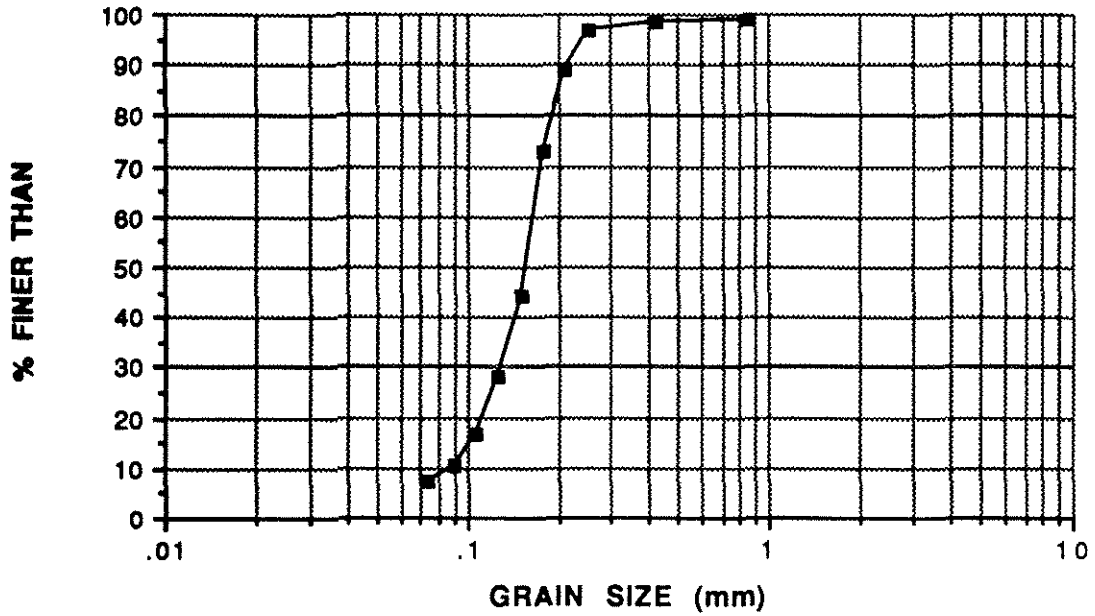


PL 10

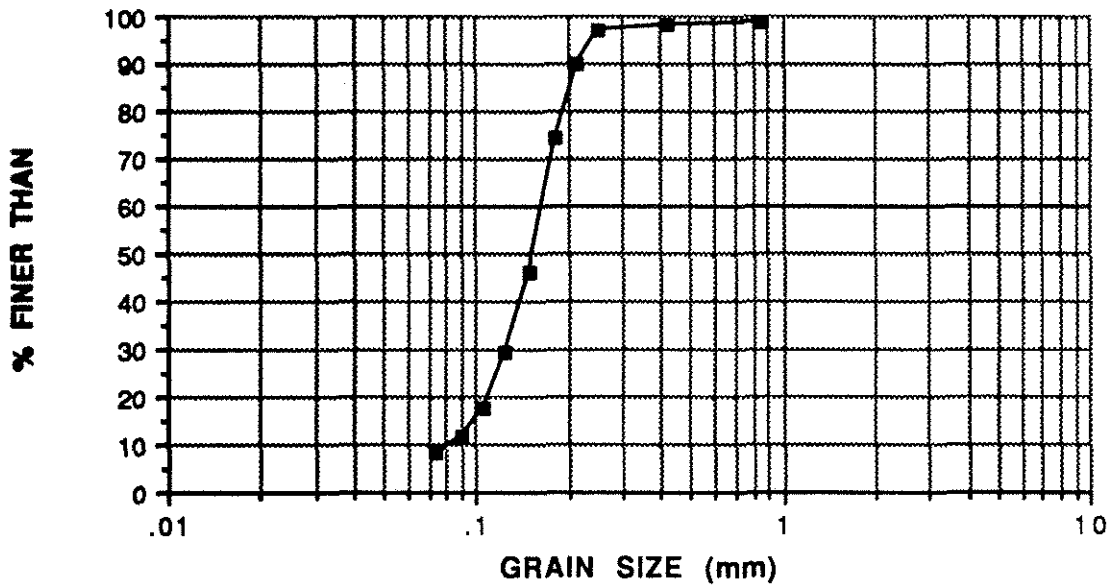


PL 12

FIGURE D-4: Grain Size Distribution for PL 10 and PL 12

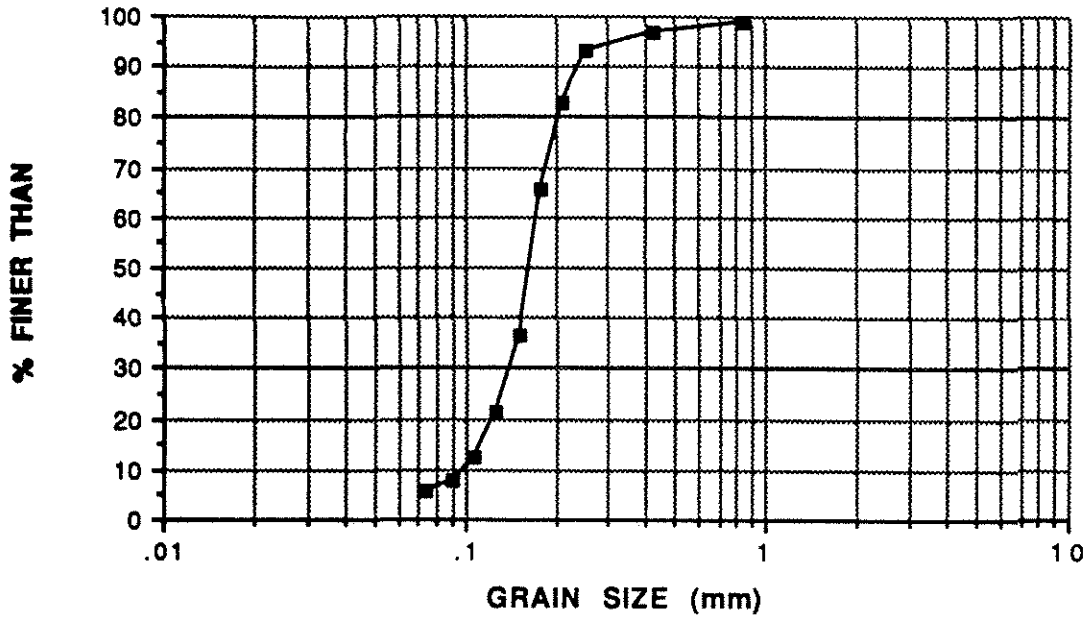


PL 15

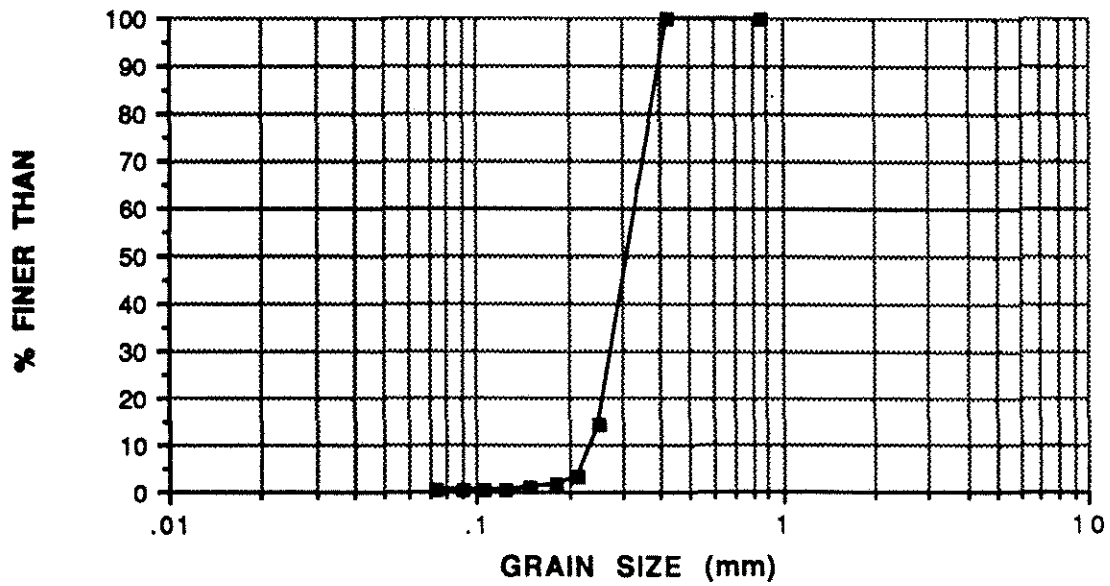


PL 16

FIGURE D-5: Grain Size Distribution for PL 15 and PL 16

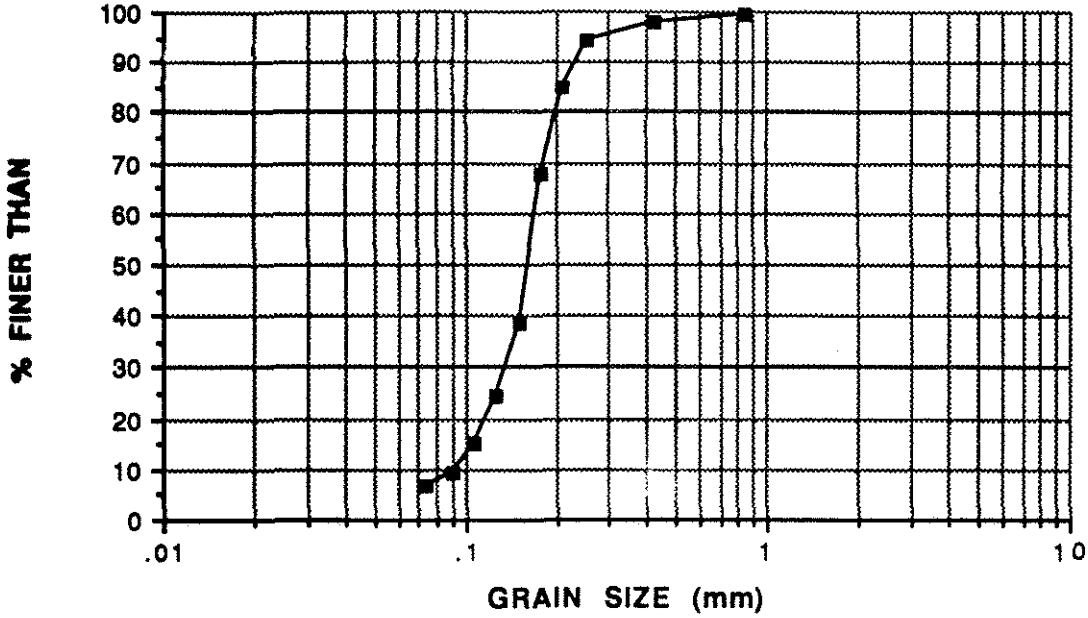


PL 17

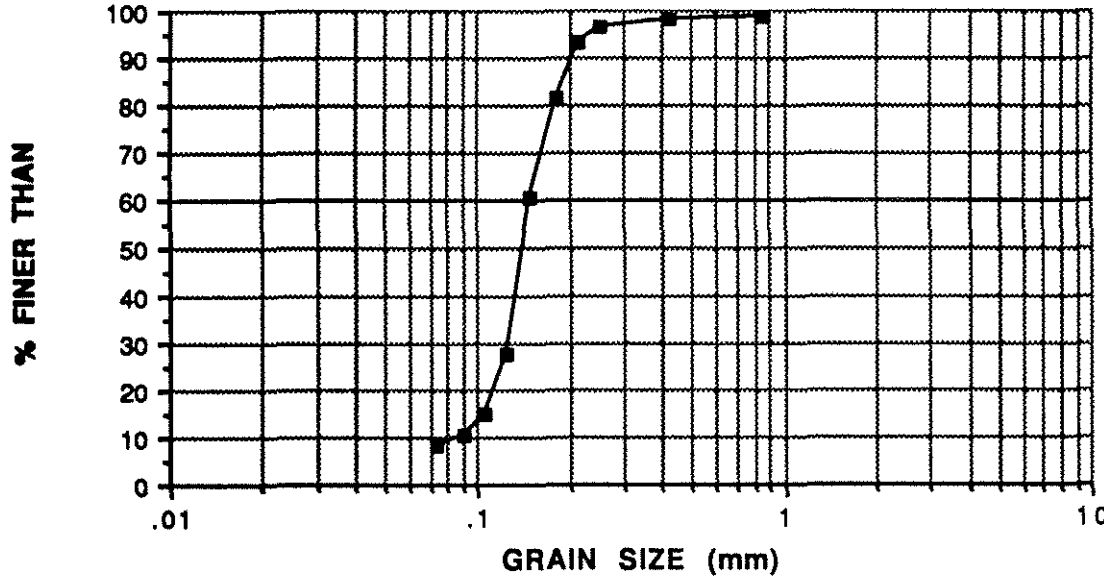


PL 18 (OTTAWA SAND)

FIGURE D-6: Grain Size Distribution for PL 17 and PL 18

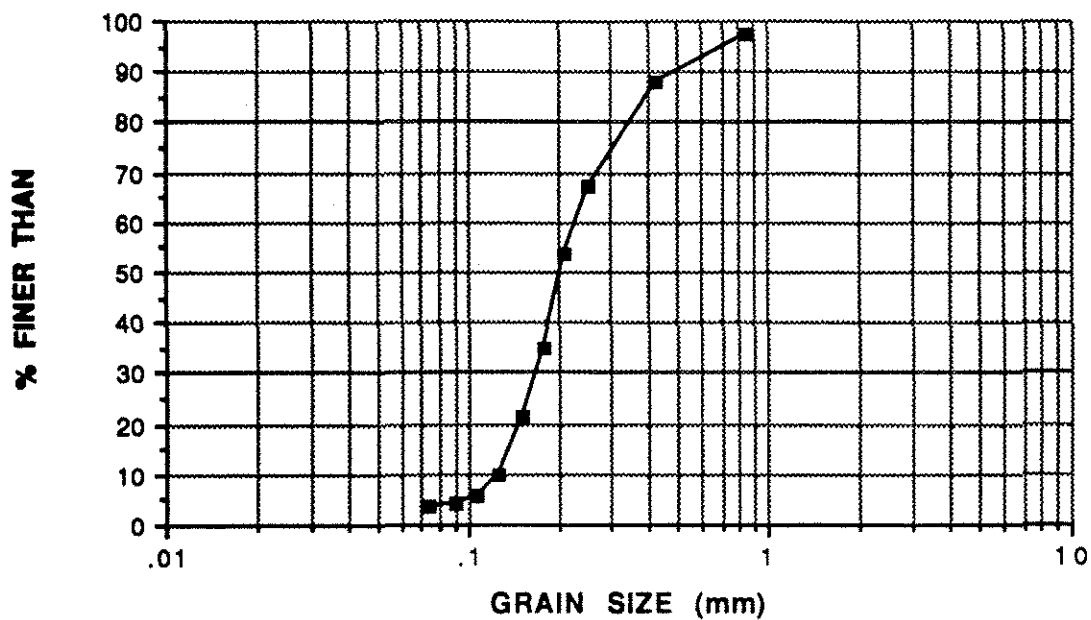


PL 19

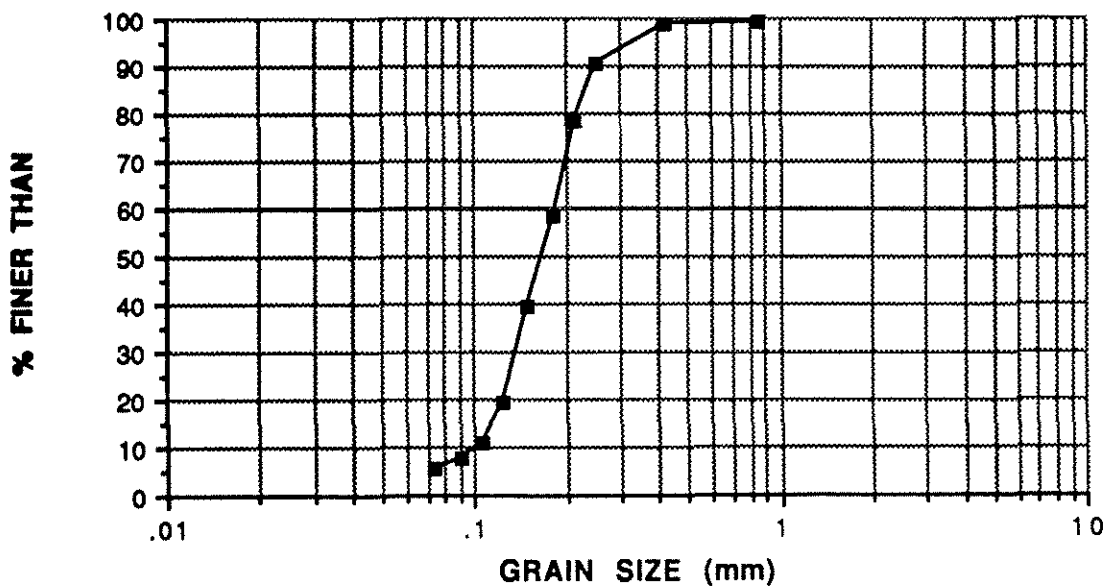


FL 3

FIGURE D-7: Grain Size Distribution for PL 19 and FL 3

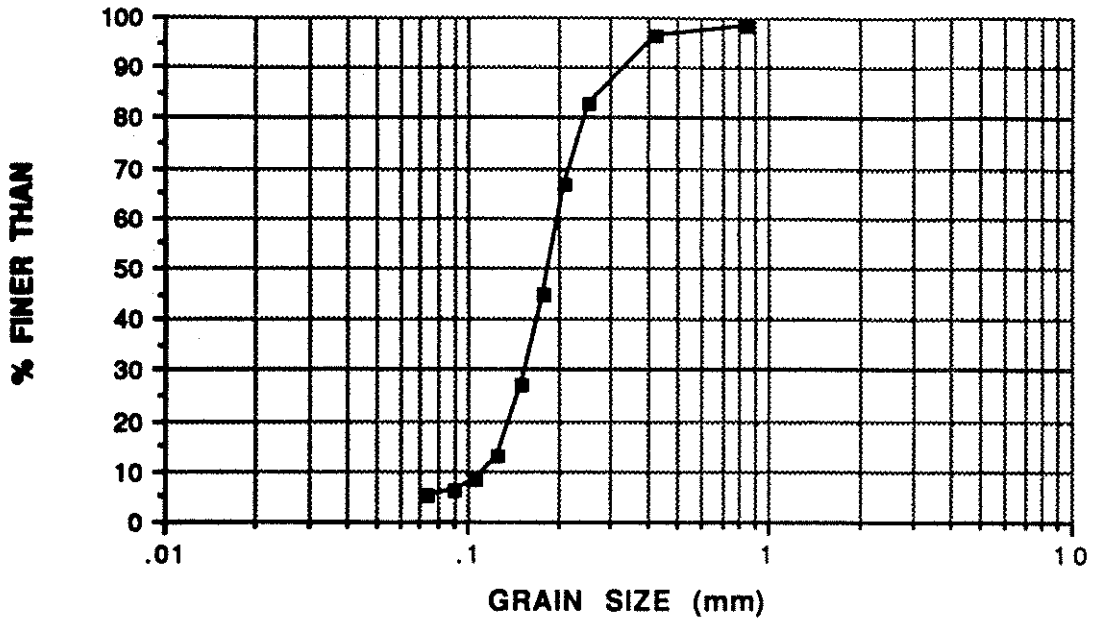


FL 4

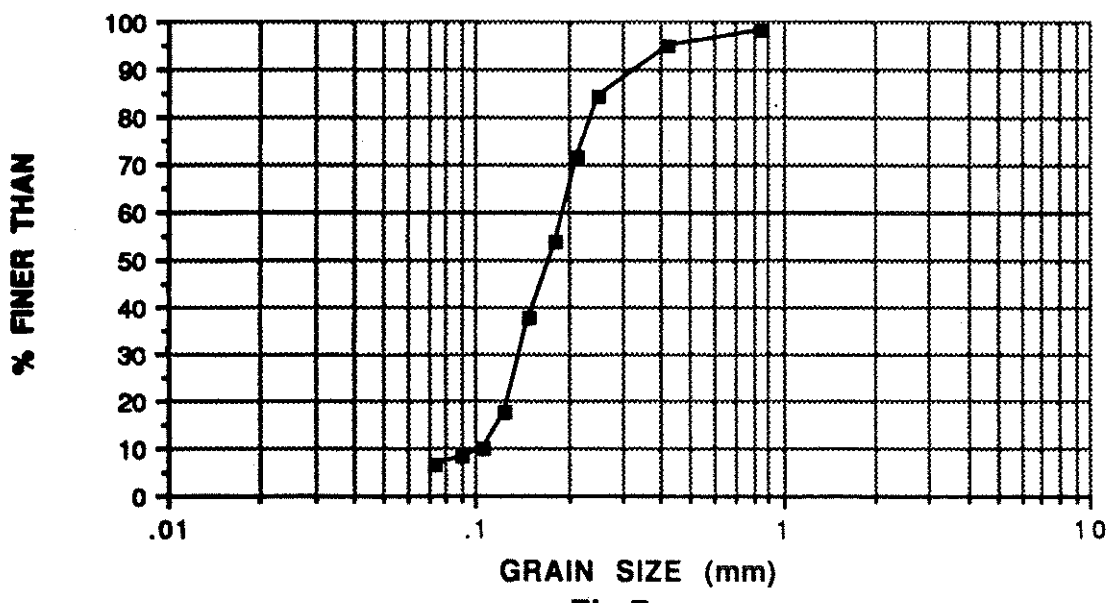


FL 5

FIGURE D-8: Grain Size Distribution for FL 4 and FL 5



FL 6



FL 7

FIGURE D-9: Grain Size Distribution for FL 6 and FL 7

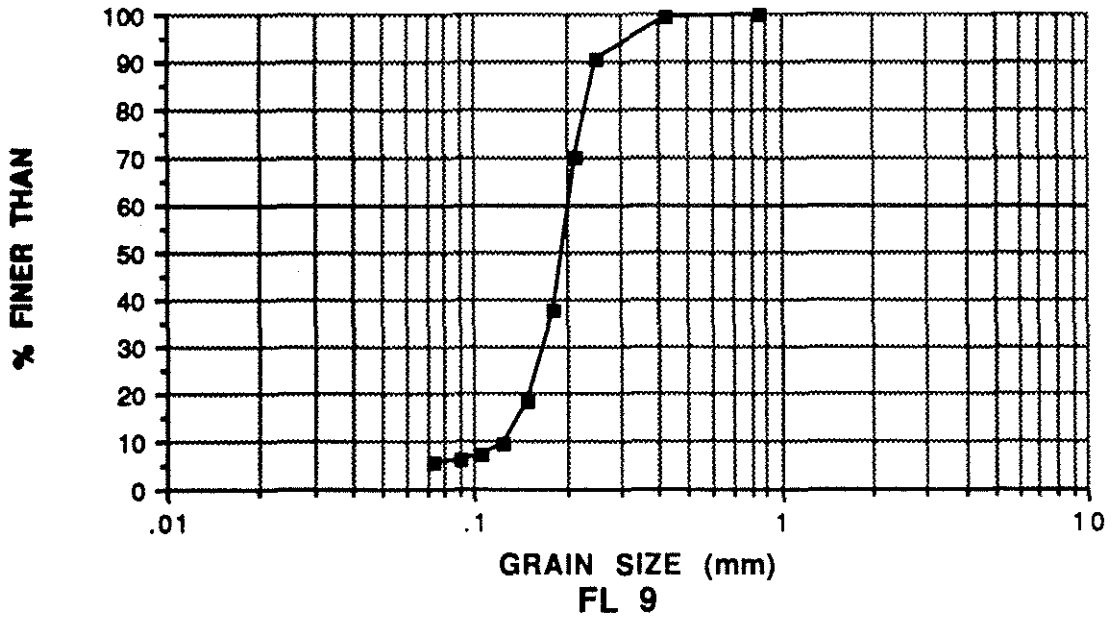
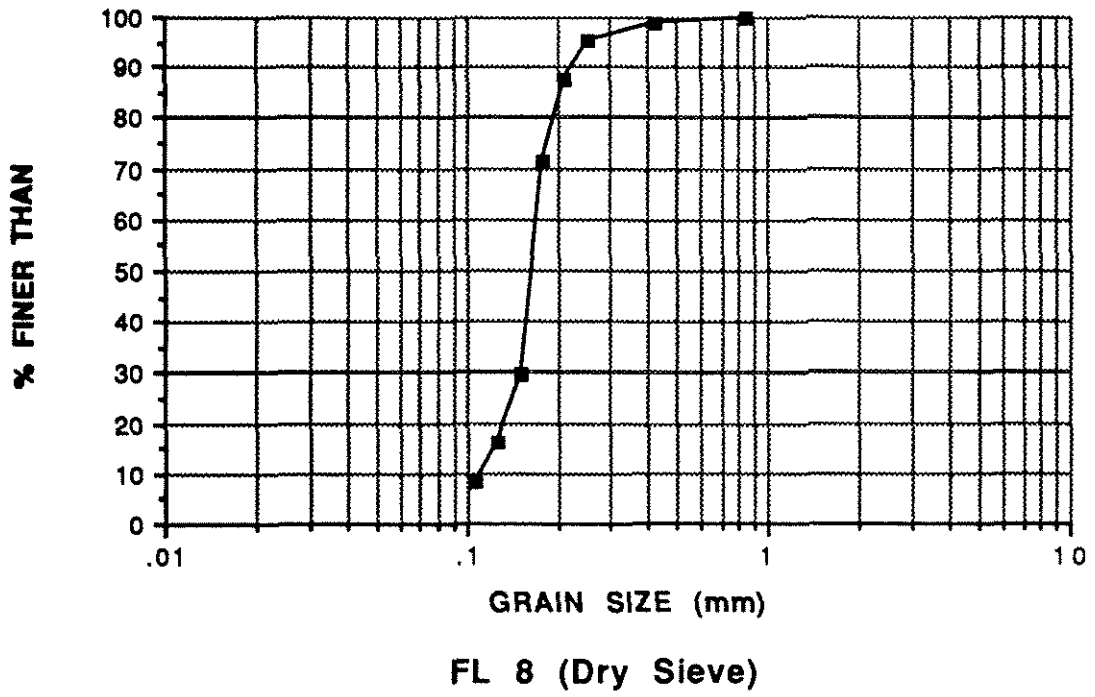
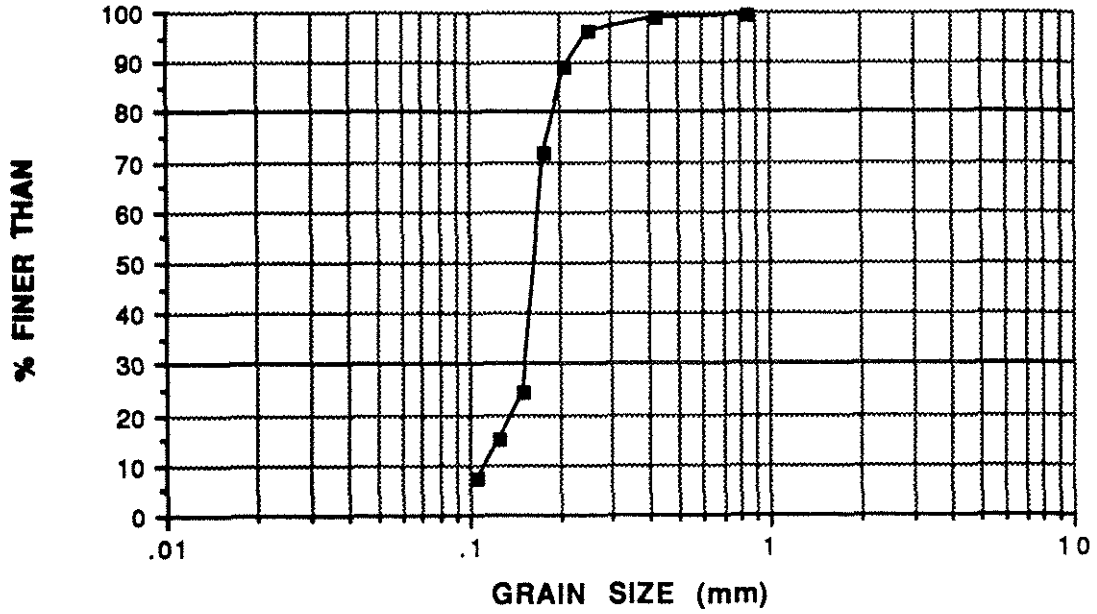
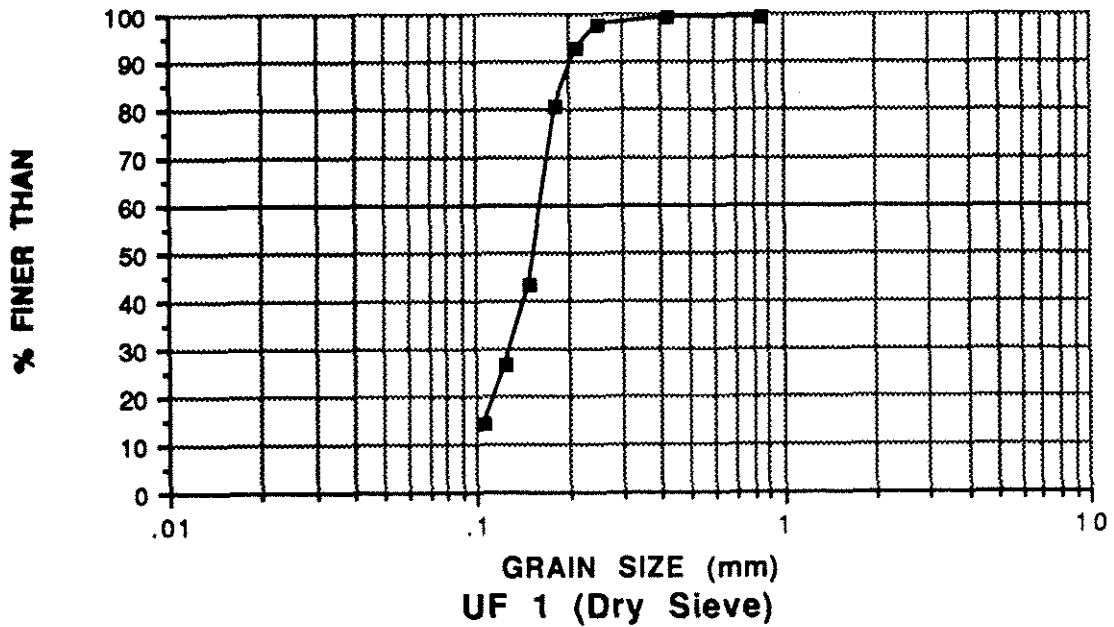


FIGURE D-10: Grain Size Distribution for FL 8 and FL 9



FL 10 (TS-4 M2)



UF 1 (Dry Sieve)

FIGURE D-11: Grain Size Distribution for FL 10 and UF 1

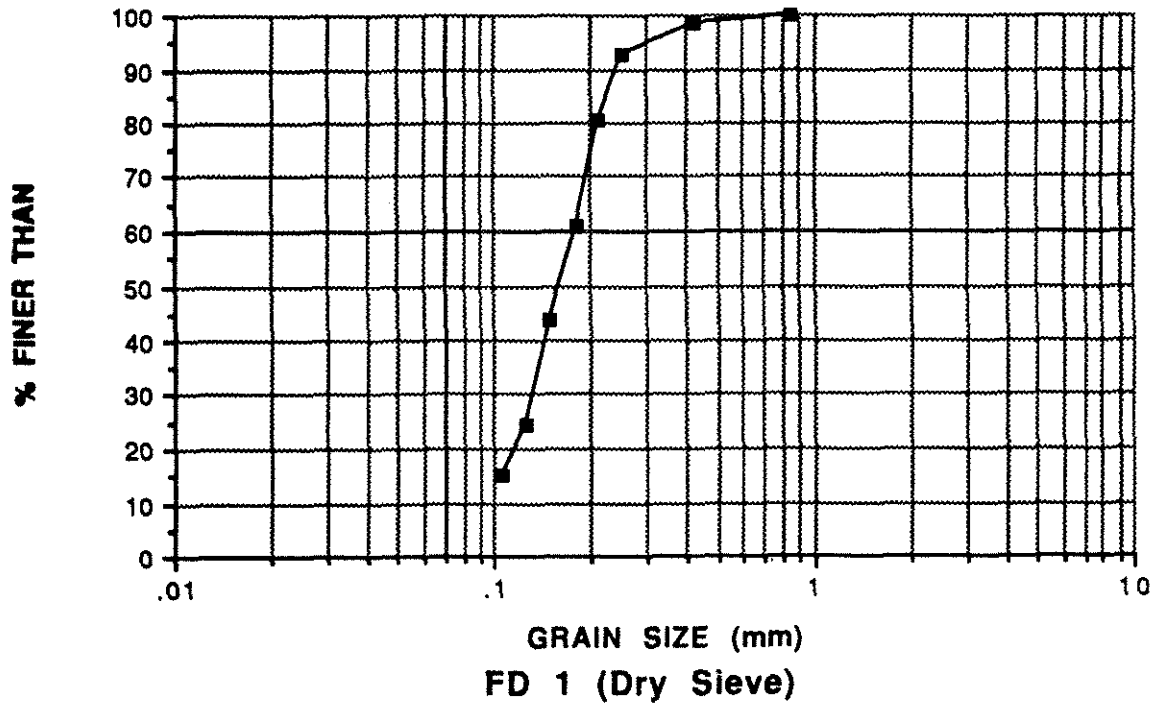


FIGURE D-12: Grain Size Distribution for F 1

**APPENDIX E - Relationship Between the Relative Density Parameter and
Various Moderate Strain Parameters**

Results of the comparison of the RD parameter with various moderate strain parameters (initial tangent and foreslope moduli, and Skempton's A parameter and the stress ratio at the elbow) are presented in Figures E-1 to E-4. No tight correlation of these parameters with the RD parameter appear to exist for this data set. However, the inspection of the individual groups of data show trends with the RD parameter and these trends are compared with expected behaviour during initial shear.

Initial Tangent Modulus

Figure E-1 shows the data from Sources 1, 2 and 4 trending to higher values of initial tangent modulus with decreasing RD parameter, although with significant scatter. This trend reflects the increased stiffness of the sand matrix expected as its pre-shear state moves across the behavioural boundary from contractive (above) to dilative (below). The scatter is believed to be added to by the well known difficulties in obtaining accurate strength moduli in laboratory tests, especially with the determination of the initial tangent modulus because of seating problems caused by the lubricated ends, and the influence of the apparatus stiffness on the measured values. The other data presented in Figure E-1 do not correlate as well as the data from Sources 1, 2 and 4. Because of the large degree of scatter, no preparation method effect could be determined.

Foreslope Modulus

The overall trend observed in Figure E-2 is that of increasing foreslope modulus with increasing RD parameter. The foreslope modulus represents the rate of increase in pore pressure observed during the initial contractive stage found in all the CU tests studied, and is analogous to the rate of volume change that would occur during a drained test during

the initial loading stage. A specimen with a strong dilative tendency (highly negative RD parameter) would likely exhibit the initial contraction at a slower rate than a contractive specimen. This is intuitively probable because the grains of a loose specimen under low initial effective confining pressures (higher RD parameter value) are more easily rearranged to a position providing a steady state resistance in undrained shear than those of a dense specimen under the same initial effective confining pressure (lower RD parameter value), due to fewer intergranular contacts constraining the rearrangement. The rate of change of position of the grains with respect to one another influences the observed pore pressure response significantly, with a higher rate producing a larger response in the same time frame.

During the initial compression of the soil skeleton, this rate of change of relative grain position is probably affected in the same manner as during rearrangement to a steady state fabric, hence the trend as observed is plausible. In the initial compression stage, however, the particles are attempting to occupy less space because of the compressive loading applied rather than changing orientation with respect to one another. The undrained boundary conditions do not let this occur, as would be observed in a drained test, but interparticle slip does occur and the pore pressure increases to compensate for the compression tendency. With more potential to compress, the loose specimen should exhibit a faster pore pressure response than that of a dense specimen (having the same p_0').

The rate of change of particle position with respect to one another is also likely affected by the initial fabric of the specimen, especially prior to the elbow where the least disruption of the initial fabric has taken place. No specific trend attributable to the method of preparation was observed. The overall trend of increasing foreslope modulus with increasing RD parameter is not exhibited well within the individual groups of data. The scatter observed is likely contributed to by the accuracy with which the foreslope modulus

can be measured. The sensitivity of the modulus to the inevitable small errors in the pore pressure response (due to membrane penetration and lubricated end compliance effects), and to errors in strain rate calculated (due to an inexact area correction) can be high.

Stress Ratio

A slight trend from higher to lower stress ratio at the elbow with increasing RD parameter is seen, in Figure E-3, both weakly overall and, somewhat stronger within the groups of data provided by Source 3 (pluviated) and Source 4. The stress ratio reported at the elbow is indicative of the rate of strength development within the specimen prior to the elbow point, after which the strength either reduces dramatically (contractive), increases substantially (dilative), or remains approximately constant (contractive-dilative). The observed trend is believed to be plausible because a higher strength can be expected to develop at the elbow in a dilative specimen than in a contractive specimen due to more intergranular contacts constraining the rearrangement, as outlined for the foreslope modulus. No specific trend attributable to the method of preparation can be discerned from this data.

Pore Pressure Parameter 'A'

The 'A' parameter is defined by the ratio of the change in pore pressure to the ratio of the change in deviatoric stress in a saturated medium from the pre-shear conditions to the stage of the test in question (the elbow, in this case). As such, the expected change in

the A parameter at the elbow with a increase in the RD parameter is to increase, due both to an increase in the pore pressure component (as described for the foreslope modulus) and a decrease in the strength component (as described for the stress ratio). This trend is observed (in Figure E-4) within the data of Source 1, 3 (compacted) and 4, but is not well defined in the remaining data. Too much scatter exists to relate this change in observed relation to the RD parameter with the change in initial fabric.

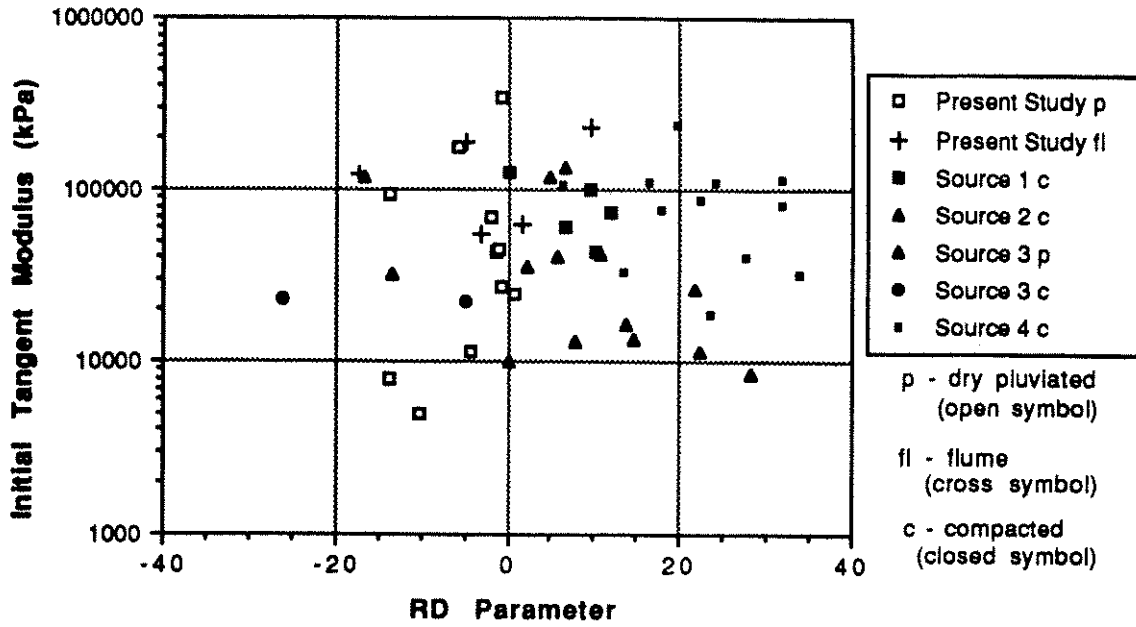


FIGURE E-1: Initial Tangent Modulus vs RD Parameter

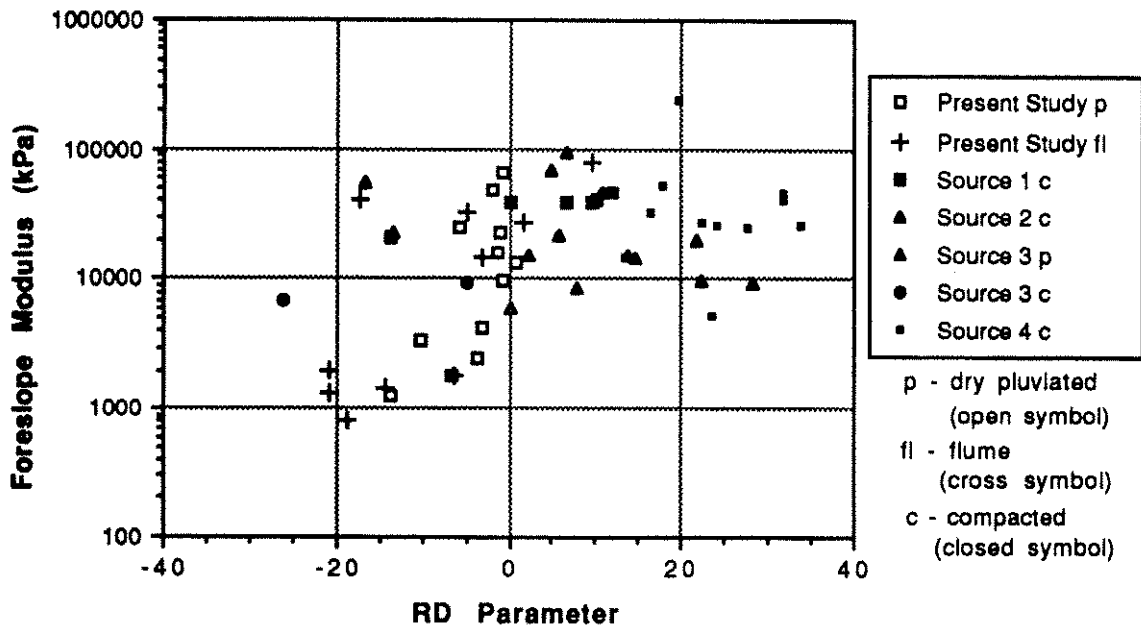


FIGURE E-2: Foreslope Modulus vs RD Parameter

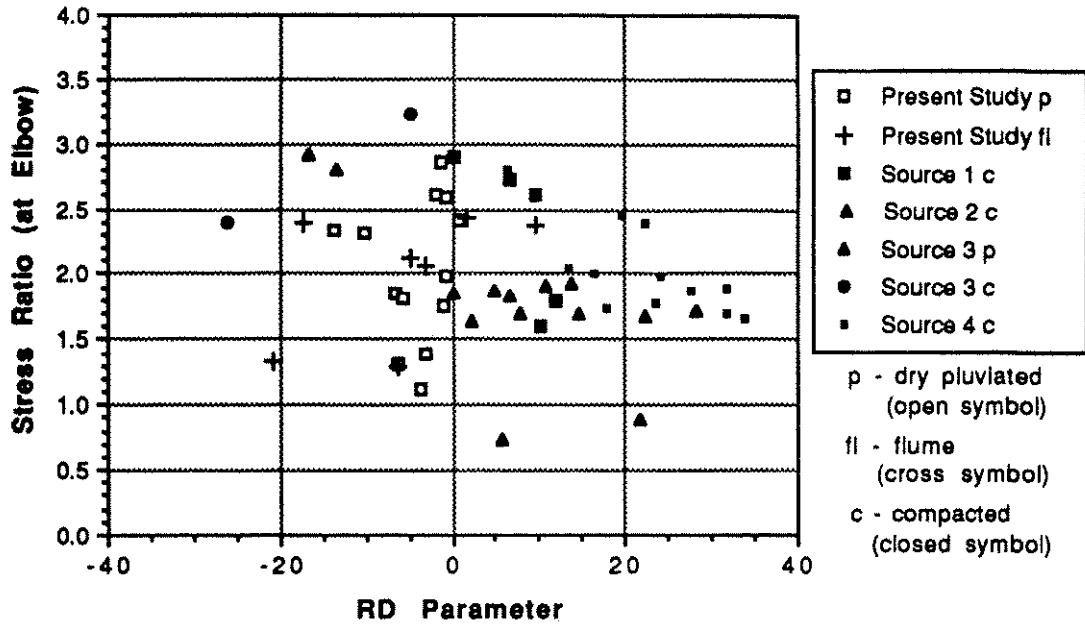


FIGURE E-3: Stress Ratio vs RD Parameter

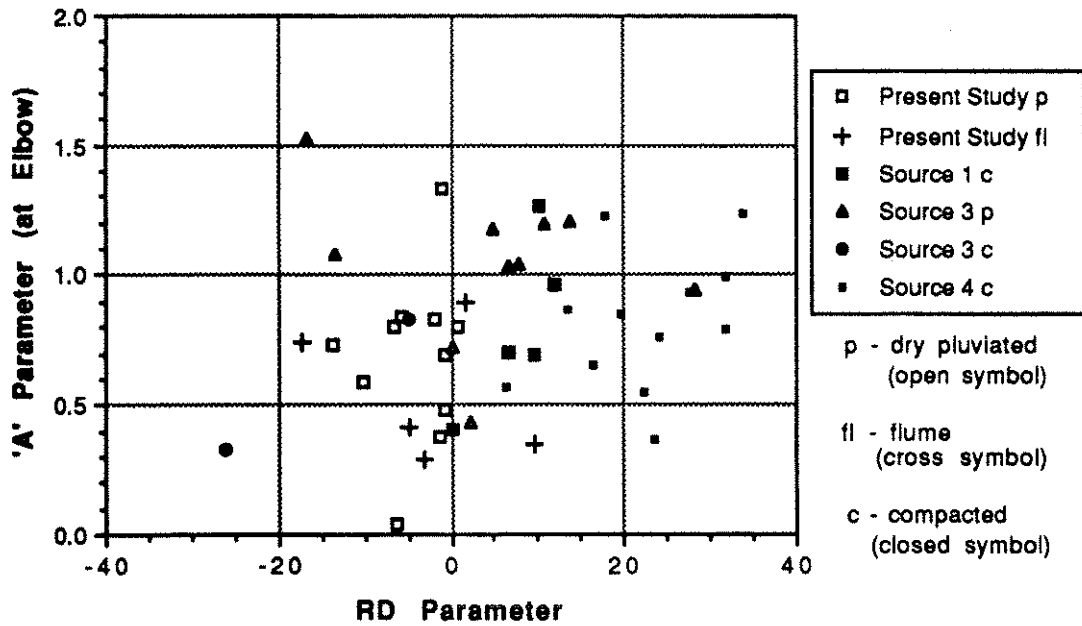


FIGURE E-4: 'A' Parameter vs RD Parameter

SOURCE 1 - Geotechnical Engineers Inc. (1978)

SOURCE 2 - Geotechnical Engineers Inc. (1981)

SOURCE 3 - Thurber Consultants Ltd. (1985)

SOURCE 4 - EBA Engineering Consultants Ltd. (1987)

SOURCE 5 - Hardy-BBT Ltd. (1987 and 1988)